Order Number 9325158

Spectroscopic studies of some Ru(II) polypyridyl complexes in solution, on porous Vycor glass (PVG), and bound to calf thymus DNA

Tysoe, Steven A., Ph.D.

City University of New York, 1993

U·M·I
300 N. Zeeb Rd.
Ann Arbor, MI 48106

A

Spectroscopic Studies of Some Ru(II) Polypyridyl Complexes in Solution, on Porous Vycor Glass (PVG), and Bound to Calf Thymus DNA.

by

Steven A. Tysoe

A dissertation submitted to the Graduate Faculty in Chemistry in partial fulfillment of the requirements for the degree of Doctor of Philosophy. The City of New York.

1993

This manuscript has been read and accepted for the Graduate Faculty in Chemistry in satisfaction of the dissertation requirement for the degree of Doctor of Philosophy.

4/23/93 — date

Thomas C. Stein — Chairman of Examining Committee

4/27/93 — date

Richard Pizza — Executive Officer

Harry D Gafney

A D Baker

D Talbot

The City University of New York

Preface

Many reports[1,2] concerning the usefulness of transition metal complexes containing Ru(II) with α–diimine ligands as light sensitizers in photochemical processes, as well as photocatalysts in electron transfer reactions have appeared in the literature within the last 20 years. This is due to several interesting qualities which these complexes possess, namely:

1) The complexes are relatively easy to prepare and characterize
2) The visible absorption spectrum is dominated by a metal-to-ligand charge transfer (MLCT) transition which is very intense
3) They are stable for long periods of time in solution
4) Optical isomers do not tend to racemize in solution
5) The excited state can decay radiatively and has a relatively long lifetime at room temperature
6) The excited state can either undergo energy transfer or electron transfer, and can behave as either an oxidant or a reductant

Numerous studies of $Ru(bpy)_3^{2+}$ and its analogues dissolved in various solvents and adsorbed onto heterogeneous supports have been undertaken, the goal being to further characterize the photophysics and photochemistry of these cations. More recently, reports have appeared[3-30] concerning the usefulness of Ru(II) complexes as a spectroscopic probe of nucleic acid structure. Perturbations of the spectroscopic properties of Ru(II) complexes in the presence of a nucleic acid are indicative of the conformation or conformations existing in the DNA or RNA, as well as an indication of the

binding characteristics of the metal complex to the nucleic acid.

In the past few years, much attention has been given to transition metal complexes and their interaction with double-stranded DNA in the B-Form. Several Ru(II) complexes are known to bind to this conformation of DNA in an intercalative fashion[4] , where a planar aromatic ligand can slip between two base pairs within the major groove. Some have also been shown to cleave DNA photolytically.[14,24,31] Upon binding to DNA, effects on the optical spectra can lead to knowledge of the binding characteristics of the metal complex, and therefore serve as a probe of DNA structure.[4]

The study of the binding behavior of Ru(II) complexes to double-stranded DNA begins with an understanding of the photophysics and photochemistry of these complexes in aqueous solution. When the spectral properties of metal complexes in aqueous solution are understood, an investigation of how and why DNA perturbs these spectra can lead to an understanding of the binding behavior of these metal complexes to the DNA duplex. Several metal complexes of the type $Ru(bpy)_2L^{2+}$ or $Ru(phen)_2L^{2+}$, where L is a bis-chelate ligand, have been shown by our laboratories[23] to bind to double-stranded DNA in aqueous solution. Binding is largely affected by the shape[32] and charge[23] of the ligands surrounding the metal, so these parameters have been varied for each complex studied. Optical isomers of the complex $Ru(bpy)_2ppz^{2+}$, which have been isolated,[33] exhibit differential binding to DNA.[23] These enantiomers have been useful in examining the effect of the ligands that are not involved in the binding (the ancillary ligands), and also how "mirroring" the structure of a

Ru(II) polypyridyl complex can influence the overall binding to DNA.

The following dissertation research investigates the spectral properties of some Ru(II) complexes in aqueous solution and examines how these properties change when bound to DNA. Chapter I contains background information on the photophysical aspects of Ru(II) complexes with emphasis on the complex cation $Ru(bpy)_3^{2+}$, which can be regarded as the prototype of all Ru(II) α-diimine complexes. Chapter II discusses preparation and characterization of some novel Ru(II) complexes. Chapter III deals with an investigation of the enhanced excited-state basicities of two similar Ru(II) complexes in aqueous solution. Chapter IV deals with some spectroscopic properties of Ru(II) complexes containing 3,3'-polymethylene bridges on bipyridyl or terpyridyl ligands. Chapter V is a study of the binding of some Ru(II) complexes to porous Vycor glass, a material which is somewhat analogous to DNA in many respects, yet different in others. Chapter VI is concerned with the criteria Ru(II) complexes must possess to be useful as probes of DNA structure, as well as a discussion of binding modes. Chapter VII is an examination of the complex $Ru(bpy)_2ppz^{2+}$ in aqueous solution and when bound to DNA. Chapter VIII discusses the complexes $Ru(bpy)_2qpy^{2+}$, $Ru(bpy)_2qpyMe^{3+}$, and $Ru(bpy)_2qpyMe_2^{4+}$ in aqueous solution and bound to DNA and compares these results to the binding characteristics of $Ru(bpy)_2ppz^{2+}$. Chapter IX is an investigation of other potential DNA binders that have been investigated. Chapter X is a summary of the photophysical data collected for the complexes studied in this dissertation. Chapter XI contains the experimental section.

Acknowledgements

I would like to express my appreciation to my research advisors, Dr. Thomas C. Strekas and Dr. Harry D. Gafney, for their commitment and patience in directing the work contained in this dissertation, and to Dr. A. D. Baker for his encouragement and support of this effort. You have all given me a great deal of confidence and have instilled in me the faculties necessary to pursue a career in Chemistry.

I would also like to express my gratitude to all the members of the Queens College Chemistry Department, especially Dr. Axelrad, for his continued support and faith in me, and to Drs. David Locke, Raymond Disch, and Robert Bittman, for their help and useful discussions. Thanks to Dr. David Lavallee, of Hunter College, for serving on my thesis committee, and Dr. Richard Pizer, of Brooklyn College, for all his assistance down at the Graduate Center. Thanks to Mr. Ottmar Safferling for his enjoyable discussions and help with the glassware. Thanks to Dr. Larry Mansfield of the Queens College Math Department for sharing his knowledge of computers with me.

I would like to thank my fellow students who have worked with me in the past and present for their help and encouragement, especially Dr. Robert Morgan, Dr. Edgar Mendoza, Mr. Eugene Wolkow, Dr. Jian Wei Fan, Mr. Larry Leung, and Dr. Suresh Tewani. Thanks for the help through the rough times. Thanks to all the members of the Academic Computer Center, especially Mr. Robert Pescinski, Mr. Salvatore Saieva, and Mr. Yan Juras, for their never-ending technical support and fruitful discussions. Thanks to Mr. Robert Bunch and Mr. Stanley Sham for their help with the electronics, and Dr. Tak Cheung for his assistance with the YAG laser.

I wish to express my love and appreciation to my parents, Mr. Alfred E. Tysoe and Mrs. Gloria Tysoe, who believed in me from the very beginning, and have always supported me in all my pursuits, and have given me confidence and faith in myself. I wish to thank my sisters Barbara and Karen, for their love, and to my brothers-in-law Gonzalo, Rodrigo, Lou, and Mike (almost) for accepting me as their brother.

Most of all, I wish to express all the love, gratitude, and appreciation within me to my loving wife, Marcela, who stood by my side for 7 years of our lives to see the completion of this project, and whom I could never begin to completely thank for her dedication and love. Thank you Marcela, from the bottom of my heart. I love you.

Table of Contents

List of Figures

Chapter I

Chapter II

Chapter V

Chapter VI

Chapter VII

List of Tables

List of Schemes

Chapter I

Chapter I. Photophysical Aspects of $[Ru(bpy)_3]^{2+}$

Introduction

Characterization of the ground and excited states of polypyridyl complexes of Ru(II) has been the subject of much controversy.[34-72] Early investigators of the photophysical phenomena make conflicting arguments supporting several types of models for radiative deactivation of the excited state (or states).[34-36,45] Studies of low temperature lifetime and emission quantum yield,[50] temperature dependence of lifetime and quantum yield,[48] and studies with Ru(II) complexes doped into crystals[37,64] give descriptions and assignments of the ground and excited states. Because of the numerous interpretations that have been presented concerning the photophysical aspects of Ru(II) complexes, it is important to mention the current theories supported by researchers in this area. First, however, a discussion of the absorption and emission processes in general will aid in understanding the photophysics of Ru(II) polypyridyl complexes.

When a molecule absorbs a photon, an excited state species is formed, i.e. an electron is promoted to an excited state. This highly energetic, unstable species must deactivate in some way. Several things can happen when deactivation occurs, mainly

(a) emission of light (luminescence),

(b) radiationless deactivation (loss of energy as heat),

(c) photochemistry (an irreversible reaction forming a new species), or

(d) energy loss to another species present (quenching process)

From electronic spectroscopy, it is known that the intensity of an absorption band is related to the probability of the transition which in turn is related to the spin quantum number S of the states involved in the transition. Transitions between states with the same spin are highly allowed, and give rise to intense absorption bands, while transitions between states with differing spin are forbidden and give rise to very weak bands. A number of molecules have a ground state of singlet character and a lowest excited state of triplet character, which would be a forbidden transition. Therefore this triplet state can only be populated indirectly by first populating a singlet excited state followed by intersystem crossing to populate the excited triplet, thus giving rise to a three state model.

A Jablonski diagram (Figure I-1) shows the possible events occurring in this three state model.[2] Each deactivation process described by the Jablonski diagram can be explained in terms of a rate constant k which is the inverse of the lifetime (τ) for that process.[73] The values of these rate constants determine how the processes compete with each other, and they are one of the factors determining whether or not the molecule will luminesce. A quantum yield (ϕ) is defined as the number of moles of either photons or photoproducts produced divided by the number of einsteins absorbed.[73] Of particular interest is the quantum yield for the process of going from the lowest excited state triplet to the ground state. This transition is generally thought to give rise to the phosphorescence observed in some aromatic molecules, and is probably the major radiative pathway in Ru(II) complexes.[48]

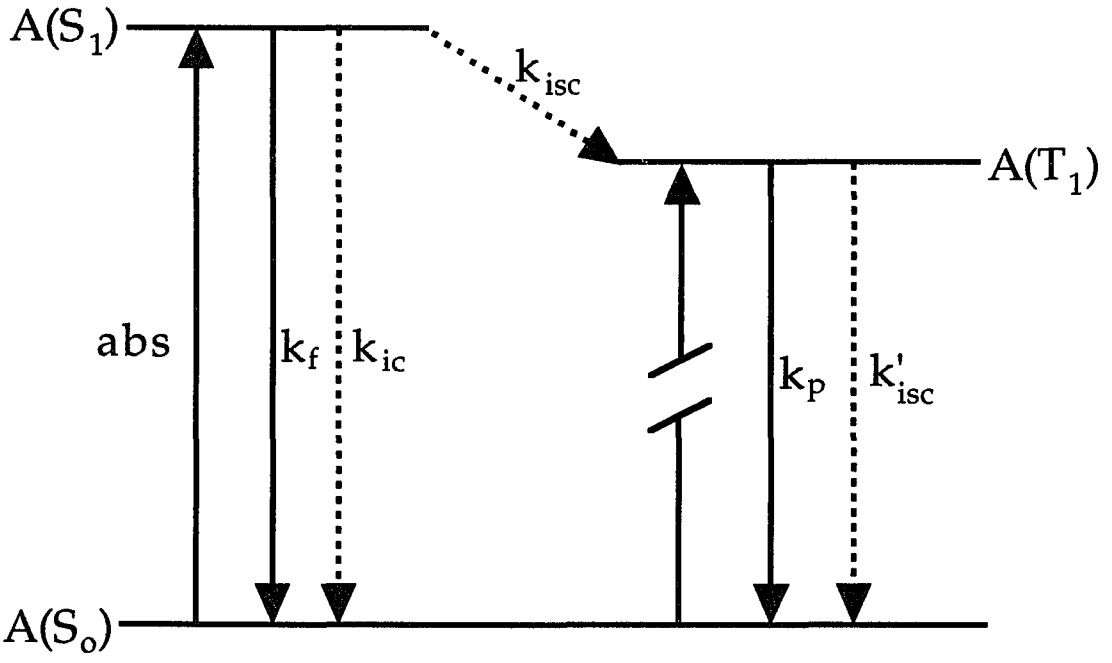

Figure I-1. Jablonski Diagram showing various deactivation processes. k_f, k_{ic}, k_{isc}, k_p and k'_{isc} are the unimolecular rate constants for fluorescence, internal conversion, singlet to triplet intersystem crossing, phosphorescence and triplet to singlet intersystem crossing, respectively.

The $[Ru(bpy)_3]^{2+}$ complex is a d^6 complex in a strong ligand field with D_3 symmetry. The ligand field induced states can be described with reference to the t_{2g} (stabilized) and e_g(destabilized) d orbitals from the metal ion and the π (bonding) and π^* (anti-bonding) orbitals from the ligand. The ground state is a low-spin complex with all 6 d electrons paired in the t_{2g} orbitals. The t_{2g}^6 ground state is defined with the term symbol $^1A_1$. The orbitals and states for a typical d^6 metal ion in an octahedral symmetry are described in Figure I-2.

Absorption

An excitation of one electron from the ground state singlet can result in four different transitions. They are the d-d*, d-π^*, π-π^*, and π-d* transitions. The excited states generated from the transitions of the electrons in the Ru metal orbitals are generally not well defined singlets and triplets, due to spin-orbit coupling and mixing of the states. The d-d* transitions or metal-centered (MC) transitions give rise to weak absorption bands (ε ~100 M^{-1} cm^{-1}) which are LaPorte forbidden. The d-π^* and the π-d* transitions involve transfer of charge from the metal to the ligand or the ligand to the metal and are called a metal-to-ligand charge transfer (MLCT) and ligand-to-metal charge transfer (LMCT) transitions, respectively. These transitions are highly allowed and give rise to very intense (ε ~20000-25000 M^{-1} cm^{-1}) visible absorption bands. The π-π^* (LC) transitions are generally ligand in character and can be seen in the free ligand as well as the complex, and occur in the UV portion of the spectrum (ε ~40000-110000 M^{-1} cm^{-1}).

Figure I-3 is the absorption spectrum of the $[Ru(bpy)_3]^{2+}$ complex at room

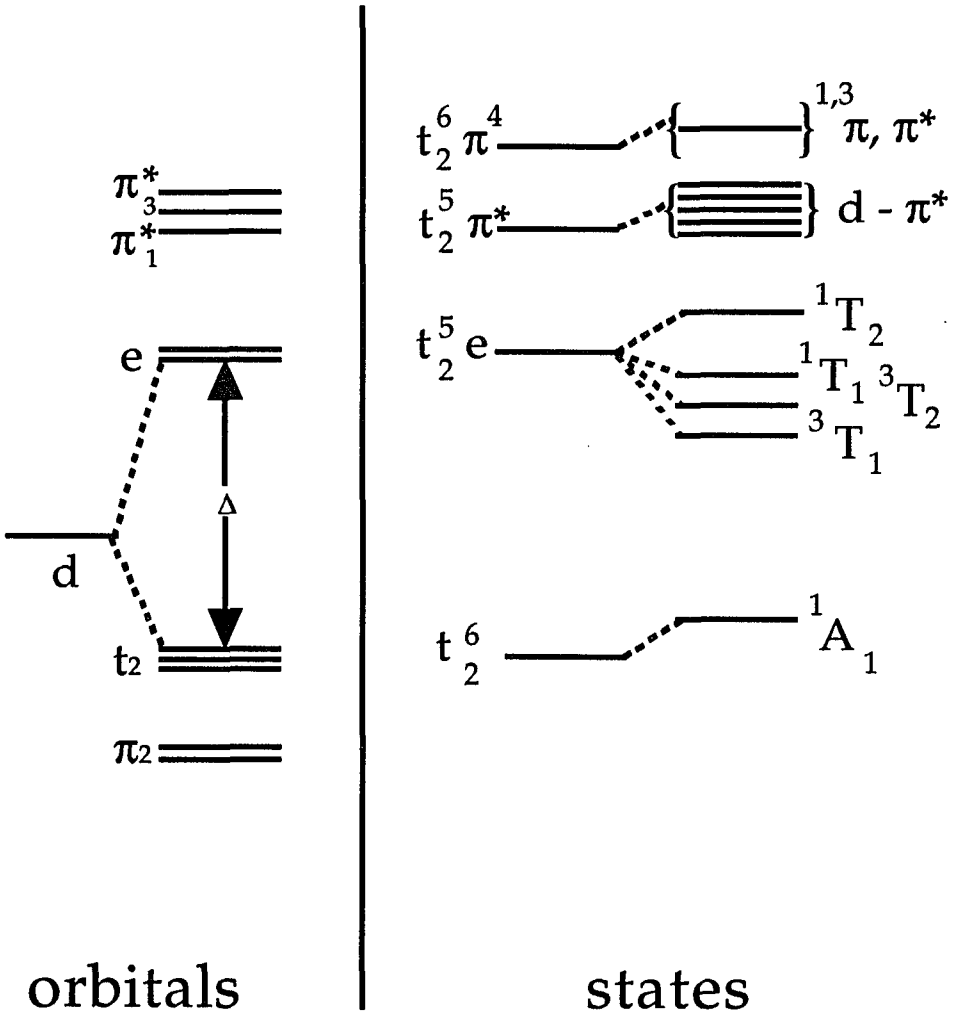

Figure I-2. Orbitals and states of a d^6 metal ion in a strong ligand field.

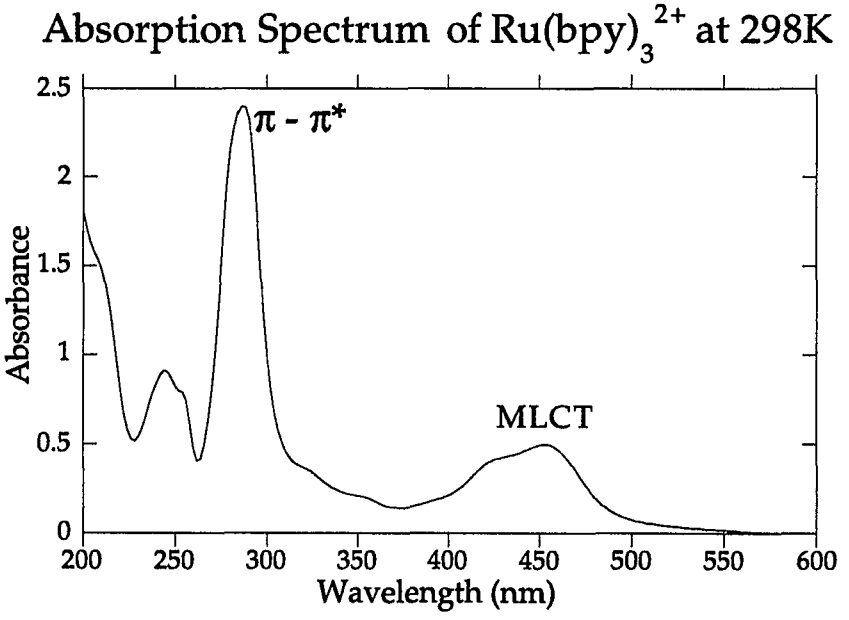

Figure I-3. Absorption Spectrum of $Ru(bpy)_3^{2+}$ at 298K. Absorption bands are designated as MLCT or π-π^*.

temperature in aqueous solution. The band assignments are as indicated. The spectrum contains MC,LC and MLCT transitions. Also some other minor bands appear in the spectrum, which have not been unambiguously assigned.

Emission

The highly energetic excited states of Ru(II) complexes can undergo several processes resulting either in radiationless deactivation or luminescence or both. They are described by Scheme 1.

Scheme 1

$[Ru(bpy)_3]^{2+*}$ ----> $[Ru(bpy)_3]^{2+} + h\nu$	luminescence
$[Ru(bpy)_3]^{2+*}$ ----> $[Ru(bpy)_3]^{2+}$ + heat	radiationless deactivation
$[Ru(bpy)_3]^{2+*}$ + Q ----> $[Ru(bpy)_3]^{2+}$ + Q	quenching processes
$[Ru(bpy)_3]^{2+*}$ ----> products	photochemistry

$[Ru(bpy)_3]^{2+}$ exhibits a broad orange emission at room temperature centered at 600-610 nm.(Figure I-4a) In glassy solutions at 77K, however, a well-resolved band at 585 nm and a shoulder at 630 nm are thought to be the emission and a vibrational progression with $\Delta\nu$ = 1300 cm^{-1}. (Figure I-4b) Originally, an assignment of π^*-d CT fluorescence was made by Paris and Brandt[34] and was debated by various researchers.[35,36,44] Later, researchers assigned the emission as d*-d phosphorescence,[35] d*-d fluorescence,[36] charge transfer,[37,40] π^*-d phosphorescence,[44] and π^*-d CT luminescence with no multiplicity specified.[40] A more recent description is of a manifold of three closely coupled spin-orbit excited states giving rise to the emission.[74] In other

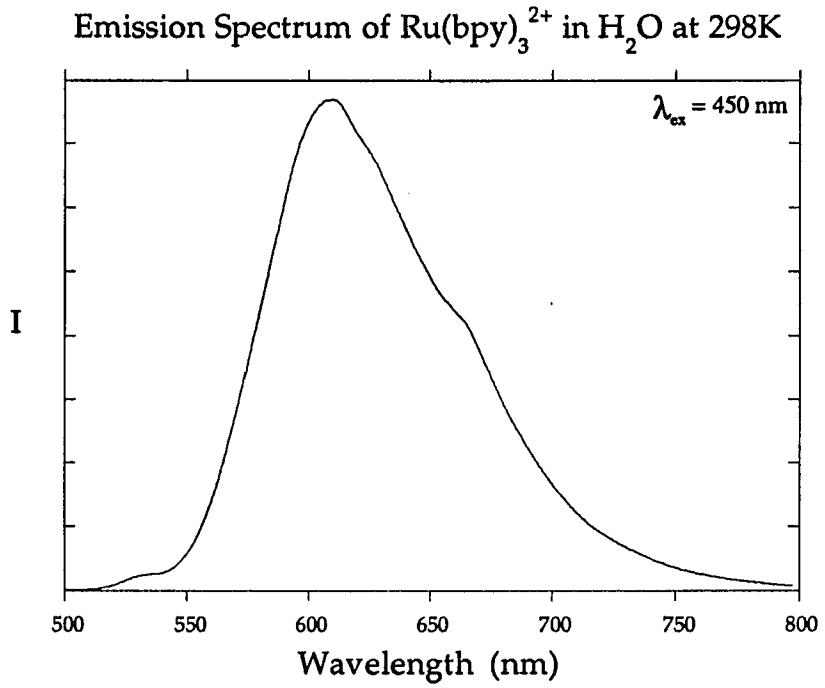

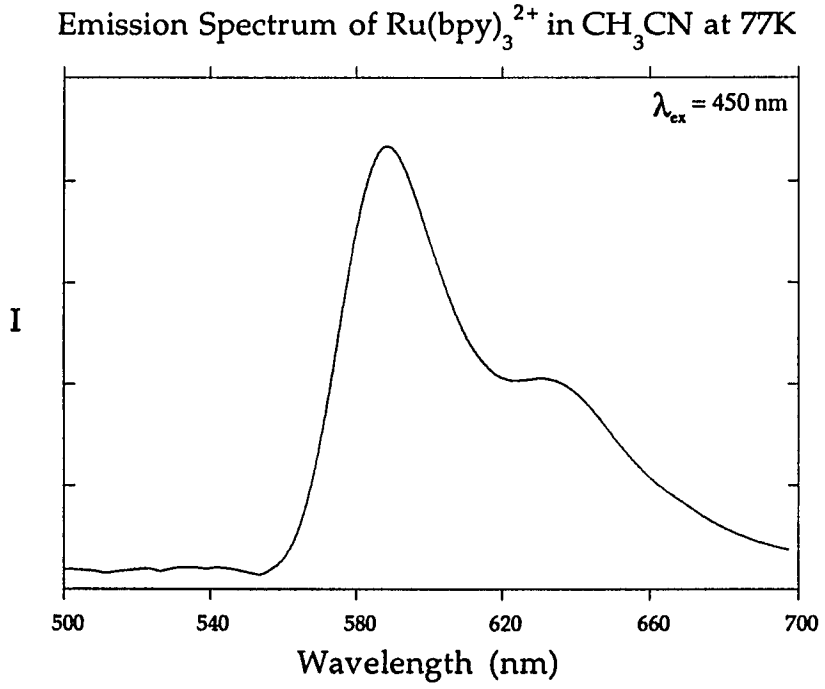

Figure I-4a and I-4b. Emission Spectra of $Ru(bpy)_3^{2+}$ at 298K and 77K.

words, only the lowest excited state and higher states accessible through the Boltzmann distribution of thermally populated states can be involved in the luminescence.[48,49,75,76] (See Figure I-5)

A four level-model was also proposed by Van Houten and Watts,[56] where lower lying MLCT excited states and higher MC excited states were used to fit experimental data for the temperature dependence of quantum yield and luminescence lifetime. This model takes into account certain solvent effects that exist, and also explains the high temperature photosubstitutional chemistry of $[Ru(bpy)_3]^{2+}$. The model also suggests a major deactivation pathway via the MC states. Because the deactivation pathway involves phonon coupling to the solvent, a study of quantum yield and luminescence lifetime vs. T in both D_2O and H_2O gave results which suggest that the complex is more closely coupled to H_2O than to D_2O. This model is portrayed in Figure I-6.

Ordering of the excited states determines to a great extent whether a complex will luminesce or not.[77] It is theorized that if MC type states lie lower in energy than the MLCT or LC type, then deactivation will occur through the MC states and no luminescence will result. If, on the other hand, the MC states lie above the MLCT or LC states, the excited state does not undergo radiationless deactivation to the same extent and luminescence is observed, except at high T where the MC states are accessible due to the Boltzmann distribution. (Figure I-7)

It is evident that luminescence properties can be altered by a logical choice of ligands coordinated to the metal.[68] The ordering of the MLCT, LC and

Crosby Model of Excited State Manifold

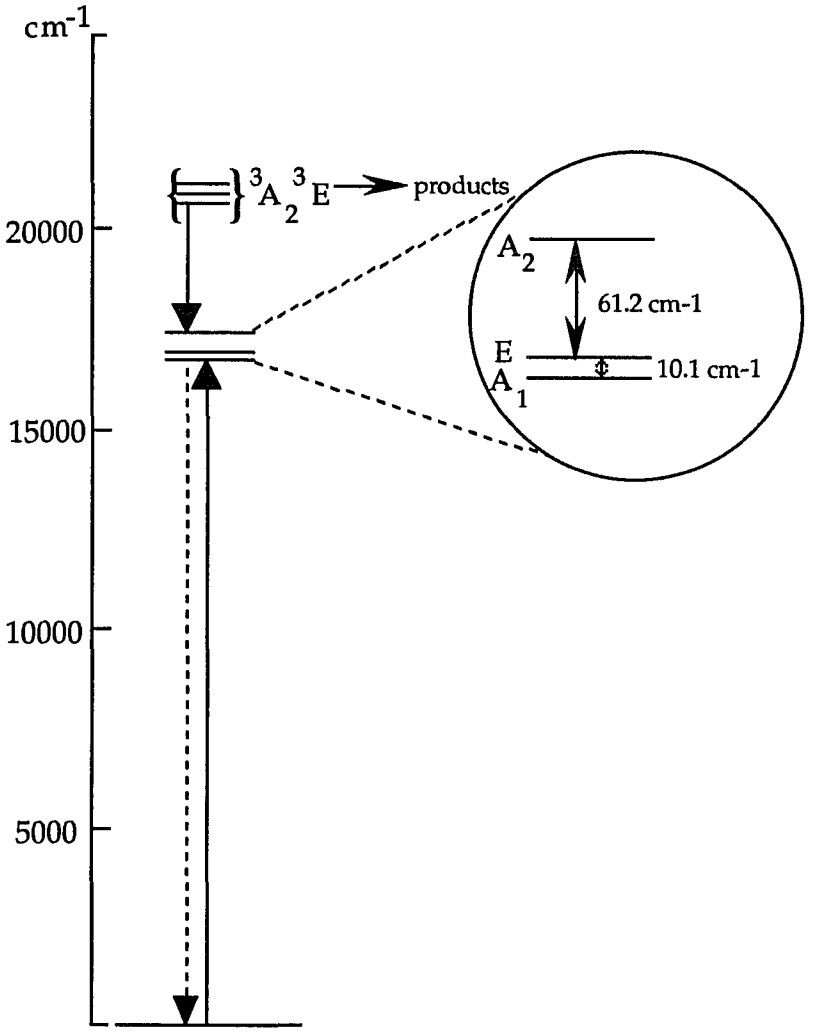

Figure I-5. Crosby model of emissive manifold of states

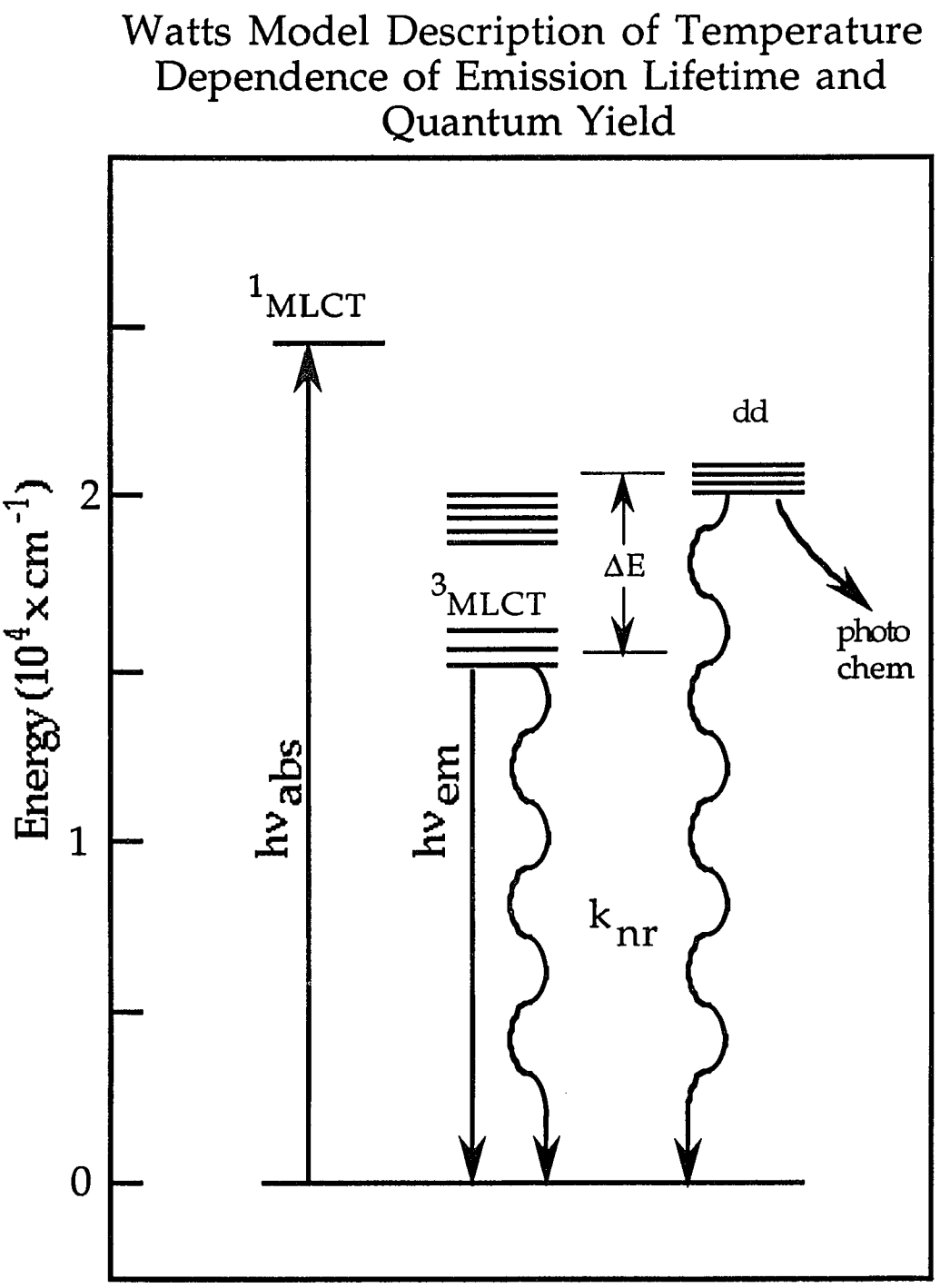

Figure I-6. Watts model of emissive excited states

MC states depends on the ligand field induced by the ligands and the properties of the ligands themselves. By designing complexes which order the states in a specified way, the desired emission properties can be obtained.

One problem in describing the emission phenomenon in Ru(II) complexes is knowing whether the state associated with the luminescence is localized on one ligand, or it is delocalized on all three.[68] For the tris-type complexes (all three ligands the same), a model, called the electron-ion parent coupling model, portraying the electron in a localized orbital on one of the three ligands, was proposed by Crosby et. al.[48] This model was further supported using evidence from resonance Raman spectroscopy,[63,72] where the vibrations could be correlated to the bpy^- anion. Other techniques such as ESR,[70] NMR[78] and emission polarization[79] have also been used to support this localized model.

Descriptions of the excited state as $Ru(bpy)_2bpy^-)^{3+}$ have appeared in the literature, which describe a $4d^5$ Ru^{3+} center and three bpy ligands with the electron associated with only one bpy forming bpy^-.[68] There are other reports, however, which are inconsistent with this model, especially when $[Ru(bpy)_3]^{2+}$ is incorporated in a frozen glass matrix, and therefore some controversy has arisen over this designation.[67] To avoid confusion, the emissive excited state will be designated in this work as $[Ru(bpy)_3]^{2+*}$, which is an MLCT state of principally triplet character.

For the bis-bpy type complexes (two bipyridines and one other ligand), it has been shown that luminescence will occur from the state associated with

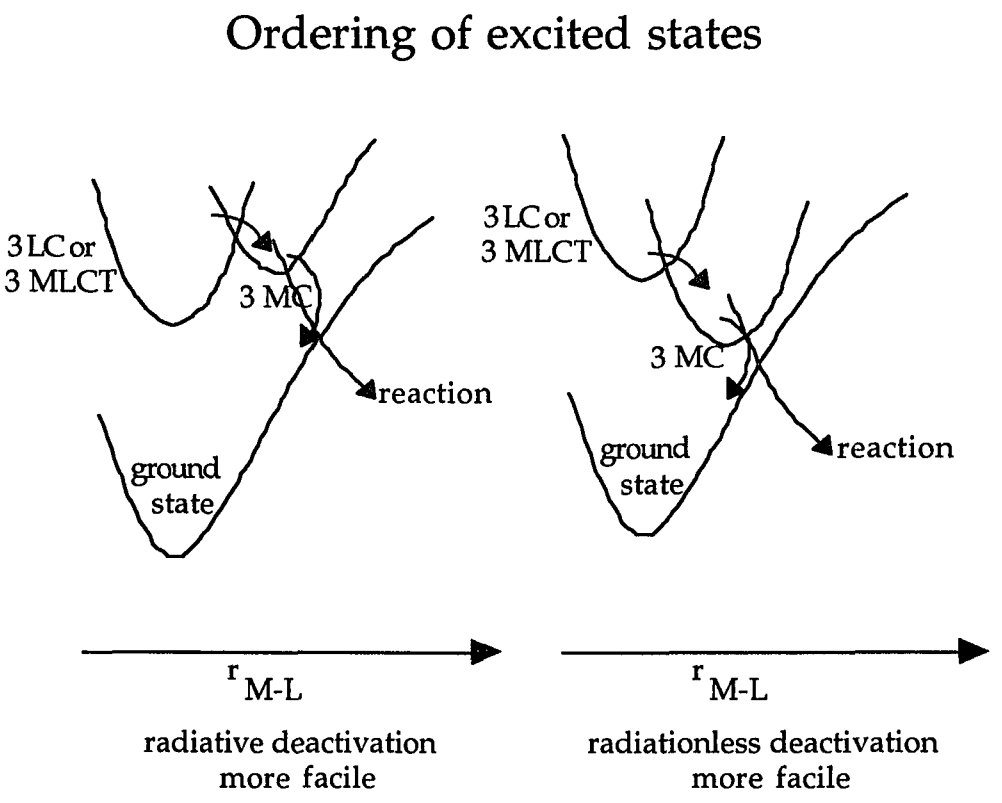

Figure I-7. Energy ordering of excited states in d^6 complexes and its implication on radiative and non-radiative processes.

the ligand with lowest lying MLCT excited state, as evidenced from resonance Raman spectroscopy.[80] This has been seen for our complexes $[Ru(bpy)_2ppz]^{2+}$ and $[Ru(bpy)_2dpp]^{2+}$, where both the dpp and ppz ligands lie lower in energy with respect to bpy. Here the designation is less ambiguous than in the $[Ru(bpy)_3]^{2+}$ case, and the electron is thought to be associated with the lower energy ligand. Therefore, the excited states of these mixed-ligand complexes can be designated as singlet and/or triplet MLCT states of the form $[Ru(bpy)_2(ppz)^-]^{3+}$ and $[Ru(bpy)_2(dpp)^-]^{3+}$, respectively.

Polarization

Several studies[47,66,67,81] of the polarized absorption and emission spectra have attempted to unambiguously assign the lowest emitting MLCT state as either a ^3E or $^3A_2$. Fujita and Kobayashi[47] measured the luminescence polarization of $Ru(bpy)_3^{2+}$ in an EPA rigid glass at 77K and determined polarizations of ~+1/7 which agrees with the theory for a planar absorption (x,y) oscillator and a planar (x,y) emission oscillator. In other words, the absorption and emission occur in the same plane. Table 1 portrays the possible polarizations of various types of absorption and emission oscillators.

Table 1

Absorption Oscillator	Emission Oscillator	Polarization (P)
Linear (z)	Linear (z)	+1/2
Linear (z)	Linear (x)	-1/3
Linear (z)	Planar (z,x)	+1/7
Linear (z)	Planar (x,y)	-1/3
Planar (x,y)	Linear (z)	-1/3
Planar (x,y)	Planar (x,y)	+1/7

The observation of a somewhat larger polarization when exciting at 21000 cm^{-1} was explained by examining the transitions from $^3A_2$ --> $^1A_1$ and ^3E ---> $^1A_1$. For the first case, this spin forbidden transition can borrow intensity through spin-orbit coupling from the planar oscillator ^1E ---> $^1A_1$ transition, but the ^3E ---> $^1A_1$ transition can have contributions from both the planar ^1E ---> $^1A_1$ transition and the linear(z) $^1A_2$ --> $^1A_1$ transition. Since the $^1A_2$ --> $^1A_1$ transition has a theoretical polarization of +1/2, a weighted contribution of this state can explain the observed polarization of 0.25 at 21000 cm^{-1}. Because of this, Kobayashi et. al[47] assigned the lowest MLCT emissive state as mainly ^3E in character.

DeArmond and coworkers[66,81] compared the possible orderings of the manifold of emissive states and measured essentially the same polarization values as Kobayashi. However, he compared the Kobayashi model with a model proposed by Crosby[48] in which the $^1A_2$ state is the origin of the emission. Crosby's model, however, did not account for the experimental evidence and predicted a decrease in polarization of the 21000 cm^{-1} band if the $^1A_2$ state is the origin of emission. DeArmond therefore was in agreement with the Kobayashi model of a ^3E emissive state.

The use of polarization data to answer the question of orbital localization or delocalization comes from understanding the symmetry changes upon excitation. Two limiting cases exist where either the orbital is delocalized on all three ligands, with D_3 symmetry, or is localized on one, with C_{2v} symmetry. In the latter case an accidental threefold degeneracy would exist ($3C_{2v}$) and all

three chromophores would be identical. A D_3 type system contains the C_2 symmetry element and can be considered to have C_{2v} symmetry when an electron "hops" into a orbital located on one chelate. By using a mixed-ligand complex, the degeneracy is removed and since all three orbitals are not identical, C_{2v} symmetry is the highest symmetry possible for the emissive MLCT state. The electron can therefore only "hop" to the lowest energy ligand π^* orbital, and it is therefore localized. This explains why using mixed ligand complexes facilitates the description of the emissive state, since it eliminates this "hopping" phenomenon and localizes the charge on only one ligand.

Luminescence Lifetime and Flash Photolysis

Luminescence lifetimes of $Ru(bpy)_3^{2+}$ in N_2 purged aqueous solution at 298K (~600 ns) fall between the typical ranges for fluorescence (ca.1-20ns) and phosphorescence (>1000 ns). This evidence also supports the model of mixed spin-orbit emissive state(s). Typically, $Ru(bpy)_3^{2+}$ and its analogs exhibit a first-order (unimolecular) luminescence decay in aqueous solution which decrease in time as a function of temperature and are also shortened by the presence of luminescence quenchers (e.g. O_2) (Figure I-8) Luminescence lifetimes are greatly affected by the local environment and are therefore a very sensitive probe of the location of the chromophore. For example, in DNA, a bi-exponential decay is often seen,[5] indicating more than one luminescing environment for the chromophore.

A laser flash photolysis apparatus can measure the transient absorption spectrum of the MLCT emissive state of $Ru(bpy)_3^{2+}$.[61] By using the 532 nm line

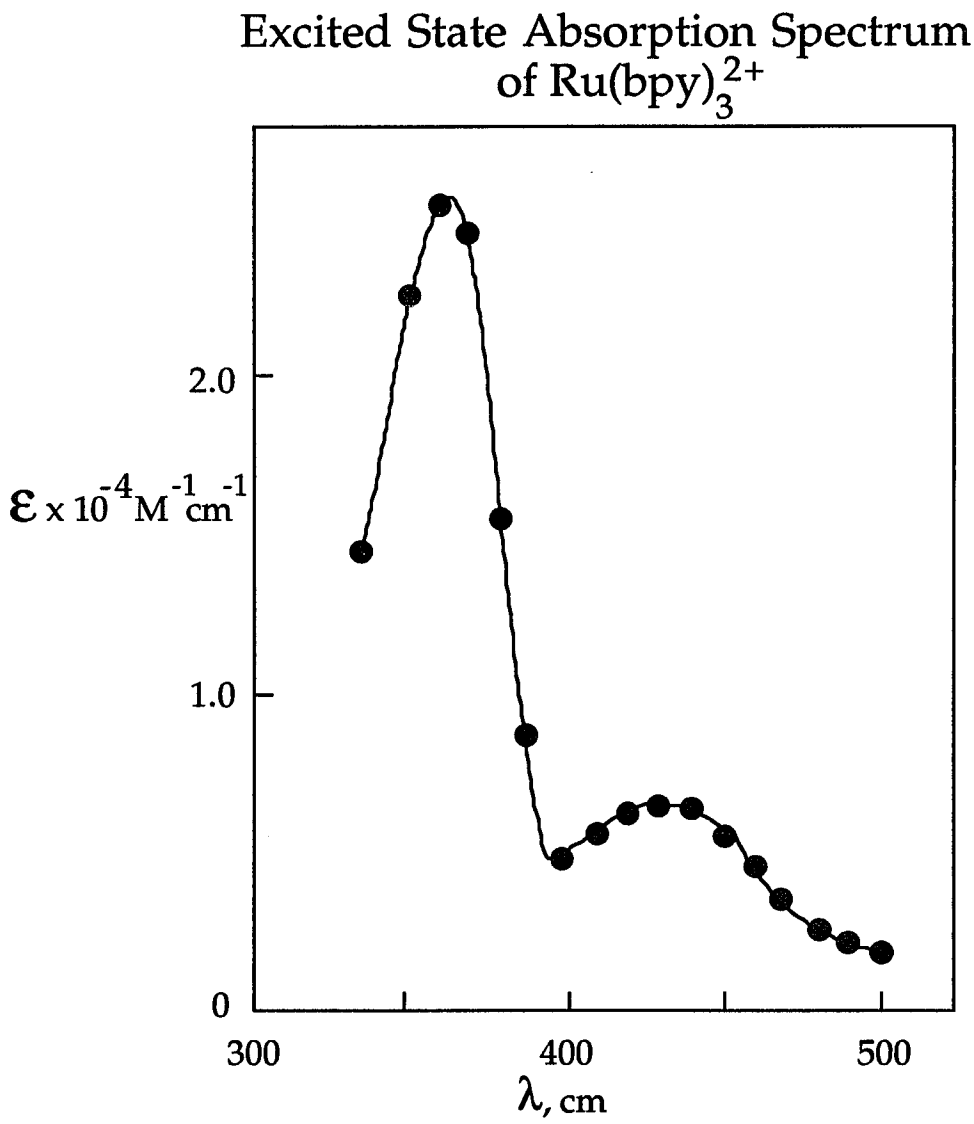

Figure I-8 Excited state absorption spectrum of $Ru(bpy)_3^{2+}$ at 298K

of a pulsed Nd:YAG laser, a 20 ns pulse can generate the emissive state with a quantum yield approaching 1.0, while the perturbation of the analyzing beam measures the absorbance decrease of the transient as a function of time. The lifetime of the excited state transient has been measured to be ~620 ns in aqueous solution at room temperature (N_2 purged).[57] The similarity of the lifetime of this transient with the luminescence lifetime of $Ru(bpy)_3^{2+}$ prompted the assignment of the absorption band at 360 nm to the emissive MLCT state. (Figure I-9)

In a separate experiment, the formation of the hydrated electron was effected by use of a conventional flash photolysis apparatus.[62] The reaction $Ru(bpy)_3^{2+*}$ ---> $Ru(bpy)_3^{3+} + e^-_{aq}$ occurs only with excitation of uv light. Using laser flash photolysis, it is sometimes possible to distinguish energy transfer processes from electron transfer processes.[61] It is also used as a probe into the redox behavior of the excited state of $Ru(bpy)_3^{2+}$.

Resonance Raman

The resonance Raman effect has been instrumental in determining the localization of charge on only one of the three bidentate ligands in $Ru(bpy)_3^{2+*}$. Early studies by Dallinger and Woodruff[63] describe vibrations in the excited state of $Ru(bpy)_3^{2+}$ which correlate to the bipyridine vibrations present in bpy^-. The good correlation of these vibrations are supportive of the existence of the $[Ru(bpy)_2(bpy^-)]^{2+}$ species.

Time resolved resonance Raman spectroscopy has given evidence of a single ligand localized excited state in the time frame of a molecular vibration.[82]

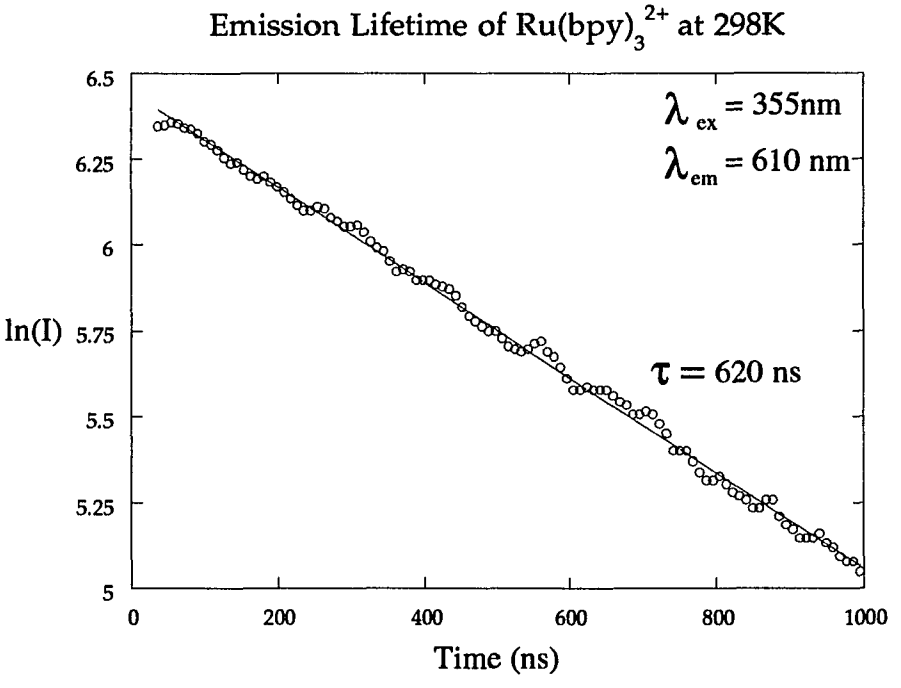

Figure I-9 Luminescence Lifetime of $Ru(bpy)_3^{2+}$ in H_2O at 298K. Exponential decay behavior is seen for this complex. Measured using air-saturated samples of $Ru(bpy)_3^{2+}$. Quenching by O_2 decreases luminescence lifetime by ~50%.

Studies with mixed-ligand complexes suggest that the electron is localized on the ligand easiest to reduce, or with the lowest energy π^* acceptor orbital.[83]

The resonance Raman spectrum of the ground state of $Ru(bpy)_3^{2+}$ is shown in Figure 10. Note the seven prominent bands which are due to seven symmetrical modes of vibration of the bpy ligand.

Increases in the intensity and/or number of vibrations associated with the ground state typically indicates a stronger coupling of the ground and excited states, via "acceptor" orbitals.[84] A stronger coupling of the ground and excited states generally is indicative of fast, radiationless processes. A weak coupling to the excited state, therefore, should show less bands with weaker intensities.

Redox Properties of $Ru(bpy)_3^{2+}$

The luminescence lifetimes of many Ru(II) complexes are on the order of microseconds. This time is sufficient (>1 ns) for the lowest lying MLCT excited state to encounter other solutes and cause either of two specific types of bimolecular reaction to occur, namely electron transfer or energy transfer.

Energy transfer is a bimolecular reaction between an excited state species and another ground state species. (e.g. a quencher) The reaction

$$*A + B \text{---}> A + B^*$$

is a representation of energy transfer where *A loses its energy to another species B to form a new excited state species B*.

Electron transfer is the other fate of a bimolecular reaction of the MLCT excited state. This process can occur by either an oxidative or reductive scheme. Scheme 2 portrays these two possibilities.

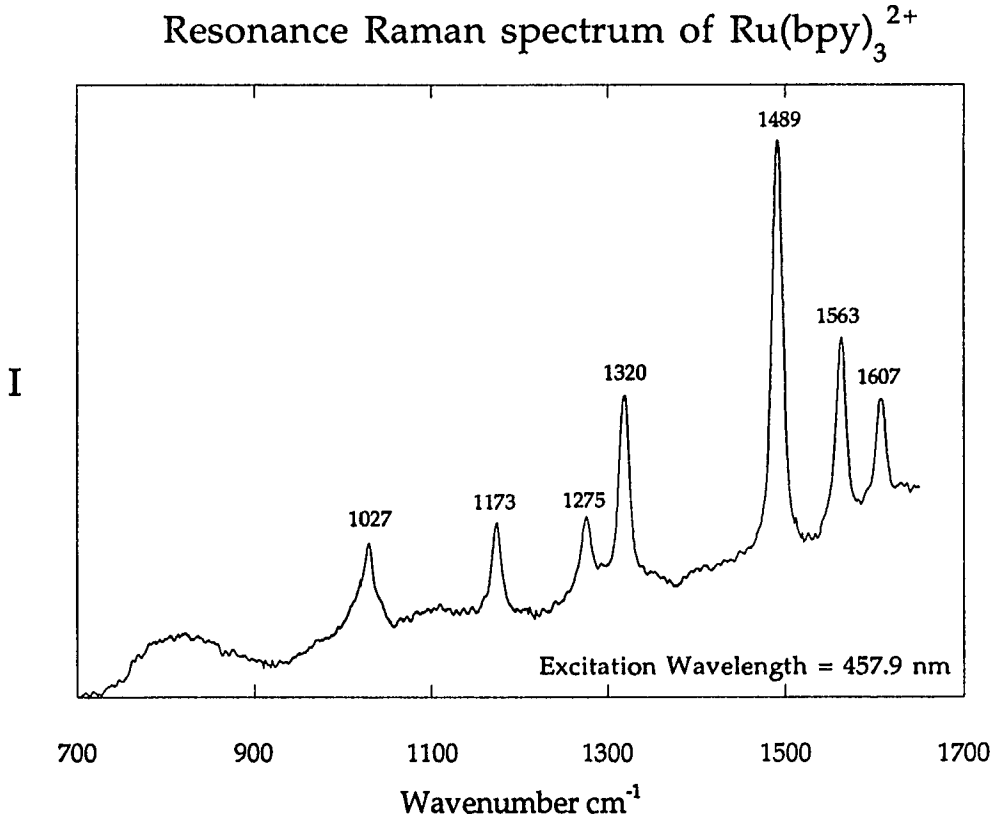

Figure I-10. Ground State Resonance Raman spectrum of $Ru(bpy)_3^{2+}$. Sample excited with 457.9 nm excitation and measured at a spectral bandwidth of ~$2cm^{-1}$.

Scheme 2

$^{*}A + B \text{---} > A^{+} + B^{-}$ oxidative electron transfer

$^{*}A + B \text{---} > A^{-} + B^{+}$ reductive electron transfer

Due to the higher energy content of the excited state, $Ru(bpy)_3^{2+*}$ behaves as both a stronger oxidant as well as a stronger reductant than the corresponding ground state ion. The redox potential for the $Ru(bpy)_3^{3+/2+}$ pair is 1.26V, and 1.24V for the $Ru(bpy)_3^{2+/1+}$ pair.[85] The excited state lies 2.12eV higher in energy, therefore a redox potential diagram can be constructed as shown in Figure I-11. Design of photochemical systems using $Ru(bpy)_3^{2+*}$ can promote either the formation of the oxidant or the reductant for use in electron transfer schemes. These in turn can be used to either oxidize or reduce other species, e.g. the catalytic reduction of water to H_2. These systems, unfortunately, were unable to perform the **catalytic** reduction of water, however, they do appear to work in a non-catalytic fashion. This lack of catalytic activity, which is attributed to a thermal back electron transfer, will be explained further in a later section explaining the use of $Ru(bpy)_3^{2+}$ as a light absorption sensitizer (LAS).

Chemiluminescence

Thermal electron-transfer reactions of metal complexes where differing oxidation states of the metal are involved often lead to the formation of an emitting MLCT excited state. This phenomenon is called chemiluminescence, since the luminescence is derived from a chemical reaction. Both $Ru(bpy)_3^{3+}$ and $Ru(bpy)_3^{+}$ are successful at forming $Ru(bpy)_3^{2+*}$ with great efficiency, with a

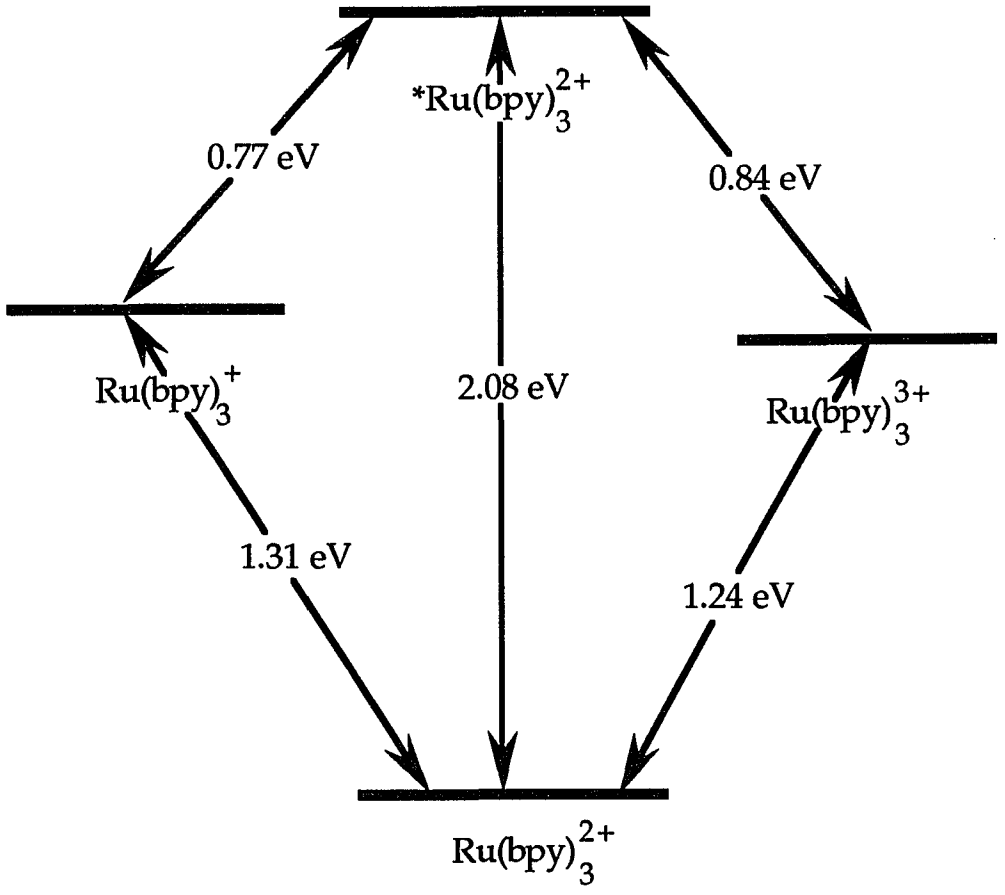

Figure I-11. Redox Energy Diagram of the $Ru(bpy)_3^{2+}$ complex with redox potentials given for each process.

generation of light upon relaxation to the ground state. This was first observed by Lytle and Hercules in 1966 by the neutralization of $Ru(bpy)_3^{3+}$ with strong base (OH^-).[86]

Mutual annihilation reactions with $Ru(bpy)_3^{3+}$ and $Ru(bpy)_3^{+}$ are also successful at generating $Ru(bpy)_3^{2+*}$ with subsequent light emission at an electrode surface. Reactions like this at an electrode surface are sometimes referred to as electrogenerated chemiluminescence (ECL) and have been studied extensively by Bard and others.[87,88]

Emission Quenching

Non-radiative deactivation arises when either the solvent system or an added solute interferes with the emissive state creating a non-luminescent pathway. Such is the case with dioxygen, which efficiently quenches luminescence. It is therefore necessary for solutions of $Ru(bpy)_3^{2+}$ to be N_2 purged or freeze-pump-thawed to remove the unwanted O_2.

Bimolecular quenching in fluid solution approaches the maximum diffusion limited value of $2 \times 10^9\ M^{-1}s^{-1}$, and often follows the Stern-Volmer relation

$$I_0/I = 1 + K_{sv}[Q]$$

where I_0 and I are the emission intensities of the unquenched and quenched species, [Q] is the quencher concentration, and K_{sv} is an experimentally determined value called the Stern-Volmer constant.[73] The rate constant can be determined experimentally from the K_{sv} if the luminescence lifetime of the unquenched species is known, via the relation $k_q = K_{sv}/\tau$.

In environments where diffusion is inhibited, (e.g. low temperature) the Stern-Volmer model does not apply. The rate constant becomes a function of the distance between the quencher and the chromophore, and quenching is described via the Perrin equation[85]

$$I_0/I = k \exp(cV)$$

where k is a constant, c is the concentration of the quencher, and V the volume of the "quenching sphere". According to this interpretation, only those quenchers inside the sphere can quench. This model also may apply to chromophores in restricted environments where mobility is inhibited.

Efficient quenching via energy transfer occurs when there is sufficient orbital overlap of the donor-acceptor pair (the zero-zero spectroscopic energy), while quenching due to electron transfer involves the redox potentials of the oxidized and reduced excited states. Figure I-12 portrays the difference in these processes in terms of measurable molecular quantities relevant to electron and energy transfer.

In addition to dynamic quenching, static quenching can occur by ion-pairing in the ground state. For some systems, this complicates the description of the quenching phenomenon, but if luminescence lifetime data are used for studying quenching, the static component is eliminated.

Quenching can occur by use of a myriad of ions and molecules, and many studies have been reported. The ions Fe^{3+}, Cu^{2+}, Eu^{3+}, Ag^{+}, and Hg^{2+} quench $Ru(bpy)_3^{2+*}$ oxidatively forming $Ru(bpy)_3^{3+}$ as the main product.[91-102]

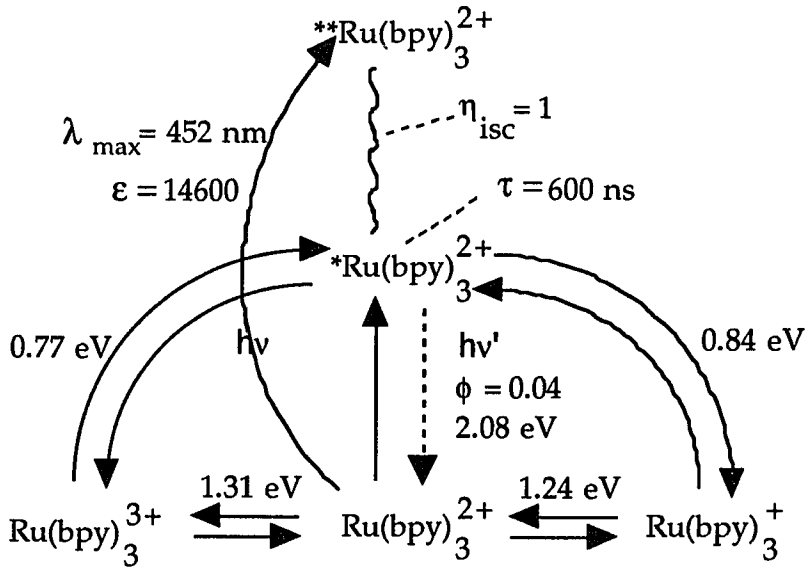

Figure I-12 Electron and Energy Transfer Processes of $Ru(bpy)_3^{2+*}$

Eu^{2+}, SO_3^{2-}, and ascorbate ion photoreduce $Ru(bpy)_3^{2+*}$.[95,104,105] Cr^{3+} and Ti^{3+} are thought to quench via energy transfer.[106-109]

The interest in the photochemistry of $Ru(bpy)_3^{2+}$ began with reports by Gafney and Adamson[110] and Fujita and Kobayashi[111-113] that $Ru(bpy)_3^{2+*}$ has the capability of facilitating decompositions of metal complexes by electron transfer to some Co(III) complexes as well as decompose Cr(III) complexes via energy transfer. Using $[Co^{III}(NH_3)_5X]^{2+}$ as an example of an electron transfer quencher, the emissive state of $Ru(bpy)_3^{2+}$ transfers an electron to the Co (II) complex yielding $Ru(bpy)_3^{3+}$, and the unstable $[Co^{II}(NH_3)_5X]^{2+}$ complex which eventually decomposes to the Co(II) aquo complex.

Quenching by organic molecules via the oxidative electron transfer pathway has been studied extensively, especially by employing the heterocyclic salt methyl viologen (MV^{2+}).[114-121] Subsequent formation of MV^+ can reduce H^+ to H_2 with use of a Pt catalyst. These systems, however, require the use of the reductant EDTA to scavenge the $Ru(bpy)_3^{3+}$ so the "back electron transfer" is inhibited. (See Scheme 3) Quinones also appear to behave similarly to methyl viologen, i.e. via the oxidative pathway.

Scheme 3

$Ru(bpy)_3^{2+*} + MV^{2+}$ -------> $Ru(bpy)_3^{3+} + MV^+$	Electron Transfer
$Ru(bpy)_3^{3+} + MV^+$ -------> $Ru(bpy)_3^{2+*} + MV^{2+}$	Back Electron Transfer
$2MV^+ + 2H^+$ ---> $2MV^{2+} + H_2$	Reduction of H_2 by MV^+
EDTA + $Ru(bpy)_3^{3+}$ + catalyst----> $Ru(bpy)_3^{2+}$ + $EDTA^+$	Use of sacrificial donor

Use of $Ru(bpy)_3^{2+}$ as a light absorption sensitizer (LAS)

Several photochemical reactions do not occur because neither of the two reactants can absorb light in the uv-visible region. Therefore the employment of a light absorption sensitizer[122] can allow these reactions to occur by excitation of the sensitizer. $Ru(bpy)_3^{2+}$ can function as a photosensitizer for many reactions because it possesses the necessary kinetic, thermodynamic, and spectroscopic properties.[123-129] The reaction of triphenylamine with methyl viologen cannot occur thermally because of an unfavorable ΔG (+1.45eV). If however, light with an energy greater than 1.45eV were to be supplied, the reaction could occur thermodynamically. It is the case that neither of these reactants can absorb visible light, so this reaction does not take place since no absorption takes place. By addition of $Ru(bpy)_3^{2+}$, the reaction is sensitized by allowing the photochemical formation of MV^+ from MV^{2+}.[130] Utilizing large concentrations of triphenylamine, the formation of the triphenylamine cation is favored over the back electron transfer reaction, which would decrease the concentration of MV^+. The end result is a photochemical reaction facilitated by the addition of a photosensitizer. (See Scheme 4)

Scheme 4

The endothermic dark reaction does not occur

$MV^{2+} + NPh_3$ ---//----> $MV^+ + NPh_3^+$ $\Delta G = +1.45eV$

Exothermic Photochemical Reaction does not occur because neither reactants absorb visible light

$MV^{2+} + NPh_3 + h\nu$---//----> $MV^+ + NPh_3^+$ $\Delta G < 0$

The formation of the excited state

$Ru(bpy)_3^{2+} + h\nu$ --------> $Ru(bpy)_3^{2+*}$

The formation of MV+

$Ru(bpy)_3^{2+*} + MV^{2+}$ -------> $Ru(bpy)_3^{3+} + MV^+$

Using high concentrations of NPh_3 to form NPh_3^+

$Ru(bpy)_3^{3+} + NPh_3$ -------> $Ru(bpy)_3^{2+} + NPh_3^+$

The net reaction is the photochemical reaction of MV^{2+} with NPh_3.

The splitting of water via photosensitization is of great practical value due to our ever increasing reliance on fossil fuels. The use of a non-carbon based fuel (H_2) eliminates formation of CO_2 and CO in the atmosphere, and therefore provides a clean burning fuel alternative. The study of the feasibility of photochemically splitting water has been the main driving force for carrying on research in the area of Ru(II) photochemistry.[124,133-142] The photosensitization of water-splitting is thermodynamically possible, yet kinetically disfavored due to the need for a two electron reduction to occur in order to form H_2 from H^+. The photochemical system $Ru(bpy)_3^{2+}$-MV^{2+}-TEOA (triethanolamine) has been extensively studied[143-170] and does lead to photochemically produced H_2 upon irradiation with visible light. Some pH dependency was found for this system, with pH >7 systems giving a larger yield of H_2. An unfortunate consequence of the reaction is that the electron donor (TEOA) is unavoidably used up and is referred to in the literature as a "sacrificial" donor. The need for the "sacrificial" donor therefore significantly diminishes this system's utility. Similar behavior is observed when using EDTA as an electron donor.

Use of $Ru(bpy)_3^{2+}$ as a light emission sensitizer (LES)

Just as there are several potential electron-transfer reactions that do not occur for various reasons, the same is true for chemiluminescent reactions. Therefore, the employment of a light emission sensitizer (LES)[122] can transform certain potential chemiluminescent reactions into reactions which will generate

light. One type of reaction is the reduction of lead dioxide by oxalate ion in acid.[17]

One of the most intriguing reactions in which $Ru(bpy)_3^{2+}$ plays the role of LES is the oscillating Belousov-Zhabotinskii reaction.[172,173] The oxidation of carboxylic acids by bromate ions catalyzed by the $Ru(bpy)_3^{3+/2+}$ redox couple proceeds as follows

$3BrO_3^- + 5CH_2(COOH)_2 + 3H^+ \text{ ---------> } 4CO_2 + 3BrCH(COOH)_2 + 2HCOOH + 5H_2O$

When it was understood that $Ru(bpy)_3^{3+}$ could be reduced by carboxylic acids, it was believed that an oscillating emission from the chemiluminescence should result. This was exactly what was found by Balzani et. al. in 1982.[173] An artificial "lightning bug" was created.

Other applications of $Ru(bpy)_3^{2+}$ as LES include the conversion of stored chemical energy into light. (Sensitized lyoluminescence)[174]

$Ru(bpy)_3^{2+}$ in Organized Assemblies and Restricted Environments

Several investigations reporting the photophysics and photochemistry of $Ru(bpy)_3^{2+}$ in heterogeneous media and organized assemblies have been the foundation for studies of Ru(II) complexes in biologically active molecules, e.g. DNA. Reports of the incorporation of $Ru(bpy)_3^{2+}$ and its analogues into various types of supports is indicated in Table 2.

Table 2

Medium	Reactions	Reference
Colloidal SiO_2/H2O	Quenching by MV^{2+}	175,176
Layered Silicates	Quenching by MV^{2+}	103,177
	Emission Studies	178
	Spectroscopic Studies	179
	Quenching by Fe^{3+}	180-182
Cellulose	Quenching by Fe^{3+}, Cu^{2+}, Cr^{3+}	183-187
Ion Exchange Resin	Quenching by Fe^{3+}	188,189
Zeolites	Formation of Ru^{3+}	190,191
Nafion Films	Emission	192
Starburst Dendrimers	Emission quenching	193
Colloidal TiO_2	Emission	194
	Water Reduction	163,170,195-199
	Emission Quenching	200
Micelles	Photoredox reactions	201
Vesicles	Electron Transfer to MV^{2+}	202,203
DNA	Spectroscopic Studies	3-33

The differences between the properties of Ru(II) complexes in solution and in organized media include differing redox behavior, differing photochemistry, and/or differing spectral properties, all as a result of the geometrical constraints and changes in mobility of the complex ion and its quenchers in this environment. Also, organization of donor and acceptor can be to some extent achieved by use of a molecular assembly of known dimensions. Because luminescence is exceptionally sensitive to changes in the local environment, emission spectroscopy (including time resolved ES) is probably the best suited technique to examine transition metal complexes in restricted environments. Ru(II) complexes, many being luminescent at room temperature, serve as excellent candidates to examine the photophysics in organized media. The differing photophysical behavior in heterogeneous

systems has been exploited in the research contained in this dissertation, where differing spectral properties of Ru(II) complexes in the presence and absence of DNA leads to the development of a model supporting several types of binding modes to the macromolecule.

Summary

A summary of the spectroscopic and redox properties of $Ru(bpy)_3^{2+}$ and $Ru(phen)_3^{2+}$ are given in Table 3 [1]. This table is useful as a standard for redox and spectral properties of Ru(II) complexes, and serves as a quick reference for comparison to novel complexes of Ru(II).

Table 3

Property	$Ru(bpy)_3^{2+}$	$Ru(phen)_3^{2+}$
Ground State Absorption		
λ_{max} (nm)	452, 345, 285	447, 422, 262
ε ($M^{-1}cm^{-1}$)	14600, 6500, 87000	19000,18300,115000
Excited State Absorption		
λ_{max} (nm)	310, 358, 452	
ε ($M^{-1}cm^{-1}$)	27300, 2100	
ϕ	1.00	
Energy	2.12eV	
Reduction Potentials	In CH_3CN (vs. SCE)	In CH_3CN (vs. SCE)
E_0 ($Ru^{3+/2+}$), V	+1.29	+1.26
E_0 ($Ru^{2+/+}$), V	-1.33	-1.36
E_0 ($Ru^{3+/2+*}$), V	-0.81	-0.87
E_0 ($Ru^{2+*/+}$), V	+0.77	+0.82

Table 3 (cont'd)

Luminescence

Em. max. (298K) (H_2O)	607 nm	593 nm
Em. max. (77K) (EPA)	580,633,692 nm	565, 610, 664, 726 nm
τ and ϕ (H_2O, 298K)	620 ns, 0.042	920 ns, 0.058
τ and ϕ (EtOH, 77K)	5.2μs, 0.38	9.8μs, 0.60

Isotope Effects	ϕ (lum.)	τ(μs)
$Ru(bpy)_3^{2+}$ in H_2O	0.04	0.62
$Ru(bpy)_3^{2+}$ in D_2O	0.07	1.02
$Ru(bpy)_3^{2+}$-*d*8 in H_2O	0.047	0.69
$Ru(bpy)_3^{2+}$-*d*8 in D_2O	0.079	1.25

-Data taken from Reference 1.

Chapter II. Preparation and Description of Ru(II) α-Diimine Complexes Under Investigation.

Discussion

Ruthenium(II) complexes possess a d^6 transition metal ion in an octahedral (O_h) ligand field which can support as much as six ligands per ion. Due to the strong ligand field established by α-diimines, the t_2g and eg d-orbitals are split sufficiently to make these metal complexes diamagnetic. Three bidenate ligands, such as bipyridine, can bond in a coordinate covalent fashion to the metal center via donation of lone pair electrons from the ligand. These ions assume a propeller-shaped symmetry which is lowered to D_3. Two tridentate ligands can surround a metal center and give C_{2v} symmetry. Mixed-ligand complexes of the type $Ru(bpy)_2L^{2+}$ or $Ru(phen)_2L^{2+}$ further lower the symmetry. Assignment of symmetry is further complicated by chelation itself, which distorts the ligand to some degree.

The complexes $Ru(bpy)_3^{2+}$ and $Ru(phen)_3^{2+}$ have been well characterized in a variety of solvents and supports.[1,2] They have provided information concerning the excited and ground state behavior of Ru(II) α–diimine complexes in general, and therefore can be considered as the prototype complexes by which all such complexes are compared. One observation that was reported early was the change in excited state behavior upon modification of the ligand surrounding the metal.[68] This has been exploited as the most useful way of modifying the photophysical and photochemical aspects of the system. By using this method the labs of Strekas,

Baker, and Gafney have synthesized various types of modified bpy's and phen's in hopes of further elucidating the effects of these modifications on the excited-state behavior of Ru(II) complexes. Emphasis has been put on synthesizing $Ru(bpy)_2L^{2+}$ and $Ru(phen)_2L^{2+}$ type complexes, since in these cases only one ligand is modified, which very often simplifies the spectral interpretation. The only exception to this are the complexes with polymethylene bridges, where the tris complexes were used for simplification of the resonance Raman spectrum.

Preparation of mixed-ligand complexes of Ru(II) begin by the preparation of the compound $Ru(bpy)_2Cl_2$. This is achieved by refluxing $RuCl_3$ with either bipyridine or o-phenanthroline.[37] After this complex is crystallized, the ligand of choice L is refluxed with $Ru(bpy)_2Cl_2$ and the new complex is isolated.

Several complexes of the type $Ru(bpy)_2L^{2+}$ and $Ru(phen)_2L^{2+}$ have been synthesized by our laboratories. Figures II-1 through II-6 show the ligands and the complexes synthesized which will be discussed in this dissertation. The complex $Ru(bpy)_2ppz^{2+}$ (Figure II-2) was emphasized since optically pure enantiomers were prepared,[33] thus allowing more useful experimental data to be obtained and compared to the other racemic complexes. The $Ru(bpy)_2$ $qpyMe_2^{4+}$ complex(Figure II-3) was also emphasized, due to its somewhat surprising binding behavior with DNA.

As shown in Figure II-1, the ppz ligand is a planar-fused analogue of the dpp ligand. Studying these two ligands and the complexes they form allows one to look at the effects of planarity on the spectra of these complexes.

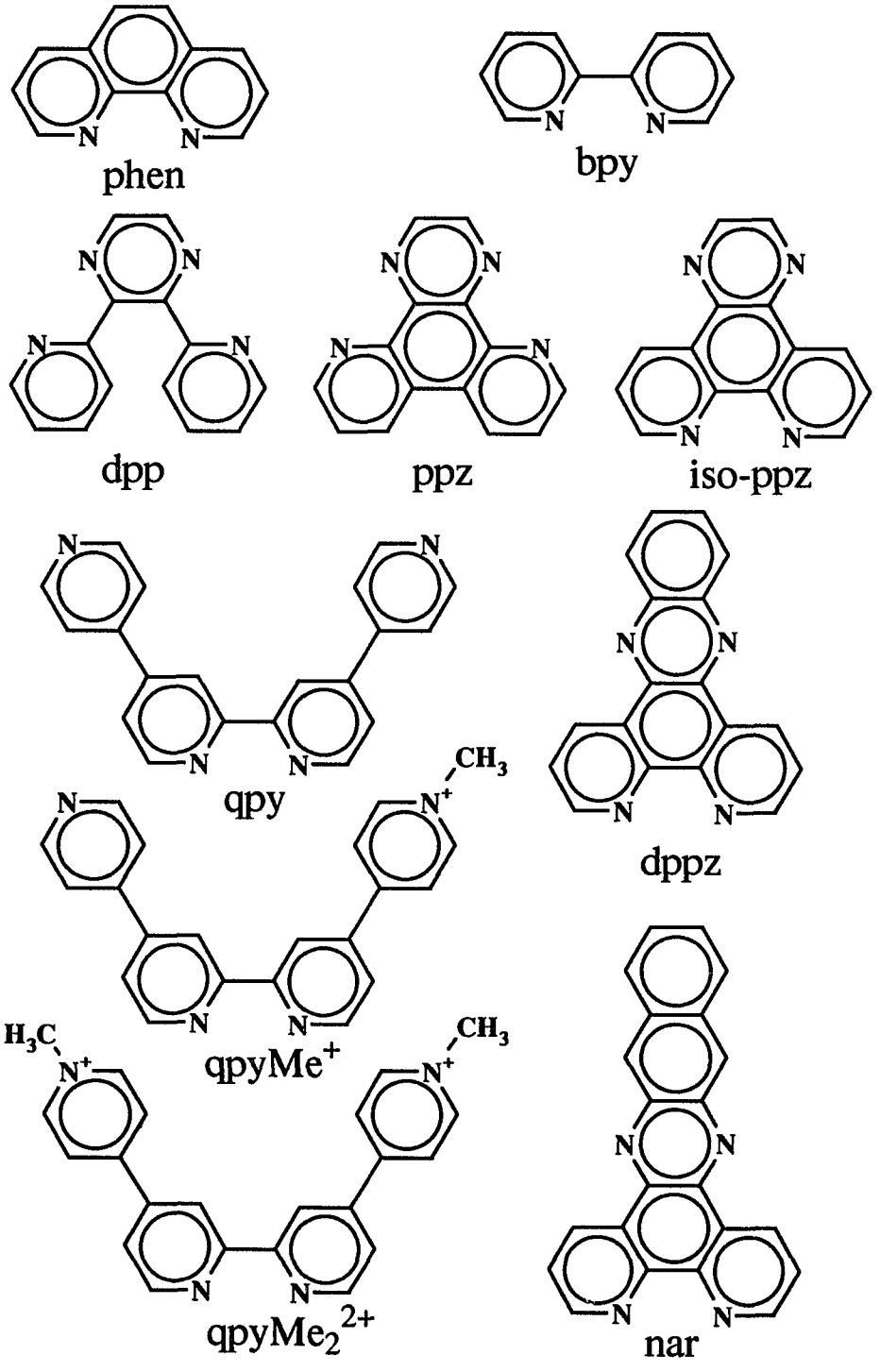

Figure II-1. Ligands used for synthesis of Ruthenium polypyridyl complexes

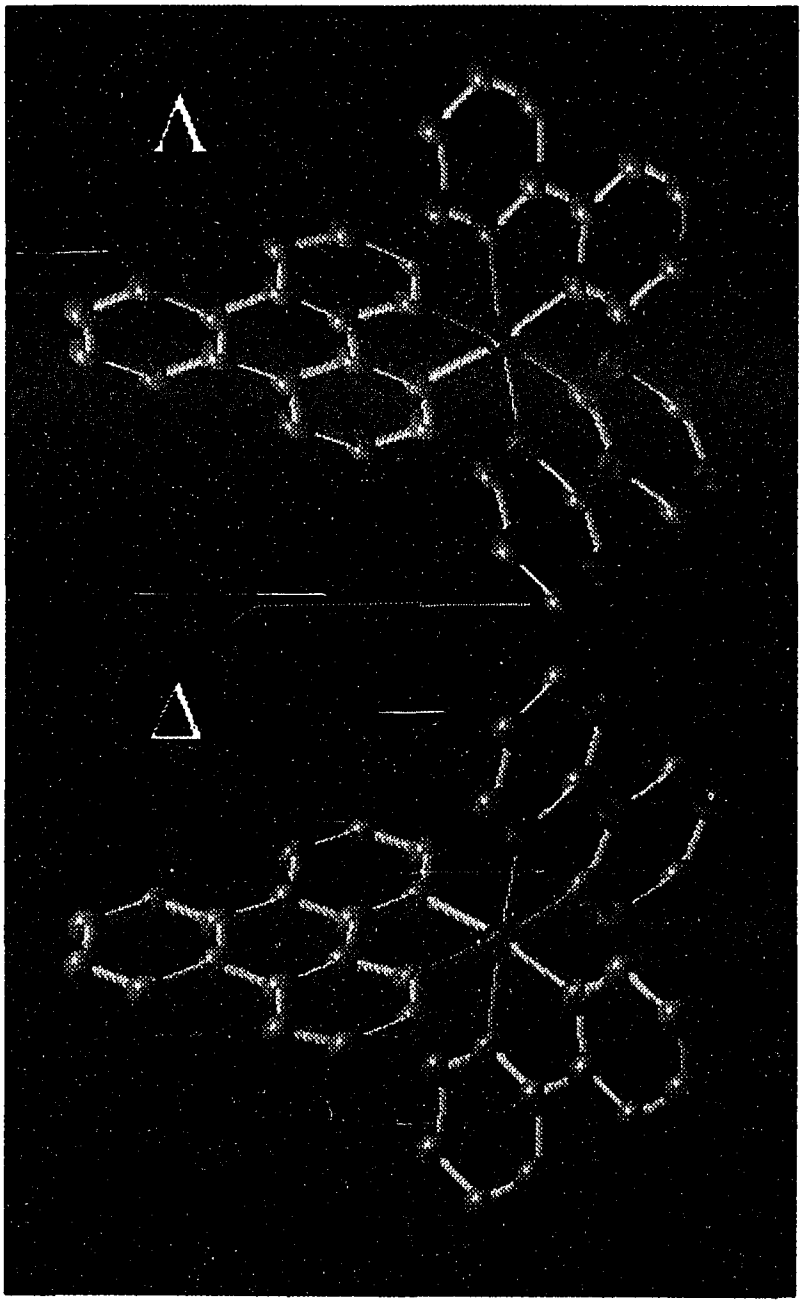

Figure II-2. Δ and Λ enantiomers of $Ru(bpy)_2ppz^{2+}$ (Without Hydrogens). Image created with MacMolecule-University of Arizona.

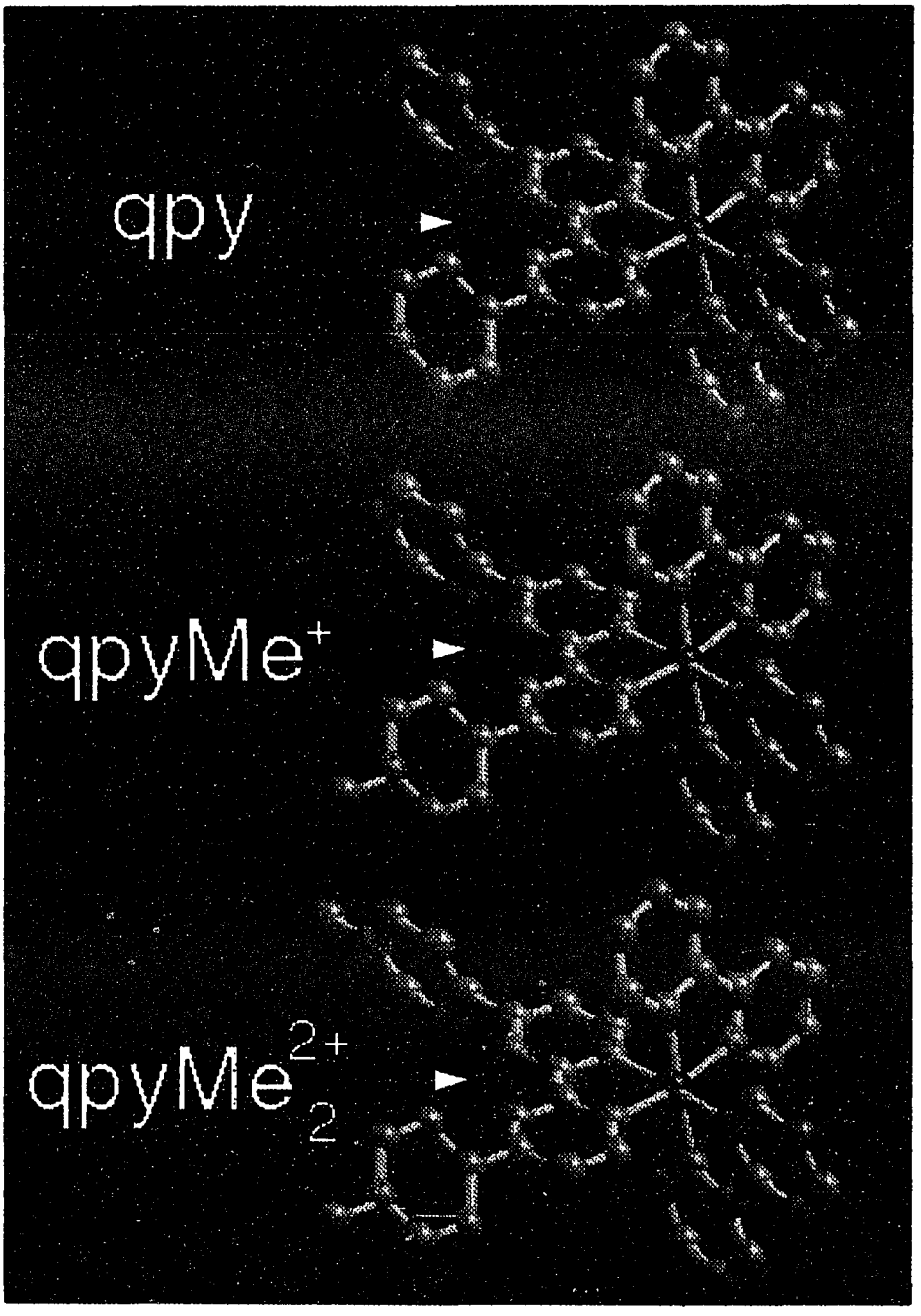

Figure II-3. $Ru(bpy)_2qpy^{2+}$, $Ru(bpy)_2qpyMe^{3+}$, and $Ru(bpy)_2qpyMe_2^{4+}$ complexes (without Hydrogens). Image created with MacMolecule-University of Arizona.

Annelated bipyridyl complexes

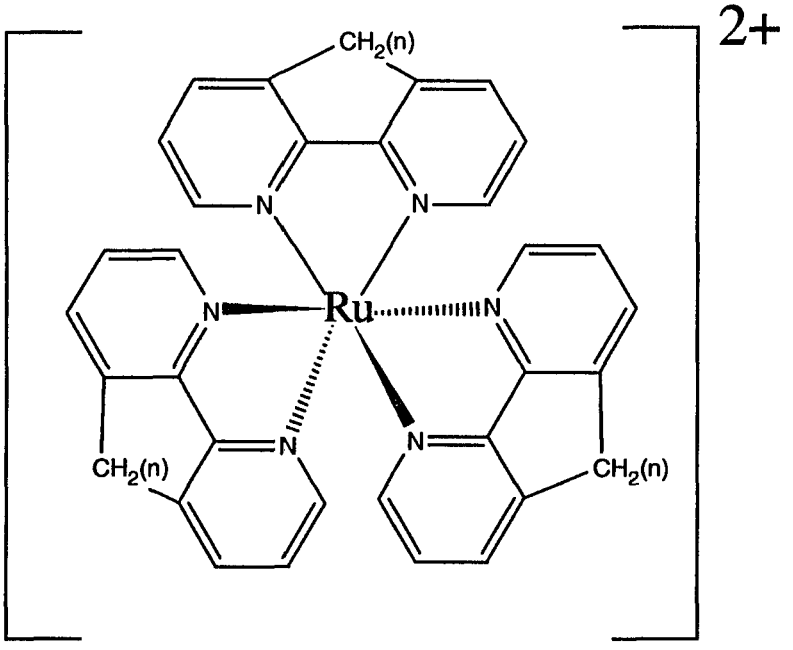

n= 0, 1, 2, 3, 4

Figure II-4 Annelated bipyridyl complexes (Chapter IV)

Annelated terpyridyl complexes

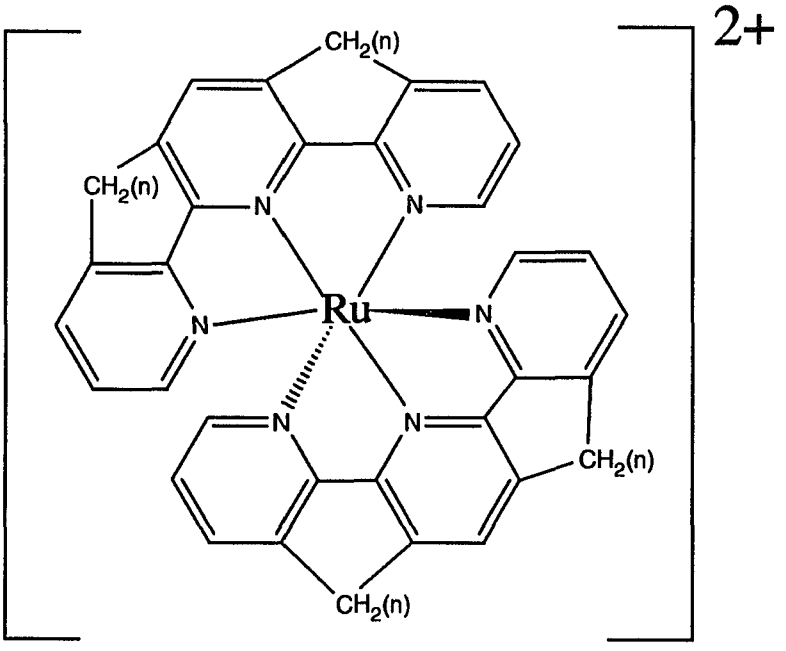

n= 0, 2, 3, 4

Figure II-5 Annelated terpyridyl complexes (Chapter IV)

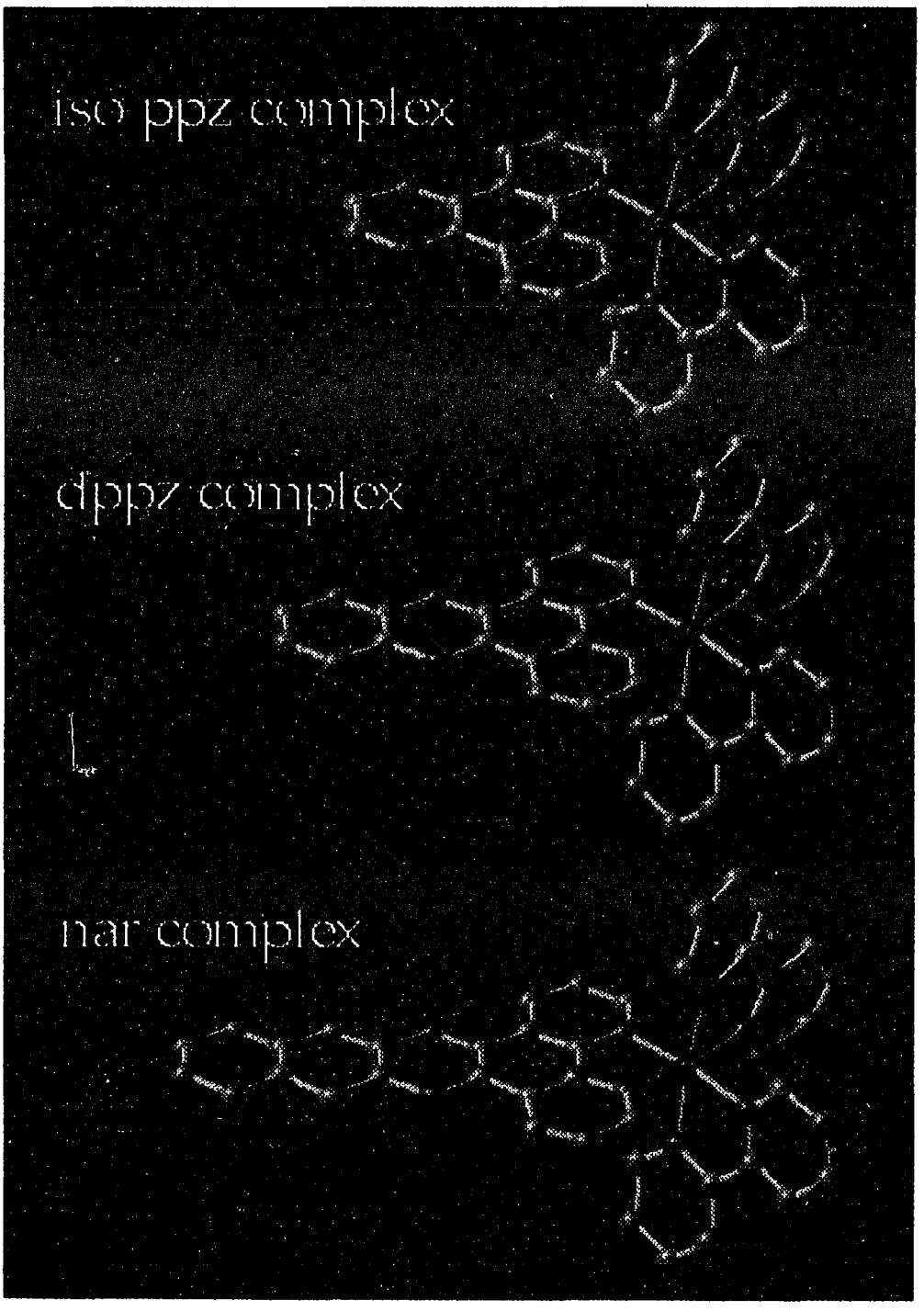

Figure II-6. $Ru(bpy)_2iso\text{-}ppz^{2+}$, $Ru(bpy)_2dppz^{2+}$, and $Ru(bpy)_2nar^{2+}$ complexes (without Hydrogens) Image created with MacMolecule-University of Arizona.

Because ppz is locked into a planar configuration, it is very different from dpp when steric hindrance is involved in the perturbation of the system. While dpp can relieve strain by rotating the pyridyl ring out of the plane of the pyrazyl ring, ppz cannot effect such a change. The differences in structural distortion emphasize the difference between otherwise analogous ligands and complexes. Also analogous to these complexes is $Ru(bpy)_2$iso-ppz^{2+}, (Figure II-6) so called because the ligand is a structural isomer of ppz. This ligand is also planar, and the complex it forms is very similar to the ppz complex, yet different because chelation occurs with two pyridyl rings instead of one pyridyl and one pyrazyl ring as in the ppz system. This greatly affects the spectroscopy of $Ru(bpy)_2$iso-ppz^{2+}, causing distinct absorption and emission properties.

The effect of peripheral charge on the spectroscopic properties of complexes can be studied by use of the bis-bipyridine complexes made from the qpy ligands (Figure II-3). The complexes formed show significant differences in their spectroscopic behavior, all due to the peripheral charge. Interaction with DNA for this series of ions shows how the charge can play a large role in the binding.[23]

The complexes in Figure II-4, prepared by Dr. Randolph Thummel and co-workers from the University of Houston, form a series of interesting tris-chelate analogues which probe the effects of a polymethylene bridge on the spectral properties of the complexes.[84] In Figure II-5 the corresponding bis-chelate complexes have also been prepared by Thummel et. al. and studied by us in a similar fashion. These complexes provide a means of studying the

influence of varying steric and electronic factors which can alter the excited-state properties dramatically.

The Ru bis-bipyridine complexes of nar, iso-ppz, and dppz (Figure II-6) make up a series of complexes which show the effect of additional aromatic rings on one ligand of the complex. These complexes are especially useful in examining the effects of ligand length on binding to DNA.

Chapter III. Enhanced Excited-State Basicities of $Ru(bpy)_2L^{2+}$ in aqueous solution.

Introduction

Results of the excited-state properties of Ru(II) polypyridyl complexes have provided important information that is useful as a guideline for designing new light conversion mechanisms which utilize a Ru(II) complex as a photosensitizer.[1,2,128] By studying quenching processes, the mechanism by which electron transfer occurs can then be more fully understood.[124] When protonatable sites are available on the ligand, such as imino or carboxyl groups, quenching can be monitored as a function of pH.[209-217] Quenching studies for several complexes of this type have shown that the excited-state is much more basic than the corresponding ground state.[210-218] There have been differing results, however, concerning the basicity of the ground state, where some reports claim an enhanced basicity, and some a decreased basicity for their complexes.[210,219] It is important to make the proper selection of the free-ligand pKa used for the purposes of comparison to the metal complex pK_a.

Two monomeric complexes, $Ru(bpy)_2(L)^{2+}$, where L= 2,3-bis(2-pyridyl) pyrazine or 4'7'-phenanthrolino-5',6':5,6-pyrazine have been prepared and characterized as well as their dimeric analogues.[23,80,220] A measurable luminescence has been detected for each of the complexes in neutral solution. At pH 1, however, all luminescence is lost. Emission spectra of the corresponding dimeric complexes show no pH effect. The pH effects on the excited state and ground state properties, ground state pK_a's, as well as

estimates of the excited-state pKa's are included in this discussion.

Results

Absorption and Emission Spectroscopy Figure III-1 are the visible absorption spectra of the dpp (top) and ppz (bottom) complexes (monomeric) from 350-650 nm at pH 7 (solid lines). The spectra of the same complexes in >10M perchloric acid are also shown (dashed lines). A decrease was evident in the two MLCT bands for both complexes, but the absorbance at 575 nm increases for the dpp complex and at 600nm for the ppz complex. This band shift was due to the protonation of the ligand, either dpp or ppz. Both complexes manifest this new band as a distinct change in color, the dpp complex going from yellow to purple and the ppz complex turning from yellow to blue. These protonated complexes bear a striking resemblance to the dimeric complexes, which also have red-shifted absorptions and no monomeric MLCT bands. After a few hours, it was observed that perchloric acid was too strong an oxidant to be used for these measurements, since decomposition of the protonated complex occurred. Sulfuric acid, therefore, was used instead, which did not cause decomposition at these concentrations.

Absorption titrations for both complexes were reversible. Isosbestic points at 511 nm for dpp and 530 nm for the ppz complex were found. The increase in absorbance of the new band at 575 for dpp and 600 for the ppz complex was plotted vs. Hammett's acidity function ($-H_0$) for the sulfuric acid solutions. The pK_a's for the protonated ligands are $H_0 = -4.9$ for the dpp ligand and $H_0 = -6.8$ for the ppz ligand. This spectral change can therefore be

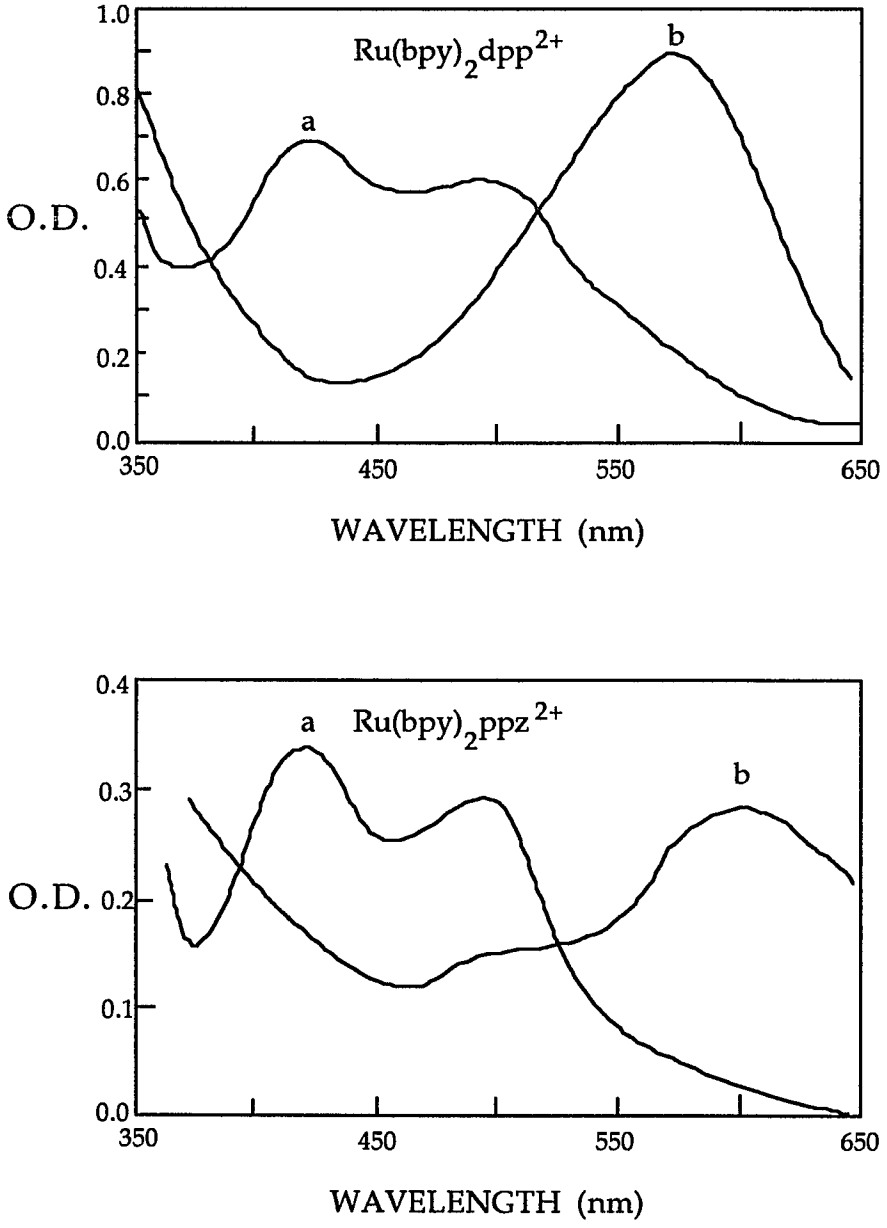

Figure III-1. Absorption spectra of $Ru(bpy)_2dpp^{2+}$(top) and $Ru(bpy)_2ppz^{2+}$ (bottom) complexes in water at pH 7 (a) and in concentrated perchloric acid (b).

considered as the protonation of the pyrazyl nitrogen opposite the coordinated Ru(II) site. It is interesting to note that the protonation of the pyridyl nitrogen opposite the Ru(II) site, which has been estimated to occur at a pH between 1 and 3, does not cause a noticeable change in the absorption spectrum, yet the protonation of the pyrazyl nitrogen at a much lower pH shows a remarkable change.

An examination of the uv spectrum of free dpp ligand shows a shift from 282 to 293 with a half-maximal change at pH 2.0. This is the only spectral change seen for the free ligand. Dpp titrates for two protons, and the two pK_a's of the pyridyl nitrogens are approximately the same value, yet, due to statistical considerations explained by Bodner,[221] the pK_a's must differ by 0.6 pH units. Therefore, approximate values of 1.7 and 2.3 for the dpp pyridyl protonation are acceptable.

Emission spectroscopy of the two complexes vs. pH show that there is no emission below 0.1M acid. Figure III-2 is a luminescence titration for both complexes between pH 1 and 6. Emission intensity was monitored at 690 for the ppz complex and 675nm for the dpp complex.

Time-resolved emission spectroscopy evidence reports that the emission lifetime decreases with pH, yet the measured lifetimes are too short below ~pH 3 to be reliable. For the dpp complex a lifetime of 120ns at pH 7 decreased to a lifetime of 91ns at pH 2.89. Similar results are seen for the ppz complex, but the emission is weaker and drops off at a slightly higher pH. For the ppz complex a lifetime of 100ns at pH 7 decreased below experimental reliablity at pH 3.5.

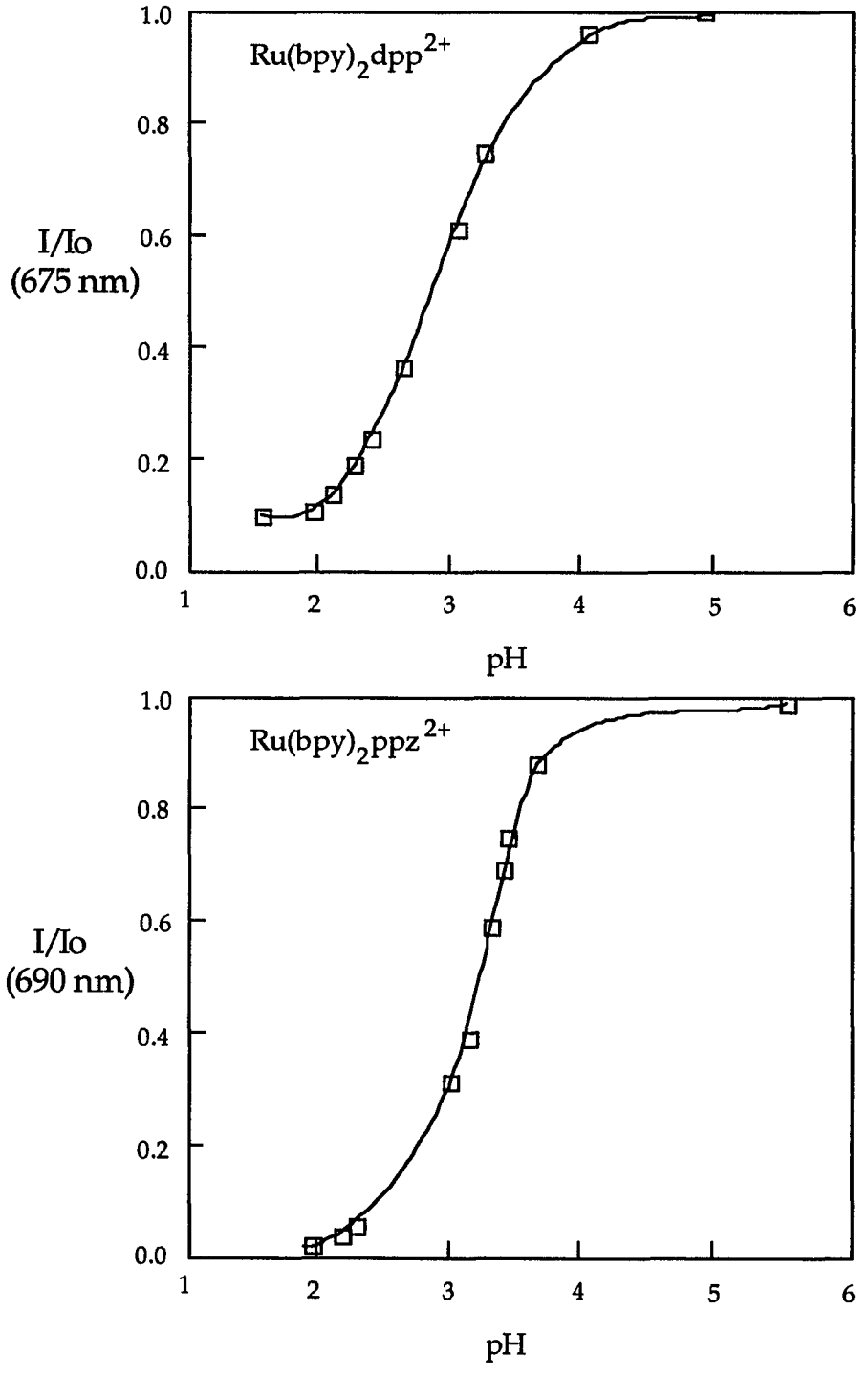

Figure III-2. Relative Emission (wavelength as indicated) versus pH for the $Ru(bpy)_2dpp^{2+}$(top) and $Ru(bpy)_2ppz^{2+}$ (bottom) complexes.

The experimental difficulty in these measurements did not permit a titration curve of luminescence lifetime vs. pH to be plotted.

Discussion

Luminescence Titration of the ppz and dpp complex The pK_a's for the ground state of each complex show that in the pH range where emission intensity decreases (i.e. pH 1-4), only the unprotonated form gives rise to the emission. Since the mono-protonated form of the complex does not luminesce, the titration curves are not valid for calculating excited-state pKa's.[222] A Stern-Volmer plot for each complex Figure III-3 gives the bimolecular quenching rate constants (k_q) of 5.5 x 10^9 $M^{-1}s^{-1}$ and 1.6 x 10^{10} $M^{-1}s^{-1}$ for the dpp and ppz complexes respectively. These values establish that the protonation is diffusion limited for each complex. If a value of 10^{10} $M^{-1}s^{-1}$ is assumed for the rate constant, and one uses the lifetimes of each complex to generate the luminescence titration curves, the values for pK_a of 3.1 for the dpp complex and 3.3 for the ppz complex are obtained. The value of k_q establishes[223,224] that the proton encounter is a site-specific protonation of the deprotonated excited base, and this is thermodynamically favored. Because the pKa of H_30^+ is -1.75, this must be the lower limit of the excited-state pKa for each complex. If the excited-state pKa's were smaller, no large change in the absorption spectrum could be observed, since H_30^+ would be protonated first.

Acid Dissociation Constants of Diimines and Ru(II) Complexed to Diimines

Protonation of pyrazine is much more difficult (pK =0.80) than pyridine (pK = 5.23),[225] indicating that basicity is reduced by the presence of the

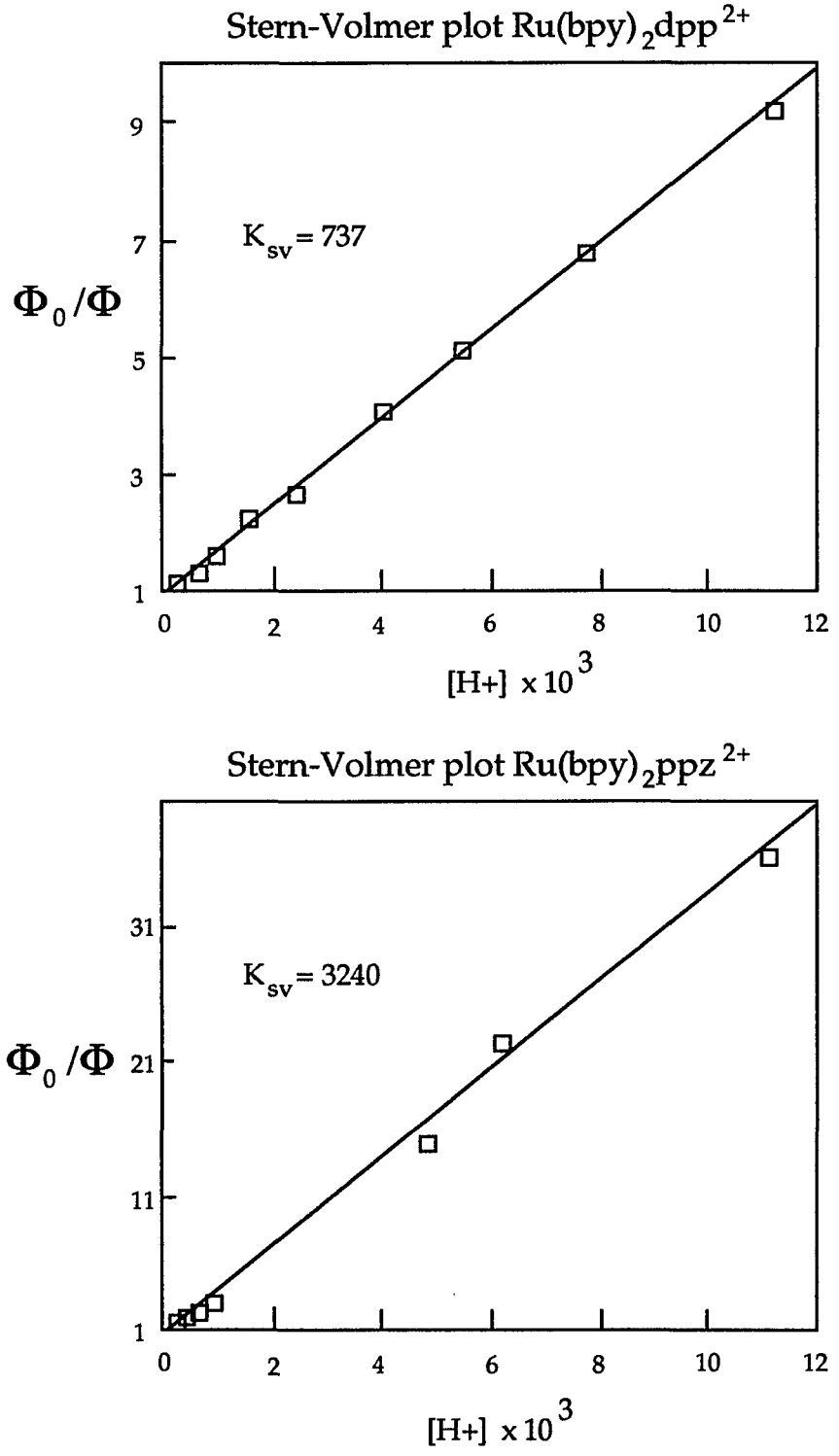

Figure III-3. Stern-Volmer quenching plots of data in Figure 2.

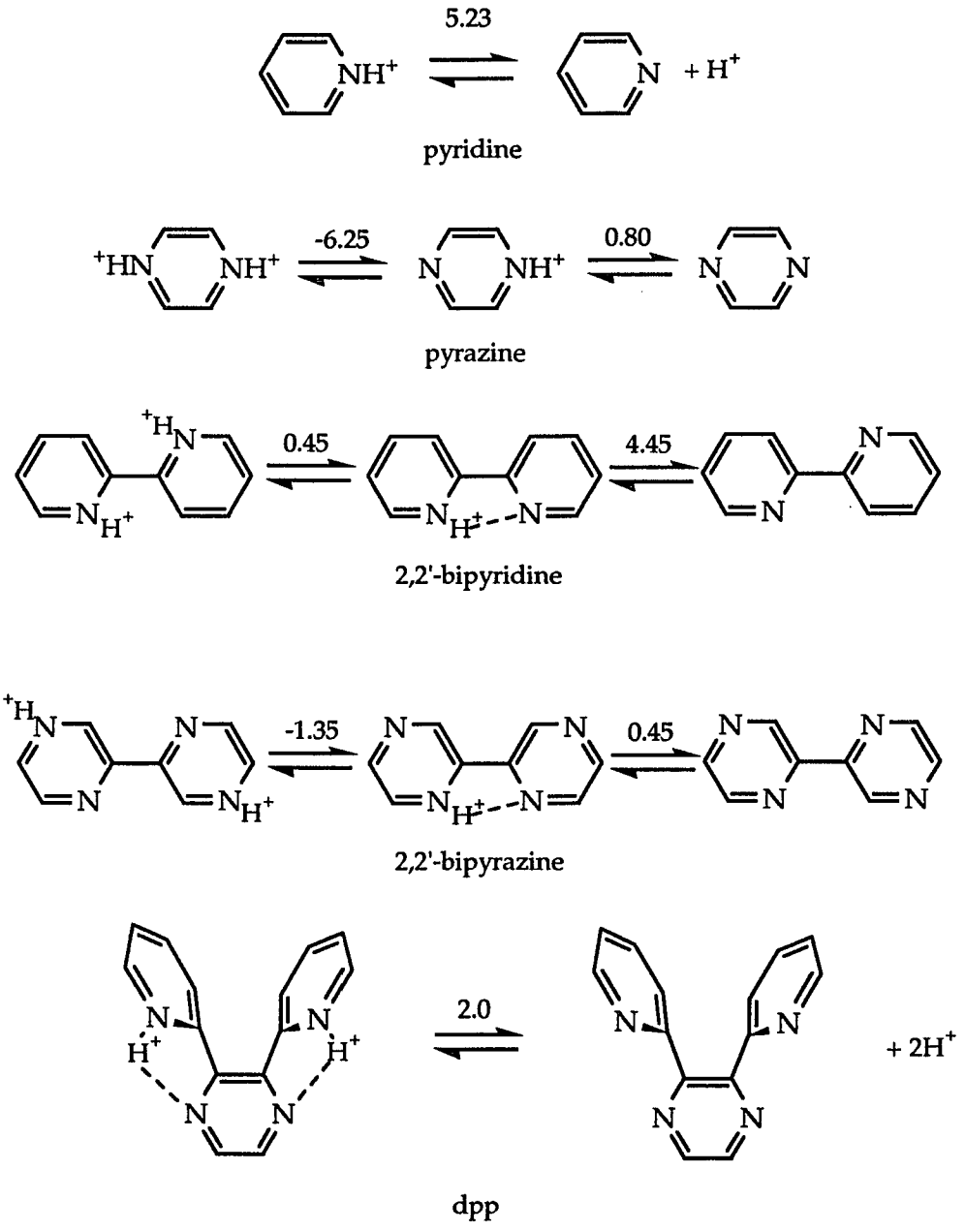

Figure III-4. Structures and pK_a's for diimine and bis(diimine) ligands

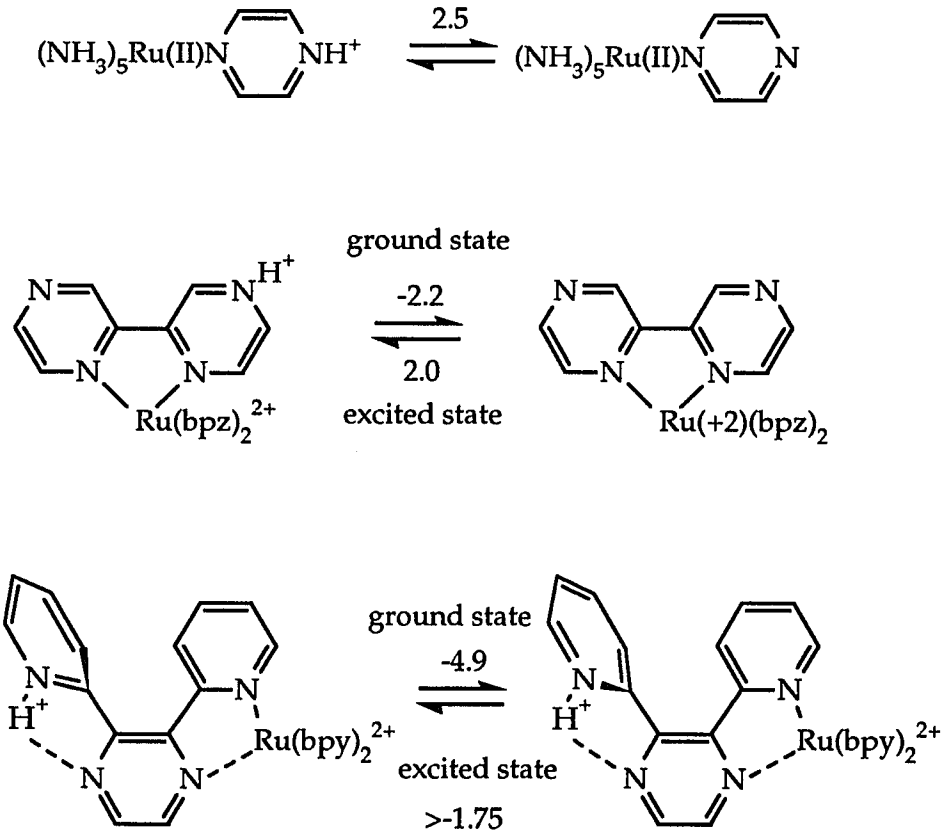

Figure III-5. Structures and pK_a's for diimines coordinated to Ru(II).

para imino nitrogen. (See Figure III-4) The second protonation of pyrazine is much less basic (pK = -6.25), thus showing a decrease in basicity of almost 7 orders of magnitude. Coordination of pentamnineruthenium(II) to pyrazine gives a pK_a of 2.5. (Figure III-5).[219] Therefore, the imino nitrogen in the complex is more basic than pyrazine by approximately 2 orders of magnitude. If this pK_a is compared to the protonation of the pyrazinium ion, it can be said that coordination to Ru(II) increases the basicity from -6.25 to 2.5, a substantial change.

With 2,2'-bipyridine[226] and 2,2'-bipyrazine,[210] the protonations become complicated because of electrostatic interactions, mainly an attraction of the proton on the adjacent ring in the mono-protonated form and a strong repulsion in the diprotonated form, due to the close proximity of the 2 protons. Because of these electrostatic interactions, the first pKa's for bpy and bpz are slightly lower than pyridine and pyrazine, respectively, but the second pKa value is only slightly lower for bpz (-1.35) and much lower for bpy (0.45). The difference in protonation behavior occurs because the 3,3' nitrogens are protonated in bpz, a somewhat easier protonation than diprotonation on a 2,2'-nitrogen. The third protonation of bpz, which for steric reasons is similar to the coordinated bpz complex, occurs at a H_0 of -10, compared to the third protonation of the tris complex of bpz (pH= -2.2) which is much more basic than bpz. An increase in the pKa to 2.0 occurs in the excited-state of $Ru(bpz)_3^{2+}$, showing that increased electron density on the ligand occurs in the excited state.

The protonation of the ligand dpp, occurring at 2.0, or 1.7 and 2.3 is

plausible, since the protonations of the first two sites are similar and isolated from each other. As is shown in Figure III-4, the pyridyl rings of dpp are rotated out of the pyrazyl plane due to some steric hindrance. We can however visualize some electrostatic attraction of these protons to the pyrazyl nitrogens from these structures.

For the complexed dpp, it was impossible to see the first protonation of the pyridyl nitrogen using absorption spectroscopy. This proton is sufficiently removed from the Ru(II) center to assume that the pK_a of this protonation is near 2.0, or possibly slightly higher. The detected protonation (second protonation) of the dpp complex is assigned to the protonation of the pyrazyl nitrogen and is electrostatically hindered by the presence of the pyridyl proton. As protonation of the second nitrogen occurs, the electrostatic repulsion pushes the pyridyl ring away from the plane of the pyrazyl ring, causing a large spectral change to occur. This is analogous to the dimeric Ru(II) dpp and ppz complexes, which show a large change in their visible absorptions in relation to the monomeric complexes. The very low pK_a value for protonation of the pyrazyl nitrogen in the dpp complex, which is probably more basic than the third protonation of dpp, leads one to believe that the third protonation of dpp ligand is probably not observable, even with 96% sulfuric acid.

For the ppz complex and ligand, the pyrazyl nitrogens of the complex must be even less basic than the corresponding nitrogens in dpp, since ppz is locked into a planar arrangement, and no alleviation of the electrostatic repulsion can occur. The pK value of $H_0 = -6.8$ supports this argument. Again,

no detection of the third protonation of the ligand itself was observed, since the complex is probably more basic than the free ligand.

Increased Basicity of the coordinated diimines in the excited state The lower limit of -1.75 for the excited-state basicities shows that the excited-states are significantly more basic than the corresponding ground-state basicities. Therefore, in the MLCT state, the complexed ligands are better bases by at least 3 orders of magnitude for dpp and at least 5 orders of magnitude for ppz as compared to their ground-state values. Resonance Raman spectra have shown[80,220] the lowest charge transfer state to be associated with these ligands and not bipyridine. Interpretation of the most enhanced modes in the resonance Raman spectrum suggest that charge is not symmetrically transferred, as it is in bpy and bpz. This supports the increased basicity of the pyrazyl nitrogen relative to the pyridyl nitrogens. Another consideration is that of the bpy radical anion, which has been shown to have pK_a's of ~24 and 8,[227] compared to neutral bpy which has pK_a's of 4.45 and 0.45, and shows how an electron in a pyridine ring can increase the basicity of the nitrogen in that ring.

The presence of a pyridyl nitrogen with a pKa of ~2, combined with the protonation of the pyrazyl nitrogen which is expected to be more facile in the excited-state, gives rise to a dynamic process which can, on the order of picoseconds, rearrange the proton between two sites that transiently possess nitrogens with similar pKa's. This may explain why no luminescence is seen in the protonated forms, since this protonation may provide pathways to non-radiative deexcitation.

Chapter IV. Spectroscopic Study of polymethylene bridged bipyridyl and terpyridyl complexes of Ru(II).

Introduction

The extent to which variation of ligand structure can influence the excited-state redox properties of Ru(II) polypyridyl complexes[232-240] has been investigated for two series of complexes which vary only by the length of a 3,3'-polymethylene bridge present in the ligand.[84] For the tris-bipyridyl complexes, a bridge length from 1 to 4 methylene units was employed. For the bis-terpyridyl complexes, a bridge length from 2 to 4 methylene units was employed on each side of the center pyridyl ring.

A recent report of NMR and X-ray crystallography[241,242] of the annelated bipyridyl complexes indicated that this series of ions provide a set of structurally similar complexes which differ only with respect to the dihedral angle of the chelate. The absorption spectra for the series of complexes are quite similar, except for the n=1 complex which is blue-shifted. The most striking variation in spectral properties of the bipyridyl complexes is the luminescence intensity in acetonitrile at room temperature. For the n =1 complex, no luminescence was seen, as reported previously.[243] For the n=2 complex, the luminescence was virtually identical to that of $Ru(bpy)_3^{2+}$. With the n=3 complex, the luminescence was decreased by an order of magnitude, and for n=4 complex, the emission was extremely weak and red-shifted to 680 nm.[84] Low temperature (77K) emission spectra of this series of complexes also exhibit changes upon alteration of the bridge length. For the terpyridyl complexes in CH_3CN

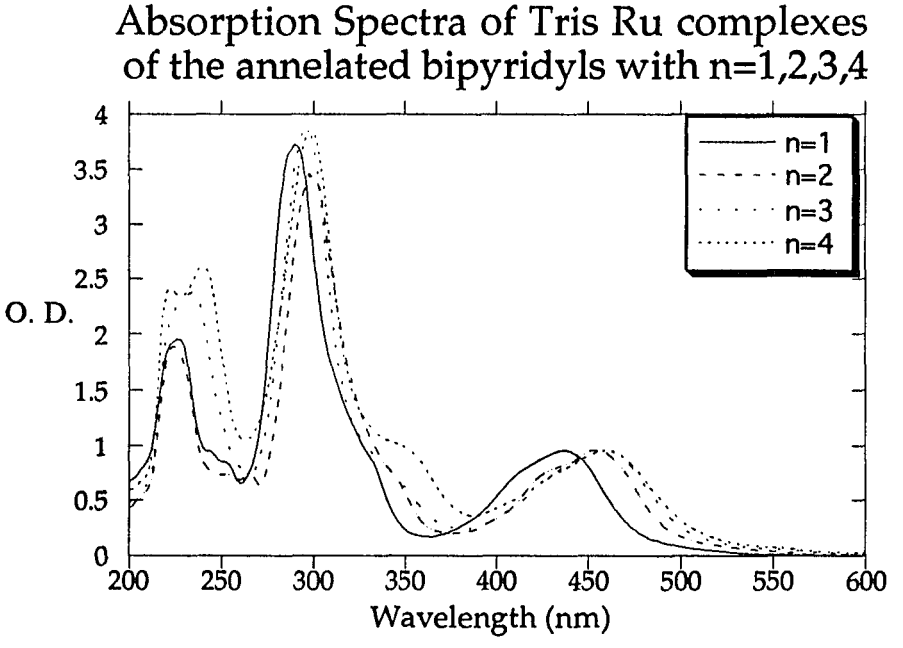

Figure IV-1. Absorption spectra for the bipyridyl series of complexes at 298K. Concentrations were adjusted such that the absorbance of the MLCT band in each complex is 1.0.

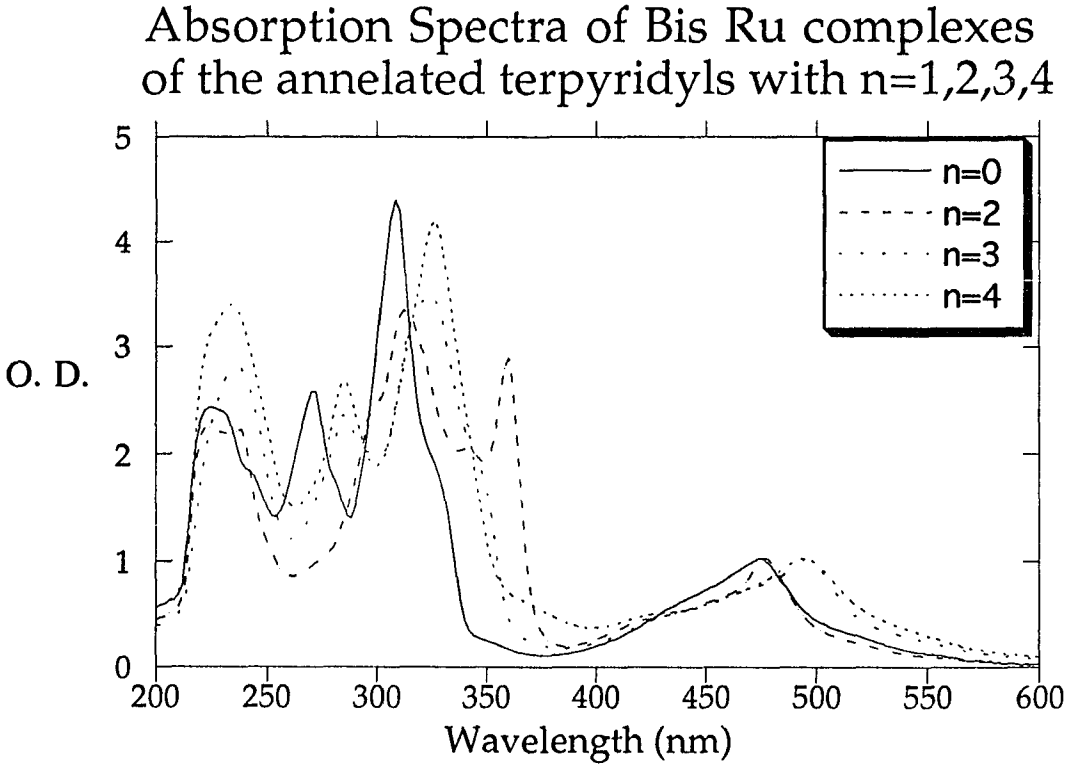

Figure IV-2. Absorption spectra for the terpyridyl series of complexes at 298K. Concentrations were adjusted such that the absorbance of the MLCT band in each complex is 1.0.

solution at room temperature, the n=0 complex showed a very weak luminescence at 618 and the n=3 complex also showed weak emission at 657. None of the other terpy complexes studied (n=2, n=4) showed any measurable emission at room temperature.

At 77K, however, large differences were apparent. The n=0 complex showed strong emission at 615 with a resolved shoulder at 663. The n=2 complex showed a very weak luminescence at 654 nm with a shoulder at 713 nm. The n=3 complex luminesced at 659 nm with a shoulder at 712 nm, ~10-20% of the intensity of n=0. The n=4 complex was the weakest emitter, with a very broad and weak luminescence at 651 nm with an unresolvable shoulder.

Resonance Raman spectroscopy (rR) of Ru(II) polypyridyl complexes has been instrumental in understanding the ground and excited state properties of these species.[80,244-251] rR gives vibrational information concerning the ground state geometries of the coordinated ligands, while rR intensities can shed light on the effectiveness of the vibration to couple the ground and excited states.[252,253] The more efficient coupling generally leads to a diminished quantum yield of luminescence as well as a shorter luminescence lifetime.

A compilation of absorption spectra, emission intensity, time-resolved emission, and resonance Raman spectroscopy data has been undertaken for these two series of complexes in hopes of understanding the effects of ligand structure on the ground and excited state properties of this class of molecules. The efficiency of coupling the ground and excited states has been investigated as a function of bridge length, and this is correlated to the emission data.

Results

Figure IV-1 is the absorption spectra for the bipyridyl series of complexes at 298K. Figure IV-2 is the absorption spectra for the terpyridyl series of complexes at 298K. All samples are in CH_3CN solution.

Figures IV-3 and IV-4 are the resonance enhanced Raman spectra from 1000 cm^{-1} to 1700 cm^{-1}, using 457.9 nm excitation, of the annelated bipyridyl complexes. Figure IV-4 is a comparison of the n=1 spectrum to $Ru(bpy)_3^{2+}$, for reference to unperturbed bpy vibrations. Comparison of the n=1 complex with the others in the series reveals that the n=1 complex is in a class by itself. Figure IV-4 is a comparison of the annelated n=2,3, and 4 complexes to $Ru(bpy)_3^{2+}$. The excitation at 457.9 nm corresponds well to the maximum MLCT absorption band for all the complexes, providing maximum resonance enhancement.[241] Excitation with 488 nm light gives essentially the same spectrum. The band at 1374 cm^{-1} is a solvent band due to CH_3CN and serves as an internal standard.

Figure IV-5 is the resonance enhanced Raman spectra from 1000 cm^{-1} to 1700 cm^{-1}, using 457.9 nm excitation, of the annelated terpyridyl complexes. Again, the excitation at 457.9 nm corresponds well to the maximum MLCT absorption band for all the complexes, providing maximum resonance enhancement.

Normalized emission spectra at 77K for both series of complexes are shown in Figures IV-6 and IV-7. The intensities were normalized in each series to allow for discussion of the vibrational progressions seen.

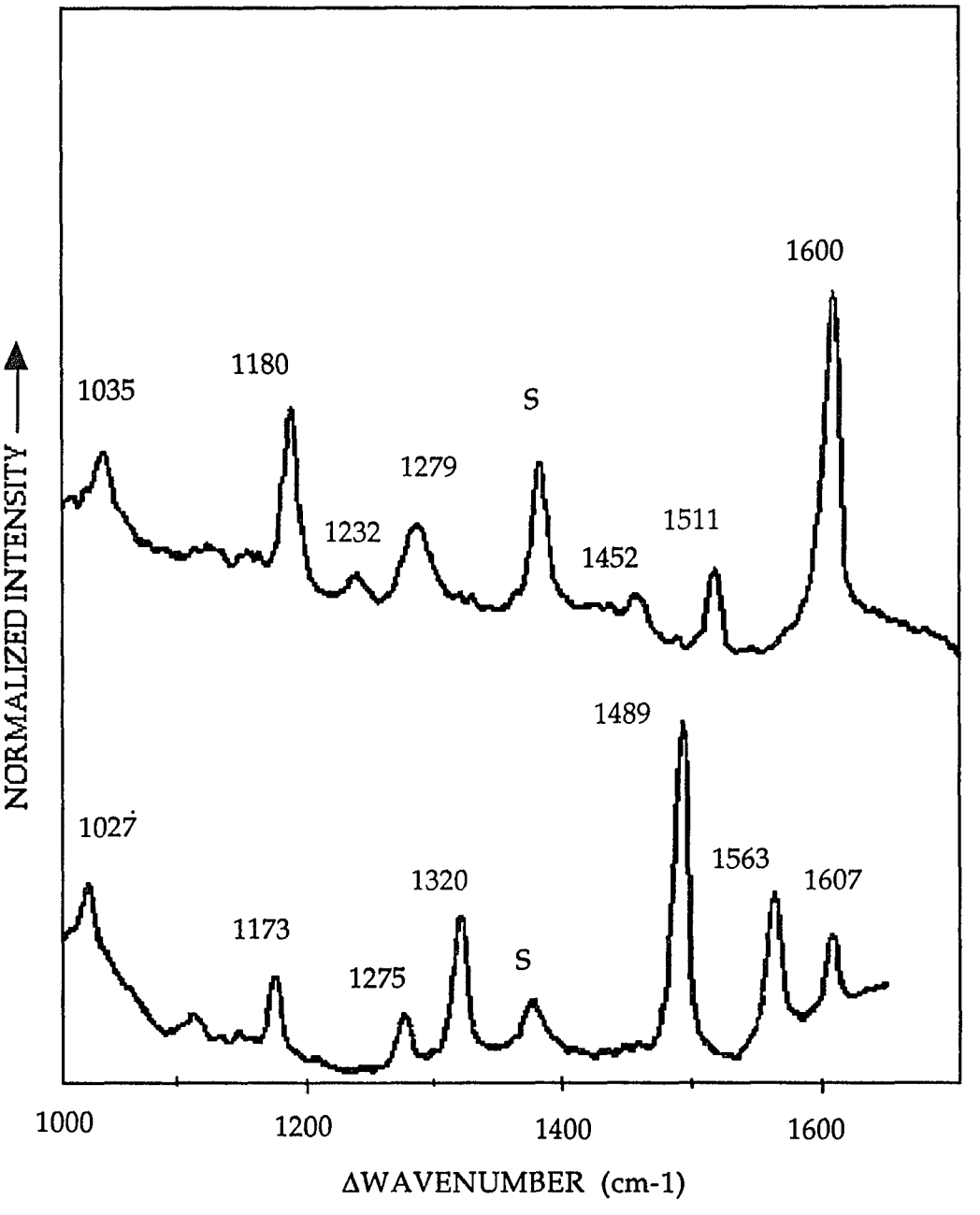

Figure IV-3. Resonance Raman spectra of $Ru(bpy)_3^{2+}$ (bottom) and Ru(bpy n=1)$_3^{2+}$ top at room temperature in acetonitrile solution at ~10^{-4} M (excitation wavelength at 457.9 nm) The spectra have been normalized to the peak height of the most prominent peak to facilitate relative intensity comparisons.

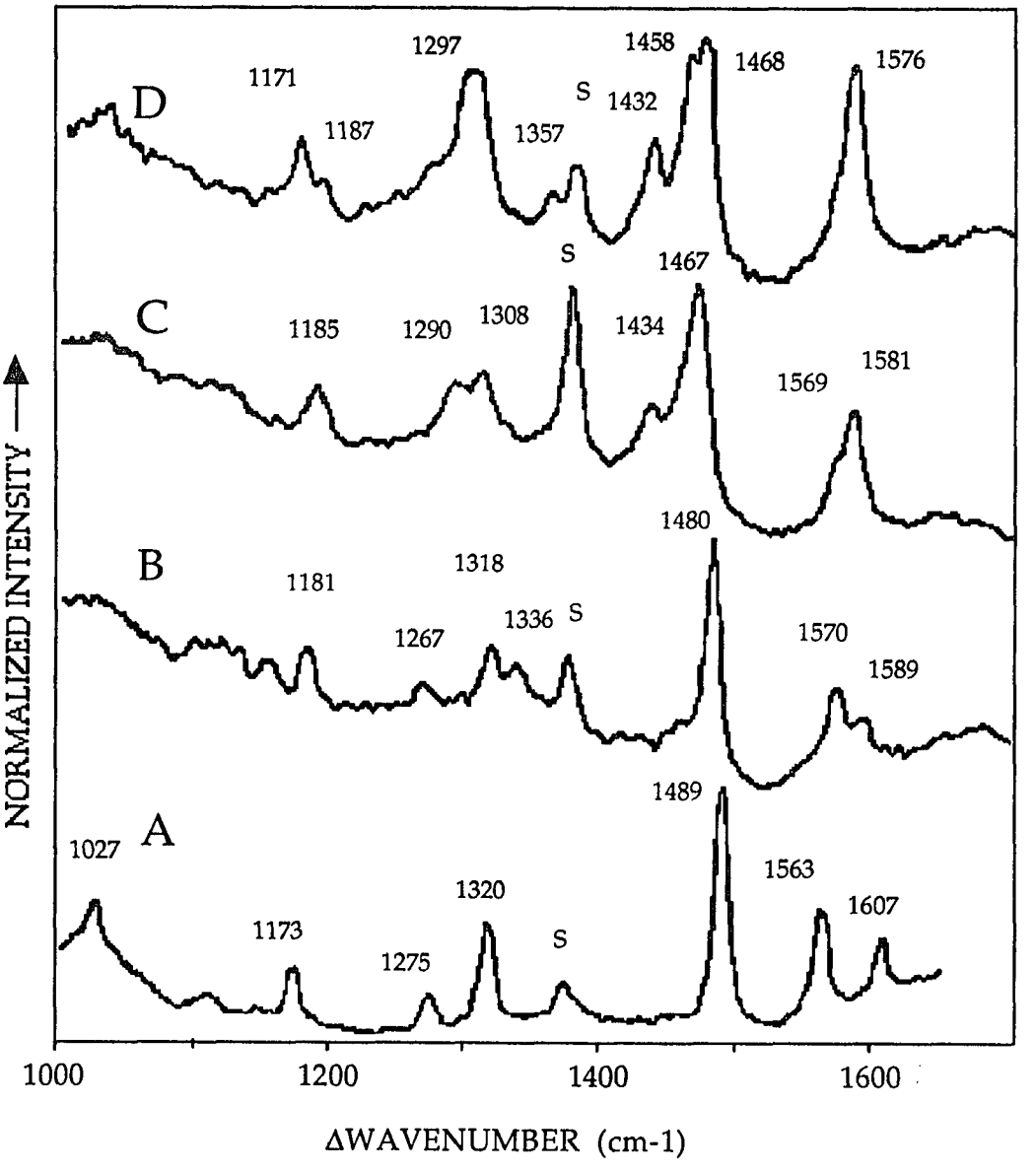

Figure IV-4. Resonance Raman spectra of $Ru(bpy)_3^{2+}$ (A), $Ru(bpy\ n=2)_3^{2+}$ (B), $Ru(bpy\ n=3)_3^{2+}$ (C), $Ru(bpy\ n=4)_3^{2+}$ (D) at room temperature in acetonitrile solution at ~10^{-4} M (excitation wavelength at 457.9 nm) The spectra have been normalized to the peak height of the most prominent peak to facilitate relative intensity comparisons.

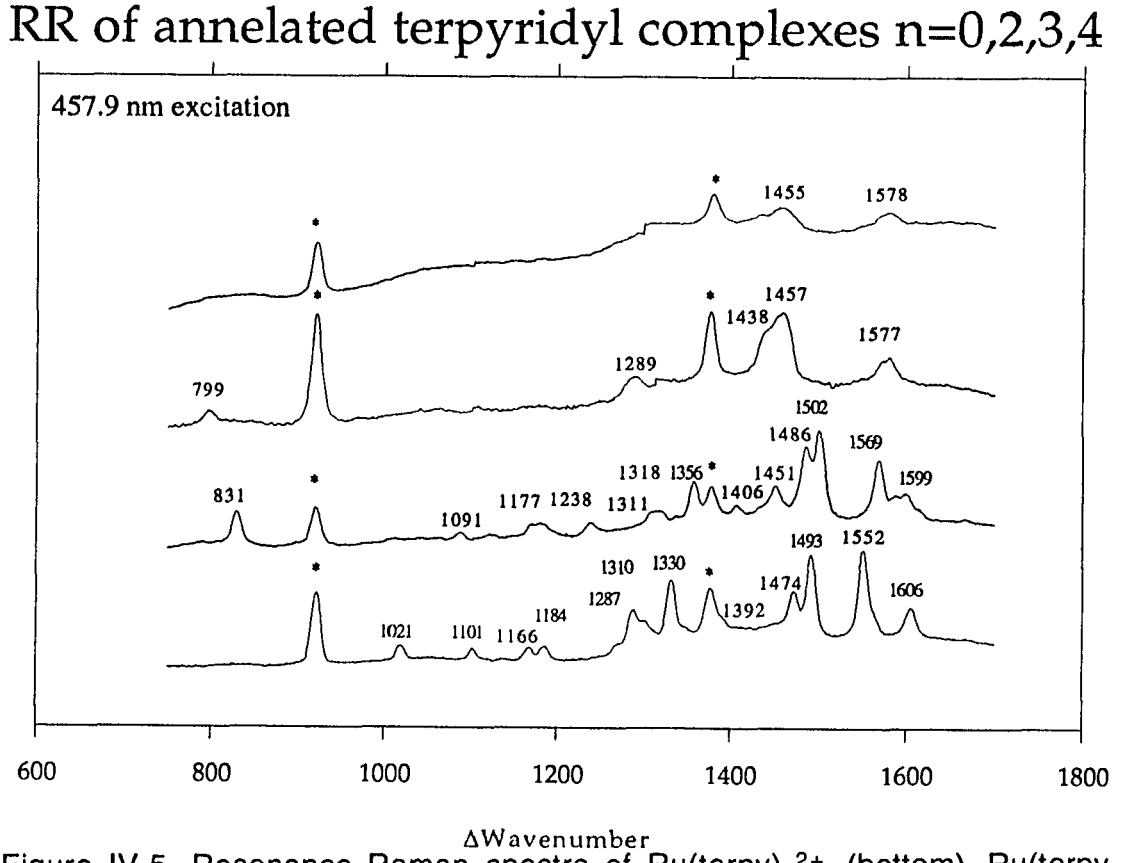

Figure IV-5. Resonance Raman spectra of $Ru(terpy)_3^{2+}$ (bottom), $Ru(terpy\ n=2)_2^{2+}$ (second from bottom), $Ru(bpy\ n=3)_2^{2+}$ (second from top), and $Ru(bpy\ n=4)_3^{2+}$ (top) at room temperature in acetonitrile solution at ~10^{-4} M (excitation wavelength at 457.9 nm) The spectra have been normalized to the peak height of the most prominent peak to facilitate relative intensity comparisons.

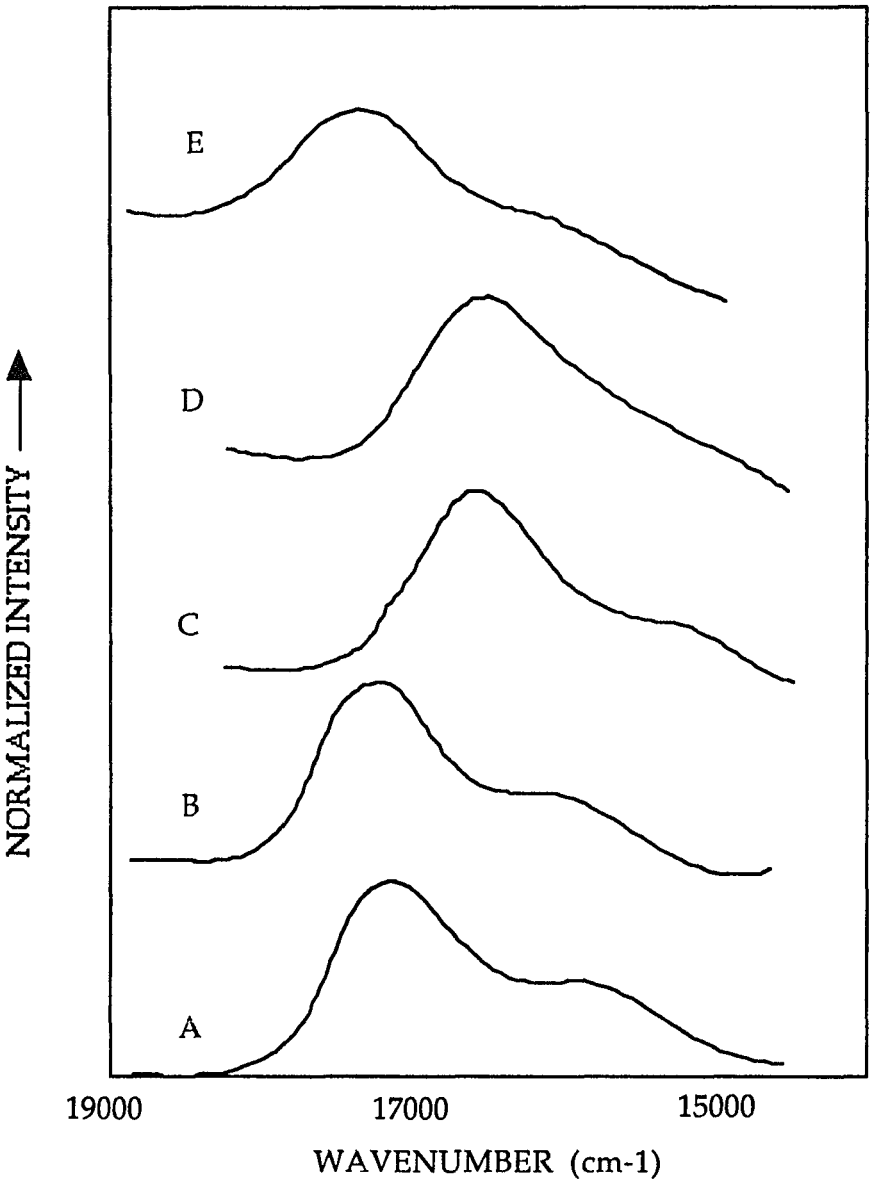

Figure IV-6. Normalized 77K emission of the annelated bipyridyl complexes. (A) -$Ru(bpy)_3^{2+}$ (B) - $Ru(bpy\ n=1)_3^{2+}$ (C) - $Ru(bpy\ n=2)_3^{2+}$ (D) - $Ru(bpy\ n=3)_3^{2+}$ (E) - $Ru(bpy\ n=4)_3^{2+}$.

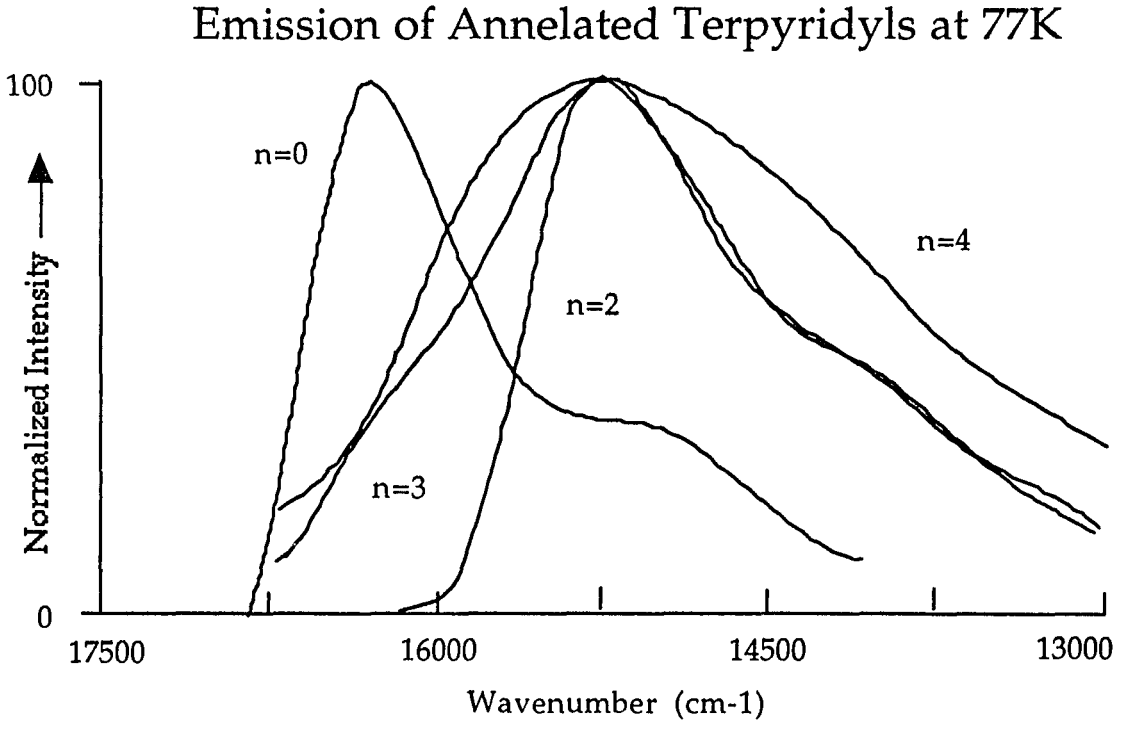

Figure IV-7. Overlay of the normalized 77K emission spectra of the terpyridyl complexes in CH_3CN glass. Each spectrum is indicated in the plot.

Luminescence lifetimes are only given for the bipyridyl complexes. Room temperature measurements were made on N_2 purged, CH_3CN solutions of the respective complexes, and 77K measurements used frozen CH_3CN solutions. Results are given in Table 1.

Table 1

Measured Lifetimes for Ru(annelated bpy n=0,1,2,3,4)$_3^{2+}$ at 25°C and 77K

complex	liq. soln., (ns)[a]	frozen soln. (μs)[b]
$Ru(bpy)_3^{2+}$	620	5.3
$Ru(bpy\ n=1)_3^{2+}$	[c]	5.5
$Ru(bpy\ n=2)_3^{2+}$	630	5.4
$Ru(bpy\ n=3)_3^{2+}$	455	2.7
$Ru(bpy\ n=4)_3^{2+}$	[d]	3.6[e]

[a]Approx. 10^{-5}M solutions in acetonitrile at 25°C [b]Same as in a, but frozen in cold finger Dewar at 77K.[c]No emission observed. [d]Signal too weak to measure lifetime at reported 680nm emission maximum. [e]Maximum at 77K is 606nm.

Discussion

Bipyridyl complexes n=0,1,2,3,4

Examination of the resonance Raman vibrational spectrum shows a continuous trend with increasing methylene units from n=0 to n=4, with the exception of n=1, which is by itself distinct. A comparison of n=2,3,4 with n=0 shows correspondence between the 1607 cm^{-1} and 1563 cm^{-1} bands in the

$Ru(bpy)_3^{2+}$ spectrum with a shifted pair at 1589 cm^{-1} and 1570 cm^{-1} for the n=2 complex, a shifted peak at 1581 cm^{-1} with a shoulder at 1569 cm^{-1} for the n=3 complex, and a single peak at 1576 cm^{-1} for the n=4 complex(probably two degenerate frequencies). The most intense 1489 cm^{-1} band in the $Ru(bpy)_3^{2+}$ spectrum is shifted to 1480 cm^{-1} in the n=2 complex, to 1467 cm^{-1} for n=3 (with asymmetric broadening on the low energy side), and a 1458 cm^{-1}, 1468 cm^{-1} pair in the n=4 complex. The 1275 cm^{-1}, 1320 cm^{-1} pair of bands in the $Ru(bpy)_3^{2+}$ spectrum is slightly shifted for the n=2 complex, move closer for n=3 (1290 cm^{-1} ,1308 cm^{-1}), and form one band (1297 cm^{-1}) in the n=4 complex. The 1173 cm^{-1} $Ru(bpy)_3^{2+}$ band splits into two bands at 1171 cm^{-1} and 1187 cm^{-1} for the n=4 complex, and the n=3 complex shows asymmetric broadening on the high frequency side. Also, a new band appears for the n=3 complex at 1434 cm-1. This is seen at 1432 cm-1 for the n=4 complex. Finally, n=4 complex shows a new band at 1357 cm-1 which is not present in any other spectra, and a low frequency shoulder on the 1297 cm^{-1} band emerges.

The resonance Raman spectra in Figure IV-3 portray the fact that the n=1 complex is significantly different from the others, yet comparable to $Ru(bpy)_3^{2+}$. The n=1 spectrum has 7 bands which likely correlate to the seven $Ru(bpy)_3^{2+}$ bands. The five highest frequency bands are all downshifted relative to $Ru(bpy)_3^{2+}$(1607/1600, 1563/1511, 1489/1452, 1320/1279, 1275/1232). The broadening that occurs with the 1279 cm-1 band is most likely due to mixing of a methylene carbon to ring carbon stretch with ring-stretching modes at the same frequency, creating another resonance enhanced vibrational mode. The

1173 cm^{-1} and 1027 cm^{-1} bands of $Ru(bpy)_3^{2+}$ are present at essentially the same wavenumbers for all spectra in this series. These are assigned to in plane C-H deformation mixed with symmetric in plane ring stretch, involving the distortion of the ring bonds simultaneously.

The X-ray structure of the n=4 complex[241] reveals the dihedral angle between the planes of the two pyridine rings to be 30.4°, reduced from 80° in free bipyridine, due to chelation constraints. While the structures of n=2 and n=3 have not been done, NMR data[241] indicates a progression of structural change from n=2 to n=4, with n=4 showing the most distorted structure. NMR data also point out the uniqueness of the n=1 complex, where the bite angle of the chelate is forced open by the short methylene bridge. These data support the X-ray data which give a bite angle of 80.1° and a dihedral angle of 7.1° from one pyridine to the other. The resonance Raman spectra for the n=2,3, and 4 complexes exemplify the change in structural variation of these complexes in absence of an X-ray structure.

The shifts in vibrational energy and the intensity changes present in the spectra of the annelated bipyridyl complexes (Figure IV-4) can be correlated to the vibrational spectrum of biphenyl.[249] For this comparison, the xy plane is the molecular plane of biphenyl with the x-axis oriented along the inter-ring bond. Biphenyl belongs to the point group D_{2h} when both phenyl rings are in the same plane. For the chelated bipyridine ligand, which has C_{2v} symmetry, xz is in the molecular plane, with the x-axis oriented along the inter-ring bond. A_g and B_{2u} in-plane modes of biphenyl will correlate as A_1 modes for molecules with C_{2v}

symmetry and therefore will probably be resonance enhanced within the MLCT band. As was shown previously,[249] several biphenyl frequencies are recognizable in the spectra of coordinated bipyridines. When twisting occurs along the inter-ring bond, the symmetry can drop to C_2 or lower. While some new resonance Raman enhanced bands should appear, comparison with biphenyl suggests that these out-of-plane modes would have vibrational frequencies lower than 1000 cm-1. Modes that are only weakly enhanced in the undistorted complexes may show significant enhancement as the complex distorts. Shifts in frequency which follow these intensity changes can be attributed to bonding changes produced by changes in the dihedral angle of the two pyridine rings and changes in the ways the normal modes are coupled. A list of the correlation of the vibrational modes of biphenyl with the complexes n=0,2,3,and 4 is given in Table 2. The similarity of the n=0 complex with the n=2 complex suggests only a small perturbation in the vibrational modes. It is clear, in comparison of the n=0 complex with the n=4 complex, that a large change in redistribution of intensities has occurred. While the most prominent band in the $Ru(bpy)_3^{2+}$ spectrum is at 1489 cm^{-1}, the n=4 complex shows three bands of similar intensity at 1567 cm^{-1} ,1468 cm^{-1} and 1297 cm^{-1}. The presence of these equal intensity bands show that there are several efficient Franck-Condon-Active vibrational modes for absorption. If the ground and excited state geometries are not too different, these normal modes would be those most efficient in coupling the ground state to the emissive excited state.

Table 2

Correlation of Ligand Modes for coordinated 2,2'-bpy and bridged 2,2'-bpy ligands with biphenyl modes (D_{2h} symmetry)

sym	biphenyl[a]	$Ru(bpy)_3^{2+}$	$Ru(bp\ n=2)_3^{2+}$	$Ru(bp\ n=3)_3^{2+}$	$Ru(bp\ n=4)_3^{2+}$
Ag	1612	1607	1589	1581	1576
B2u	1570	1563	1570	1569	1576
Ag	1507	1489	1480	1467	1468
B2u	1432	1448		1460 sh	1458
B2u	1383			1434	1432
$-(CH_2)n-$ C_3 ring			1336		1357
Ag	1285	1320	1318	1308	1297
B2u	1272	1275	1267	1290	1297
Ag	1190	1173	1181	1185	1187
B2u	1156	1109		1185	1171
B2u	1074	1067[b]			
Ag	1030	1041[b]			
Ag	1003	1027			1035

[a]From reference 254. [b]From reference 250. All frequencies in units of cm^{-1}.

The 77K emission spectra of the complexes (Figure IV-6) exhibit a maximum corresponding to the 0-0 transition and a shoulder for the 1-0 transition. The separation of these peaks in wavenumbers roughly corresponds to the frequencies of those normal modes which efficiently couple the excited state to the ground state. As can be seen, the shoulders become less well resolved as n increases, suggesting that more than one coupling frequency is present in these complexes. The equal distribution of maximum intensities in the resonance Raman spectrum of the n=3 and n=4 complexes corresponds with the trend of spectral broadening of the 77K emission spectra for these complexes as n increases.

The luminescence lifetime at room temperature and at 77K of the n=2 complex is notably similar to the n=0 ($Ru(bpy)_3^{2+}$) complex. This is not surprising since the n=2 complex is the least distorted of all the complexes in the series except for $Ru(bpy)_3^{2+}$ itself. For the n=3 complex at room temperature, the lifetime drops by ~30% and at 77K drops by ~50% relative to $Ru(bpy)_3^{2+}$. The room temperature emission for the n=3 complex is ~90% weaker than either the n=2 or the n=0 complex. For the n=4 complex, the weak emission intensity prevented reliable measurement of the luminescence lifetime at room temperature, yet at 77K a blue shifted emission and a luminescence lifetime comparable to n=3 was observed. The similarities of the n=1 and n=4 emission spectra have been previously described in the literature.[241]

The significant drop in quantum efficiency of emission going from n=2 to n=3 with only small changes in luminescence lifetime, points to a change in the

radiative rate constant for the n=3 complex in relation to n=2. For the n=4 complex. Evidence suggests that "acceptor modes" that depopulate the excited state non-radiatively are ring-stretching modes in the 1000-1700 cm-1 range.[82,252] Also, those frequencies most likely to be enhanced in the resonance Raman spectrum are these same modes involved in coupling the excited state to the ground state. Highly allowed (i.e. intense) vibrations within the MLCT absorption band are believed to act as the "acceptor" modes for radiationless deactivation. The resonance enhanced Raman spectra of the complexes indicate that twisting along the inter-ring bond leads to a redistribution of the vibrations in the 1000-1700 cm^{-1} region. A greater number of efficient modes for coupling of the ground and excited states exists, and radiationless deactivation is facilitated via these "acceptor" modes.

Terpyridyl complexes n=0,2,3,4

Examination of the resonance enhanced Raman vibrational spectra in Figure IV-5 shows a continuous trend with increasing methylene units from n=0 to n=4. The n=1 complex is not shown since this complex was not synthesized. Increases in the number of bands in the n=3 and n=4 spectrum and band broadening are obvious, probably due to the existence of more "acceptor" modes promoting radiationless deactivation. This explains why the n=4 complex is the weakest emitter of the series at 25°C and at 77K, and also why the emission is very broad for this complex. Figure IV-7 is an overlay of the normalized emission spectra at 77K for the terpyridyl complexes showing the increasing broadness of the spectra as n increases. Note also that the n=2, n=3

and n=4 complexes are all red shifted relative to the n=0 complex, which suggests that the methylene bridges distort the ligand appreciably.

Unlike the $Ru(bpy)_3^{2+}$ complex, the $Ru(terpy)_2^{2+}$ complex and most of its analogues do not luminesce strongly at room temperature.[255,257,259-261] This has been attributed to a more labile nature of the terpyridyl ligand structure[262] compared to $Ru(bpy)_3^{2+}$, and is also due to the weaker ligand field induced by terpy compared to bpy. The weaker induced ligand field may cause the metal-centered (dd) states to lie lower in the terpy complexes compared to complexes of bpy, and this can allow an increase in the Boltzmann distribution of these states. An increase in the population of these states is believed[56] to cause radiationless deactivation at higher temperatures, and thus less intense luminescence at room temperature is found. It is also speculated that one of the outer rings of terpy (whose Ru-N bond is longer and weaker than the Ru-N bond for the central pyridyl ring) can detach relatively easily and allow aquation of the metal center.[263] Furthermore, it is speculated that the terpy "bite" angle is not favorable and does not bond to the Ru(II) core with the same proficiency as does bpy in $Ru(bpy)_3^{2+}$.[263] As a result, the quantum yield of luminescence at room temperature for $Ru(terpy)_2^{2+}$ has been unmeasurable and its luminescence lifetime <0.005ns.[61] This is significantly different behavior from $Ru(bpy)_3^{2+}$ and can be attributed to the additional distortions in the molecule.

At 77K, the emission of $Ru(terpy)_2^{2+}$ shows that the ligand structure is significantly different from room temperature and luminescence is even stronger than $Ru(bpy)_3^{2+}$ at this temperature.[61,76] The quantum yield of luminescence of

$Ru(terpy)_2^{2+}$ at 77K has been measured to be 0.48, compared to 0.35 for $Ru(bpy)_3^{2+}$ under similar conditions. Also, the luminescence lifetime is 11.0 μs for $Ru(terpy)_2^{2+}$ compared to 5.3 μs for $Ru(bpy)_3^{2+}$. This is an indication that in rigid media the non-radiative pathway to deexcitation is inhibited by either the increased rigidity of the $Ru(terpy)_2^{2+}$ structure (which decreases the vibrational energy necessary to access the MC states), or due to the smaller population of the MC states which lead to radiationless deactivation.

By adding additional methylene bridges, more resonance enhanced modes are allowed, and a more efficient mode of coupling the ground and excited states results in decreased emission intensity.[82,84,252] This does not explain, however, why the n=2 complex shows a significantly weaker emission than the n=3 complex. In the n=2 complex, the steric interference of the hydrogens protruding into the opposing ligand cannot be overcome due to the lack of sufficient flexibility along the methylene bridges. This geometrical arrangement may induce a very facile pathway to non-radiative deexcitation in the n=2 complex. It may also prevent formation of the emissive excited state due to the inability of the terpy ligands to twist out of planarity in the n=2 complex. Also, several new vibrational bands appear for the n=2 complex, not present in $Ru(terpy)_2^{2+}$, which can account for the decrease in luminescence intensity via coupling of the ground and excited states. For the n=3 and n=4 complexes, the methylene bridges are sufficiently flexible to find a more suitable (less sterically hindered) geometry, yet this increased flexibility undoubtedly enhances new modes of vibration, which decreases luminescence intensity via

the "acceptor" mode theory. The emission spectra of the n=3 and n=4 complex appear flatter due to many new vibrational modes introduced by increasing the bridge length. The presence of at least 6 new bands in the n=2 spectrum relative to the n=0 complex supports the "acceptor" model of deactivation. The appearance of a new vibrational band in the n=2 spectrum at 831 cm^{-1} is interesting because no band is within 150 cm^{-1} of this in the n=0 spectrum. It is also present in the n=3 spectrum at 799 cm^{-1}. Although the "acceptor" mode theory[82,252] appears valid for vibrations between 1000-1700 cm-1(ring stretch modes), it remains to be seen if deactivation via this low frequency (~800cm^{-1}) mode is possible. It seems plausible that deactivation through this vibrational mode can lead to another type of radiationless deexcitation, yet this remains to be proven.

Chapter V. Binding of $Ru(bpy)_3^{2+}$ to Porous Vycor Glass

Part A. Temperature Dependence of Emission ϕ and τ

Introduction

Several attempts to characterize the excited state of $Ru(bpy)_3^{2+}$ using the temperature dependence of its photophysical properties have led to an understanding of the nature of its luminescence. At low temperature, intersystem crossing is independent of excitation wavelength, and believed to have a quantum efficiency of ~1.0.[46] The manifold of emissive states is believed to consist of three closely spaced levels which differ in energy by only 80 cm^{-1}. Below 120K, relaxation is described by the decay times of the individual levels, while above 120K, decay is best described as the average of the lifetimes of the individual levels in thermal equilibrium.[48,49,52,56]

In aqueous solution, relaxation to the emissive manifold via intersystem crossing is believed to occur with unit efficiency. Three modes of deactivation of the emissive state include a radiative pathway which is temperature independent, a non-radiative pathway which is temperature independent, and a temperature dependent non-radiative pathway.[56] The rate constants describing these pathways are k_r for the radiative pathway, k_{nr} for the non-radiative temperature independent pathway, and k_{nr} multiplied by a Boltzmann factor for the non-radiative temperature dependent pathway. Van Houten and Watts[56] have previously described the temperature dependence as due to the population of a thermally accessible d-d or ligand field manifold of states lying ca. 3600cm^{-1} above the emissive manifold of states. It is theorized that at T >

80°C, a non-radiative relaxation pathway via these d-d states becomes the dominant pathway, which can also explain some of the photochemistry that occurs with $Ru(bpy)_3^{2+}$ at higher temperatures.[56]

The model first proposed by Watts was applied to several other d^6 diimine complexes. In several systems, however, such as mixed-ligand complexes, this model did not fit. With these complexes, the energy proposed for the d-d state manifold does not parallel ligand field strength,[125,131,237] and several complexes do not show photolabilization even though it should occur with greater efficiency with these complexes due to a smaller energy of activation. These states which have significantly lower energies (300-800 cm^{-1}) above the emissive state are described as MLCT states in the literature,[125,131,132,237] and do not lead to photolabilization or photochemistry. Evidence for such states can be found in polarized emission spectra of $[Ru(bpy)_3](PF_6)_2$ which position a low lying MLCT state ($^2A_2$) ca. 800 cm^{-1} above the emissive manifold.[144]

The excited state properties of $Ru(bpy)_3^{2+}$ have been shown to be dependent on the local environment. Deviations from aqueous solution behavior can be attributed to this dependence, and several studies attempting to clarify the effect of a rigid support on the photophysics of $Ru(bpy)_3^{2+}$ have been undertaken.[59,146,264-269] Incorporation of $Ru(bpy)_3^{2+}$ into a cellulose acetate film decreases the energy needed to access the temperature dependent deactivation pathway to 810 cm^{-1}, compared to ~3600 cm^{-1} in aqueous solution.[59] The decrease in activation energy relative to aqueous

solution is described by a "matrix effect" where the rigidity of the matrix decreases the contribution of the vibrations necessary to access the d-d states.[132] As a result, non-radiative decay in this rigid medium is thought to occur via population of an MLCT state lying significantly lower in energy than the d-d states.[132]

Examining the emission properties of $Ru(bpy)_3^{2+}$ on porous Vycor glass (PVG) as a function of temperature in the 5-90°C range was undertaken to describe the excited state dynamics of the complex on this glass. Fits of the experimental data of luminescence lifetime vs. temperature and emission quantum yield vs. temperature for both aqueous solutions of $Ru(bpy)_3^{2+}$ and for $Ru(bpy)_3^{2+}$ adsorbed onto PVG yield a model which is consistent with the existence of a lower lying manifold of MLCT states ~1168 cm^{-1} above the emissive state and a higher lying ligand localized state located ~1117 cm^{-1} above the ^{1}MLCT absorptive state.

Results

Spectroscopic Properties

In the 300-600 nm region, the absorption spectra of $Ru(bpy)_3^{2+}$ in solution and on PVG are, within experimental error, the same. The spin-forbidden MLCT absorptions (460-520 nm) are not as well resolved as they are in single crystal spectra of $Ru(bpy)_3(PF_6)_2$.[65] The only apparent change in the absorption spectrum occurs with the 286 nm π-π^* band associated with bipyridine transitions. The ratio of the 286 nm band relative to the 452 nm band decreases from 6.3 in aqueous solution to 5.8 in the adsorbed complex.

No temperature dependence of the absorption spectrum is observed for either sample, yet the emission spectrum shows large changes in intensity for both. Small, but noticeable shifts in emission maxima are also evident.

Resonance enhanced Raman spectra with 457.9 nm excitation indicate that similar ground state vibrational modes are present for both samples, however the intensity of the 1492 cm^{-1} vibration is lower by ~25% when $Ru(bpy)_3^{2+}$ is adsorbed onto PVG.[195,196] This perturbation of the vibration at 1492 cm^{-1} is preserved as the temperature is raised to 85°C.

Emission Quantum Yields and Lifetime

At each temperature, the emission decay of a degassed aqueous sample of $Ru(bpy)_3^{2+}$ was recorded. The emission intensity was also measured under identical conditions, and τ and ϕ were tabulated (Table 1). Excellent agreement with data obtained by Van Houten and Watts[56] verifies accuracy of the equipment used for the measurements. The ratio of ϕ/τ (the emission quantum yield divided by the emission lifetime) was found to be independent of temperature within the range of 5-90°C.

For $Ru(bpy)_3^{2+}$ adsorbed onto PVG, the longer component of the emission decay and the quantum yield of luminescence are tabulated in Table 2. τ is shown to decrease with increasing temperature, but the quantum yields differ only when approaching the phase transitions of water. As a result, the ϕ_{em}/τ ratio declines with increasing temperature. Since ϕ_{em}/τ is $\eta_{isc}k_r$, the temperature dependence is radically different from solution behavior, where η_{isc}

Table 1

Measured and calculated τ,ϕ_{em} of $Ru(bpy)_3^{2+}$ in aqueous solution

T(°C)	τ_m [a]	τ_c [b]	ϕ_{em} [c]	ϕ_{calc} [d]	ϕ_{em}/τ_m [e]
5	720±25	721	0.052±.003	0.051	7.2×10^{-5}
15	690±21	677	0.048±.003	0.048	6.9×10^{-5}
25	600±20	616	0.042	0.043	7.0×10^{-5}
35	527±15	529	0.035±.002	0.037	6.7×10^{-5}
45	420±18	422	0.029±.002	0.030	6.9×10^{-5}
55	320±25	328	0.023±.002	0.023	7.1×10^{-5}
65	244±10	241	0.017±.001	0.017	7.0×10^{-5}
75	157±10	168	0.012±.001	0.012	7.6×10^{-5}
85	123±8	118	0.0091±.001	0.0083	7.3×10^{-5}

[a]Measured emission lifetimes of N_2 purged aqueous $Ru(bpy)_3^{2+}$ at $5 \leq T \leq 85$

[b]Calculated lifetimes from computer fit of equation 3.

[c]Measured emission quantum yields of N_2 purged $Ru(bpy)_3^{2+}$ at $5 \leq T \leq 85$

[d]Calculated lifetimes from computer fit of equation 6.

[e]Ratio of the measured emission quantum yield to the measured emission lifetime at $5 \leq T \leq 85$.

Table 2

Measured and calculated τ,ϕ_{em} of $Ru(bpy)_3^{2+}$ adsorbed onto PVG

T(°C)	τ_m [a]	τ_c [b]	ϕ_{em} [c]	ϕ_{calc} [d]	ϕ_{em}/τ_m [e]
5	1049±15	1044	0.078±.004	0.077	7.4×10^{-5}
15	892±15	891	0.063±.004	0.064	7.0×10^{-5}
25	754±16	776	0.050±.002	0.052	6.6×10^{-5}
35	680±30	674	0.041±.002	0.041	6.0×10^{-5}
45	591±6	585	0.032±.001	0.032	5.4×10^{-5}
55	518±7	519	0.026±.002	0.025	5.0×10^{-5}
65	468±16	461	0.021±.001	0.021	4.4×10^{-5}
75	412±20	408	0.018±.001	0.018	4.3×10^{-5}
85	346±14	366	0.015±.001	0.016	4.3×10^{-5}

[a]Measured emission lifetimes of N_2 purged aqueous $Ru(bpy)_3^{2+}$ at $5 \leq T \leq 85$

[b]Calculated lifetimes from computer fit of equation 3.

[c]Measured emission quantum yields of N_2 purged $Ru(bpy)_3^{2+}$ at $5 \leq T \leq 85$

[d]Calculated lifetimes from computer fit of equation 6.

[e]Ratio of the measured emission quantum yield to the measured emission lifetime at $5 \leq T \leq 85$

is temperature independent and assumed to be of unit efficiency, and k_r, by its very nature, must be temperature independent.

Attempts to explain this contrasting behavior between the solution and PVG samples by the presence of self-quenching interactions or impurity quenching were discounted due to the low concentrations used which minimize these effects. Self quenching can occur on PVG, but it was shown that loadings $\geq 10^{-4}$ mol/g were needed to achieve it. Since typical loadings were 10^{-6} mol/gram, self-quenching was ruled out. Self quenching due to mobility of the adsorbate is also not likely to contribute to this behavior since it was shown earlier that the emission polarization for $Ru(bpy)_3^{2+}$ on PVG is 0.16 in the temperature range 5-85°C, similar to $Ru(bpy)_3^{2+}$ in rigid glass at 77K,[47] and thus the complex is immobilized in the PVG matrix at room temperature.[196]

Photochemistry

At 83°C, 350 nm photolysis of degassed samples of a 0.1M HCl solution of 55μM $Ru(bpy)_3^{2+}$ decreases the absorbance at 450, with an increase at 370 nm. These results are similar to that found by Van Houten and Watts,[56] except the 500 nm shoulder they reported did not appear during the beginning of photolysis.

The experiments could not be duplicated on the glass since the concentration of H^+ necessary to capture the dissociated ligand would dissolve the matrix of the glass. A photoproduct was noticed, however, after photolysis of the PVG sample without H^+, and the increase of absorbance in the 510-520 nm region indicated the formation of a disproportionation product, not a ligand

labilization product.[207]

Discussion

When $Ru(bpy)_3^{2+}$ is adsorbed onto PVG, the absorption spectrum is almost identical to the aqueous solution spectrum. Between 5 and 90°C, all vibrations which are resonance enhanced do not differ in frequency by more than 1 cm^{-1} from solution spectra. A significant decline in the intensity of the most prominent 1492 cm^{-1} vibration (~25%) occurs upon adsorption onto PVG. The spectral evidence indicates that the structural differences occur in the excited state of $Ru(bpy)_3^{2+}$ when it is adsorbed onto PVG, rather than occur in the ground state.[195]

Resonance Raman band frequencies are related to ground state properties, while changes in the intensity of the bands indicate the efficiency of coupling the ground and excited states through molecular vibration.[84,208] In other words, vibrations which lead to the excited state conformation are expected to be strongly resonance enhanced. Therefore, molecular motions leading to the excited state conformation are inhibited when $Ru(bpy)_3^{2+}$ is adsorbed onto PVG, as evidenced by the decrease in the 1492 cm^{-1} vibration intensity, and the decrease of absorptivity in the π-π^* absorption band. These occurrences are attributed to "matrix effects"[132] imposed on $Ru(bpy)_3^{2+}$ as a result of adsorption.

In aqueous solution (N_2 purged), the temperature dependence of the lifetime and the quantum yield can be fit empirically to equations 1 and 2,

$$\tau(T) = (k_{0r} + k_{0nr} + k_{1nr} e^{-\Delta E/kT})^{-1} \quad [1]$$

$$\phi_{em}(T) = k_{0r}\,\tau \quad [2]$$

where k_{0r} and k_{0nr} are the rate constants for the radiative and non-radiative decays of the emissive MLCT manifold of states.[56] ΔE and k_{1nr} are parameters describing the activation energy needed to populate the higher lying d-d states, and the associated rate constant of non-radiative decay from these states, respectively. Fitting of our solution data with equations 1 and 2 yielded parameters that are in excellent agreement with those results published by Van Houten and Watts previously.[56]

The lifetime data collected for the adsorbed $Ru(bpy)_3^{2+}$ could be fit using the equation

$$\tau(T) = (k_0 + k_1 e^{-\Delta E/kT})^{-1} \quad [3]$$

where $k_0 = k_{0r} + k_{0nr}$ and $k_1 = k_{1nr}$.[132] The lifetime data could also fit the more general expression which incorporates a second Boltzmann factor.[132]

$$\tau(T) = [(k_0 + k_1 e^{-\Delta E/kT})^{-1}/(1 + k_1 e^{-\Delta E/kT})]^{-1} \quad [4]$$

It was later shown that this fitting equation is different than the previous one only if $\Delta E \leq 3kT$. Calculated values of τ at each measured T obtained from computer fits are given in Table 1, which for the lifetime data, are in excellent agreement with the measured temperature dependence.

Solution data indicate a d-d state ~3600 cm^{-1} above the emissive state, which leads to substitutional photochemistry and/or non-radiative decay. Results for $Ru(bpy)_3^{2+}$ on PVG suggest that population of a lower state only ~1168 cm^{-1} above the emissive state is responsible for the observed

temperature dependence.

Using the values obtained from the computer fit for $Ru(bpy)_3^{2+}$ on PVG, the temperature dependence of quantum yield was calculated and found to be vastly different than the measured values. The aqueous solution model could fit the temperature dependence of luminescence lifetime, but not the temperature dependence of emission quantum yield.

To resolve this dilemma, a new model was proposed.[256] Since the quantum yield of emission is described by

$$\phi = \eta_{isc} k_r \tau \qquad [5]$$

where η_{isc} is the efficiency of intersystem crossing to the emissive states, k_r is the radiative rate constant and τ is the measured luminescence lifetime. Because of the the evidence that the ratio of ϕ_{em}/τ is temperature dependent, a unit efficiency of the intersystem crossing to the emissive state cannot be assumed. Therefore, population of a state or states in thermal equilibrium with the ^{1}MLCT state (which gives rise to the 452nm absorption band) can create a new pathway for deactivation to the ground state, which does not pass through the emissive state. (See Figure V-1.) Applying the fitting equation

$$\phi_{em} = \frac{k_{isc}}{k_{isc} + k_{2nr} e^{(-\Delta E2/kT)}} \quad \frac{k_{0r}}{k_{0r} + k_{0nr} + k_{1nr} e^{(-\Delta E1/kT)}} \qquad [6]$$

generates values for the parameters $\Delta E1$, $\Delta E2$, k_{0r}, k_{0nr}, k_{1nr} and k_{2nr}.[256] $\Delta E1$ is the energy required to access the states lying above the emissive state, $\Delta E2$ is the energy required to access the states lying above the absorptive state,and

k_{0r}, k_{0nr}, k_{1nr} and k_{2nr} are rate constants describing the radiative and non-radiative processes described in Figure V-1. The values found are reported in Table 3. It is important to note that the values obtained for this fit are within experimental error of the values obtained for the temperature dependence of the lifetime fit. This agreement gives confidence to the proposed model.

According to the energy gap law,[230] decay from the ^{1}MLCT lying above the absorptive state to the ground state would be slow due to the large energy

Table 3

Parameters generated from fit to proposed model[256]

Parameter	Fit Using Lifetime Data	Fit Using Quantum Yield Data
$k_{0r}+k_{0nr}$	$3.30\pm0.6 \times 10^5$ s^{-1}	$2.56\pm0.5 \times 10^5$ s^{-1}
k_{1nr}	$3.18\pm0.5 \times 10^8$ s^{-1}	$2.36\pm0.8 \times 10^8$ s^{-1}
ΔE_1	1168±160 cm^{-1}	1122±100 cm^{-1}
ΔE_2	*	1117±70 cm^{-1}

* The existence of a higher lying ^{1}MLCT is not necessary for fitting the lifetime data to the proposed model. Addition of a Boltzmann term describing this ^{1}MLCT state does not significantly alter the fit of the lifetime data, but explains the temperature dependence of the quantum yield data.

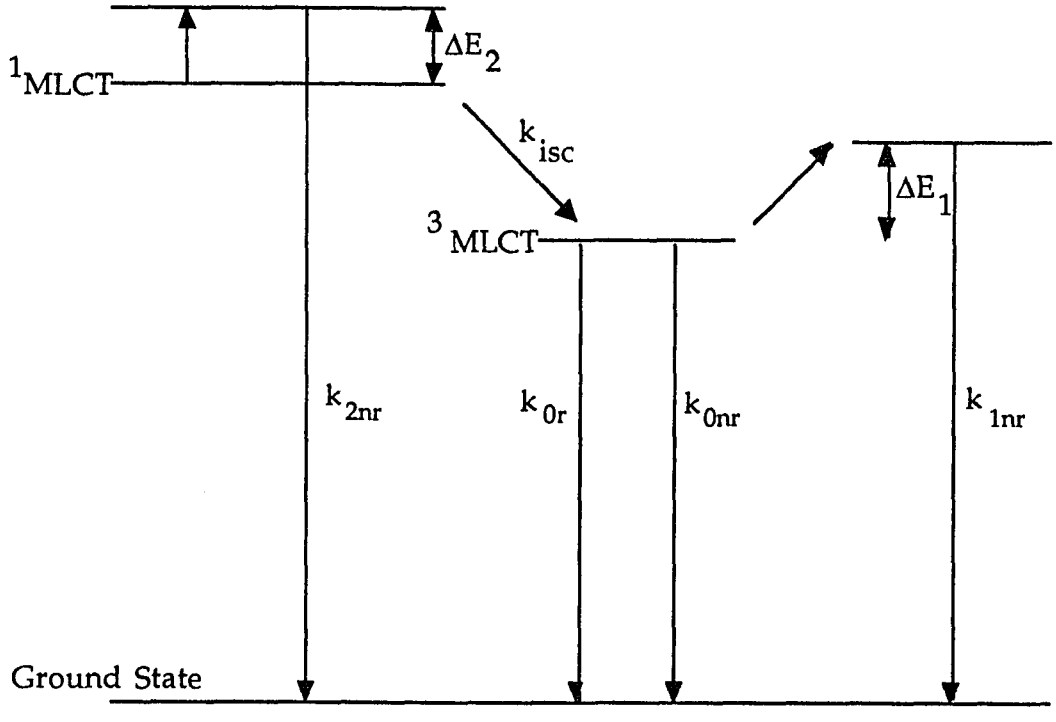

Figure V-1. The proposed model for excited state decay processes of $Ru(bpy)_3^{2+}$ (ads).

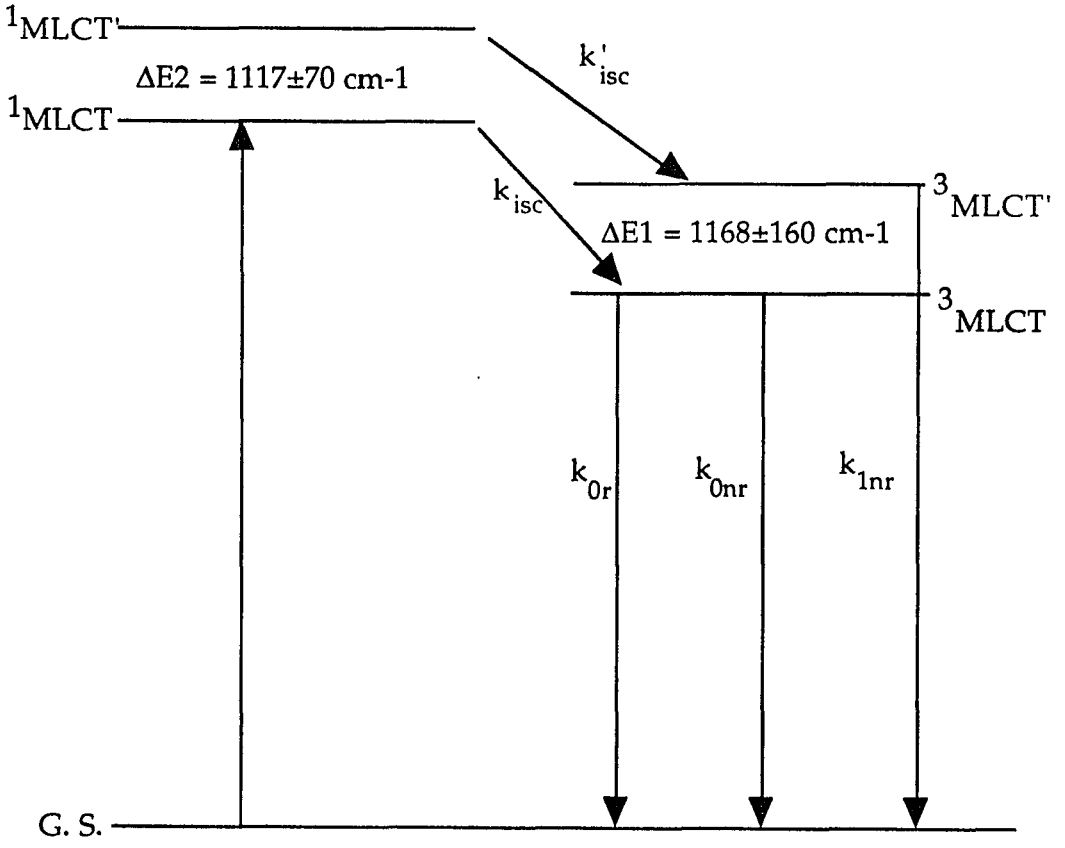

Figure V-2 The modified excited state energy level diagram for $Ru(bpy)_3^{2+}$(ads)

gap. Decay through the ^{3}MLCT' lying above the emissive state would be more facile and therefore it is reasonable to propose a modified model for the energy levels of $Ru(bpy)_3^{2+}$ adsorbed on PVG which is still consistent with the data. This is portrayed in Figure V-2.

Due to the much smaller energy gap found for ΔE_1 when $Ru(bpy)_3^{2+}$ is adsorbed onto PVG, a ^{3}MLCT state rather than a d-d state lying above the emissive state is proposed to be the thermally populated state. Since there is a lack of substitutional photochemistry in the matrix, transitions to the d-d states are prevented by the existence of this lower lying non-emissive ^{3}MLCT state. "Matrix effects" are believed to play a role in the inability to populate the higher d-d states.[132]

Although the calculated values of k_1 and ΔE_1 for the $Ru(bpy)_3^{2+}$ on PVG are different than those values found in solution, they are quite similar to data found for $Ru(bpy)_3^{2+}$ in a cellulose acetate matrix.[59]

Summary

The excited state dynamics of $Ru(bpy)_3^{2+}$ can be represented by the following scheme[256]

GS ---> ^{1}MLCT

^{1}MLCT ----> ^{3}MLCT --->GS + hν or GS + heat

^{3}MLCT ----> ^{3}MLCT' ---->GS + heat

^{1}MLCT ----> ^{1}MLCT' ----> ^{3}MLCT' ----> GS + heat

Using this scheme, and applying the proposed model, the temperature dependence of luminescence lifetime and quantum yield of $Ru(bpy)_3^{2+}$ adsorbed onto PVG can be rationalized.

Part B. Temperature Dependence of the Photoinduced Disproportionation of $Ru(bpy)_3^{2+}$ on Porous Vycor Glass

The photophysical and photochemical properties of $Ru(bpy)_3^{2+}$ bound to porous Vycor glass have been determined as a function of temperature. In the 5-95 °C range, the spectroscopic properties of the adsorbed complex are equivalent to aqueous solution spectra at the same temperature. The emission lifetime of the adsorbed complex declines with increasing temperature, but the emission polarization ratio is independent of temperature and equivalent to that measured in hydrocarbon glasses at 77 K. Photolysis of the adsorbed complex leads to disproportionation, and the quantum yield of the reaction increases with increasing temperature. The latter is interpreted within a surface conduction model where an Arrhenius plot of the quantum yield data indicates that the barrier to electron transport on the glass surface is 6.87±0.11 kcal/mol.

Introduction

The use of heterogeneous media to control the photoredox chemistry of $Ru(bpy)_3^{2+}$ has received considerable attention.[258,270-275] There is now a growing body of evidence that hydroxylated silicas and cellulose films promote charge separation. Thomas and co-workers, for example, report that incorporating $Ru(bpy)_3^{2+}$ into silica colloids enhances electron transfer between the complex and methylviologen, MV^{2+},[175] while photolysis of $Ru(bpy)_3^{2+}$ adsorbed onto "dry" cellulose leads to disproportionation.[183] We find that 450-nm photolysis of $Ru(bpy)_3^{2+}$ adsorbed onto Corning's code 7930 porous Vycor glass, PVG, leads to disproportionation[207] and, with coadsorbed MV^{2+}, a net

formation MV^+ in the absence of external electron donors.[276] PVG is a porous, transparent glass that, like silica gel, possesses a hydroxylated surface.[207,277-279] The band gap in SiO_2 is 6.9 eV[194] while the excitation energies used in the above experiments are <5 eV.[207,276] Therefore, unlike reactions on semiconductive metal oxides, where charge separation occurs via population of a conduction band, the reactions on hydroxylated silica surfaces must involve a different mechanism of charge separation.[207]

$Ru(bpy)_3^{2+}$ cation exchanges onto the glass surface, and emission polarization measurements indicate that the reactions occur between a fixed array of immobilized adsorbates.[195,207] Flash photolysis data confirm the presence of a photodetached electron, and quantum yield measurements indicate that disproportionation depends on the mean separation between the redox partners.[207,276] These data led to the postulation of a surface conduction model, where biphotonic excitation of (ads) (an adsorbed species) leads to ionization

$$Ru(bpy)_3^{2+}(ads) + 2h\nu \text{ ---> } Ru(bpy)_3^{3+}(ads) + e^- \quad [1]$$

Surface conduction of the photodetached e^- is thought to involve the population of intermediate surface acceptor sites, S

$$e^- + S \text{ ---> } S^- \quad [2]$$

These are thought to be shallow energy wells from which the photo-detached electron can be thermally activated but, nevertheless, present an energy barrier, albeit slight, that prevents immediate recombination.[207] Net electron transfer occurs when the redox partners are within the electron

migration distance, 50±10 Å, and when this distance exceeds that for the thermal back-reaction, < 13 Å in the disproportionation reaction, the redox products are stable.[207]

Surface conduction implies that the quantum yield of electron transfer on the glass surface will exhibit an activation energy that reflects the average depth of the proposed surface acceptor sites. In this section, the results of a study of the temperature dependence of the photoinduced disproportionation of $Ru(bpy)_3^{2+}$(ads) are given. To determine the effect of temperature on the mobility of the adsorbed complex, its photophysical properties have been measured at temperatures between 5 and 90 °C.

Results and Discussion

Thermal gravimetric analysis and diffuse reflectance FTIR spectra of calcined PVG indicate a surface composed of free and associated silanol groups and small amounts of chemisorbed water.[277-279] $Ru(bpy)_3^{2+}$ cation exchanges onto this surface, and optical density measurements indicate a uniform distribution of the complex on the glass surface.[207] Regardless of the number of moles adsorbed, however, $Ru(bpy)_3^{2+}$(ads) penetrates no more than 0.45± 0.05 mm and uniformly impregnates volumes of glass defined by the penetration depth and the area of a particular side.[207,253] The interior of the glass, ca. 80% of the total volume, remains vacant.[253]

With the exception of a slight broadening of the 452-nm MLCT transition at higher temperatures, UV-visible spectra of room temperature, 22±1 °C, aqueous solutions of $Ru(bpy)_3^{2+}$ are equivalent to spectra of 85 °C solutions.

Similar results are found with the adsorbed complex. Increasing the temperature causes a slight broadening of the MLCT absorption, but otherwise the spectrum of $Ru(bpy)_3^{2+}$(ads) at 80 °C is the same, within experimental error, as that at room temperature. At both temperatures, spectra of $Ru(bpy)_3^{2+}$(ads) agree in band maximum, relative extinction coefficient, and band half-width with the corresponding aqueous solution spectra.[195] Absolute extinction coefficients are 10-15% larger than the corresponding solution values,[195] although as previously noted the difference is due in part to differences in light scattering and/or penetration depth.[195,207]

Resonance Raman spectra of aqueous solutions of $Ru(bpy)_3^{2+}$ are also independent of temperature. In the 1000-1600 cm^{-1} bipyridine region, the seven-band pattern of a room-temperature solution is equivalent in band frequency and relative intensity to that of a 95 °C solution. However, these spectra differ from that of $Ru(bpy)_3^{2+}$(ads). At 22±1 and 80±1 °C, the seven band maxima of $Ru(bpy)_3^{2+}$(ads) are within 1 cm^{-1} of those in the aqueous solution spectrum, but both spectra show a significant decline ca. 25% in the relative intensity of the prominent 1492 cm^{-1} band.[195]

Resonant Raman frequencies are a ground-state property, whereas changes in relative intensity are related to the nuclear displacements that distort the ground-state configuration to that of the excited state, i.e., the origin shift.[208] At room temperature and 80 °C, therefore, the ground state of the adsorbed complex is equivalent to that in aqueous solution, whereas the structures of the excited states appear to differ in the two media.[195] With the exception of

apparently less structural distortion of the MLCT state, however, the spectral data offer no indication that increasing the temperature causes any significant changes in the adsorbed complex.

The similarity of the Vycor and aqueous solution spectra belies the strength of the adsorbate-adsorbent interaction. A strong adsorbate-adsorbent interaction on other supports is signaled by changes in either absorption or emission spectra of the complex. Van Damme and co-workers, for example, suggest that molecular distortions caused by intercalating $Ru(bpy)_3^{2+}$ into hectorite, a magnesium silicate, reduce the intensity of the bpy π-π^* transition relative to the intensity of the MLCT transition from 6:1 in aqueous solution to 2:1 in the silicate.[178,281] Wheeler and Thomas report a 27-nm blue shift in the emission maximum and a ca. 6-fold increase in emission quantum yield when $Ru(bpy)_3^{2+}$ is incorporated in polymerized silica.[175] In spite of the absence of a spectral change when $Ru(bpy)_3^{2+}$ cation exchanges onto the PVG, emission polarization suggests a relatively strong interaction.

Polarization ratios, P, for $Ru(bpy)_3^{2+}$(ads) at 22±1 °C are, within experimental error, the same as those measured in rigid EPA solutions at 77 K when excited with 400-, 465-, and 510-nm light.[195] (P~0.16) Furthermore, with 465-nm excitation, P is independent of temperature over the 5-90 °C range. Since emission polarization precludes rotational motion, and it is difficult to envision translational motion without concurrent rotational motion, emission polarization implies no $Ru(bpy)_3^{2+}$ (ads) translational mobility. Of course, the latter refers only to mobility during the excited-state lifetime. Yet, there is no

indication of a macroscopic redistribution of the adsorbed complex. Even after 8 h in boiling water or several months in room-temperature water, the distribution of $Ru(bpy)_3^{2+}$ (ads) in samples containing (5.0±0.2) x 10^{-7} mol/g is, within experimental error, the same as that determined immediately after preparation.[253] Emission polarization and the absence of macroscopic redistribution indicate that $Ru(bpy)_3^{2+}$ cation exchanges onto a specific site, and the electrostatic interaction that binds the complex to that site is sufficient to prevent exchange with other sites. Therefore, changes in the disproportionation quantum yield that occur in the 5-90 °C range are not biased by increases in adsorbate mobility.[207]

Difference spectra recorded during 457.9-nm photolysis of degassed samples containing (1.0±0.1) x 10^{-6} mol of $Ru(bpy)_3^{2+}$ (ads)/g show a decline in absorbance at 452 nm, characteristic of $Ru(bpy)_3^{2+}$(ads), and concurrent increases at 350 and 510 nm characteristic of $[Ru(bpy)_2(bpy)^-)]^+$(ads).[207] Spectroscopically, the reaction pathway is independent of temperature, but the quantum yield of $[Ru(bpy)_2(bpy^-)]^+$(ads) formation, $\phi_{Ru(I)}$ is temperature dependent. Four independent values of $\phi_{Ru(I)}$ at the different temperatures were determined for each sample with a 457.9-nm excitation power of 10 mW. The values of $\phi_{Ru(I)}$ (Table 4), calculated from the initial increase in absorbance at 510 nm and the average absorbance at the excitation wavelength, 457.9 nm, show a ca. 6-fold increase when the temperature is raised from 0 to 65 °C.

In keeping with the previous notation, [207] the quantum yield of disproportionation, i.e., $\phi_{Ru(I)}$ is given by

Table 4

Values of $Ru(bpy)_3^{2+}$(ads) Emission Lifetimes and Observed and Corrected Values of $\phi_{Ru(I)}$ at Different Temperatures

T °C	τ, ns	τ_T/τ_0	$\phi_{Ru(I)}$	$\phi_{Ru(I)}$ (corr.)
0	845±45	1.00±0.05	0.49±0.05	0.49±0.02
22	675±30	1.25±0.06	1.0±0.1	1.25±0.06
45	505±45	1.67±0.13	1.63±0.2	2.72±0.21
65	406±33	2.08±0.16	2.43±0.3	5.05±0.39

$$\phi_{RuI} = \phi_P f_{ej} k_7/(k_7 + k_8) \quad [3]$$

where ϕ_P and f_{ej} represent the quantum efficiency of photoionization and the fraction of photodetached electrons ejected from the surface acceptor sites, respectively. k_7 and k_8 are the rate constants for $[Ru(bpy)_2(bpy^-)]^+$(ads) formation

$$e^- + Ru(bpy)_3^{2+}(ads) \text{ ----> } [Ru(bpy)_2(bpy^-)]^+(ads) \quad [4]$$

and recombination

$$e^- + Ru(bpy)_3^{3+}(ads) \text{ ----> } [Ru(bpy)_3^{2+}(ads)]^* \quad [5]$$

In aqueous solution, recombination leads to population of the MLCT state with essentially unitary efficiency.[280] Since the spectrum of e^- on PVG is transient at all temperatures, f_{ej} is taken to be unity[207] and independent of temperature.

$[Ru(bpy)_2(bpy^-)]^+$(ads) formation exhibits a second-order dependence on excitation intensity.[207] Since the luminescent MLCT state of $Ru(bpy)_3^{2+}$ absorbs at 450 nm ($\varepsilon_{450} \sim 5 \times 10^3\ M^{-1}\,cm^{-1}$),[284] photoionization of $Ru(bpy)_3^{2+}$ (ads) is

taken to be a sequential biphotonic process.[207] The first photon generates the MLCT state which then absorbs the second photon. Therefore, ϕ_P in eq 3 is the product

$$\phi_P = \phi_{isc} P_{MLCT} \phi_{ion} \quad [6]$$

ϕ_{isc}, P_{MLCT} and ϕ_{ion} represent the quantum yield of intersystem crossing, the probability of secondary excitation, and the quantum yield of ionization following absorption of the second photon.

Demas and Crosby have shown that ϕ_{isc} is independent of excitation wavelength and unity, within experimental error, at both 77K and room temperature.[46] Van Houten and Watts report that the $Ru(bpy)_3^{2+}$ emission quantum yield in degassed aqueous solution decreases from 0.049±0.003 at 5 °C to 0.0075±0.0006 at 90 °C, while the lifetime decreases from 730±39 ns at 5 °C to 100±8 ns at 90 °C.[56] Since the ratio of quantum yields at the two temperatures, 6.53±0.20, is essentially the same as the ratio of lifetimes, 7.2±0.2, the decline in emission quantum yield is due principally to an increase in the nonradiative rate. Consequently, ϕ_{isc} is taken to be independent of temperature and essentially unity. ϕ_{ion} is the quantum yield for ionization following absorption of the second photon. Since kT at 90 °C, 0.16 eV it is considerably smaller than the excitation energy required for ionization, $2.2 < E < 5.0$ eV,[207] ϕ_{ion} is taken to be independent of temperature in the 5-65 °C range examined in these experiments.

P_{MLCT} represents the probability for secondary excitation of the MLCT state. Since the absorption and emission spectra of $Ru(bpy)_3^{2+}$(ads) are

independent of temperature, we assume that the absorption cross section for the MLCT state is also temperature independent. Therefore, the temperature dependence of P_{MLCT} reflects the temperature dependence of MLCT state lifetime, τ. The emission lifetime of thoroughly degassed samples of $Ru(bpy)_3^{2+}$(ads) decreases from 820±20 ns at 5 °C to 320±16 ns at 85 °C. The decrease in lifetime with increasing temperature is not due to self-quenching. The lack of change in the emission polarization ratio over the entire temperature range precludes a sudden increase in adsorbate mobility. With the immobilized complex, self-quenching occurs when the adsorbates are within an effective quenching volume, which requires $\geq 1.2 \times 10^{-5}$ mol/g.[195] Rather, the change in emission lifetime with increasing temperature is due principally to changes in the rates of the radiative and nonradiative processes.

The probability of secondary excitation increases with increasing lifetime of the MLCT state. Therefore, the quantum yield of $[Ru(bpy)_2(bpy^-)]^+$(ads) formation is written as

$$\phi_{RuI} = \phi_{isc} P_{MLCT} (\tau_T/\tau_0) \phi_{ion} k_7/(k_7+k_8) \qquad [7]$$

where τ_T/τ_0 is the ratio of the lifetime at a temperature T relative to that at 0 °C. The values of ϕ_{RuI} corrected for the temperature dependence of the MLCT state lifetime according to eq 7, ϕ_{RuI}(corr), are listed in Table 1. An Arrhenius plot of the log of these values vs 1/T (Figure V-3) is linear, and the slope yields an activation energy of 6.87±0.11 kcal/mol.

The quantum yield of $[Ru(bpy)_2(bpy^-)]^+$(ads) formation reflects photoionization of $Ru(bpy)_3^{2+}$(ads), electron transport on the glass surface, and

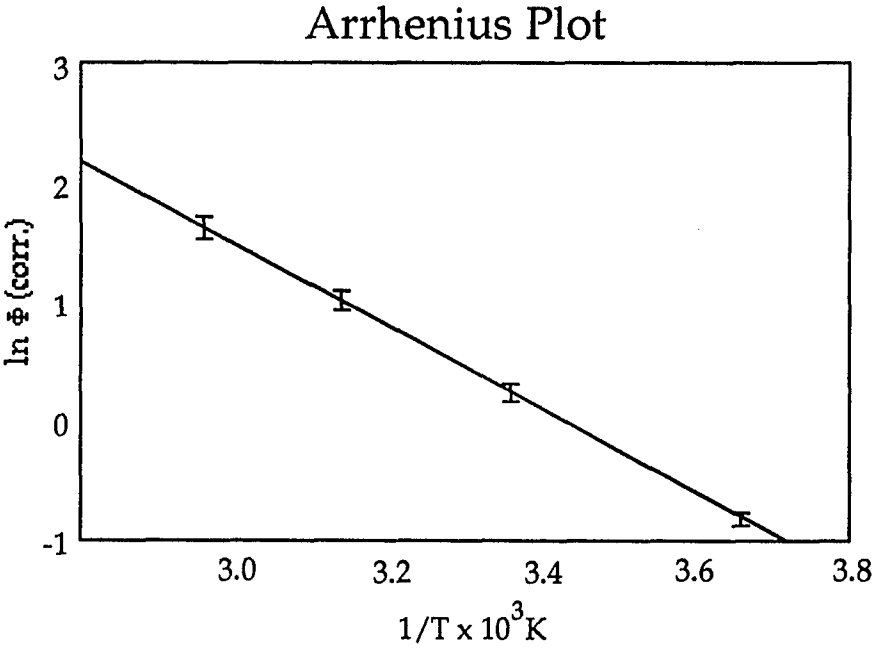

Figure V-3 Arrhenius plot of corrected ϕ_{RuI} vs. 1/T

reduction of a second $Ru(bpy)_3^{2+}$(ads) (eq 4) that lies within the electron migration distance.[207] As described above, ϕ_{isc} and ϕ_{ion} are taken to be independent of temperature in the 5-95 °C range. Meisel, Matheson, and Rabani report that the rate constant for reduction of $Ru(bpy)_3^{2+}$ by the hydrated electron in aqueous solution is 6.0×10^{10} M^{-1} s^{-1},[282] which is in close agreement with the value 8.0×10^{10} M^{-1} s^{-1}, reported by Baxendale and Fiti.[283] Both values suggest a reaction unfettered by an activation barrier. Furthermore, assuming that the reduction potential of the electron on the glass is equivalent to that in aqueous solution, 2.7 eV,[284,285] since its optical spectrum is essentially equivalent to that in aqueous solution,[207,286] reaction 4 has a net driving force of ca. 1.5 eV, while that for reaction 5 is ca. 4 eV. In view of these exothermicities, we assume that reactions 4 and 5 possess little or no activation barriers, and their respective rate constants, k_7 and k_8, are essentially independent of temperature. Consequently, the measured activation energy, 6.87±0.11 kcal/mol, is attributed principally to barriers encountered during electron transport on the glass surface. Within the proposed surface conduction model,[207] this suggests that the average depth of the surface acceptor site(s) is ≤6.87±0.11 kcal/mol.

Conclusion

Emission polarization and the lack of macroscopic redistribution of $Ru(bpy)_3^{2+}$ on PVG establishes that the electrostatic interaction binding $Ru(bpy)_3^{2+}$ to PVG is of sufficient strength to prevent adsorbate mobility in the 5-90 °C range. The quantum yield of $[Ru(bpy)_2(bpy^-)]^+$(ads) formation at each

temperature, corrected for the temperature dependence of the MLCT state lifetime, increases with increasing temperature and, within the proposed surface conduction model, suggest that the average depth of the surface acceptor site(s) is $\leq 6.87 \pm 0.11$ kcal/mol.

Chapter VI. DNA-Drug interactions (dyes, antibiotics, and metal complexes).

Introduction

DNA and RNA, the molecules of life, have the ability to interact with certain classes of molecules, including drugs, carcinogens, mutagens, complex ions, and organic dyes.[287-290] These types of molecules contain extended heterocyclic aromatic chromophores, and most if not all possess planar portions of the molecule which interact with the nucleic acid double helix.[290] Judging by the major role which DNA and RNA plays in biological replication and protein biosynthesis, it is not surprising that interactions of nucleic acids with molecules such as these alter cell metabolism, decrease cell growth, and cause mutations and cancer.[289]

Three general types of laboratory studies are carried out concerning DNA-drug interactions. They are:

1) chemical modification of DNA (e.g. modifying a base pair).[291]
2) covalent linkage of drugs to DNA.[292-294]
3) binding of small molecules to DNA non-covalently through electrostatic, intercalative, and other types of interactions.[295]

This discussion will deal primarily with the third class of studies, where interaction with DNA via non-covalent (and reversible) processes are dominant.

Nucleic Acid Structure

Since Watson and Crick deduced the structure of B-DNA,[296,297] an onslaught of research resulted in the determination of several other conformations of DNA besides the B-form. The structure of the nucleic acids,

DNA and RNA, vary according to solvent conditions and chemical modification. Some of the more common types of structures, the A- B- and Z- types are shown in Figure VI-1. It has been shown that the binding of drugs to DNA is sensitive to the DNA conformation,[26] and therefore the way in which the drug interacts with DNA can be an indication of the type of DNA present.[3,13] This differential binding to various conformations of DNA can be exploited in several technologies, including recombinant DNA technology and cancer research.

From Figure VI-2, the structure of a portion of a strand of B-DNA is given. The yellow atoms represent phosphorus, the red atoms oxygen, the blue atoms nitrogen, and the gray atoms carbon (Hydrogen atoms not shown). The structure is of a double helix composed of an alternating sequence of sugar and phosphate forming the backbone of the structure. The ribose or deoxyribose sugars (5 carbon sugars) are bonded to the phosphates via phosphodiester linkages at the 5' position of one sugar and the 3' position on another sugar. The sugar is substituted at the C1' position and a nitrogenous base is covalently bonded there, aligned perpendicular to the helical axis. This repeating unit (sugar-phosphate-nitrogenous base) is referred to as a nucleotide. (Figure VI-3) Paired to a complementary base via hydrogen bonding interactions, the structure essentially consists of two sugar-phosphate backbones wrapped around each other forming the double helix.

Several aspects of the structure of B-DNA should be noted. First of all, the outer region of the molecule is hydrophilic and negatively charged, due to the presence of the phosphate moieties. Second, due to hydrogen bonding

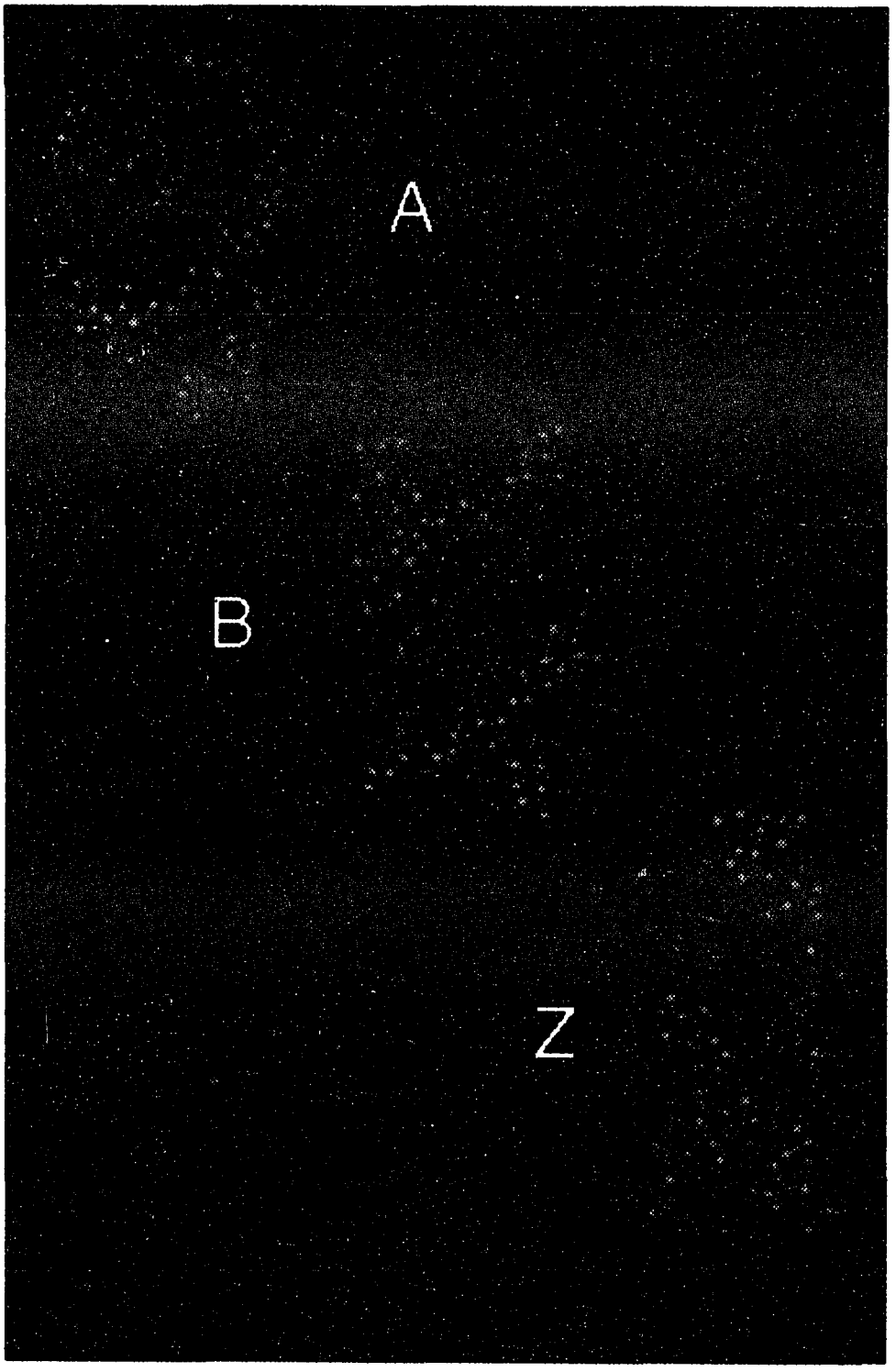

Figure VI-1. Stuctures of A-, B- and Z-form DNA. The sugar-phosphate backbone is green and the base pairs are purple.

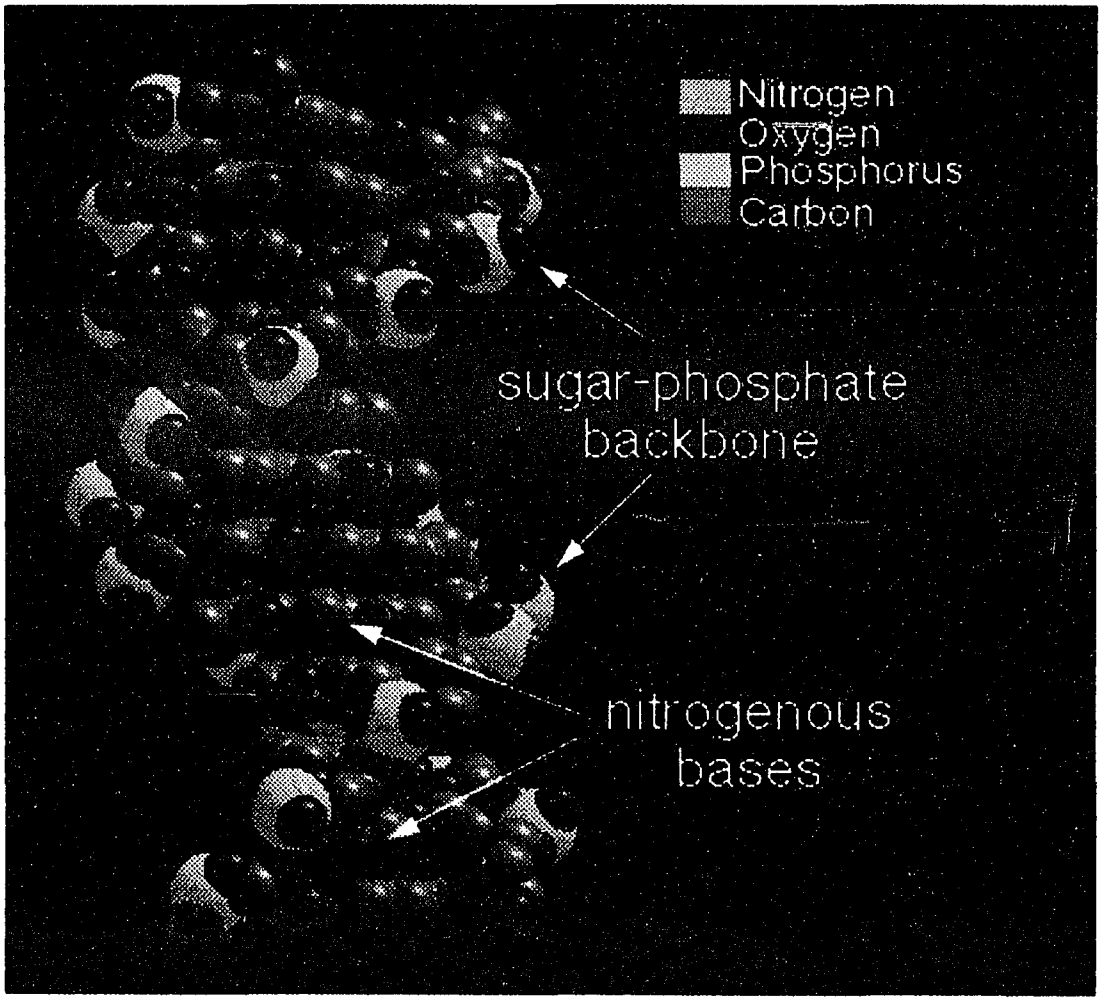

Figure VI-2. Detailed view of B-form DNA. Atoms are as indicated. Image created with MacMolecule-University of Arizona.

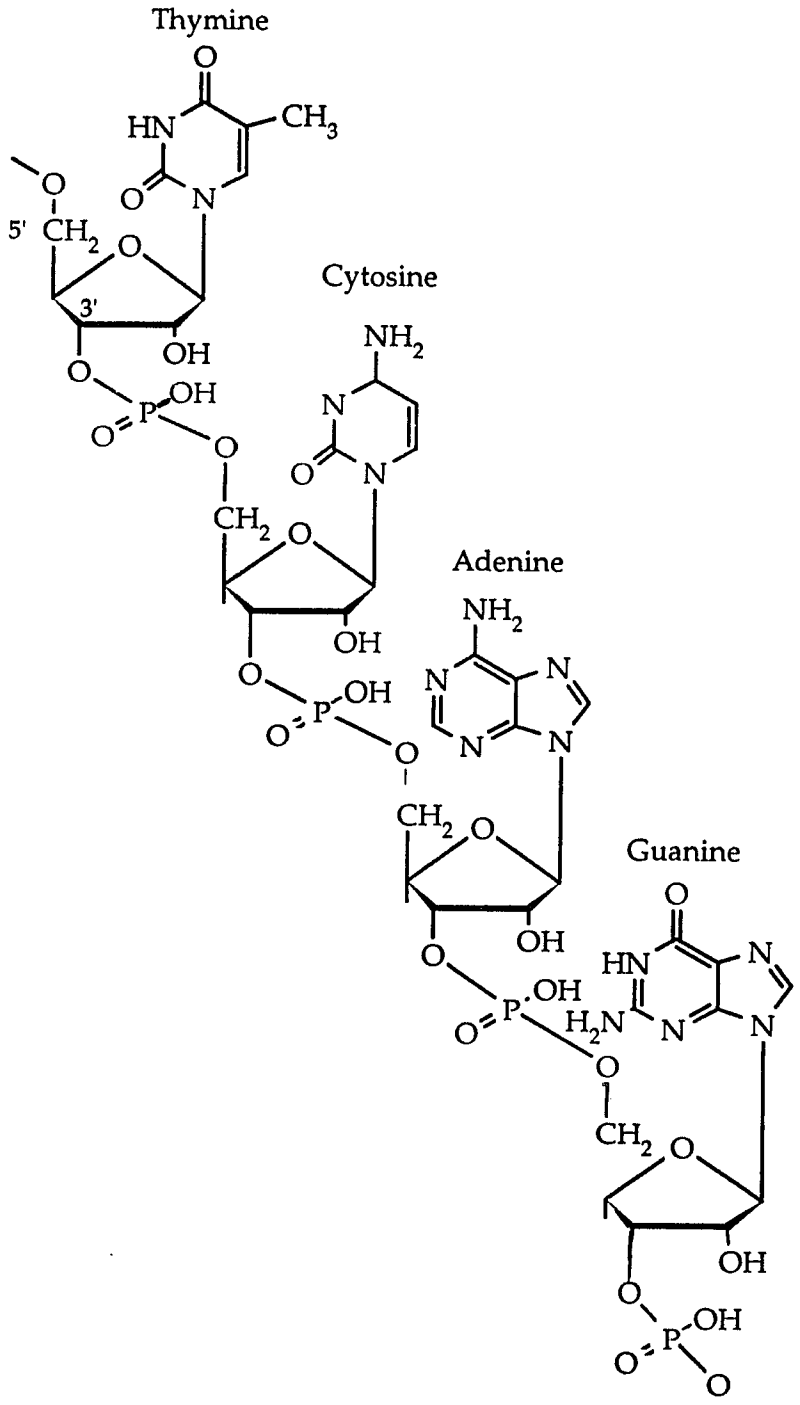

Figure VI-3. Nucleotides

considerations, adenine bases will pair only with thymine bases (uracil bases in RNA), and guanine will only pair with cytosine. (Figure VI-4) This aspect is what makes DNA a "template" molecule and suggests how complimentary base pairing can effect replication and repair of DNA. Thirdly, the inner region of the macromolecule is mainly hydrophobic due to the presence of the aromatic heterocyclic base pairs in this location. Fourthly, in B-type DNA, a "major" groove and a "minor" groove are formed as a consequence of the way the nucleotides are spatially arranged. The major groove is known to be deeper and wider than the corresponding minor groove. The depths and widths of these grooves change with DNA conformation as well as DNA sequence. Figure VI-5 depicts the two different grooves in B-DNA.

Lengths of nucleic acid may vary from a few base pairs in synthetic oligonucleotides to several million in native DNA. The diameter of the helix in B-DNA is known to be ~1.8nm, and the adjacent bases are stacked so that the distance from one base pair to the next is ~0.34nm. Each base pair is rotated by ~36° , thus approximately 10 base pairs correspond to a full helical turn in B-DNA. DNA and RNA can be found in nature as linear or circular, and have been synthesized as either type.

Conformations of DNA

Although DNA is often depicted by the classical Watson-Crick description,[296,297] several different conformations can exist in local regions along the strand or along its entire length. Some local regions of DNA in addition to the A and Z forms (Figure VI-1) that exist are depicted in Figure VI-6.

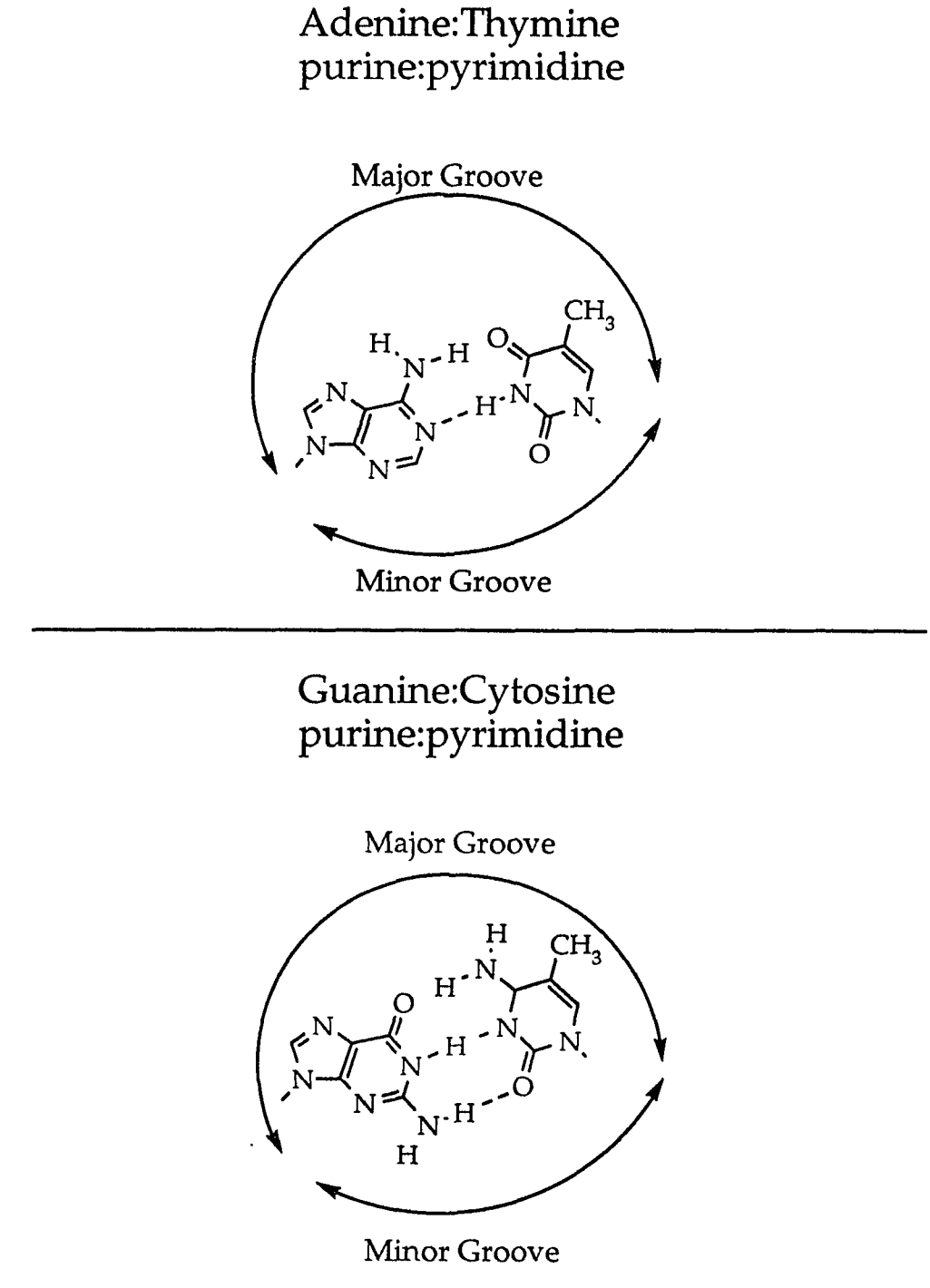

Figure VI-4. Watson-Crick base pairing in DNA.

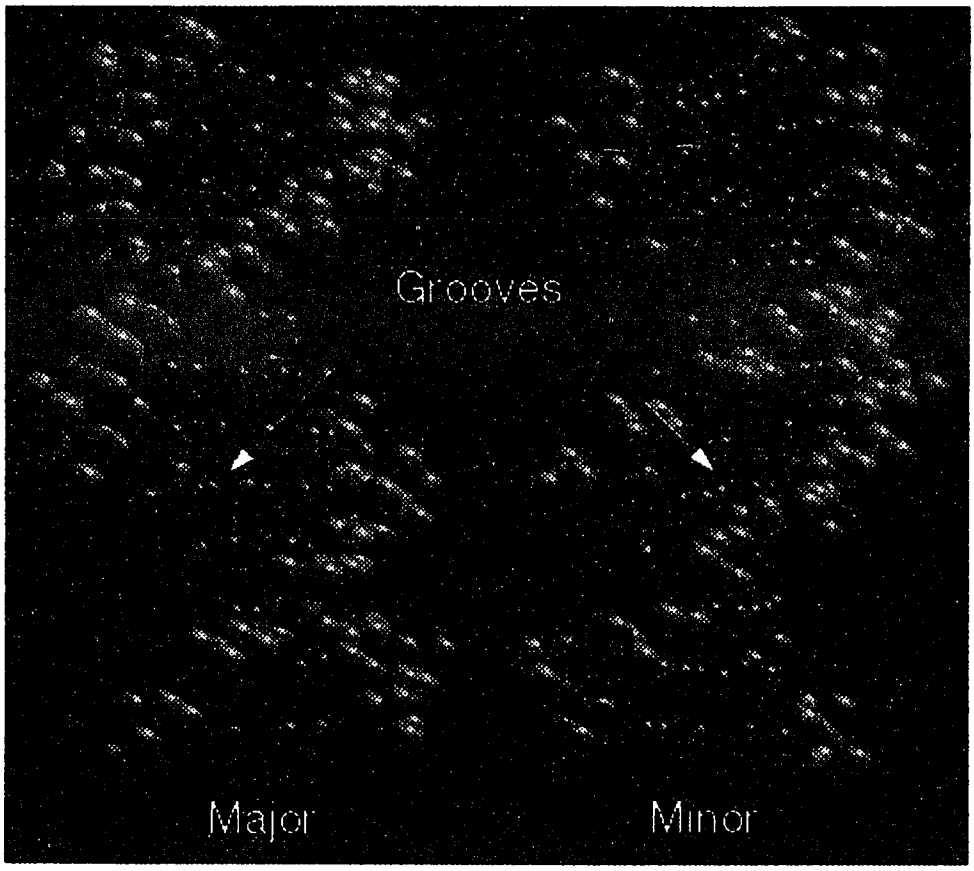

Figure VI-5. Views of the major and minor grooves in B-DNA. Image created with MacMolecule-University of Arizona.

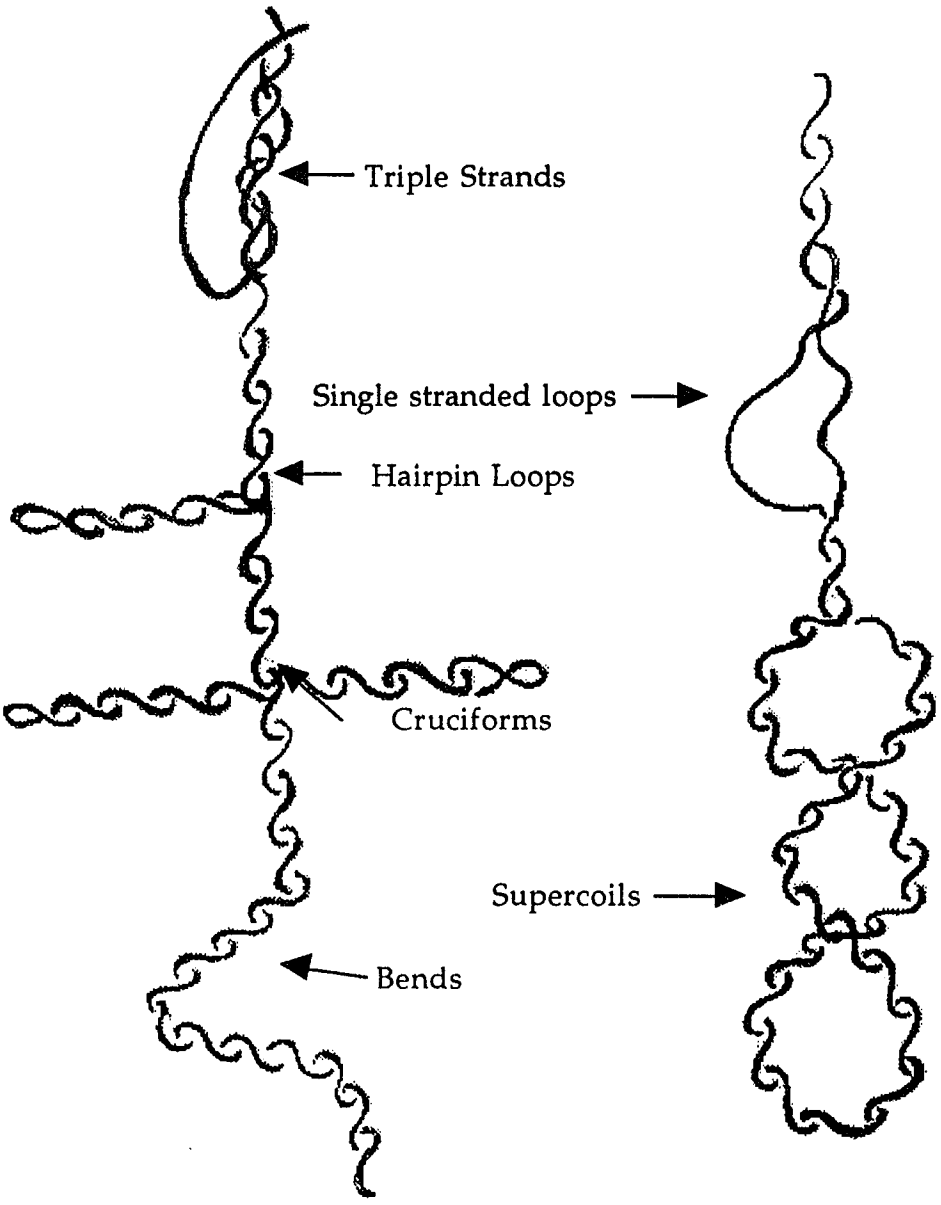

Figure VI-6. Several DNA conformations.

The B-form, thought to be most common, is a right handed helix with base pair stacking normal to the helical axis. The A-form is also a right handed-helix, but differs significantly from the B-form. Due to change in the sugar conformation, the bases are pushed outward toward the minor groove and are tilted with respect to the helical axis. As a result of this conformational change, the minor groove is very wide and shallow, and the major groove becomes pulled into the interior of the molecule, making this groove inaccessible to molecular binders. Double stranded RNAs typically adopt the A-conformation, but local regions of DNA which contain specific sequences can under certain conditions adopt the A-conformation as well.

Z-DNA, being a left-handed helix, is drastically different in conformation from either A- or B- forms.[298] Z-DNA is a zig-zag helix, with the repeating unit on each strand being a dinucleotide (GC) instead of a mononucleotide. Due to this drastic conformational change, the major groove is very shallow and the minor groove is a shallow, zigzagging groove. Alternating guanine-cytosine sequences in the presence of high salt are most likely to adopt this conformation.

Other conformations, such as triple stranded DNA,[299] contain regions of base-pairing which differs from the Watson-Crick description. Some DNA contains regions which link via a cross-like structure known as a cruciform.[300,301] Other regions of DNA form bends in the helical axis.[302-304] Some native DNAs have glucosylated base-pairs (e.g. T-even phage DNA)[305] which essentially block access of the major groove and as a result prevent

binding via the major groove.

Targeting these regions of DNA by use of molecular probes which bind preferentially to these conformations has been the emphasis of several major research efforts.[11,26,306] The recognition of these DNA conformations using molecular probes can prove useful when developing site specific reagents or drug delivery systems. It is clear, therefore, that an understanding of how molecular probes interact with DNA is crucial in examining their effectiveness towards these applications. Some examples of well-studied molecular probes of DNA are given in Figures VI-7 and VI-8. Non-covalent binding of these probes to DNA can occur in several different ways.

Types of non-covalent binding

Electrostatic

Several types of non-covalent interactions are believed to exist when binding drugs to DNA.[8,292-294] (Figure VI-9) Perhaps the simplest to visualize is a purely electrostatic (coulombic) attraction of a positively charged drug (cation) with the negatively charged phosphate backbone of DNA. These types of interactions exist with all positively charged molecular probes, e.g ethidium bromide.

Bridging electrostatic interactions are thought to occur with polycations, where a phosphate on one strand of DNA can bind one portion of the probe, and a phosphate either on the same strand or the opposing strand binds to another portion of the probe, forming a bridge.[23] It is proposed that this type of DNA interaction may exist with our $Ru(bpy)_2qpyMe_2^{4+}$ complex.

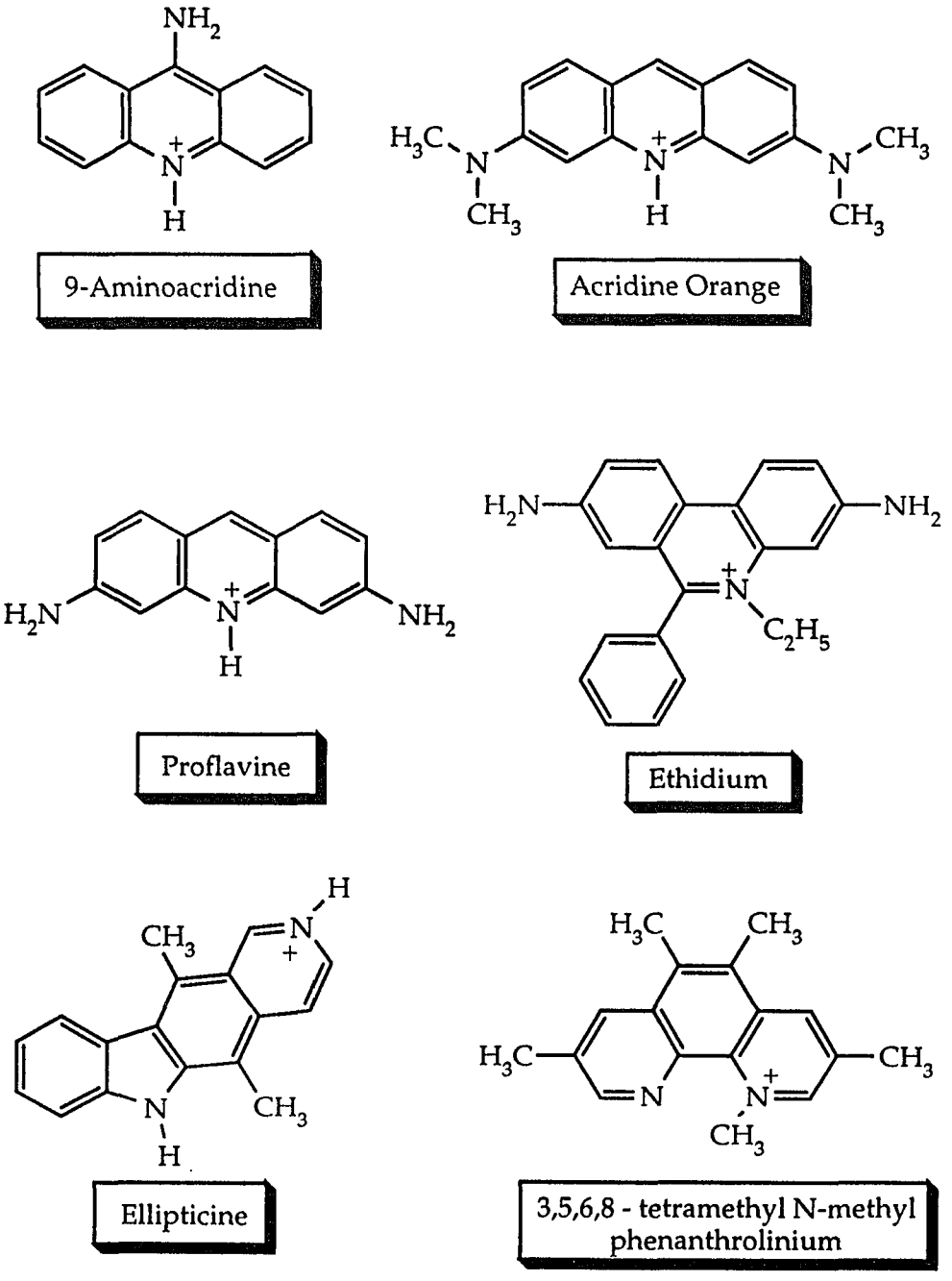

Figure VI-7. Molecular Probes

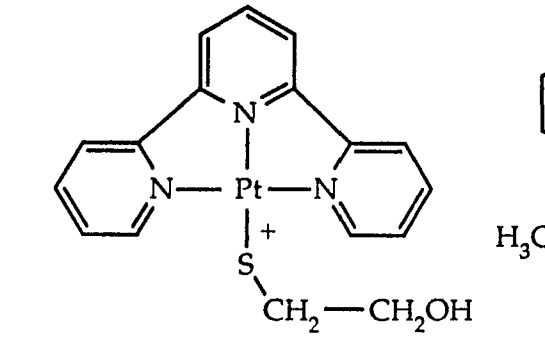

2-hydroxy-ethanethiolato -2,2',2''-terpyridine -platinum (II)

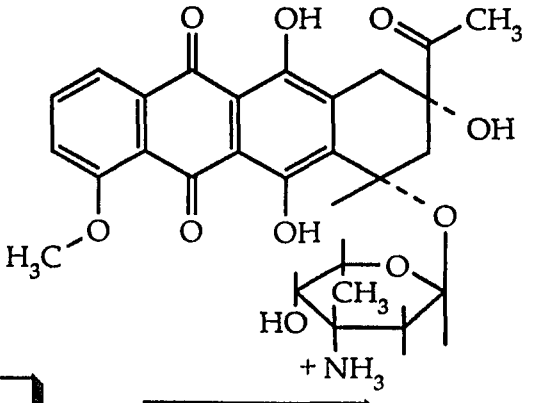

Daunomycin

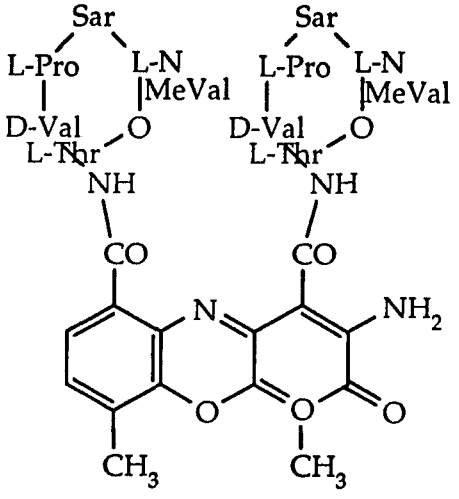

Actinomycin

Figure VI-8. Molecular Probes

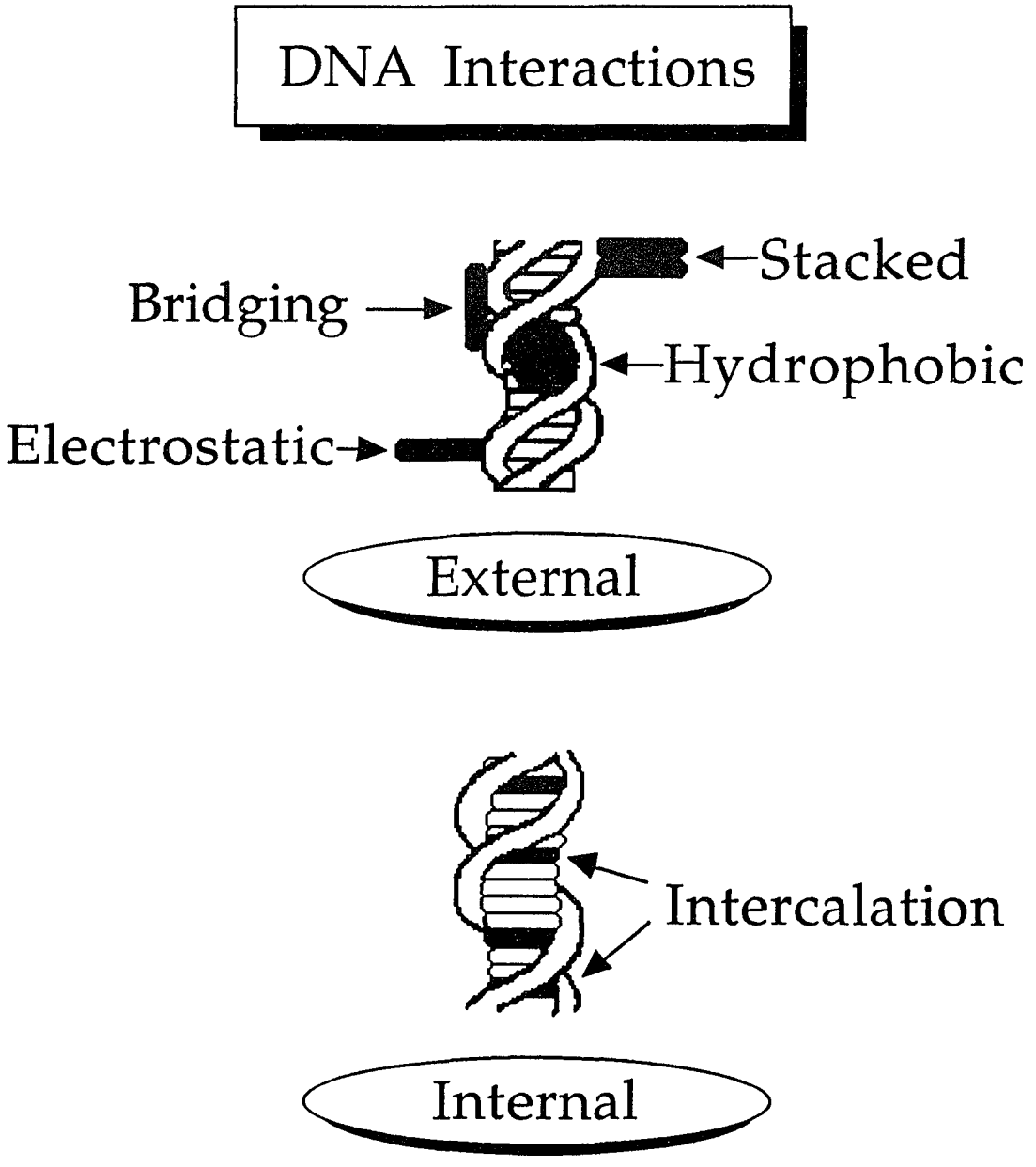

Figure VI-9. Binding modes of organic molecules to DNA.

Intercalation

In 1956, Peacocke and Skerrett[307] found that proflavine (an acridine dye), when bound to DNA, exhibited two or more distinguishable binding processes, a strong and weak binding mode. They proposed that the strong binding was an electrostatic interaction, while stacking interactions of the bound proflavine were attributed to the weak binding. This evidence was based on equilibrium dialysis data. Subsequent research[295] disproved their proposition based on physical and spectroscopic evidence.

Physical measurements of increased DNA viscosity upon binding of acridine dyes, and initial decrease of the sedimentation coefficient of DNA when the concentration of the dye was below a certain value, led Lerman in 1961 to propose the model of **intercalation.**[295] This model is one where the planar dye slips between the base pairs of DNA and is stabilized by favorable hydrogen bonding and van der Waals interactions. Intercalation lengthens and stiffens the DNA duplex, decreasing the mass per unit length, which increases the viscosity and decreases the sedimentation coefficient.[295]

Further evidence to support the intercalation model came from X-ray crystallographic data of intercalated DNA fibers.[295,308] These findings showed that the planar acridine dyes sit between the two planar base pairs, pushing the base pairs apart so as to accommodate the dye. Isenberg, Baird and Bersohn[309] showed that the binding of aromatic hydrocarbons to DNA depends on the molecular dimensions of the bound molecule. Müller and Crothers[310] determined that the chromophore of actinomycin is intercalated between the

base pairs, while the peptide portion of the molecule binds to the phosphate backbone. Ethidium bromide, studied by Fuller and Waring, was also found to exhibit intercalative binding.[311]

Spectroscopic study of the binding of drugs to DNA using fluorescence,[312] polarized fluorescence, flow dichroism, and absorption[313] further support the intercalation model for these molecules. NMR studies by Blears and Danyluk[314] showed two binding types, a tight non-rotational binding and a weak and rotationally less restrictive binding. CD and ORD studies[315] of bound acridines showed at least two optically active compounds formed from the optically inactive acridine dyes.

Intercalation is believed to involve binding between two base pairs, in other words, the binding site consists of four nucleotides. This can occur via either the major or minor grooves. Furthermore, from Scatchard[316] and X-ray analyses, it is believed that nearest neighbor sites exclude binding[317], because the base pairs are pushed apart to accommodate the intercalator, and the adjacent sites do not allow binding via an intercalative mode. (Figure VI-10)

Several studies have again and again confirmed intercalation for the strong binding process, and electrostatic binding for the weak binding process first described by Peacocke and Skerrett[307] as a stacking interaction. Stacking of the dye along the helix was found to be a very weak interaction,[318] and was completely lost when ionic strength was increased. The model of intercalation first proposed by Lerman[295] is now supported by researchers as the most stable type of interaction of planar aromatic dyes and drugs with DNA, yet it is

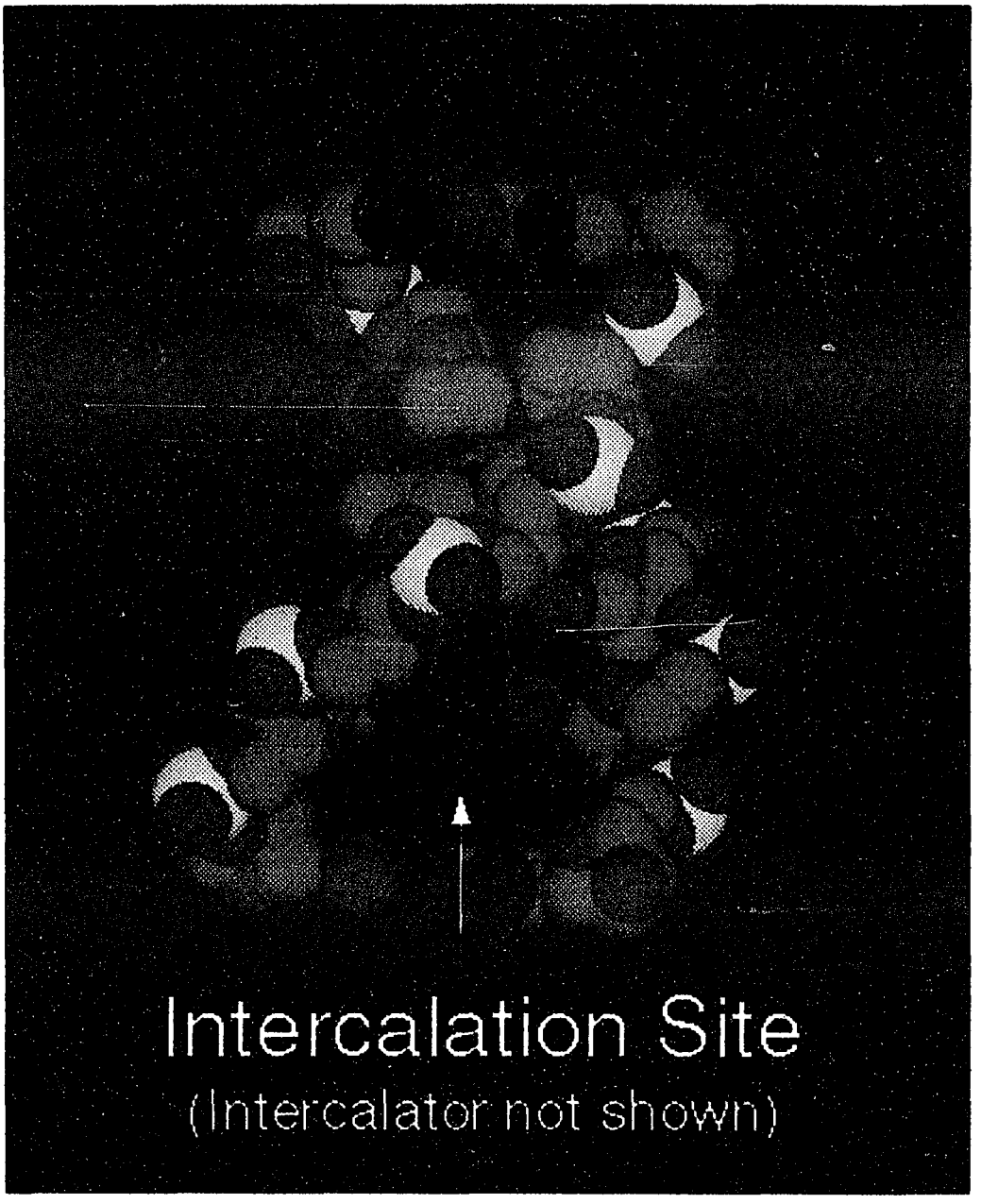

Figure VI-10. X-ray fiber structure of intercalated B-DNA (Intercalator removed) Intercalator-Daunomycin. From the Nucleic Acid Database-Rutgers University.

generally accepted that electrostatic interactions must be also be present to promote intercalative binding.

Surface (Groove Binding)

Another type of binding, surface binding (or groove binding) is also believed to occur with certain drugs and dyes.[193,319] Binding in this fashion is believed to involve both electrostatic and hydrophobic interactions. This binding mode is much more difficult to characterize because the physical and spectroscopic properties of the bound molecule would not be expected to change significantly in this process. Further complications in characterizing this mode arise from the fact that this binding mode would be expected to have a binding affinity to DNA similar to the weak electrostatic binding process, and may not be distinguishable from purely electrostatic binding. Binding of this type can occur either in the major or minor groove, and planarity is not necessary to induce this type of binding.

Binding of transition metal complexes to DNA

We now consider the binding of transition metal complexes to DNA. Metal complexes bind to DNA via several modes, some similar to the organic dyes and some very different. Metal complex ions serve as very sensitive reporters of the binding site, and by chemical modification of the ligands,[23] metal complex ion probes can be fine-tuned to recognize DNA conformations.[11,26]

Several metal ions bind to DNA covalently via coordination to the N7 of guanine. Cis-diamminedichloroplatinum(II), or cis-platin, is a well-known anti-

tumor drug which forms an intrastrand crosslink between two guanine residues created by covalent binding of the complex to two purine nitrogen atoms.[292-294] Several coordinatively unsaturated heavy metal complexes similar to cis-platin are believed to bind in this manner. Lighter metal ions such as sodium and magnesium bind to the sugar-phosphate backbone electrostatically, or less commonly through association with the sugar.[292-294]

Non-covalent interactions between the ligands surrounding a coordinatively saturated metal center and DNA can involve hydrogen bonding of coordinated NH_3 with either phosphate oxygen or base pair nitrogens. $Co(NH_3)_6^{3+}$ bound to Z-DNA apparently adopts this type of binding.[321]

Several studies on complexes thought to bind to DNA via metallointercalation have appeared.[322-323] Metallointercalation is similar to intercalation of ethidium bromide or acridine dyes, yet more restrictive since metallointercalation typically occurs via the major groove exclusively. Lippard and coworkers in 1974 first reported on metallointercalation of Pt(II) complexes containing the terpyridine ligand.[322-323] The crystal structure of the square planar complex ion $[Pt(trpy)SCH_2CH_2OH]^+$ bound to a synthetic oligonucleotide reveals metallointercalation of the terpyridine ligand via the major groove, with the minor groove being too narrow to allow intercalation via this inlet. X-ray crystallographic data of the intercalating 2,2'-bipyridyl Pt(II) complex compared with the non-intercalating bis(pyridine)Pt(II) complex further suggest that planarity of the probe is a necessary requirement for intercalation.[325]

Recently, studies on the binding of polypyridyl complexes of Zn(II),[320]

Co(III),[324,327,328] Cr(III),[328] Rh(III),[329] and Ru(II)[5,6,13,15] to DNA by Barton, Turro, and coworkers have led to a binding model of partial intercalation of one of 3 planar polypyridyl chelating ligands in the tris complexes of 1,10-phenanthroline (phen) and related complexes. In addition, electrostatic and surface bound modes were proposed. (Figure VI-11) Studies with tris(bipyridyl) complexes indicated that the bpy ligand was not sufficiently extended from the metal core to bind in this fashion.[7] Some $Ru(bpy)_2L^{2+}$ complexes appear to bind intercalatively, if the ligand L is sufficiently extended from the Ru core. However, with these complexes, the ancillary (non-intercalating) bpy ligands do not restrict insertion by interaction with the sugar-phosphate backbone to the same extent as in the $Ru(phen)_2L^{2+}$ complexes. Partial intercalative binding is believed to occur primarily via the **major** groove.[4,5] This method of binding occurs concurrently with electrostatic binding, and evidence for groove binding (both major and minor) has also been presented for these complexes.[6,21] Studies by Norden et. al.[17] using linear dichroism (LD) evidence suggest that partial intercalation may be evident for only one enantiomer of the $Ru(phen)_3^{2+}$ complex ion (the Λ isomer). Reference to these and other studies will be made as a comparison for the binding modes of the complexes used for this dissertation.

Due to the right-handed helical structure of B-DNA, metal complexes of D_3 or related symmetry can bind enantioselectively,[320] in other words, one enantiomer of the complex ion may bind more strongly than its mirror image complex ion. It is thought that steric restrictions imposed by van der Waals

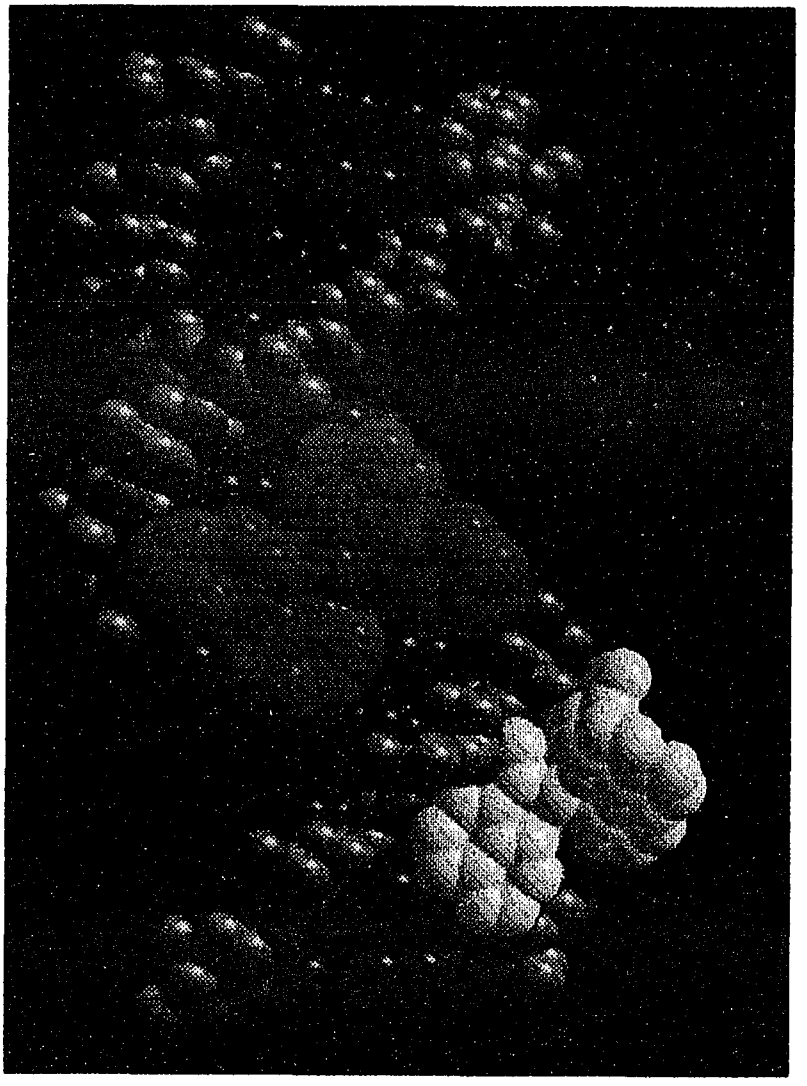

Figure VI-11. Binding modes of D_3 metal complexes. Green-Intercalation (partial insertion). Purple-Electrostatically bound. Yellow-Surface bound in minor groove. Image created with MacMolecule-University of Arizona.

Basis for the Enantioselectivity

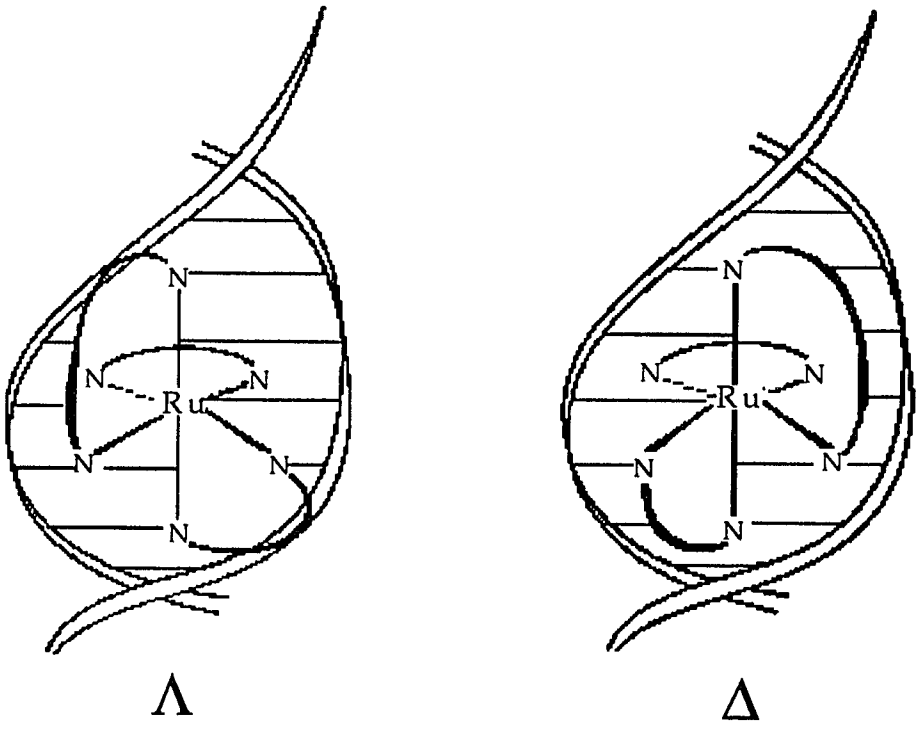

Figure VI-12. Basis for enatioselectivity

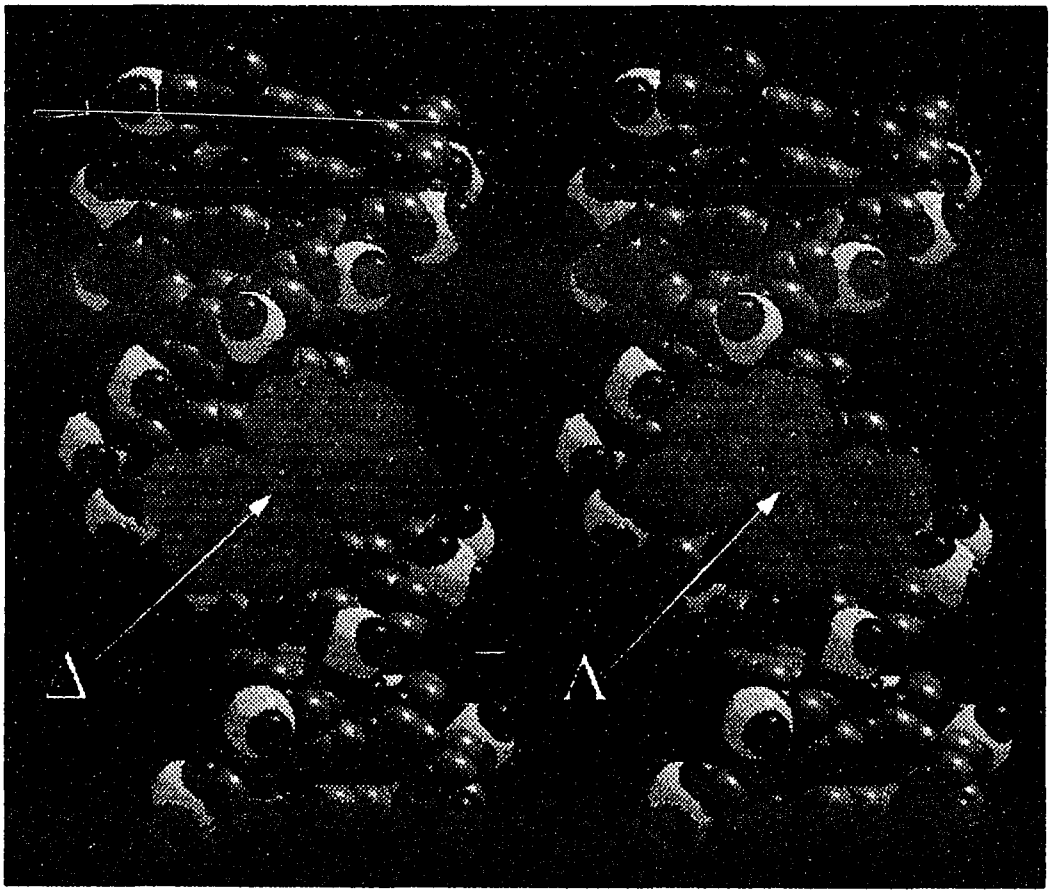

Figure VI-13. The basis for enantioselectivity in the complex $Ru(phen)_3^{2+}$. Note the interaction of the Λ complex with the sugar-phosphate backbone is more sterically disfavored compared with the Δ complex.

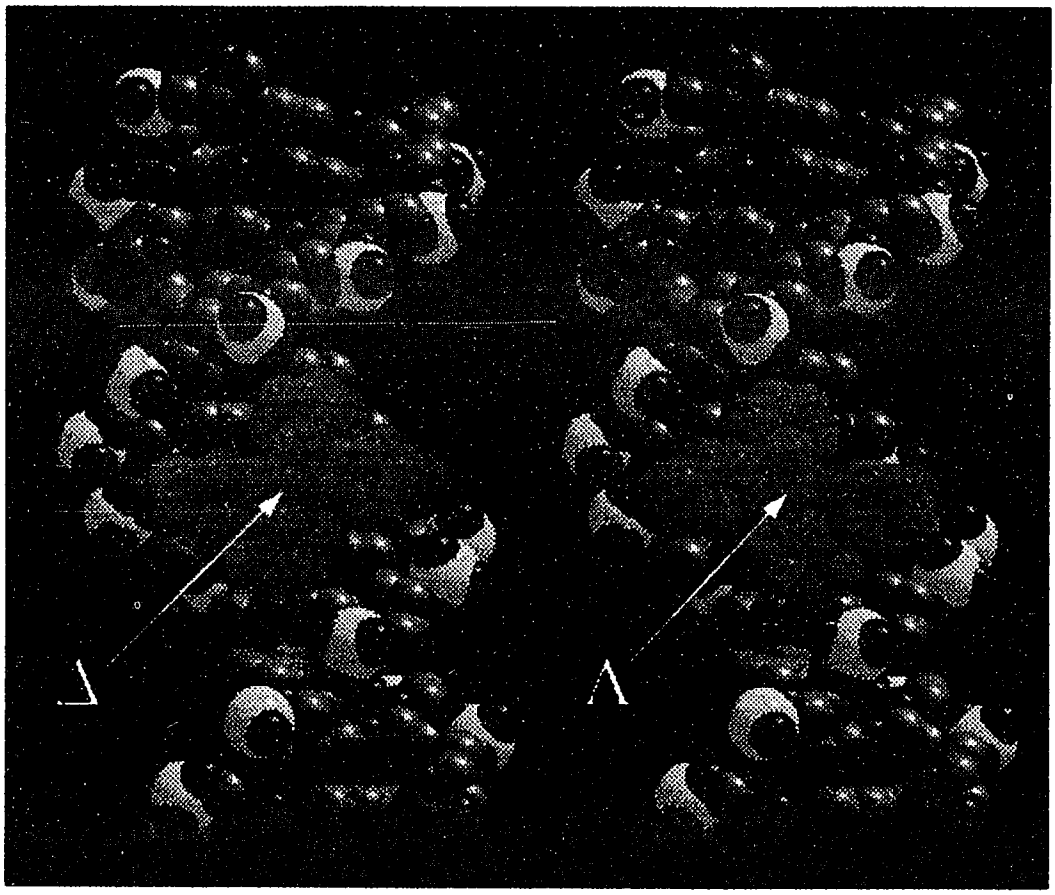

Figure VI-14. The basis for enantioselectivity in $Ru(bpy)_2ppz^{2+}$. Note that the steric interactions of both isomers with the sugar-phosphate backbone are more similar to each other compared to $Ru(phen)_3^{2+}$. (Portrayed in Figure VI-13)

contacts within the major groove for the intercalating complex favor one enantiomer. (Figure VI-13) Molecular model building suggests that the Δ isomer of $Ru(phen)_3^{2+}$ binds better than the Λ isomer. For the corresponding $Ru(bpy)_2phen^{2+}$ complex, the bpy ligands are much less restrictive. Comparing Figure VI-13 to VI-14, one can visualize why $Ru(phen)_2L^{2+}$ complexes should be more enantioselective (more restrictive of the weaker binding isomer) than $Ru(bpy)_2L^{2+}$ complexes.

Aspects of Ru(II) and Rh(III) polypyridyl complexes

Several studies have attempted to describe the binding of Ru(II) and Rh(III) polypyridyl complexes to various types of DNA.[20] They are indicated in Table 1. $Ru(phen)_3^{2+}$ is perhaps the best studied system,[4,5,6,7] which is no surprise since it is relatively easy to prepare and has been well characterized in a variety of solvents and on supports.[1] $Ru(phen)_3^{2+}$ and several other Ru(II) and Rh(III) complexes are luminescent at room temperature, and emission spectroscopy can provide information on the binding environment of the probe. The Λ enantiomer of $Ru(DIP)_3^{2+}$ (DIP = 4,7-diphenylphenanthroline) has been shown to be a selective binder to Z-DNA conformations.[3] Others have been shown to selectively cleave DNA.[24] Some conclusions arrived at from these and other studies will be presented when pertinent to the research in this dissertation.

Table 1

Studies of Binding of Ru(II) and Rh(III) complexes to DNA

Subject	Reference
Stereoselective binding of $Ru(phen)_3^{2+}$ to calf thymus DNA	4
Photophysics of $Ru(phen)_3^{2+}$ bound to DNA	5
Binding modes and base specificity:Tuning stereoselectivity	6
Interactions of Ru(II) complexes with DNA using fluorescence, topoisomerisation, and thermal denaturation	7
Chiral probes of Z-DNA conformation	3
Ru(II) polypyridyl sensitizers for photocleavage of DNA	10
Accelerated Electron Transfer between metal complexes mediated by DNA	330
$Rh(DIP)_3^{3+}$: a shape-selective metal complex which targets cruciforms	329
Tris(tetramethylphenanthroline)Ru(II): A chiral probe that cleaves A-DNA conformations	13
Study of some Ru(II) polypyridyl complexes as DNA binders and photocleavage agents	14
Mixed-ligand complexes of Ru(II) bound to DNA	15
Ligand dependent interaction of Ru(II) polypyridyl complexes with DNA probed by emission spectroscopy	16
Enantiopreferential DNA binding of $Ru(phen)_3^{2+}$ studied with linear and circular dichroism	17
Molecular Light Switch for DNA: $Ru(bpy)_2(dppz)^{2+}$	27
Synthesis and characterization of 9,10-phenanthrenequinone diimine complexes of Ru(II) and Rh(III)	18
^1H NMR studies of $Ru(phen)_3^{2+}$ bound to oligonucleotides	19,20
Sequence selective binding to the DNA major groove	21
Photoinduced electron transfer quenching of Ru(II) polypyridyls	22

Table 1 (cont'd)

bound to DNA. The role of the double helix	
Luminescence of Ru(II) polypyridyls: evidence for intercalative binding to Z-DNA	29
Enantiomeric resolution of $Ru(phen)_3^{2+}$ and $Ru(bpy)_2(ppz)^{2+}$ on a DNA-hydroxylapatite column	33
Effects of ligand planarity and peripheral charge on the intercalative binding of $Ru(bpy)_2(L)^{2+}$ to calf thymus DNA	23
DNA photocleavage by phenanthrenequinone diimine complexes of Rh(III): Shape selective recognition and reaction	32
Minor groove binding of $Ru(phen)_3^{2+}$ to $[d(CGCGATCGCG)]_2$ evidenced by two-dimensional nuclear magnetic resonance spectroscopy	25
Enantiospecific cleavage of DNA using Cu(II) chelated to the periphery of a ligand on a chiral tris-chelate of Ru(II)	24
Recognition of G-U mismatches by $Rh(DIP)_3^{3+}$	331
Novel dipyridophenazine complexes of Ru(II): Exploring luminescent reporters of DNA	30
Neither Δ nor Λ tris(phenanthroline) Ru(II) binds to DNA by classical intercalation	332
Characterization of dipyridophenazine complexes of Ru(II) The light switch effect as a function of nucleic acid sequence and conformation	28

Evidence for the binding of probes to DNA

Introduction

Spectroscopic perturbations of the molecular probe on binding report on the local environment of the chromophore, and serve to indicate the DNA duplex conformation.[306] Several spectroscopic observations have been made with "classic" intercalators and Ru(II) polypyridyl complexes when bound to DNA. Characterization of the binding as being intercalative, surface or

electrostatic is supported by various spectral perturbations. Spectral characteristics of intercalative binding are presented below. This evidence is presented with the understanding that these spectral changes do not unambigously lead to the description of the binding as intercalative in nature, but that the evidence is highly suggestive of this binding mode.

Absorption Hypochromism

Upon binding to DNA, intercalation tends to decrease the intensity of the absorption bands of the molecular probe.[333] This has been attributed to a hypochromic effect, (i.e. less color) or the decrease in absorbance due to ordering (stacking) of the chromophore which is absorbing light. A shift in energy of the absorption bands of the chromophore involved in the intercalative binding are also observed. Typically these shifts are to lower energy (bathochromic). For example, the ethidium bromide absorption band shifts from 480nm to 520nm upon DNA binding,[334] accompanied by a hypochromic effect. The theory of hypochromism has been worked out by Tinoco et. al.[335] and is beyond the scope of this dissertation.

Ru(II) polypyridyl complexes generally show a much smaller hypochromic effect than intercalators such as ethidium bromide.[4,23] This has been attributed[4] to the fact that only partial intercalation occurs, and also due to the symmetry of the molecule. For example, with $Ru(phen)_3^{2+}$, a D_3 complex ion, the predominant polarization of the charge-transfer band is perpendicular to the molecular C_3 axis, rather than parallel to the plane of the intercalator as it is with organic intercalators. This reduces the hypochromic effect seen in

$Ru(phen)_3^{2+}$ and several other Ru(II) complexes. Furthermore, charge transfer to the two non-intercalated ligands would lead to less of a hypochromic effect, since these ligands are not thought to be perturbed upon binding to DNA to the same extent as the intercalated phen ligand.

The absence of hypochromism in the absorption band of the $Ru(bpy)_3^{2+}$ complex ion is indicative of a lack of intercalative binding for this cation.[4,7] It is thought that the bpy ligand is not sufficiently extended from the metal to promote intercalative binding, and this evidence supports that theory.

Electrostatic binding, however, does not induce a hypochromic effect, since the $Ru(bpy)_3^{2+}$ complex ion must bind this way to some extent due to the dipositive charge on the Ru metal. Therefore, the **presence** of hypochromism in an absorption spectrum indicates only binding modes that **differ** from purely electrostatic binding.

Emission Enhancement and Luminescence Lifetime Increase

Upon binding to DNA, intercalators exhibit an increase in the quantum yield of luminescence (ϕ) and increase in luminescence lifetime.(τ)[5] This is attributed to the shielding of the chromophore from solvent and quenchers, and also to restrictions on the vibrational modes for radiationless deactivation.[336] Substantial increases in ϕ and τ have been seen with the intercalator ethidium bromide,[337] and to a lesser extent with $Ru(phen)_3^{2+}$.[5] Biexponential behavior was seen in measurements of τ for the $Ru(phen)_3^{2+}$ complex ion,[5] supporting the existence of a short (electrostatic binding) component and a long (intercalative binding) component. However, similar values of τ for both

components of the emission found for the $Ru(phen)_3^{2+}$ enantiomers failed to adequately differentiate the luminescing environments expected to be found for these isomers.

No change in ϕ or τ has been observed for the $Ru(bpy)_3^{2+}$ complex ion upon binding to DNA,[5] indicating that binding of this complex ion via the proposed intercalative scheme does not occur. This has also been attributed to the lack of extension of the bpy ligands from the Ru(II) metal center, and parallels the lack of absorption hypochromism seen for this complex ion.[4,23]

Often, blue shifts in the emission maxima of intercalating molecular probes are accompanied by emission enhancement, similar to effects observed upon going from polar to non-polar solvents. Emission bands tend to be narrower due to the redistribution and decrease in intensity of vibrational modes of the excited state that occur when going from a polar to a non-polar solvent. Similar shifts have been observed with intercalators such as ethidium bromide,[337] where the binding to DNA shifts the emission maximum to higher energy (blue shift) as well as increases the quantum efficiency. This is consistent with the chromophore luminescing from a more non-polar environment, such as the interior of the double helix of DNA, when intercalatively bound. While the band shift for bound $Ru(phen)_3^{2+}$ is ~2 nm to the red,[4] this small shift does not disprove intercalation, since luminescence in this complex ion may originate from MLCT states associated with the non-intercalated ligands, and van der Waals and electrostatic interactions of these ligands within the major groove can possibly shift emission maxima to lower

energy (red shift). Indeed, we have seen red shifted emissions from non-intercalating tetrapositive Ru(II) complexes bound to DNA, presumably induced by electrostatic interactions.[23] (Chapter VIII)

Emission Polarization

The electrostatic binding of molecular probes to DNA does not restrict rotational freedom of the cation, whereas binding via intercalation fixes the orientation of the chromophore during the lifetime of the excited state.[5] This can occur for a long enough time to induce a polarization of the emission by restricting rotational freedom of the probe. This restriction of motion can be monitored by steady state or time-resolved emission polarization experiments, where the polarization P is given by

$$P = I_{parallel} - I_{perpendicular} / I_{parallel} + I_{perpendicular} \quad [1]$$

I is the intensity of the emission in the parallel and perpendicular directions of polarization.[47]

DNA, being a large molecule, rotates only very slowly in solution. Therefore, emission polarization is a probe of the DNA motion itself, which orients the chromophore and gives rise to the polarization. Only those chromophores bound in the intercalative fashion will be oriented, and as a result of electrostatic binding occurring in conjunction with intercalation, polarizations less than the theoretical maxima are usually observed.[5,236] Polarization is also influenced by emission lifetime, where long luminescence lifetimes tend to allow more rotation which depolarizes the emission during the

luminescence decay.

Emission Quenching

Quenching by anions has been investigated for Ru(II) polypyridyl complex ions bound to DNA.[5,6] A pronounced decrease in the effectiveness of the anion $Fe(CN)_6^{4-}$ to quench the emission of Δ-$Ru(phen)_3^{2+}$ in the presence of DNA led Barton and others to the conclusion that the chromophore responsible for the emission is shielded from the quencher and is therefore intercalated within the DNA duplex.[5] While a decrease in the quenching ability of $Fe(CN)_6^{4-}$ with Λ-$Ru(phen)_3^{2+}$ was also observed, it was less pronounced than for the Δ-isomer.

Nonlinear Stern-Volmer quenching plots are characteristic of multiple luminescing environments, and Barton attributed the curvature of the quenching plots of bound $Ru(phen)_3^{2+}$ to the existence of intercalative, surface, and electrostatic binding modes.[5]

Using luminescence lifetime quenching data, the persistence of the short component after addition of $Fe(CN)_6^{4-}$ indicates that either electrostatic and/or surface binding occurs concurrently with intercalation, however its contribution to the overall luminescence becomes much less at higher ratios of [DNA-phosphate]/[Ru], where most of the Ru(II) complex ion is in the intercalatively bound form.[5] The persistence of the short component was used by Barton et. al as evidence for a surface bound mode, where those $Ru(phen)_3^{2+}$ complex ions bound to the surface of DNA via electrostatic and hydrophobic interactions are somewhat better shielded from the anionic quencher than those electrostatically

bound or free (i.e. in solution) ions. These surface bound ions would be expected to exhibit a luminescence lifetime similar to the free solution value, and therefore the assignment of a surface bound mode for $Ru(phen)_3^{2+}$ from this evidence seems plausible.

Equilibrium Dialysis

Equilibrium dialysis studies on organic dyes and Ru(II) polypyridyl complexes lead to non-linear Scatchard plots, which plot the ratio r/C_f versus r.[4] The variable r is the concentration of bound chromophore divided by the concentration of DNA phosphate (or nucleotide), while C_f is the concentration of the free chromophore. Scatchard plots have been instrumental in estimating the binding constant of the probe to DNA.[316] The non-linearity in these plots is attributed to the existence of multiple binding sites, but it is difficult to extract more than two binding sites from such Scatchard plots. Average binding constants to the DNA duplex are obtained by fitting the binding curve to the McGhee and von Hippel equation,[338] which is modeled after the non-cooperative nearest-neighbor exclusion model. From fits to this equation, average binding constants (K_b) and site sizes (l) are calculated.

For $Ru(phen)_3^{2+}$, average binding constants on the order of 10^3 were found corresponding to a site size of l=4 (8 base pairs).[4] The value of the binding constant for $Ru(phen)_3^{2+}$ is smaller than what is found for planar aromatic intercalators, where values of 10^4 to 10^6 and higher have been measured.[335,337] Also, for planar aromatic intercalators, site sizes are typically l=2 (4 base pairs). The larger site size found with Ru(II) complexes can be

attributed to the opposing non-intercalating ligands preventing access to the four adjacent sites on the DNA duplex.[4] This argument is plausible when considering the D_3 symmetry of the $Ru(phen)_3^{2+}$ complex, the size of the phenanthroline ligand, and the intercalative mode of binding, which causes the non-intercalating ligands to align themselves in the major groove such that the adjacent binding sites are effectively blocked. Electrostatic binding would be expected to have a smaller relative site size, I, due to the increased availability of sites (phosphates) compared to the intercalative binding mode sites.

Enantioselectivity

Differential binding of the enantiomers of Ru(II) polypyridyl complexes to DNA has been informative in the description of the strong binding process as intercalative. For $Ru(phen)_3^{2+}$, the Δ-enantiomer was found to bind stronger to DNA than the Λ-enantiomer.[4] Molecular modeling[4] and recent calculations[21] suggest that the right-handedness of B-DNA accommodates the Δ-isomer better than the Λ-isomer for intercalative binding. The Λ-isomer has its ancillary (non-intercalating) ligands opposed to the direction of the groove, while the Δ-isomer has its non-intercalating ligands aligned along the major groove. (Figure VI-12) The binding mode is further stabilized for the Δ-isomer by favorable van der Waals interactions of the ancillary ligands along the groove, which are not complementary for the Λ-isomer, and may even destabilize the intercalative binding of the Λ-isomer due to steric factors.[4]

Determination of the stronger binding enantiomer is achieved by dialyzing the racemic complex against DNA and measuring the circular

dichroism (CD) of the solution outside the dialysis bag. If a CD signal is found, then binding of one enantiomer is stronger than the other, and enantioselectivity is the cause. The weaker binding enantiomer is enriched outside the dialysis bag, since the stronger binding enantiomer binds well to the DNA, and decreases the concentration of the stronger binder outside the bag. For $Ru(phen)_3^{2+}$, the Λ-isomer is the weaker binder, since it is found outside of the dialysis bag.[4]

The assignment of absolute configuration have been made for $Ru(phen)_3^{2+}$ from X-ray structure data. The Δ isomer shows the larger spectroscopic effect in the presence of DNA. This assignment of configuration is assumed for the complex $Ru(bpy)_2ppz^{2+}$, (Chapter VII) where the isomer which fits better to a right-handed helix (due to molecular modeling considerations) and binds stronger to DNA (from dialysis evidence) is assigned Δ. (See Figure II-2 -pictures of Δ and Λ $Ru(bpy)_2ppz^{2+}$)

Other evidence presented for the binding of probes to DNA

Several other techniques for describing the binding of dyes and metal complexes to DNA are given in Table 2. References are provided for the techniques described. These techniques are included for the sake of giving a more complete survey of the work that has been done in this area, and further mention of them will be included only if applicable to the current discussion.

Table 2

Technique	Reference
Topoisomerisation	7
Thermal denaturation (DNA melting)	7
Helical unwinding of supercoiled DNA	339
X-ray structure of drug-bound fibers	295
Increase in viscosity	340
Decrease in sedimentation coefficient	295
Studies with glucosylated T4 DNA	6
Kinetic T-jump	337
Differential scanning calorimetry (DSC)	319
Circular dichroism and linear dichroism	17
Cyclic Voltammetry	341

Structural modification of the molecular probe

It was realized early on that variation of the structure of the molecular probe has a profound effect on the binding ability of the probe to DNA, RNA, and synthetic polynucleotides.[309] Reports by Kelly et. al.[7] found no significant binding for $Ru(terpy)_2^{2+}$ or $Ru(bpy)_3^{2+}$, with calf thymus DNA, poly(dA•dT)•poly(dA•dT), or poly(dG•dC)•poly(dG•dC). Barton et. al. found exclusive binding for the Δ enantiomer of $Ru(DIP)_3^{2+}$ with B-DNA, which in turn made the Λ-enantiomer a useful spectroscopic probe for the Z-DNA conformation (i.e. poly(dG•dC)•poly(dG•dC) in the presence of $Co(NH_3)_6^{3+}$), since the Λ isomer will bind in Z-DNA sites but not B-DNA sites.[3]

Several other reports further illustrate that the structure of the molecular probe is perhaps the single most useful method for altering the binding characteristics of the probe to nucleic acids. To this end, the following chapters deal with molecular analogs of $Ru(phen)_3^{2+}$ and their binding to DNA. Based on these alterations of structure, comparisons of the binding behavior of these analogs relative to the well studied $Ru(phen)_3^{2+}$ complex ion are made. Differences and similarities of the binding as a function of structural alteration are discussed. Also, a novel application of a spectroscopic technique (resonance Raman), which leads to descriptions of the binding behavior of these molecular probes (Raman hypochromism), is introduced and discussed.

Chapter VII. DNA binding modes of the complex ion $Ru(bpy)_2ppz^{2+}$.

Introduction

Several studies of the binding of cationic transition metal polypyridyl complexes to DNA, RNA, and synthetic polynucleotides have been undertaken in recent years, in hopes of characterizing the interactions of these small molecules to nucleic acids.[26] A model of partial intercalation, where one wing of a tris-chelate ion is inserted between adjacent DNA base pairs via the major groove, is a fundamental feature of the models proposed by Barton et. al. to characterize the binding of such cations to nucleic acids.[5] In addition, partial intercalative major groove binding is consistent with the observed enantioselective binding of these complexes.[4] Attempts to model the enantioselective binding via electrostatic or surface bound modes are less well defined, and it becomes evident that partial intercalative binding provides a more rational basis for the observed enantioselectivity.

Despite the fact that several Ru(II) and Rh(III) polypyridyl complexes have been shown to bind enantioselectively, only a handful of reports have appeared which detail the characteristic binding of the individual enantiomers to DNA[5,6,17,19,20,25,29,342] (e.g. trisphenanthroline complexes of Rh^{3+}, Co^{3+} Ni^{2+} and Cr^{3+}). Barton et. al. have examined the binding of Δ- and Λ- $Ru(phen)_3^{2+}$ (phen=1,10-phenanthroline) to several synthetic and native DNAs.[5,6] Analysis of their spectroscopic and physical data have led them to the conclusion that the Δ- isomer favors binding in the partial intercalative fashion, with the other two

(ancillary) ligands providing van der Waals interactions with atoms lining the major groove. The "fit" of the Λ- isomer is more sterically disfavored, and does not bind favorably in this way. Minor groove surface binding is thought to be the most favored binding mode for the Λ-isomer.

In studies of the complex $Ru(DIP)_3^{2+}$ (DIP = 4,7-diphenylphenanthroline), Barton et. al. arrived[29] at the conclusion that the binding of the Λ-isomer to B-form DNA was **totally** restricted based on similar arguments given for the disfavored intercalative binding mode of the Λ- $Ru(phen)_3^{2+}$ isomer.

Binding studies by Barton et. al.[19,20] using NMR data with several transition metal complex ions and a self-complementary hexameric oligonucleotide did **not** provide conclusive evidence of the intercalative major groove binding mode. Rather, evidence for a non-intercalative minor-groove binding was observed. Similar observations were made by other researchers for the enantiomers of $Ru(phen)_3^{2+}$ bound to a self-complementary decanucleotide complex.[25] In that study, however, no other spectroscopic data was reported for possible correlation of the NMR results with spectroscopic findings.

Norden and coworkers[17] have examined the binding of $Ru(phen)_3^{2+}$ to DNA by linear and circular dichroism measurements in a flow system and have concluded the favored binding to be in the major groove for both enantiomers, yet only the Λ isomer being partially inserted between the adjacent base pairs.

Physical evidence for the binding has come in the form of viscosity measurements of DNA in the presence of the enantiomers of $Ru(phen)_3^{2+}$.

Chaires et. al.[332] concluded from their measurements that neither the Δ nor the Λ enantiomer affected the viscosity in a way that well studied intercalators do. Also, thermodynamic parameters were presented for the binding as a function of salt concentration and Chaires et. al.[332] arrived at the conclusion that the binding of $Ru(phen)_3^{2+}$ to DNA is largely electrostatic.

Cleavage studies by Barton et. al.[342] with the complex ion $Rh(phen)_2phi^{3+}$ (phi=9,10-phenanthrenequinone diimine) give different cleavage patterns for each enantiomer. Cleavage studies in our laboratories[24] with enantiomers of the complex ion $Ru(bpy)_2ppz^{2+}$ (ppz=4,7-phenanthrolino-[6,5-b]pyrazine) have shown that only the Λ isomer promotes the cleavage of plasmid DNA in the presence of Cu(II), peroxide, and a thiol. The Δ isomer is almost completely ineffective in cleaving DNA using this scheme.

This chapter is a report on spectroscopic evidence collected for the resolved enantiomers of the complex ion $Ru(bpy)_2ppz^{2+}$. While preliminary findings on the racemic $Ru(bpy)_2ppz^{2+}$ complex ion have been published,[23] this chapter provides all the evidence collected to date concerning DNA binding of the racemic $Ru(bpy)_2ppz^{2+}$ as well as the Δ and Λ enantiomers of $Ru(bpy)_2ppz^{2+}$. A useful feature present in this complex ion and its enantiomers is the spectral resolvability of the MLCT bands associated with the potentially intercalated ligand (ppz), combined with the inability of the bpy ligand to bind intercalatively. This combination improves the ability to probe the complex ion interaction with the DNA duplex, by resolving the observable effects of the binding on the spectrally different ligand types.

By fortunate circumstance, a complex ion analogous to $Ru(bpy)_2ppz^{2+}$, $Ru(bpy)_2dpp^{2+}$ (dpp=2,3-dipyridylpyrazine), which differs from the $Ru(bpy)_2ppz^{2+}$ by only one bond (hence making the non-bpy ligand non-planar), was synthesized previously and provides an extremely useful comparison probe for analyzing the effects of ligand planarity on the ligand which is presumed to intercalate between the DNA base pairs. (See Figure II-1) Since the $Ru(bpy)_2dpp^{2+}$ complex ion exhibits virtually no spectral differences in the presence of DNA, the necessary criterion of planarity for the intercalating ligand can be inferred. Also, characterization of the binding of the $Ru(bpy)_2ppz^{2+}$ by **only** electrostatic means cannot explain the observed differences between the spectral properties of $Ru(bpy)_2ppz^{2+}$ and $Ru(bpy)_2dpp^{2+}$ ions when in the presence of DNA.

The following are the results and conclusions of the binding of $Ru(bpy)_2ppz^{2+}$ to calf thymus DNA, poly(dA•dT)•poly(dA•dT), and poly(dG•dC)•poly(dG•dC). Absorption and emission spectroscopy, including polarization, steady state quenching, quantum yield, and emission lifetime measurements, combined with resonance enhanced Raman spectroscopy and viscometry, form the basis for describing the binding modes of the two enantiomers of $Ru(bpy)_2ppz^{2+}$ to B-form DNA.

Results

Absorption Hypochromism and Band Shift

Presence of a decrease in the allowedness of an optical transition (i.e. a decrease in molar extinction coefficient) has been observed for virtually every

molecular probe that binds to DNA in an intercalative fashion. For the racemic $Ru(bpy)_2ppz^{2+}$ bound to B-form DNA, a decrease in absorbance for the metal-to-ligand charge transfer band (MLCT) transition associated with the ppz ligand relative to free solution spectra is apparent. (Figure VII-1) The MLCT band at 475nm shifts to 485nm and decreases in absorbance by ca 20%. This band has been previously assigned[80,228] from resonance Raman studies to transitions from the ground state to excited states associated with the ppz ligand. The MLCT band at 422nm, previously assigned to a charge transfer transition to the excited states associated with the bpy ligands, is little changed. The spectrum was measured at a relatively high [DNA-phosphate]/[Ru] ratio (~62) with a salt concentration of 50mM NaCl in a Tris buffer (pH 7.4). Large ratios were typically used in these measurements to maximize the effect. At higher salt (0.2M), hypochromism decreased significantly, and at very high salt (>2M), the effect was lost completely.

For the resolved enantiomers, which are ~90% pure, the maximal hypochromic effect was seen for the Δ-isomer. Figure VII-2 portrays both isomers in free solution and bound to calf thymus DNA. The Δ-isomer shows approximately double the hypochromic effect compared to the Λ-isomer for the band at 475nm (~25% for Δ, ~12% for Λ) at a [DNA-P]/[Ru] =159. The 475nm absorption band shifts to ~495nm for the Δ-isomer, but only to ~480nm for the Λ-isomer. Again, for the resolved complexes, the MLCT band at 422nm is little affected.

A plot of the ratio of the the absorbances of the unperturbed MLCT band

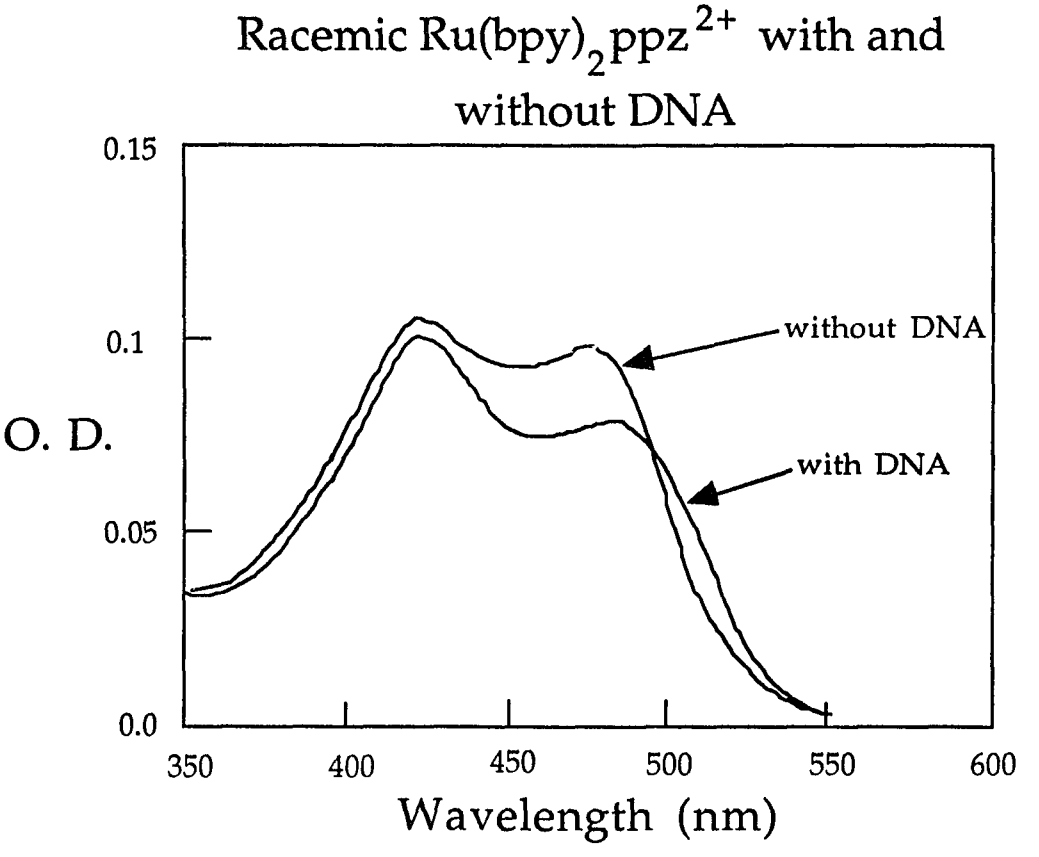

Figure VII-1 Visible absorption spectra of racemic $Ru(bpy)_2ppz^{2+}$ (9.6μM) alone (———) and in the presence of calf thymus DNA (---). [DNA-P]/[Ru] = 62. All solutions measured at 25°C in 5mM Tris, pH 7.4, 50mM NaCl.

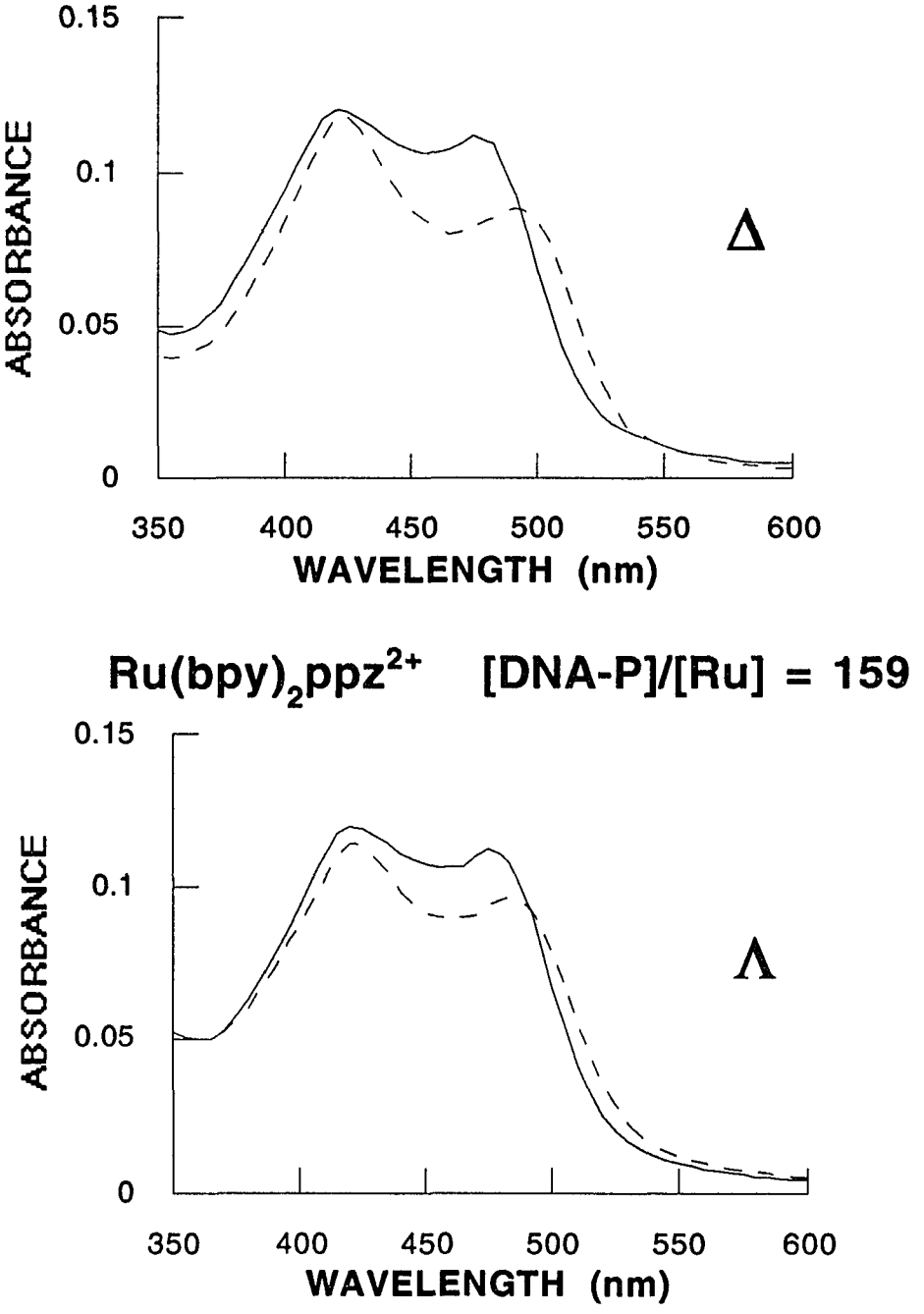

Figure VII-2 Absorption spectra of Δ and Λ $Ru(bpy)_2ppz^{2+}$ with (---) and without (—) DNA. [DNA-P]/[Ru] = 159 for both spectra. All spectra measured at 25°C in 5mM Tris, 50mM NaCl, pH 7.4.

(422nm) divided by the absorbance of the band exhibiting the hypochromism (A_{422} / $A_{475\text{-}495}$) versus [DNA-P]/[Ru] yields the plot shown in Figure VII-3. This serves to indicate the ratios at which the hypochromic effect levels off. It also serves as a quick reference to the amount of hypochromism present. For example, in free aqueous solution, the ratio A_{422} / $A_{475\text{-}495}$ is equal to 1.07. For the Δ-isomer at a [DNA-phosphate]/[Ru] = 159, the A_{422} / $A_{475\text{-}495}$ ratio is ~1.24. Therefore, the larger the A_{422} / $A_{475\text{-}495}$ ratio, the greater the hypochromic effect. Since Beer's law holds for absorbances of these complexes, this method has been useful as a quick measure of hypochromicity for this complex.

For the binding of racemic $Ru(bpy)_2ppz^{2+}$ to poly (dA•dT)• poly (dA•dT) (Figure VII-4), a A_{422} / $A_{475\text{-}495}$ ratio of ~1.28 was found at a [DNA-phosphate]/[Ru] > 20. For the binding of racemic $Ru(bpy)_2ppz^{2+}$ to poly (dG•dC)• poly (dG•dC), the A_{422} / $A_{475\text{-}495}$ ratio was found to be only 1.13 at similar [DNA-phosphate]/[Ru] ratios and salt concentrations. Red shifts of the low energy (ppz) MLCT band were also evident, being more pronounced when bound to poly (dA•dT)• poly (dA•dT), and only slight when bound to poly (dG•dC)• poly (dG•dC). Again, the bpy MLCT bands were only slightly perturbed. While binding constants have not been measured for racemic $Ru(bpy)_2ppz^{2+}$ bound to these oligonucleotides, qualitatively it is evident from our experiments that the $Ru(bpy)_2ppz^{2+}$ complex ion prefers A-T rich sites, and binds stronger to poly (dA•dT)• poly (dA•dT) than to calf thymus DNA, which has has 58% A-T content.

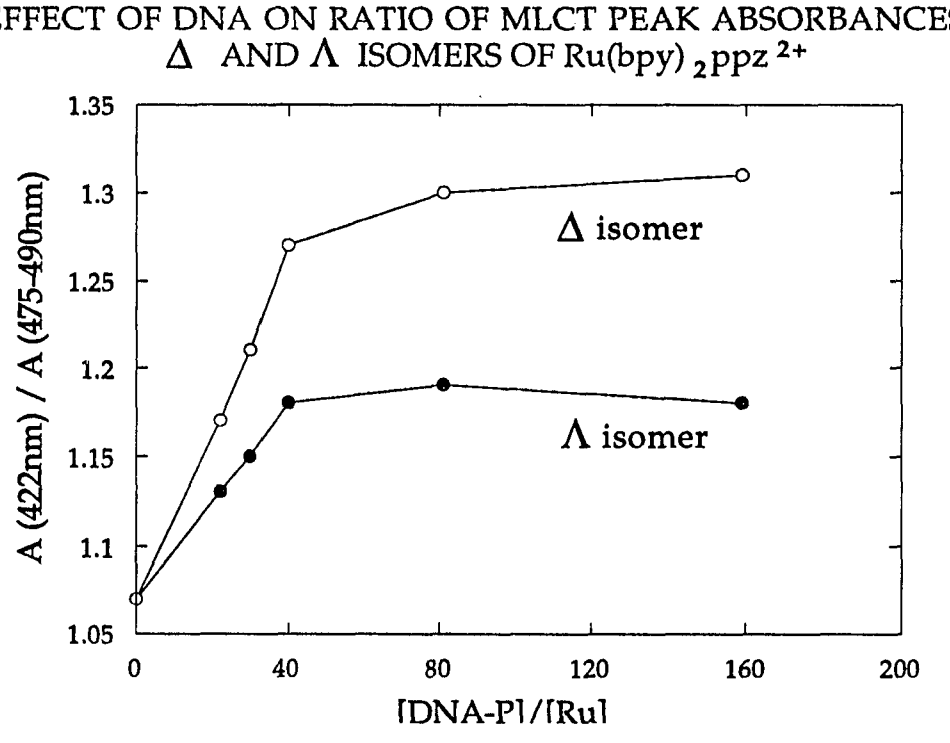

Figure VII-3. Ratio of high energy MLCT band (bpy) to low energy MLCT band (ppz) of Δ and Λ $Ru(bpy)_2ppz^{2+}$ vs [DNA-P]/[Ru] ratio. All spectra measured at 25°C in 5mM Tris, 50mM NaCl, pH 7.4.

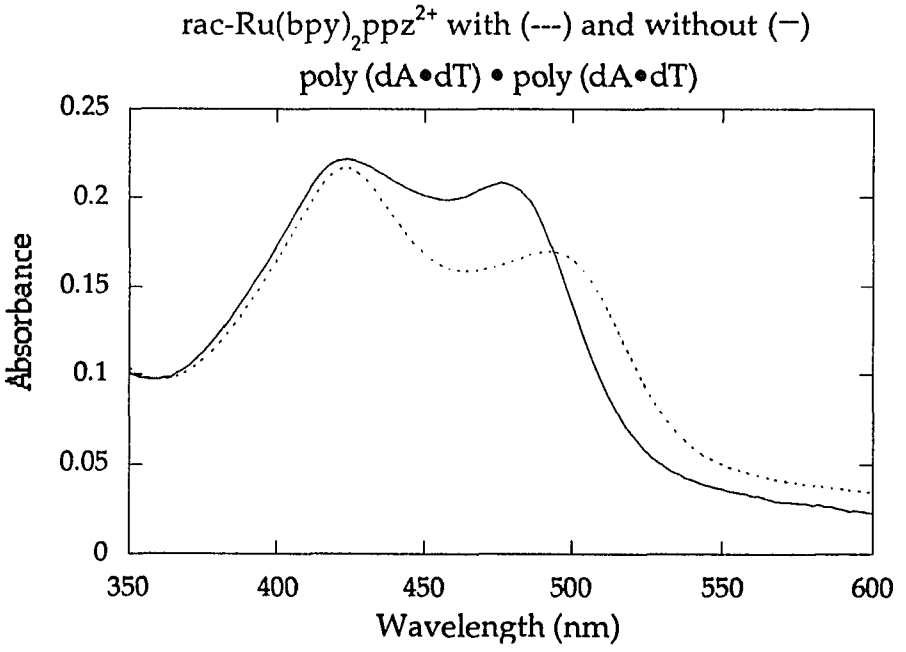

Figure VII-4. Visible absorption spectra of racemic $Ru(bpy)_2ppz^{2+}$ (20μM) alone (——) and in the presence of synthetic poly(dA•dT)•poly(dA•dT) DNA (----). [DNA-P]/[Ru] = 100. All solutions measured at 25°C in 5mM Tris, pH 7.4, 50mM NaCl.

Studies with $Ru(bpy)_2dpp^{2+}$ bound to calf thymus DNA indicate no absorption hypochromism observed at any [DNA-P]/[Ru] ratio. Likewise, no band shifts occur, indicating very weak binding to the DNA duplex.

Preliminary findings with $Ru(phen)_2ppz^{2+}$ bound to calf thymus DNA indicate similar hypochromic effects with the lower energy (ppz) MLCT band. Studies with this complex ion and its enantiomers are now underway in our laboratories, and comparisons to $Ru(bpy)_2ppz^{2+}$ will certainly increase our understanding of the binding behavior of the $Ru(bpy)_2ppz^{2+}$ complex ion.

Emission Enhancement (Increase in Quantum Efficiency)

Upon binding to DNA, luminescence enhancement of the emission band occurring at 690nm is observed for the $Ru(bpy)_2ppz^{2+}$ complex ion. This emission band is attributed to a transition from a π^* orbital on the ppz ligand to a Ru(II) d orbital. Figure VII-5 shows the emission enhancement of the calf thymus DNA bound racemic $Ru(bpy)_2ppz^{2+}$ relative to its emission in free aqueous solution. In addition, a shift of the band maximum to ~670nm (blue shift) and a band narrowing is evident in the spectrum. The quantum yield of emission when bound to DNA increases ~12-fold at large [DNA-P]/[Ru] ratios.

For the resolved enantiomers of $Ru(bpy)_2ppz^{2+}$, emission enhancement is observed for both isomers, yet the effect is more pronounced with the Δ-isomer. Figure VII-6 is the emission enhancement of the Δ- and Λ- isomers at a [DNA-P]/[Ru] ratio of 196. For the Δ-isomer, the maximal emission enhancement upon binding to calf thymus DNA is 17-fold, with a blue-shift to 668nm, compared to an enhancement of 5.2-fold and a blue shift to only 671nm for the

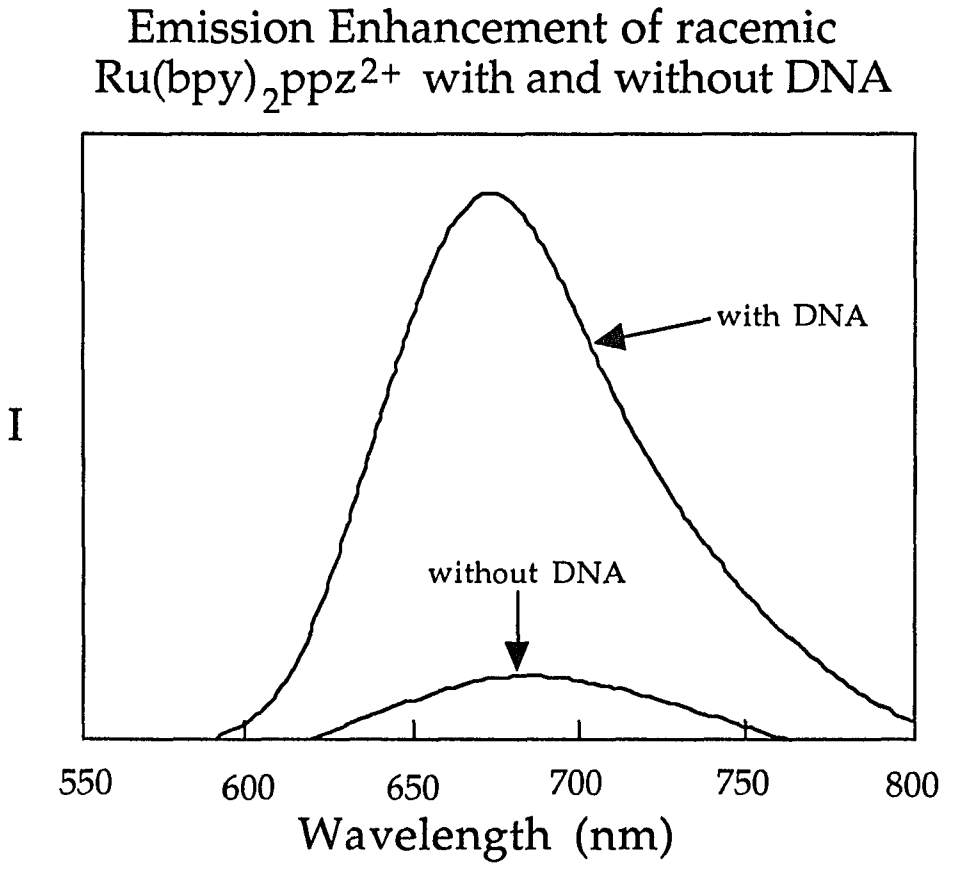

Figure VII-5. Steady-state emission spectra of racemic $Ru(bpy)_2ppz^{2+}$ (9.6μM) alone (——) and in the presence of calf thymus DNA. [DNA-P]/[Ru] = 62. All solutions measured at 25°C in 5mM Tris, pH 7.4, 50mM NaCl.

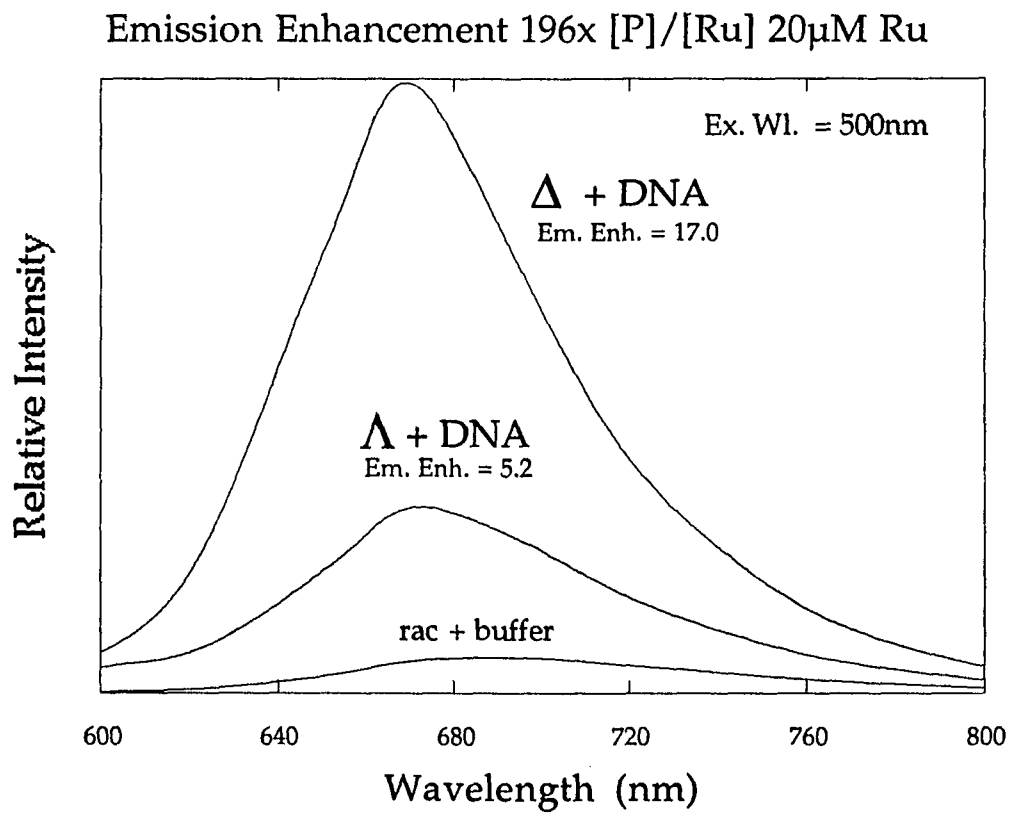

Figure VII-6. Steady-state emission spectra of Δ and Λ $Ru(bpy)_2ppz^{2+}$ (20μM) in the presence of calf thymus DNA and racemic $Ru(bpy)_2ppz^{2+}$ (20μM) in buffer. [DNA-P]/[Ru] = 196. All solutions measured at 20°C in 5mM Tris, pH 7.4, 50mM NaCl.

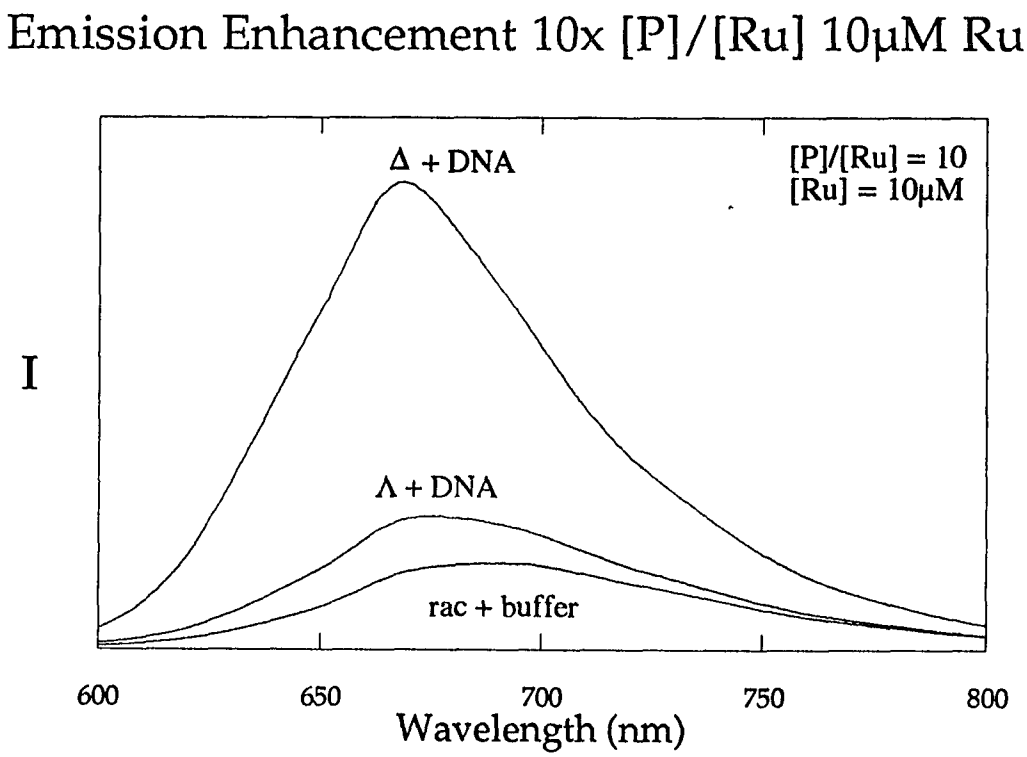

Figure VII-7. Steady-state emission spectra of Δ and Λ $Ru(bpy)_2ppz^{2+}$ (10μM) in the presence of calf thymus DNA and racemic $Ru(bpy)_2ppz^{2+}$ (10μM) in buffer. [DNA-P]/[Ru] = 10. All solutions measured at 20°C in 5mM Tris, pH 7.4, 50mM NaCl.

Λ-isomer. At a [DNA-P]/[Ru] ratio of 10, (Figure VII-7), the emission enhancement for the Δ isomer is much more pronounced than for Λ.

Normalization of emission enhancement plots yield information on the band shapes of the emission and of relative binding strength. Figures VII-8 and VII-9 are the normalized emission bands at [DNA-P]/[Ru] ratios of 196x and 10x, respectively. Figure VII-10 shows the normalized emission enhancement as a function of [DNA-P]/[Ru] ratio of the two enantiomers of $Ru(bpy)_2ppz^{2+}$. For comparison purposes, the normalized emission spectrum of $Ru(bpy)_2ppz^{2+}$ in acetonitrile, DNA and buffer is shown in Figure VII-11, with an emission maximum measured at 668nm. What is evident from Figures VII-8 and VII-9 is the 371 cm^{-1} decrease in the half-width (FWHM) of the emission band (Figure 7), from 1980 cm^{-1} (no DNA) to 1609 cm^{-1} (with DNA) for the Δ-isomer, but to only 1726 cm^{-1} for the Λ-isomer (a 254 cm^{-1} decrease). Already, at a [DNA-P]/[Ru] ratio of 10x (Figure VII-8), the half-width of the emission band of the Δ isomer at is essentially the same as that observed in the higher [DNA-P]/[Ru] ratio, but the Λ-isomer shows a blue shift to only 675nm, with a half-width of 1880 cm^{-1} (100 cm^{-1} decrease).

The normalized emission curves allow a comparison of the relative dependence of the increase in emission enhancement on the [DNA-P]/[Ru] ratio for both isomers. One can see from Figure VII-10 that the onset of emission enhancement occurs at lower ratios for the Δ-isomer. Qualitatively this indicates a higher binding constant for this isomer. A Scatchard analysis[316] of the binding using emission data, and employing the McGhee and von Hippel equation,[338]

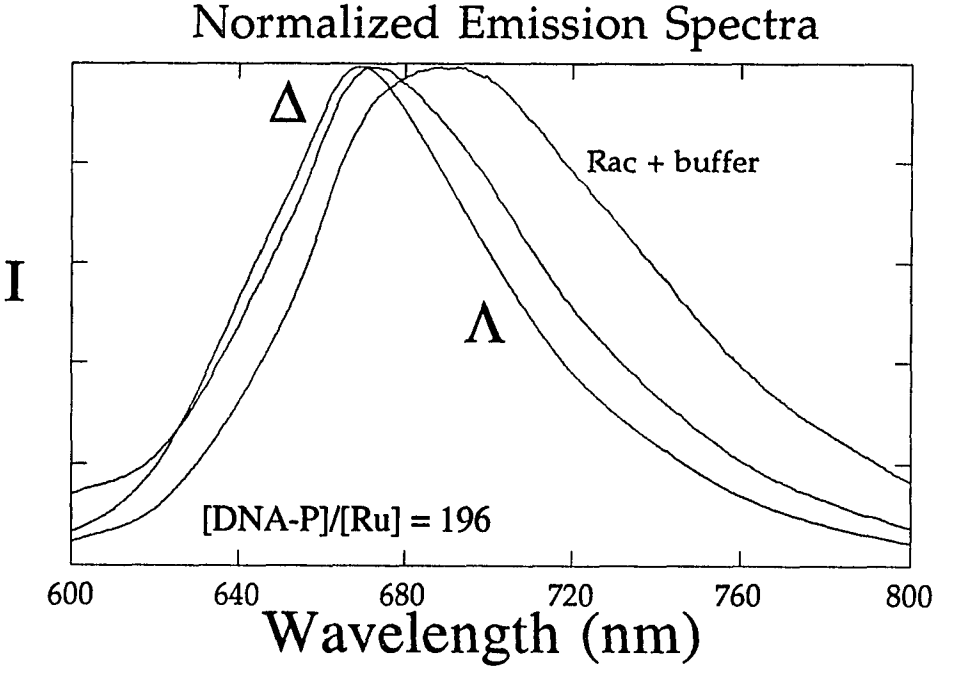

Figure VII-8. Normalized steady-state emission spectra of Δ and Λ $Ru(bpy)_2ppz^{2+}$ (5μM) in the presence of calf thymus DNA and racemic $Ru(bpy)_2ppz^{2+}$ (5μM) in buffer. [DNA-P]/[Ru] = 196. All solutions measured at 20°C in 5mM Tris, pH 7.4, 50mM NaCl.

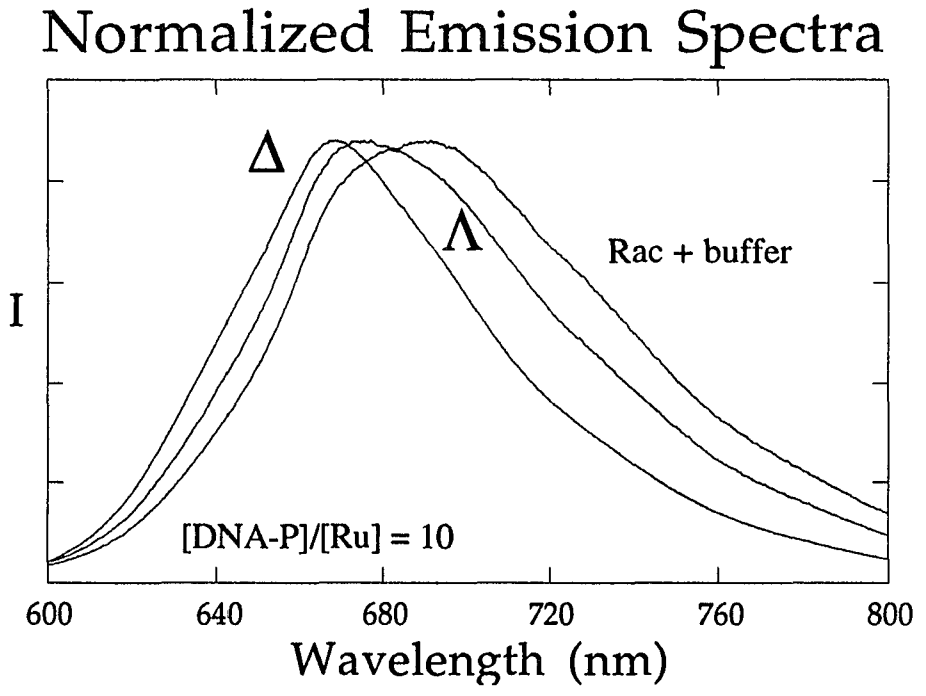

Figure VII-9. Normalized steady-state emission spectra of Δ and Λ $Ru(bpy)_2ppz^{2+}$ (5μM) in the presence of calf thymus DNA and racemic $Ru(bpy)_2ppz^{2+}$ (5μM) in buffer. [DNA-P]/[Ru] = 10. All solutions measured at 20°C in 5mM Tris, pH 7.4, 50mM NaCl.

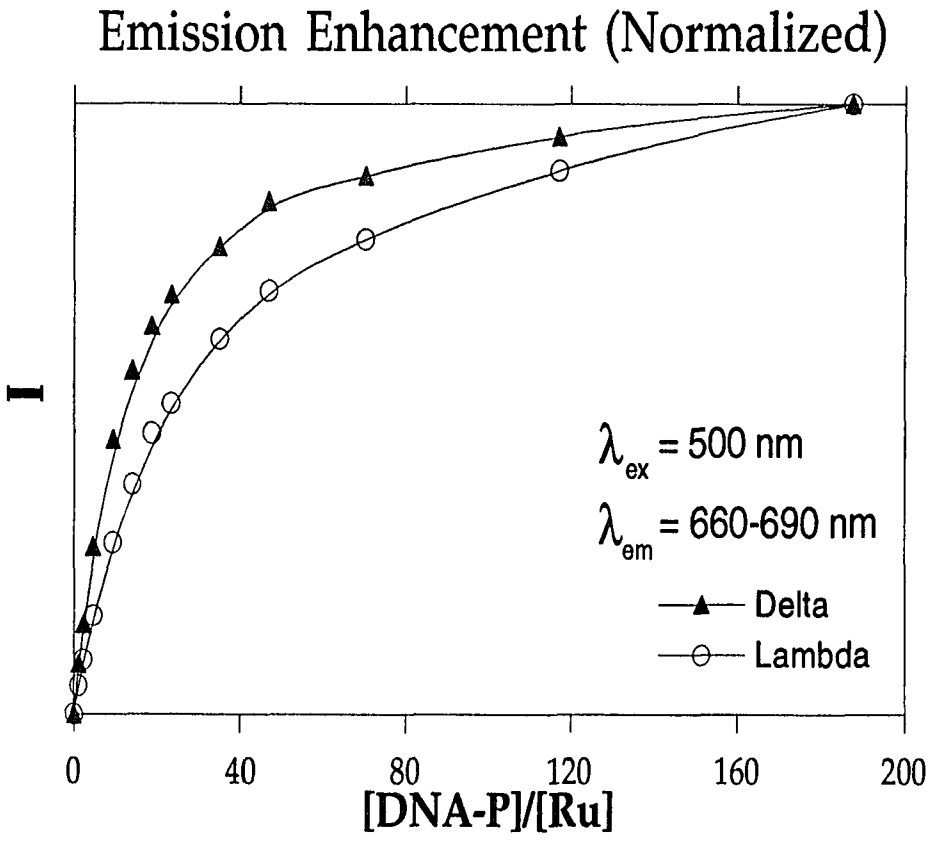

Figure VII-10 Normalized emission enhancement (Intensities at λ_{max}) vs. [DNA-phosphate]/[Ru] ratio for the Δ and Λ enantiomers of $Ru(bpy)_2ppz^{2+}$. All samples excited with λ_{ex} = 500nm at 10.0nm bandwidth. λ_{em} = 660-690nm. All samples measured at 20°C in 5mM Tris, 50mM NaCl buffer, pH 7.4. (▲ -Delta, O-Lambda)

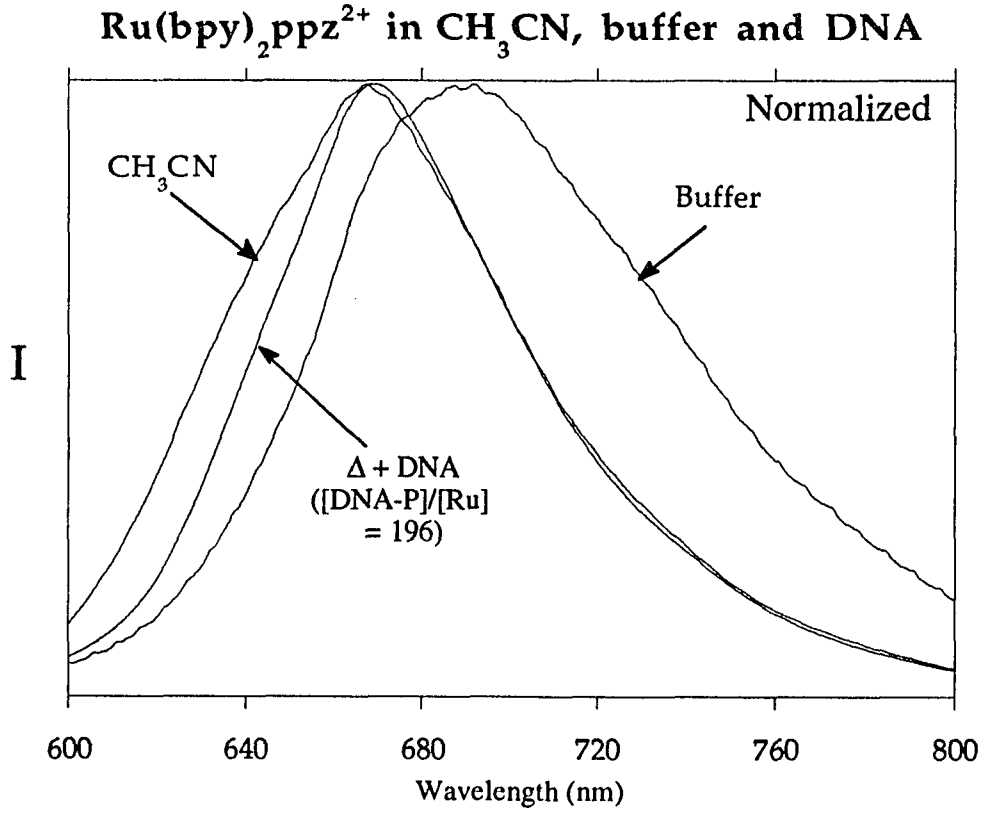

Figure VII-11. Normalized emission spectra of racemic $Ru(bpy)_2ppz^{2+}$ (5μM) in acetonitrile and in 5mM Tris, pH 7.4, 50mM NaCl buffer, and the Δ isomer in the presence of DNA ([DNA-P]/[Ru] = 196).

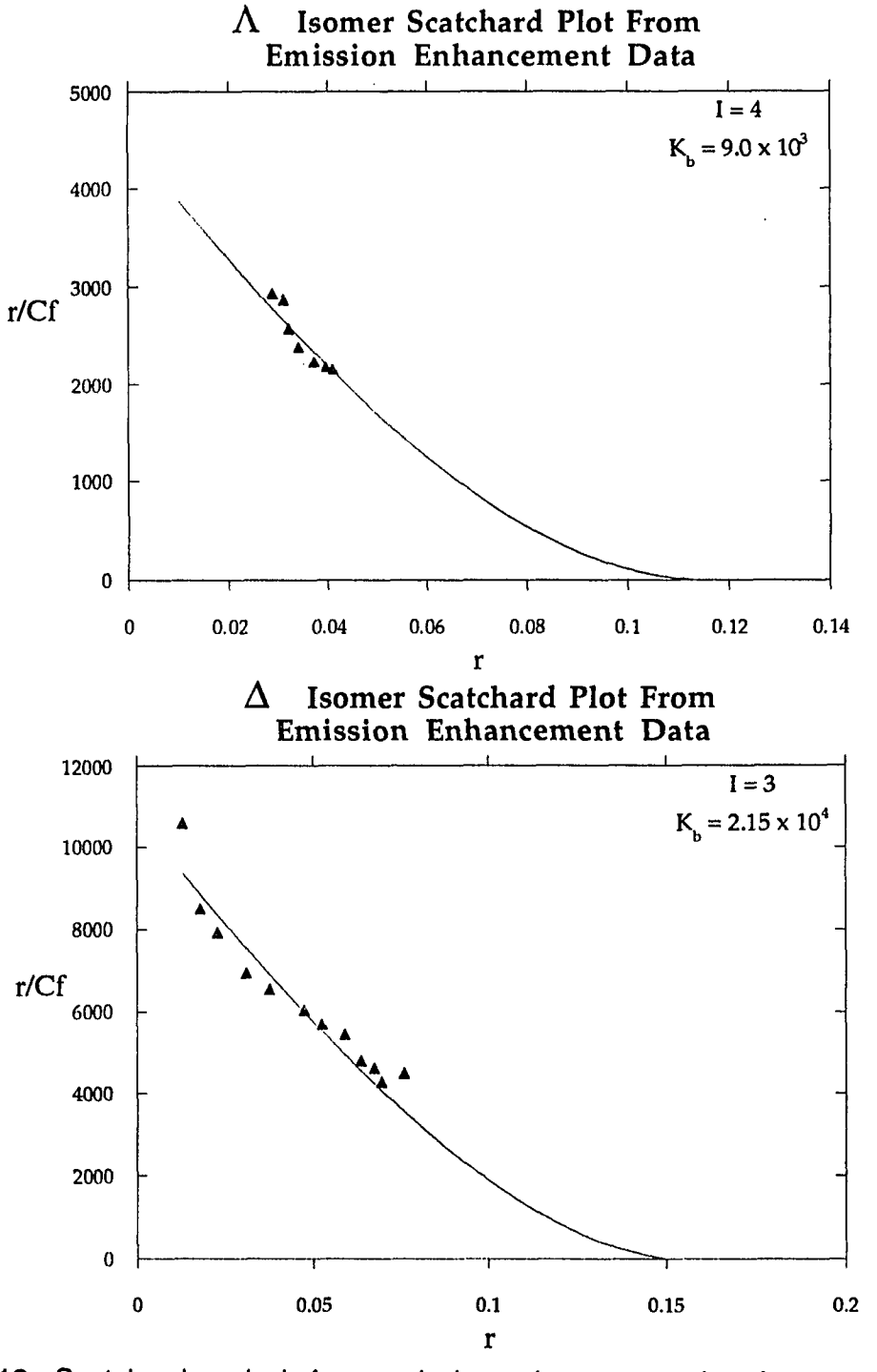

Figure VII-12. Scatchard analysis from emission enhancement data for Δ and Λ $Ru(bpy)_2ppz^{2+}$ (5μM). (▲) actual data, (——) best fit to the McGhee and von Hippel equation. Site sizes and binding constants are indicated in plot.

yields the following binding constants for the two isomers: 2.15 x 10^4 M^{-1}(Δ) and 9.0 x 10^3 M^{-1}(Λ).(Figure VII-12) The site size parameter giving the best fit in both cases was I=3. Fits using I=4 were not significantly worse. These numbers compare well with values obtained from equilibrium dialysis data of racemic $Ru(bpy)_2ppz^{2+}$. (6.0 x 10^3 M^{-1} I=3,4)

For the $Ru(bpy)_2dpp^{2+}$ complex ion, no change in emission intensity or band shape was observed in the presence of calf thymus DNA at high [DNA-P/[Ru] ratios. Figure VII-13 is the normalized emission spectrum of $Ru(bpy)_2dpp^{2+}$ in the presence and absence of DNA and in CH_3CN. Notice that the broad and structureless emission band shape is retained for $Ru(bpy)_2dpp^{2+}$ in the presence of DNA, while the band shape of the $Ru(bpy)_2ppz^{2+}$ ion changes significantly. (See Figure VII-11) The $Ru(bpy)_2ppz^{2+}$ emission band gets narrower and more gaussian in DNA. Also, the emission spectrum qualitatively indicates that the dpp complex does not bind in a hydrophobic environment, contrary to the results found for the ppz complex.

Preliminary results of luminescence studies of racemic $Ru(phen)_2ppz^{2+}$ bound to DNA show enhancement, yet smaller maximal emission enhancement than the corresponding racemic $Ru(bpy)_2ppz^{2+}$. It can be argued that the phen ligands are more restrictive than bpy, and therefore $Ru(bpy)_2ppz^{2+}$ can penetrate deeper than $Ru(phen)_2ppz^{2+}$ into the major groove of DNA.

Emission Lifetimes

Luminescence lifetime measurements are a sensitive probe of the local environment of the chromophore, and report on the binding of the chromophore

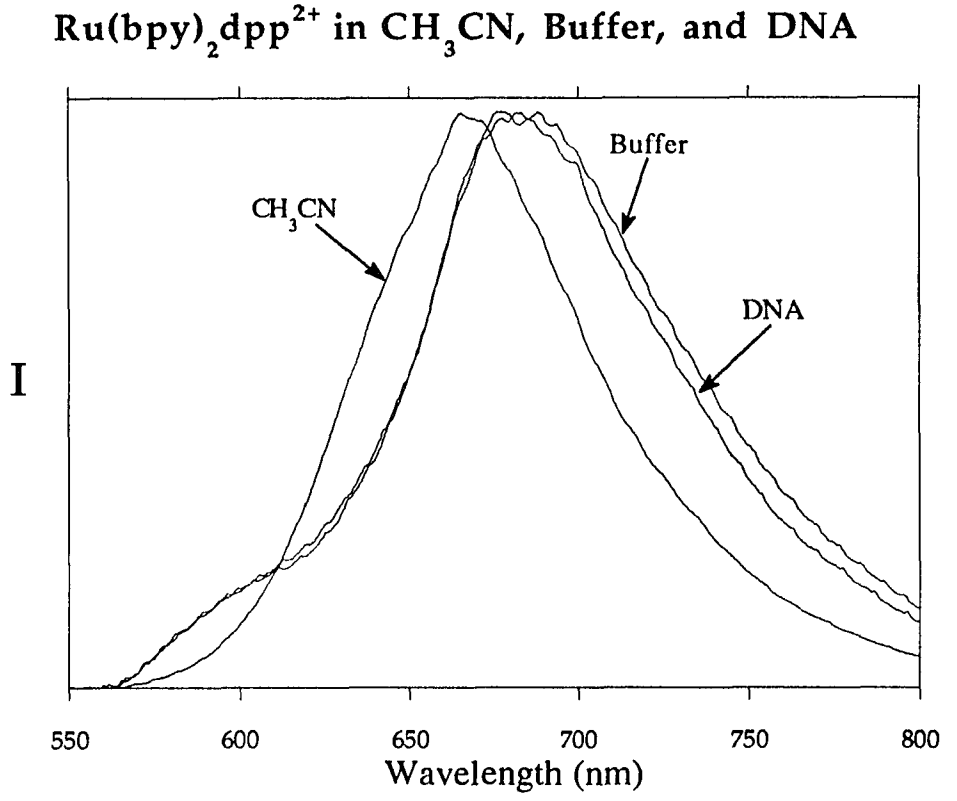

Figure VII-13 Normalized emission spectra of racemic $Ru(bpy)_2dpp^{2+}$ (5μM) in acetonitrile and in 5mM Tris, pH 7.4, 50mM NaCl buffer, in the presence of DNA ([DNA-P]/[Ru] = 196).

to a macromolecule.[333] The above described emission enhancements for Δ and Λ isomers of $Ru(bpy)_2ppz^{2+}$ are associated with emission lifetime increases as a result of binding to DNA. Previous studies[5] have attributed the longer component of a biphasic emission decay curve when bound to DNA to an intercalated, major groove bound complex, and the shorter component with a surface bound mode.[5,6] For the enantiomers of $Ru(bpy)_2ppz^{2+}$, a biphasic emission decay is found for both isomers in DNA, (Figure VII-14) which can be resolved into two components (Figure VII-15). The shorter component for both isomers is comparable to the monophasic solution values (~120-130ns). The longer lifetime component is given in Figure VII-16 and plotted as a function of [DNA-P]/[Ru] ratio. The limiting values for luminescence lifetime are different for each isomer. For the Δ isomer, a maximal value of 950 ns is obtained. For the Λ isomer, a maximal value of ~550 ns is obtained, but as the DNA concentration is increased, there is less contribution from the long component relative to the Δ-isomer at similar [DNA-P/[Ru] ratios. Lifetime values distinguish a difference in degree (i.e. a quantitative difference) between the modes of the strong binding of the two enantiomers, and these different values for the long component are an indication of the differential binding modes present for the two enantiomers. Figure VII-15 indicates the contributions of the modes of binding for each enantiomer at 2 different binding ratios.

It is interesting to point out here that **no** differences in the lifetimes of the long component of the luminescence were found for the enantiomers of $Ru(phen)_3^{2+}$ when studied by Barton et. al.,[6] and they failed to explain these

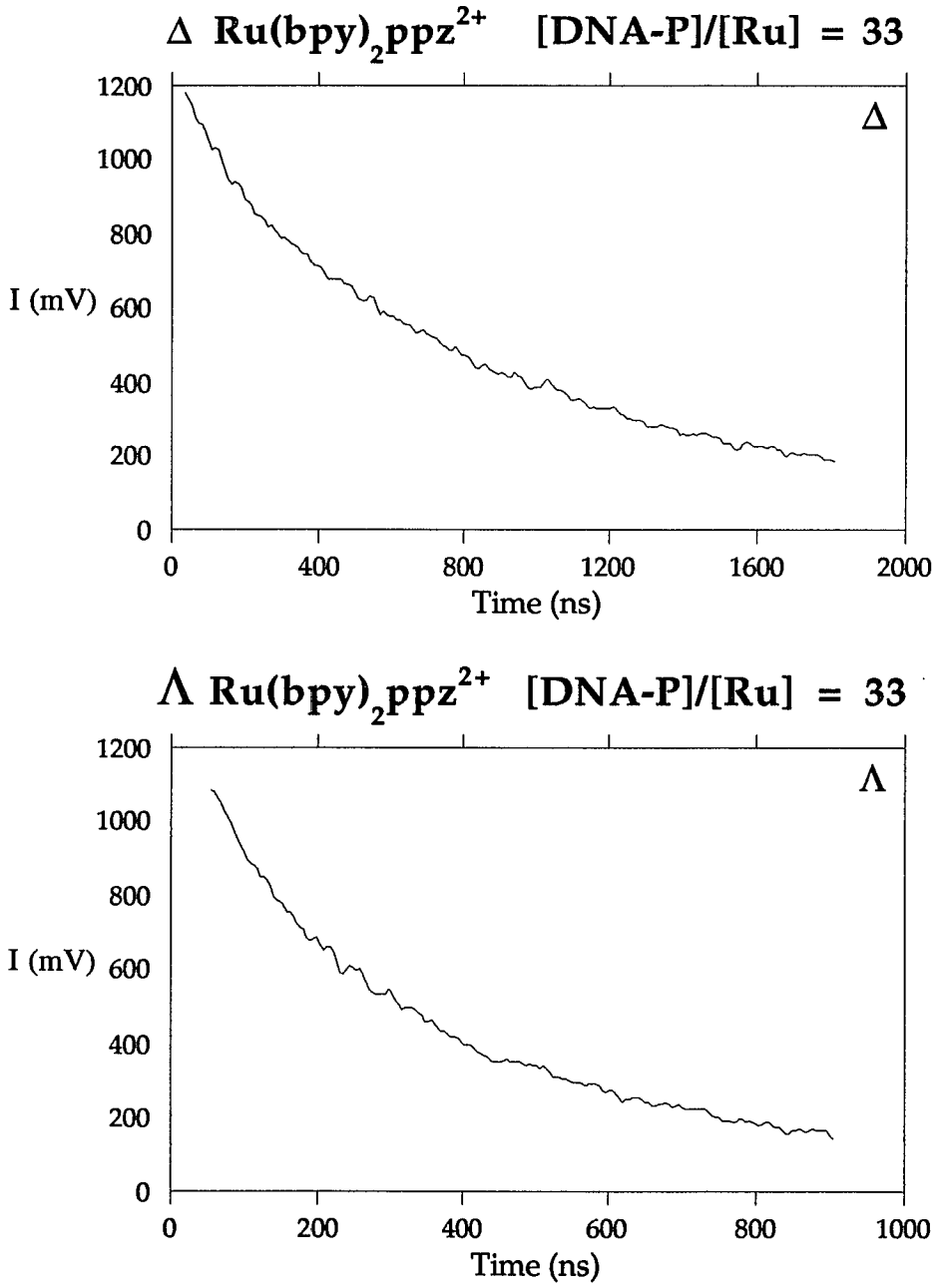

Figure VII-14. Emission decay curves of Δ and Λ $Ru(bpy)_2ppz^{2+}$ (5μM) in the presence of calf thymus DNA and racemic $Ru(bpy)_2ppz^{2+}$ (5μM) in buffer. [DNA-P]/[Ru] = 33. The 355nm line of a Nd:YAG laser was used for excitation. All solutions monitored at 680nm and measured at 20°C in 5mM Tris, pH 7.4, 50mM NaCl.

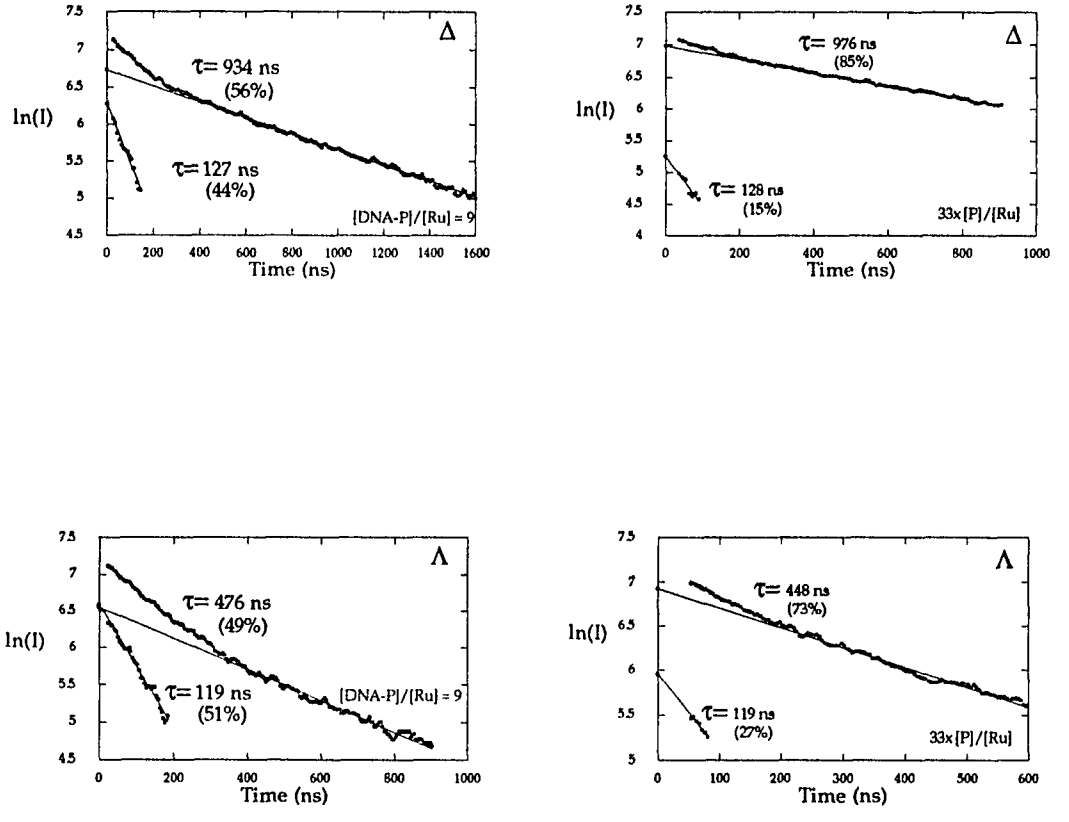

Figure VII-15. Natural logarithm of luminescence intensity vs. time for Δ (top) and Λ (bottom) $Ru(bpy)_2ppz^{2+}$ (5μM) in the presence of calf thymus DNA. [DNA-P]/[Ru] = 9,33. All solutions measured at 20°C in 5mM Tris, pH 7.4, 50mM NaCl. Solid lines represent best fit for lifetimes (pre-exponential weighting factors given in parentheses).

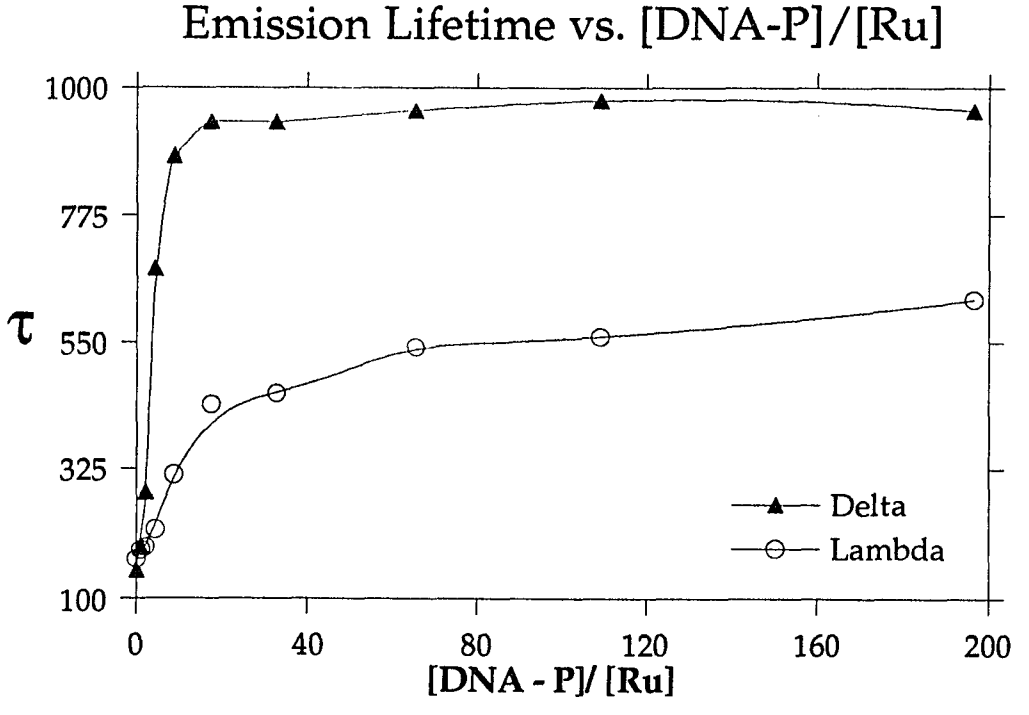

Figure VII-16. Luminescence lifetime of the long component emission of the Δ and Λ $Ru(bpy)_2ppz^{2+}$ isomers (5μM) vs. [DNA-P]/[Ru] ratio. Emission lifetimes measured at 20°C using 355nm Nd:YAG excitation and monitored at 680nm using 8.0 nm bandwidth. (▲ -Delta, ○-Lambda) All samples measured in 5mM Tris, 50mM NaCl buffer, pH 7.4.

findings in subsequent research. These results seem to indicate a more similar type of binding for both isomers of $Ru(phen)_3^{2+}$ when compared with the isomers of $Ru(bpy)_2ppz^{2+}$, which show significantly different behavior as evidenced by the different luminescence lifetimes of the long component of emission. We conclude from our data that for $Ru(bpy)_2ppz^{2+}$, the binding modes that account for the long component of the emission decay are substantially different for the two enantiomers. Furthermore, the short component contribution is diminished at higher [DNA-P/[Ru] ratios for both isomers, suggesting that intercalation (which would give rise to the long component) is the preferred binding mode at low metal complex concentrations (i.e. at high [DNA-P/[Ru] ratios) for both enantiomers, and surface (or minor groove) binding modes become appreciable only when all possible intercalation sites are occupied, i.e at low [DNA-P/[Ru] ratios. The extent to which intercalation occurs (i.e. the depth of penetration by the ligand into the helix) can therefore be understood from the point of view of enantioselectivity and emission lifetime. A "better fitting" Δ isomer would be allowed to penetrate the helix to a greater extent than the Λ isomer, and as a result, the emission lifetime of the Δ isomer would be longer than Λ, due to the fact that Δ would presumably be buried deeper into the non-polar region of the double helix, increasing its lifetime.

The data presented here represent the first well characterized report of differential binding modes for enantiomers distinguished by luminescence lifetimes, and strongly suggest that partial intercalation of the ppz ligand is an accurate description of the binding mode for both enantiomers. Partial

intercalation however, occurs to a greater extent with the Δ isomer (i.e. deeper penetration), as evidenced by the longer lifetime of its long component of emission decay. This description is compatible with the absorption hypochromism and emission enhancement observed for the two enantiomers, where the larger effect was seen for the Δ isomer.

Emission Polarization

When an emitting chromophore becomes sufficiently immobilized during its absorption and emission lifetime, the emission may be polarized as a result of this immobilization.[47] Upon binding to DNA, emission polarizations are only expected to arise from those chromophores sufficiently oriented during the lifetime of the excited state. As a consequence, the longer the lifetime of the excited state, the more likely depolarization of the emission will occur.

Emission polarizations are more likely to be the result of a tight binding interaction, and surface or electrostatic binding is not thought to give rise to this emission property. An intercalative interaction, on the other hand, is a very rigid binding mode and would be expected to show large polarizations associated with this binding process.

Emission polarizations of DNA solutions are actually measures of DNA motion as well, since the rigidly held chromophores rotate with the DNA helix, and DNA, being a large macromolecule, is expected to rotate only very slowly even at room temperature.[333] In this respect, emission polarizations indicate a lower limit of the residence time of the chromophore within the macromolecule, since the reorientation of DNA occurs only slightly during the typical lifetime of a

Ru(II) tris-chelate luminescence. (~100-1000ns)

For the racemic $Ru(bpy)_2ppz^{2+}$ complex, a maximum emission polarization of 0.09 was found for the complex bound to DNA at 20°C exciting within the ppz MLCT band. A maximum theoretical polarization of ~0.14 (fully oriented) is calculated for RuL_3^{2+} complexes of D_3 symmetry,[47] yet with these complexes, higher polarizations (~.25) have been found in 77K glass matrices,[47,66] perhaps due to anisotropy caused by molecular distortions or by the charge transfer process itself (symmetry lowering events). Similar arguments can be made for the $Ru(bpy)_2ppz^{2+}$ complex, however its symmetry is also lowered from D_3 by the presence of the ppz ligand. A plot of polarization vs. [DNA-P]/[Ru] is given in Figure VII-17, overlayed with a plot of the polarization measured for $Ru(bpy)_3^{2+}$, which is essentially zero for all [DNA-P]/[Ru] ratios examined.

For the enantiomers, emission polarizations are given in Figure VII-18, which show that the enantiomers of $Ru(bpy)_2ppz^{2+}$ have similar polarizations (0.09-0.10) at the highest [DNA-P]/[Ru] ratios. The slightly higher polarization found for the Λ-isomer at higher [DNA-P]/[Ru] ratios can be understood in light of the emission lifetime data, where the excited state of this isomer would be expected to be less depolarized than the excited state of the Δ-isomer, due to the shorter emission lifetime of the Λ-isomer. In other words, since the emission lifetime of the Δ-isomer is ~2x that of the Λ-isomer, it has approximately twice the amount of time to depolarize the emission.

Excitation polarization data, presented in Figure VII-19, show significant

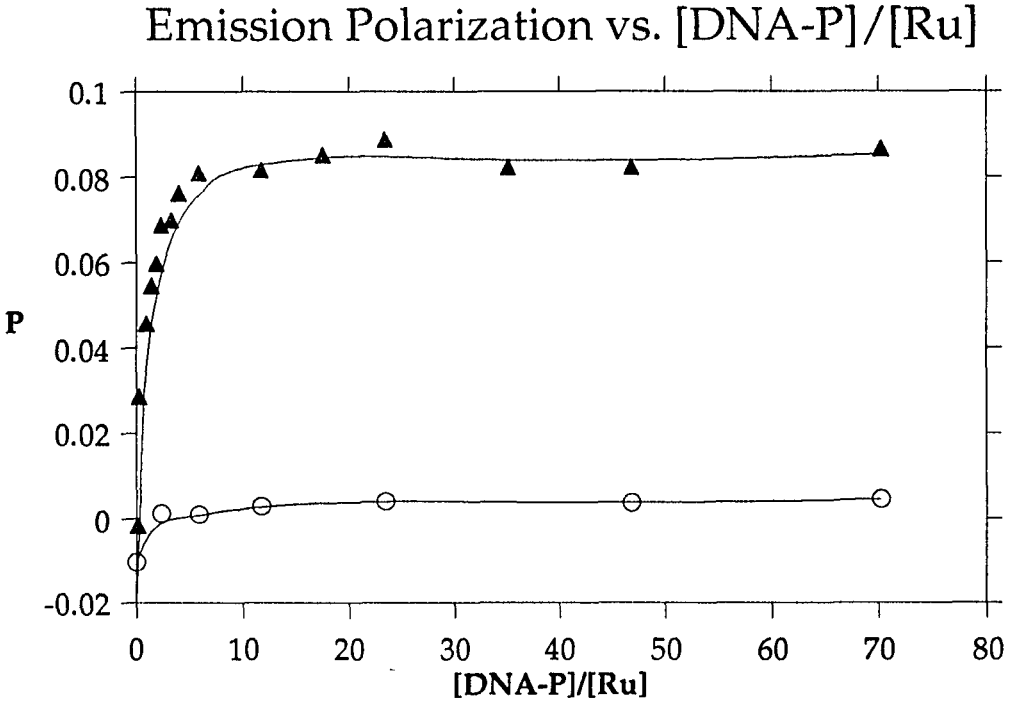

Figure VII-17. Luminescence polarization of the racemic $Ru(bpy)_3^{2+}$ and $Ru(bpy)_2ppz^{2+}$ (5μM) vs. [DNA-P]/[Ru] ratio. Emission polarizations measured at 20°C using 500nm excitation and monitored at 680nm using 10.0 nm bandwidth. (▲ - $Ru(bpy)_2ppz^{2+}$, ○- $Ru(bpy)_3^{2+}$) All samples measured in 5mM Tris, 50mM NaCl buffer, pH 7.4.

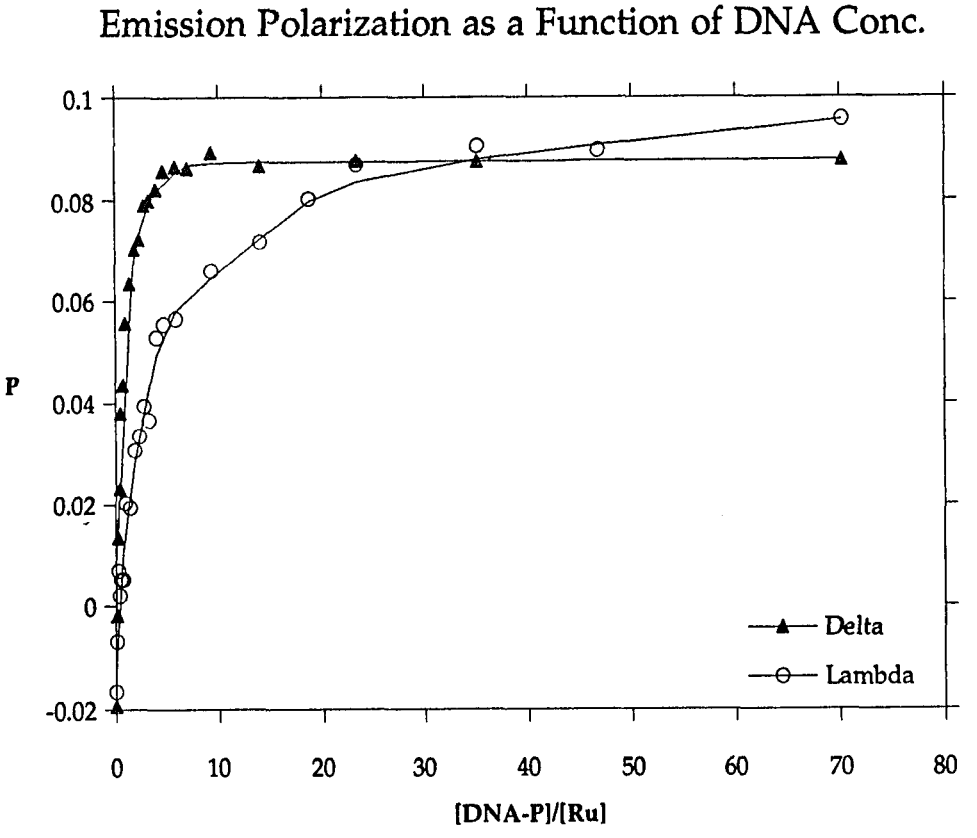

Figure VII-18 Emission Polarization of the $Ru(bpy)_2ppz^{2+}$ enantiomers vs. [DNA-phosphate]/[Ru] ratio. All data points were collected over an average of 2 minutes sampling every 0.1 second and measured at 20°C (▲ -Delta, O-Lambda) All samples measured in 5mM Tris, 50mM NaCl buffer, pH 7.4.

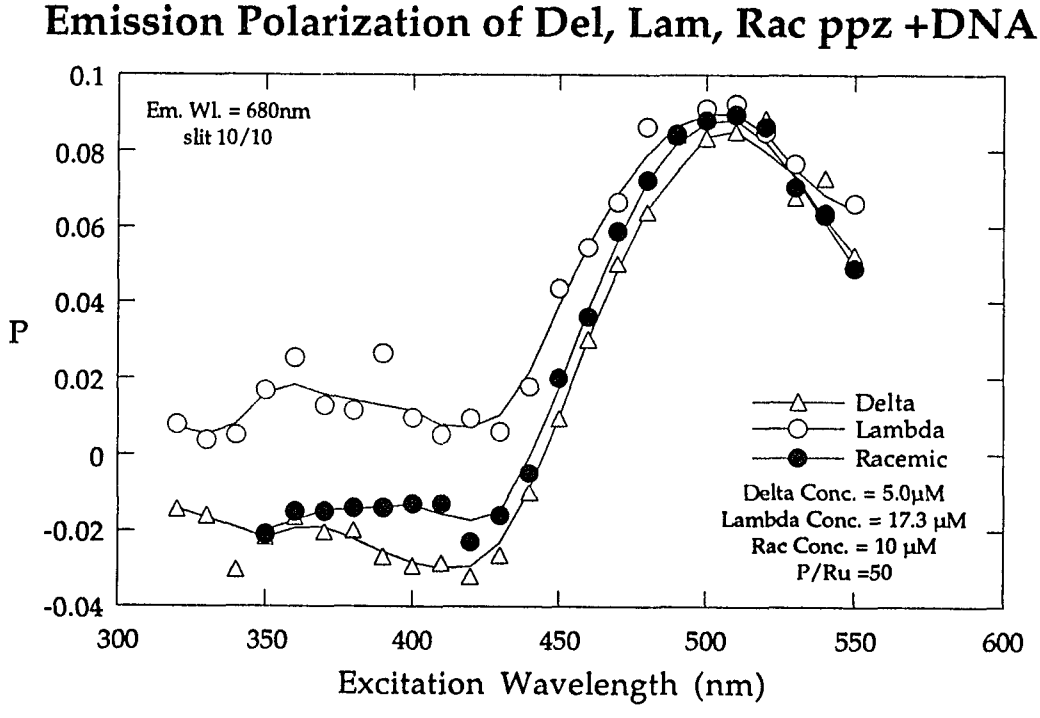

Figure VII-19. Excitation polarization (Ex. Wavelength vs. P) of Δ, Λ and racemic $Ru(bpy)_2ppz^{2+}$ monitored at 680nm. All data points were collected over an average of 2 minutes sampling every 0.1 second and measured at 20°C (△ -Δ, ○-Λ, ●-Racemic) All samples measured in 5mM Tris, 50mM NaCl buffer, pH 7.4.

polarization for excitation within the MLCT band associated with the ppz ligand, but virtually no polarization for excitation within the bpy MLCT band. According to the proposed binding model, ground and excited state vibrational modes of the bpy ligands should not be perturbed to the same extent as the ppz ligands, nor should the bpy ligands be as rigidly oriented. The relative flexibility of the bpy ligands relative to the ppz ligand may account for the lack of polarization seen for excitation via the bpy MLCT bands, but other explanations are possible.

While the observed emission in $Ru(bpy)_2ppz^{2+}$ is believed to be attributed to transfer of charge from a ppz π^* orbital to a metal d orbital, the mechanism for this process has not been completely elucidated. When thebpy MLCT band is excited, it can be envisioned that the process of transferring the charge from a bpy ligand to the ppz ligand, in preparation for luminescence from the ppz π^* orbital, depolarizes the luminescence. Also, the orientation of the bpy ligands with respect to the ppz ligand places the absorption and emission oscillators in different planes when exciting through bpy, leading to depolarization. Furthermore, the absorption oscillator lies in two planes, and the emission oscillator lies in yet a third plane. All of these may contribute to the effect of depolarizing emission when exciting through the bpy MLCT band.

The polarization of the emission for excitation within the ppz MLCT band, in the 475nm-525nm range, has the absorption and emission oscillators oriented in the same plane. In DNA solutions, since the luminescence arises from a transition from the ppz π^* orbital to a metal d orbital, large emission

polarizations associated with metal to ppz ligand transitions can only be interpreted as arising from a rigidly held (i.e. intercalated) ppz ligand.

Rate constants

The quantum yield of luminescence and luminescence lifetime for the rac, Δ- and Λ- isomers of the $Ru(bpy)_2ppz^{2+}$ ion in the presence and absence of DNA, and in acetonitrile, are given in Table 1. Quantum yields of luminescence are relative to N_2 purged $Ru(bpy)_3^{2+}$ in aqueous solution (ϕ= 0.042).[344]

Measurements of ϕ_{em} and τ allow the calculation of the rate constants k_r and k_{nr}, which represent the corresponding rate constants for the radiative (k_r) and non-radiative (k_{nr}) deactivation processes. The ratio of τ/ϕ_{em} is also calculated, which is the radiative lifetime (τ_r) in the absence of all quenchers. These values are given in Table 1. The parameters k_r and k_{nr} are calculated from the equations

$$\tau = 1 / k_r + k_{nr} \quad [1]$$

$$\phi_{em} = k_r / k_r + k_{nr} \quad [2]$$

where τ is the observed lifetime, ϕ is the relative quantum yield, and k_r and k_{nr} represent the first order rate constants for the processes of radiative and non-radiative deactivation.[73]

Table 1

Measured and calculated values of ϕ_{em}, τ, k_r, k_{nr}

	ϕ_{em}	τ (ns)	k_r (s^{-1})	k_{nr} (s^{-1})	τ_r(μs)
rac-ppz (buffer)	0.0023	120	1.9×10^4	8.2×10^6	52
rac-ppz (CH_3CN)	0.009	450	2.0×10^4	2.2×10^6	50
Δ - ppz (DNA)*	0.039	950	4.1×10^4	1.0×10^6	24
Λ - ppz (DNA)*	0.012	550	2.1×10^4	1.7×10^6	47

*Both isomers are fully bound at [DNA-P]/[Ru] = 196

The radiative lifetimes for *rac*-$Ru(bpy)_2ppz^{2+}$ in buffer (5 mM Tris, 50mM NaCl, pH 7.4) and with *rac*-$Ru(bpy)_2ppz^{2+}$ in CH_3CN are similar. This is what is typically found for chromophores introduced into different solvents, whereas the quenching environment of the solvent is altered, changing the non-radiative rate constant, but leaving the radiative rate constant relatively unchanged.

From Table 1, a decrease in the radiative lifetime for the Δ-$Ru(bpy)_2ppz^{2+}$ enantiomer by a factor of ~2 is seen in the presence of DNA, where the radiative lifetime for the Λ isomer is slightly lower and for *rac*-$Ru(bpy)_2ppz^{2+}$ in both acetonitrile and buffer the values are similar. Since the radiative lifetime is a property of the chromophore, and not of the quenching environment, a decrease in the radiative lifetime seen for Δ-$Ru(bpy)_2ppz^{2+}$ enantiomer can only be explained as a distinct alteration in the chromophore which is responsible for the luminescence, i.e the ppz ligand. Immobilization of the ppz ligand via partial intercalation and interactions with the neighboring DNA chromophores has profound effects on MLCT excited states associated with the ppz ligand, and a change in the radiative lifetime found for the Δ isomer is indicative of the perturbation of these states upon binding. Since the reciprocal of the radiative lifetime is k_r, a larger k_r found for Δ signifies an increase in the "allowedness" of radiative luminescence with this isomer, and makes this mode of deactivation more competitive with the other radiationless deactivation modes (given by the nonradiative rate constant, k_{nr}).

One other possible interpretation of the change in radiative lifetime involves change of the intersystem crossing efficiency to the emissive state.

While several researchers have accepted the assumption of an intersystem crossing efficiency of ~1.0[46] to the emissive state at room temperature, recent research based on studies in heterogeneous media[256] has challenged this assumption. If one assumes an intersystem crossing efficiency of <1.0 for the Δ-$Ru(bpy)_2ppz^{2+}$ complex in aqueous solution, then as the complex inserts into the DNA, the efficiency may increase and approach more closely an intersystem crossing efficiency of 1.0. This can explain the observed spectroscopic evidence, however, it is difficult to determine whether the k_r is changing or the intersystem crossing efficiency is changing in absence of a temperature dependence study. This type of study is not easily performed on complexes bound to DNA, since both the structure of DNA and the binding constant change as a function of temperature.

The slightly smaller value of k_r found for the Λ isomer compared to the k_r's for the racemic complex in CH_3CN and in buffer indicates that significantly less perturbation of the ppz ligand states occurs for the Λ isomer, and the chromophore is not altered sufficiently to notice a large change in the k_r. This is consistent with the proposed binding model for this isomer, which infers that the ppz ligand may not be radically altered when the Λ isomer binds to DNA, since binding of this isomer proceeds with significantly less penetration of the ppz ligand into the duplex. The amount of penetration of the Λ isomer into the duplex may not be deep enough to radically alter the MLCT excited states of ppz in this isomer, and hence a k_r similar to the free solution k_r's is found for this isomer.

Emission Quenching

Quenching by ferrocyanide ion has been used to infer an intercalative mode of binding for tris-chelates with DNA.[5,6] The intercalated complex within the major groove is less accessible to anionic quenchers in solution, than to electrostatic or surface bound complexes. Figure VII-20 shows Stern-Volmer plots I_o/I for racemic $Ru(bpy)_2ppz^{2+}$ in buffer and for each enantiomer in the presence of DNA at low [DNA-P]/[Ru] (10), and high [DNA-P]/[Ru] (43) ratios. Note that the Δ isomer is weakly quenched at both ratios, with little difference evident between the two curves, and both vary strongly from the free solution curve.

The Λ isomer, however, shows a more marked decrease in quenching at the higher [DNA-P]/[Ru] ratio (43), indicating that the typical binding site for the Λ isomer is less accessible to the ferrocyanide at these higher ratios, and indeed, may be qualitatively different than the typical binding site at lower [DNA-P]/[Ru] ratios. Also, the characteristic non-linear curvature of such plots has been attributed to the differential accessibility of bound complex to the quencher due to a variety of binding sites on the DNA.[5,6]

Luminescence lifetime quenching (τ_o/τ) of the racemic $Ru(bpy)_2ppz^{2+}$ at a [DNA-P]/[Ru] ratio = 10 indicates that the short component of the lifetime profile (attributed to both electrostatically bound and free complex) is quenched at a faster rate (i.e. quenched more efficiently) than the long component, and this short component disappears almost entirely at quencher concentrations of 0.010M $Fe(CN)_6^{4-}$. At these quencher concentrations, the long component of

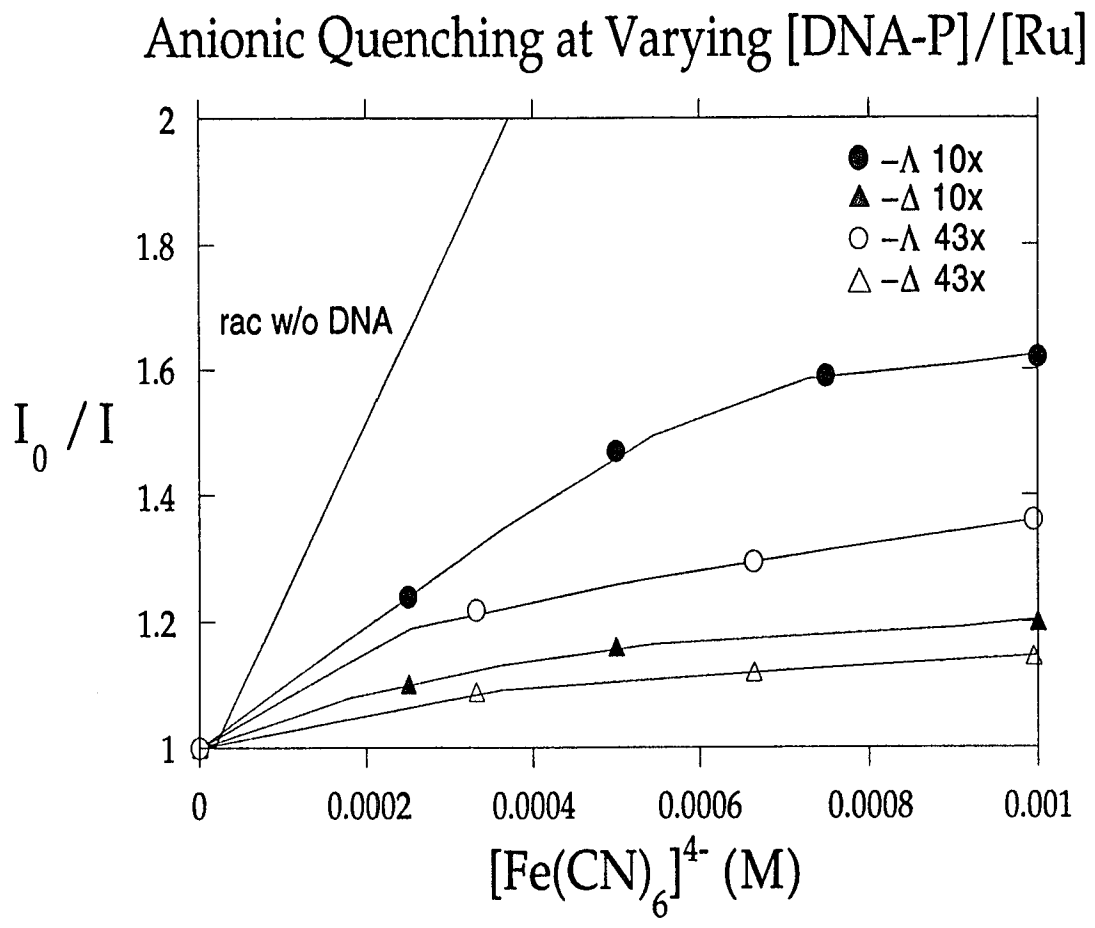

Figure VII-20 Quenching with $Fe(CN)_6^{4-}$ ion for the Δ and Λ enantiomers of $Ru(bpy)_2ppz^{2+}$ at [DNA-phosphate]/[Ru]=10 (filled symbols, ▲-Delta,●-Lambda) and [DNA-phosphate]/[Ru] =43 (hollowed symbols, △-Delta,○-Lambda). Quenching of *rac*-$Ru(bpy)_2ppz^{2+}$ by $Fe(CN)_6^{4-}$ ion in the absence of DNA shown for comparison (straight line) All samples measured at 20°C in 5mM Tris, 50mM NaCl buffer, pH 7.4.

the lifetime profile is still prominent. A very short (<15 ns) component was still visible in the lifetime profile at these quencher concentrations, but was attributed to the laser pulse via comparison to solutions with no $Ru(bpy)_2ppz^{2+}$ present. Figure VII-21 shows lifetime traces of racemic $Ru(bpy)_2ppz^{2+}$ with and without quencher. Plots of the ln(Intensity) vs. time of the quenched and unquenched racemic $Ru(bpy)_2ppz^{2+}$ solutions using a ratio of [DNA-P]/[Ru] =10 were used in Figure VII-22 to allow visualization of the disappearance of the short (electrostatic) component.

Luminescence lifetime quenching (τ_o/τ) reports on dynamic quenching, where emission intensity quenching (I_o/I) reports on both static and dynamic quenching processes.[73] Therefore, luminescence lifetime quenching is a more revealing technique for analyzing the quenching processes that occur in the excited state, and it also gives more information on the possible binding sites present in DNA.

Equilibrium Dialysis Binding Studies

Equilibrium dialysis experiments provide parameters K_b, the binding constant, and *l*, the average binding site size in base pairs, from a fit to the McGhee and von Hippel equation, as used by Barton et. al.[4]

$$r/C_f = (K_b/2)(1-2lr)[(1-2lr)/(1-2(l-1)r)]^{l-1} \qquad [3]$$

where r is the fraction of DNA phosphate sites occupied and C_f is the free solution concentration of the Ru(II) complex.[338]A best fit curve and the parameters generated from this fit are given in Figure VII-23 for the racemic $Ru(bpy)_2ppz^{2+}$ complex ion bound to calf thymus DNA.

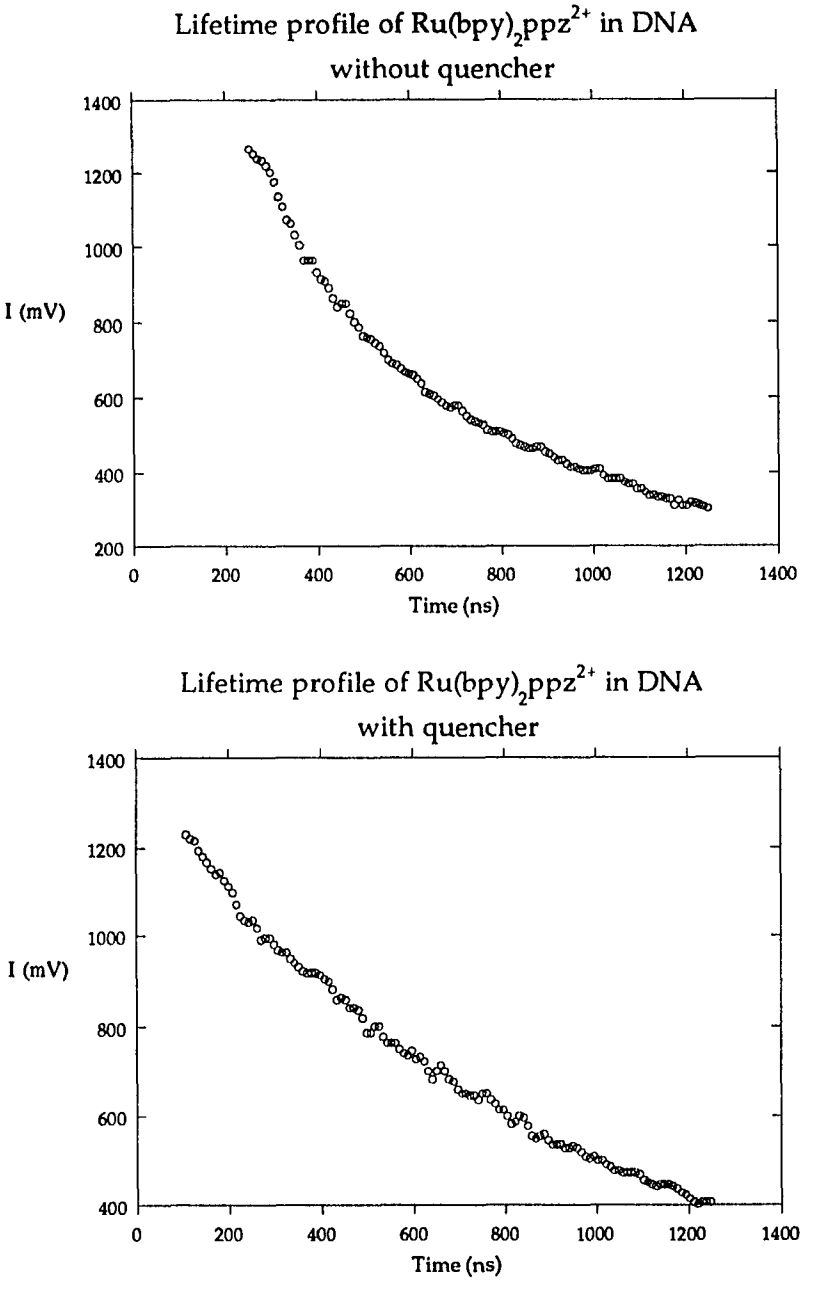

Figure VII-21. Luminescence lifetime traces of racemic $Ru(bpy)_2ppz^{2+}$ in DNA ([DNA-P]/[Ru] = 10) without (top) and with (bottom) $Fe(CN)_6^{4-}$ (anionic quencher). Samples excited at 355nm with a Nd:YAG laser and monitored at 680nm.

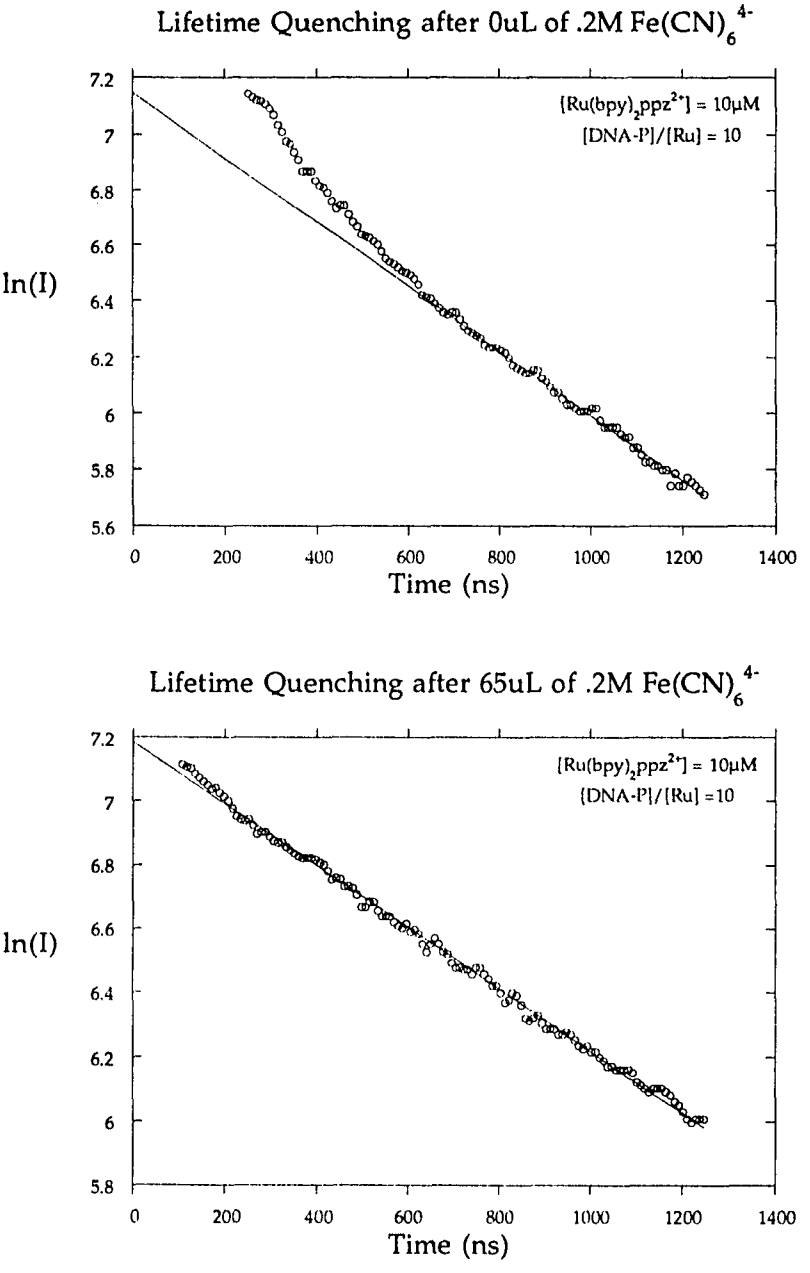

Figure VII-22. Disappearance of the short component of emission lifetime for racemic $Ru(bpy)_2ppz^{2+}$ in DNA ([DNA-P]/[Ru] = 10) upon addition of $Fe(CN)_6^{4-}$ (anionic quencher). Samples excited at 355nm with a Nd:YAG laser and monitored at 680nm.

Racemic $Ru(bpy)_2ppz^{2+}$ gives a binding constant of 6.0×10^3 and a site size I = 3 to 4. While binding constants of this magnitude are significantly lower than those found for organic intercalators (e.g. Ethidium bromide), only a portion of the entire molecule is intercalatively bound, and therefore it is less intimately held, lowering the binding constant.

Enantioselectivity

Dialyzates from experiments in which racemic $Ru(bpy)_2ppz^{2+}$ is dialyzed against 1.6mM calf thymus DNA for 41 hours were subjected to circular dichroism analysis. The presence of a CD signal is indicative of enrichment of the dialyzate with the isomer that binds less strongly to DNA, as described by Barton et. al.[4] In Figure VII-24, the CD spectrum of the $Ru(bpy)_2ppz^{2+}$ dialyzate in the 220-320 nm range is displayed. Although a CD signal would be expected to be found for the visible MLCT bands, the ellipticities are more than an order of magnitude smaller. A strong CD signal with a positive peak at 273nm and a stronger negative peak at 289nm is shown.

No CD signal was found for similar studies with the $Ru(bpy)_2dpp^{2+}$ complex (dpp ligand = non-planar analogue of ppz), indicating no enantioselective binding with this cation. These results therefore indicate that only the complex with the planar intercalating ligand, $Ru(bpy)_2ppz^{2+}$, binds enantioselectively with DNA, and this type of binding is precluded by the presence of the non-planar dpp ligand portion of the $Ru(bpy)_2dpp^{2+}$ complex ion.

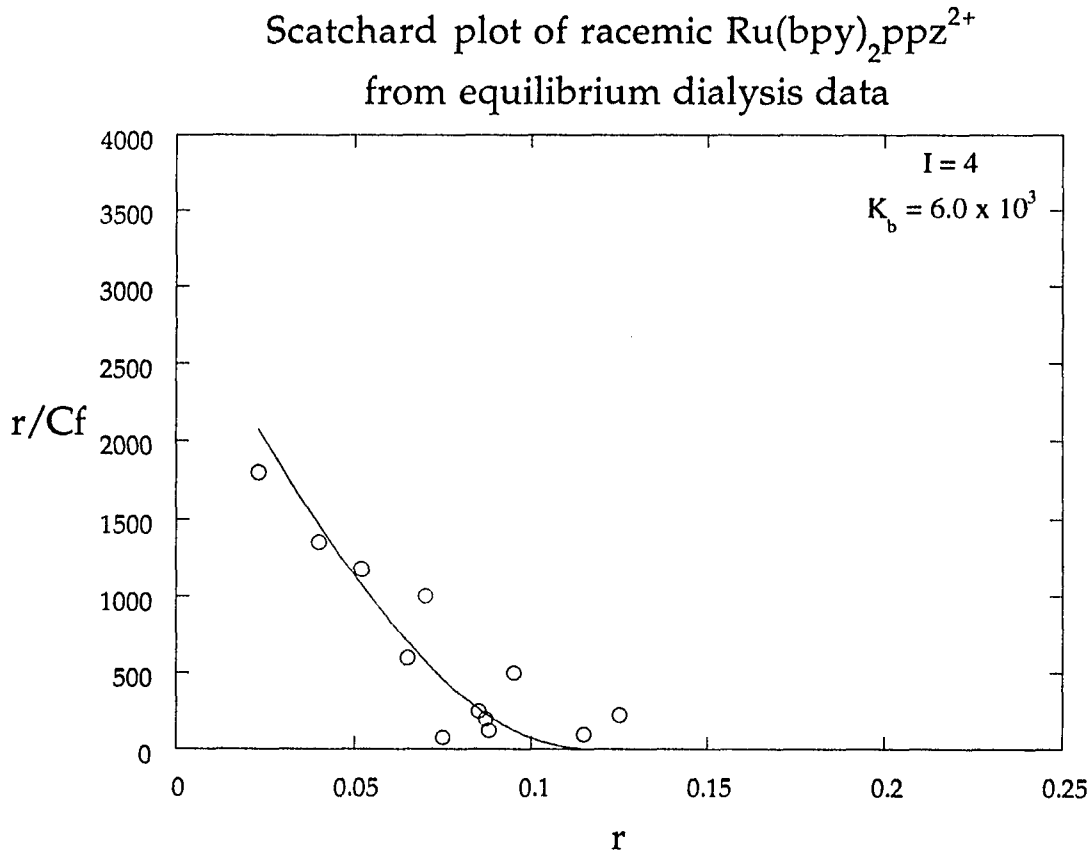

Figure VII-23. Scatchard analysis from equilibrium dialysis data for racemic $Ru(bpy)_2ppz^{2+}$. (○) actual data, (——) best fit to the McGhee and von Hippel equation. Site sizes and binding constants are indicated in plot.

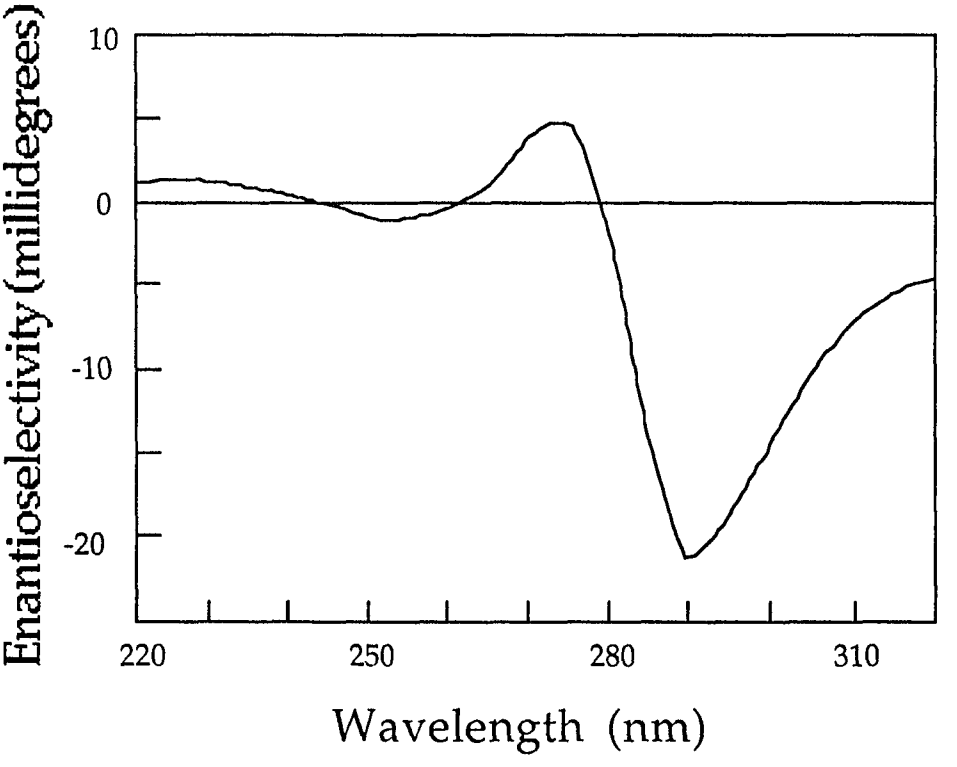

Figure VII-24. Circular dichroism spectra of 41hour dialyzates vs. calf thymus DNA ([DNA-P] = 1.6mM) for racemic $Ru(bpy)_2ppz^{2+}$. Sample measured at 25°C in 5mM Tris, 50mM NaCl buffer, pH 7.4.

Resonance Raman Spectroscopy (Raman Hypochromism)

Resonance enhanced Raman vibrational spectra for racemic $Ru(bpy)_2ppz^{2+}$ in buffer and the Δ and Λ isomers in the presence of calf thymus DNA ([DNA-P]/[Ru]=41) using 488nm and 457.9nm Ar ion excitation are displayed in Figures VII-25 and VII-26. 488nm excitation is utilized to maximize the resonance enhancement of the ppz ligand, which would be the only ligand expected to intercalate. 457.9nm excitation is used for comparison purposes. Because the emission is enhanced for the complex in the presence of DNA, the signal to noise ratio is correspondingly smaller, in particular for the Δ isomer.

Nevertheless, several differences are evident in the resonance enhanced spectra excited at 488nm. In particular, the relative intensities of the prominent bands vary from one spectrum to another, but no frequency changes of more than a wavenumber are observed. Using the buffer spectrum as a reference, the Δ and Λ isomer spectra are more similar to one another than to the buffer spectrum. In particular, note the 1271cm^{-1} shoulder on the 1256 cm^{-1} band in the buffer spectrum. Its intensity relative to the main peak is 0.33 in the buffer spectrum and ~0.50 in the Λ spectrum and a bit lower in the Δ isomer spectrum. Also, a shoulder on the low frequency side of the 1491 cm^{-1} peak in the buffer spectrum is not clearly observed in either the Δ or Λ isomer spectra. Likewise, the 1533 cm^{-1} band decreases in intensity relative to the 1491 cm^{-1} band in both DNA spectra (ratio of 1533 to 1491 cm^{-1} in buffer spectrum is 1.35, drops to 1.21 for Δ + DNA and 0.95 and Λ + DNA). Several more minor bands (e.g. 1214 cm^{-1}, 1578 cm^{-1}) seem to be nearly absent in the Δ isomer spectrum.

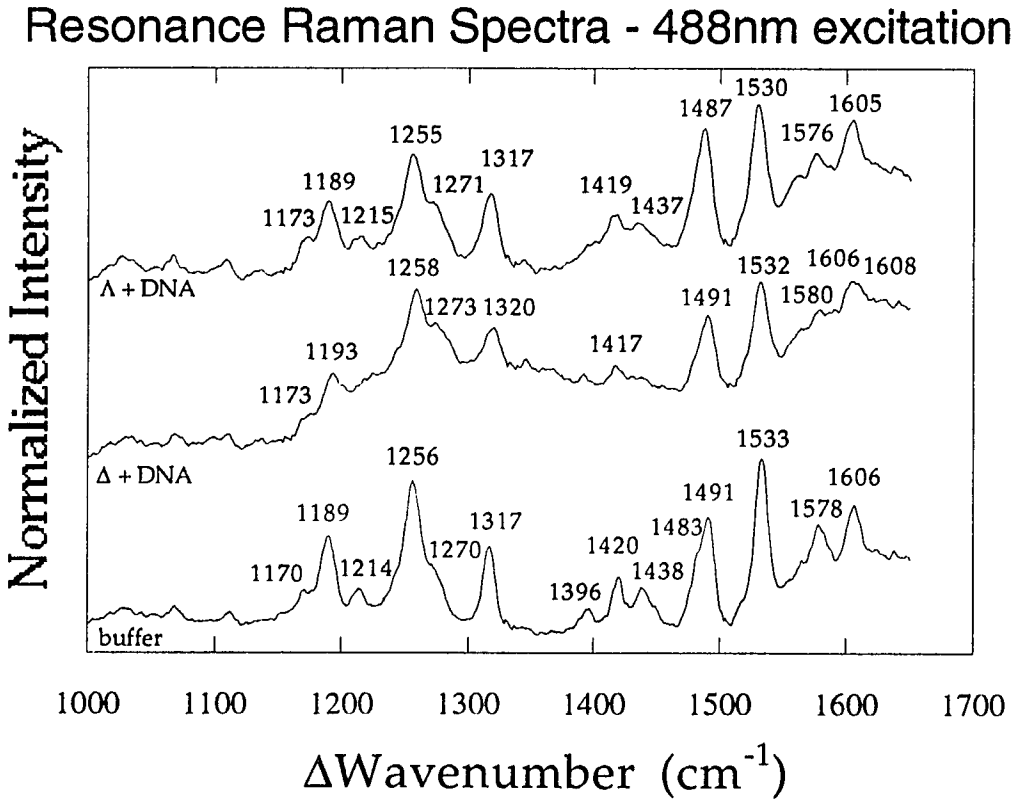

Figure VII-25. Resonance Raman spectrum of the Δ and Λ enantiomers of $Ru(bpy)_2ppz^{2+}$ at [DNA-P]/[Ru] =41 using 488nm Ar^+ excitation and 4.0 cm^{-1} spectral bandwidth. [Ru] = 45μM for all spectra. The spectrum of racemic $Ru(bpy)_2ppz^{2+}$ in buffer is shown for comparison.

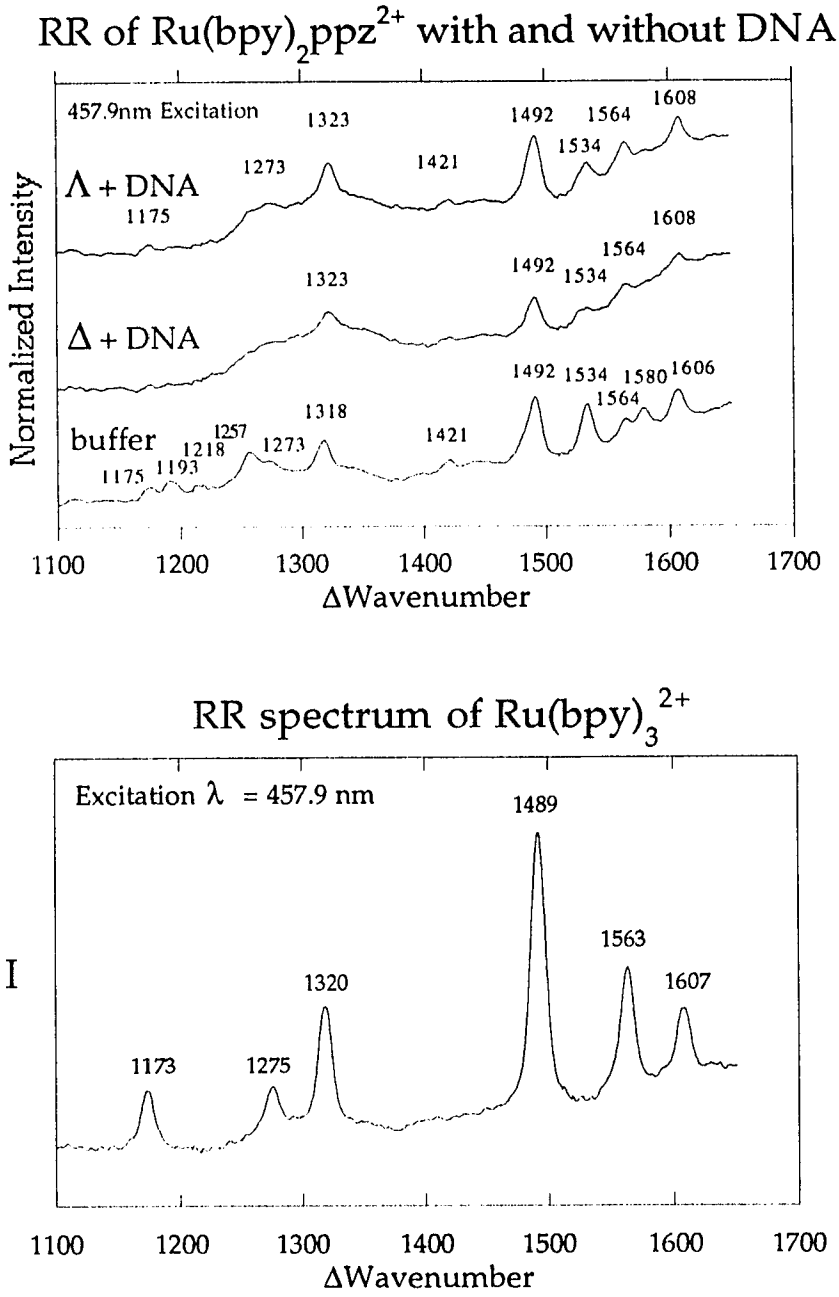

Figure VII-26. Resonance Raman spectrum of the Δ and Λ enantiomers of $Ru(bpy)_2ppz^{2+}$ at [DNA-P]/[Ru] =41 using 457.9nm Ar^+ excitation and 4.0 cm^{-1} spectral bandwidth. [Ru] = 45μM for all spectra. The spectrum of racemic $Ru(bpy)_2ppz^{2+}$ in buffer is shown for comparison, as well as the spectrum of $Ru(bpy)_3^{2+}$ in buffer.

Also, a flattening of the spectrum in the region from 1330-1440 cm^{-1} found for the Δ isomer is unique for this series of spectra, in a spectral region where no bpy bands exist (i.e. these bands are attributed to ppz ligand vibrations). The resonance Raman spectra of the same series of complexes under similar conditions were recorded with 457.9 nm excitation for comparison. (Figure 23) This spectrum is slightly different from the spectrum using 488nm excitation yet yields no new information.

Overall, the resonance Raman data are consistent with the hypochromicity observed in the visible spectra of both the Δ and Λ isomers in the presence of DNA. The corresponding Raman hypochromic effect would be expected to affect the intensities of only that part of the chromophore which is most strongly perturbed via the intercalative interaction with DNA base pairs. Although our knowledge of the nature of the normal mode structure of the ppz ligand is not detailed enough to yield specific structural information, it is encouraging to observe the differential intensity effects. Furthermore, the Raman evidence indicates that the interaction with DNA for the two isomers must be quite similar at higher [DNA-P]/[Ru] ratios.

Viscometry

We observedf DNA viscosity enhancement upon binding of racemic $Ru(bpy)_2ppz^{2+}$ to DNA, consistent with results by Lerman[295] for organic dye intercalators bound to DNA. DNA intercalators are expected to cause an increase in the length of the helix, thus stiffening it and causing DNA solutions to be more viscous. For the enantiomers of the $Ru(phen)_3^{2+}$ complex ion,

Chaires et. al.[332] reported no viscosity enhancement upon addition of $Ru(phen)_3^{2+}$ to DNA. This led these researchers to conclude that neither Δ nor Λ $Ru(phen)_3^{2+}$ bind via the scheme proposed by Barton (i.e. partial intercalation).

Viscometric data for our racemic $Ru(bpy)_2ppz^{2+}$ therefore show markedly different effects than the $Ru(phen)_3^{2+}$ complex ion, presumably because the $Ru(bpy)_2ppz^{2+}$ is more competent at binding via the proposed model due to the larger size of the ppz ligand, and the smaller size of the non-intercalating bpy ligands.

Discussion

Spectroscopic and photophysical data for both of the enantiomers of $Ru(bpy)_2ppz^{2+}$ when bound to DNA, contribute a strong case for a mode of binding involving a variable degree of intercalation of the ppz ligand, most likely within the major groove of B-form DNA, is important for each, particularly at high [DNA-P]/[Ru] ratios. In the presence of DNA, each isomer shows hypochromicity only in the visible MLCT absorption maximum associated with the ppz ligand, a substantial increase in emission quantum yield, and a blue-shifted emission maximum, reduced quenching by ferrocyanide, and a long lifetime component of a biphasic emission decay. The disappearance of the short component of the emission decay upon quenching while retaining the long component supports of the partial intercalative binding model for these isomers. The resonance Raman spectra of the individual isomers bound to DNA both show similar Raman hypochromicity effects when bound to DNA. The increase of the

radiative rate constant for the Δ isomer is highly suggestive of a more rigidly bound isomer relative to the Λ isomer. Perhaps most significantly, the emission polarization values for both isomers are the same at high [DNA-P]/[Ru] ratios, indicating a similar degree of rigidity with a fixed orientation for the two enantiomers bound to DNA. It is further notable that these limiting polarizations are achieved at relatively low [DNA-P]/[Ru] ratios (5 for the Δ isomer and 30 for the Λ isomer). The shorter timeframe of luminescence for the Λ isomer suggests that even though both isomers have the same limiting polarizations, the Λ isomer is less depolarized than the Δ isomer. The radiative rate constant found for the Λ isomer, being little affected, indicates a qualitatively weaker binding for this isomer, (i.e. less penetration and less perturbation of the ppz ligand), and therefore these two pieces of evidence account for the similar polarizations found for the two isomers.

Most of these measurements (with few exceptions) are consistent with similar measurements reported for the individual enantiomers of $Ru(phen)_3^{2+}$ and $Ru(DIP)_3^{2+}$, which have been interpreted as substantiating an intercalative mode of binding, via major groove access to B-Form DNA.[3,4,5,6] One notable exception is the disappearance of the short component upon emission lifetime quenching, which was **not** seen for the studies with $Ru(phen)_3^{2+}$, and it should be noted here that Barton assigned the persistence of the short component at high quencher concentration to a surface bound binding mode.[5] We have no evidence to support such a binding mode for either isomer of $Ru(bpy)_2ppz^{2+}$.

Intercalative binding of the Δ isomer is almost always favored over similar

binding of the Λ isomer, even at high [DNA-P]/[Ru] ratios. This is what has been found in the literature for most other enantiomeric studies, with the exception of $Ru(phen)_3^{2+}$ bound to poly [d(AT)], where binding either was not enantioselective for the Δ isomer (based on polarization data) or even favored the Λ isomer (based on equilibrium dialysis data) at [DNA-P]/[Ru] ratios of 20-40.

The clearest measurable evidence for a difference between the intercalative binding modes for the enantiomers of $Ru(bpy)_2ppz^{2+}$ are the emission quantum yields and emission lifetimes at high [DNA-P]/[Ru] ratios. The difference in the **radiative** lifetime (τ/ϕ) for the Δ isomer at these ratios compared to the Λ isomer and free solution data are completely consistent with the proposed partial intercalative (and enantioselective) binding. We surmised therefore that only the Δ isomer can penetrate the helix sufficiently to effect a change in the radiative lifetime, while the Λ isomer, though slightly intercalated, cannot penetrate sufficiently to effect a change in this parameter.

Our findings are by and large consistent with the basic model proposed by Barton et. al.[5,6] for binding of tris-chelates of this type to DNA. For this particular complex, partial intercalation of a single bidentate aromatic diimine ligand (ppz) provides a significant part of the driving force for binding to B-form double stranded DNA, and van der Waals interactions with the additional non-intercalating bpy ligands result in a measurable degree of difference between the Δ and Λ isomers in binding within the major groove of B-form DNA. The spectroscopic and photophysical evidence and the viscosity data indicate that

the ppz ligand is more deeply inserted between DNA base pairs for the Δ isomer than for the Λ isomer. Additional, surface bound or minor groove bound modes are of lesser importance. Because 2,2'-bipyridine is the ancillary ligand for this complex, significant intercalation of these ligands is precluded and only the ppz ligand intercalates. Compared to 1,10-phenanthroline, and certainly DIP, the bipyridine ligands provide significantly less steric resistance to partial intercalation of the ppz ligand for either enantiomer. Thus it seems that a mode of binding involving partial intercalation of ppz is highly favorable for both isomers at higher [DNA-P]/[Ru] ratios. However, chiral discrimination is still significant at [DNA-P]/[Ru] ratios of ~20 or less, because a quantitative preference for binding of the Δ isomer over the Λ isomer is still preserved via differential van der Waals interactions of the non-intercalating bpy ligands for the two enantiomers within the DNA major groove. Previously reported CD results,[23] and column chromatographic separation using DNA adsorbed on hydroxylapatite,[33] are entirely consistent with the emission polarization data, which indicate a maximal preference for the Δ isomer over the Λ isomer of about 65:35 at a [DNA-P]/[Ru] ratio of 2.5.

Energy minimization calculations for $Ru(phen)_3^{2+}$ binding to various polynucleotides have indicated[21] that major groove binding with partial insertion (intercalation) of one of the phen ligands is a favored mode of binding for both isomers. For the Δ isomer, another mode of binding, with two ligands within the major groove, but not inserted between bases, is only slightly less favored. The results presented here are to our satisfaction consistent with these

calculations.

The recent report of enantioselective cleavage of plasmid DNA by our group[24] utilizing a OP/Cu-like system can be interpreted in light of the evidence presented here. Cleavage was significant only in the presence of the Λ-isomer of $Ru(bpy)_2ppz^{2+}$ for experiments carried out at [DNA-P]/[Ru] ratios of 10, where intercalative binding of the Δ isomer is favored over that of the Λ isomer (~60:40). More importantly, polarization studies show that the Δ isomer is almost completely intercalated within the major groove at this [DNA-P]/[Ru] ratio, while the Λ isomer is only 60-70% intercalated at this ratio and is therefore able to deliver the active copper species to other sites, including most probably the minor groove sites determined to be effective in cleaving DNA in the Sigman OP/Cu system.

The observation that racemic $Ru(bpy)_2ppz^{2+}$ interacts with poly (dA•dT)•poly (dA•dT) to a greater extent than poly (dG•dC)•poly (dG•dC) is the first step on the path of determining the base specificity of the binding sites of this molecular probe. It is hoped that research with this probe continues and perhaps the base specificity of both of the enantiomers of $Ru(bpy)_2ppz^{2+}$ can be determined. This knowledge will be of fundamental importance for applications in the areas of genetic engineering, molecular biology, and cancer research.

Chapter VIII. DNA interactions of the complex ions $Ru(bpy)_2qpy^{2+}$, $Ru(bpy)_2qpyMe^{3+}$, and $Ru(bpy)_2qpyMe_2^{4+}$.

Introduction

The series of polypyridyl complexes $Ru(bpy)_2qpy^{2+}$, $Ru(bpy)_2qpyMe^{3+}$, $Ru(bpy)_2qpyMe_2^{4+}$, (qpy = 2,2':4,4":4',4"'-quaterpyridyl, $qpyMe^+$ = 4" N-methyl 2,2':4,4":4',4"'-quaterpyridyl, $qpyMe_2^{2+}$ = 4",4"' di-N-methyl 2,2':4,4":4',4"'-quaterpyridyl) form the basis for studying the effect of peripheral charge on the overall binding to DNA.[23] The mono- and di- methylated complexes possess interesting properties, one being that these ligands possess a positive charge on the ligand, and the charge transfer to these ligands would be expected to be enhanced. (see page 38 for structures of these complexes) Furthermore, in structural terms, they can be considered as an intramolecular assembly of a Ru(II) diimine and a viologen (quencher) site.

In studies with these complexes, the variable charge on the periphery of the qpy ligand provides a probe of the effect of peripheral charge on binding to DNA of the mixed-ligand complexes containing these ligands. Photophysical and spectroscopic data obtained in the presence and absence of DNA for this series of complexes, is given here in hopes of elucidating the type of binding found for these molecular probes. It is proposed by our group[23] that the binding of this series of complexes to DNA consists largely of electrostatic and/or surface bound interactions, with partial intercalation being a prohibited mode due to the structure of the qpy ligand (i.e. the free rotation of the two upper pyridyl rings, causing non-planarity). However, for one complex in the series,

$Ru(bpy)_2qpyMe_2^{4+}$, enantioselective binding is found, and all the possible binding modes proposed for Ru(II) polypyridyl complexes must be analyzed and discussed in terms of this finding. Partial intercalation (which gives rise to the enantioselectivity found for $Ru(bpy)_2ppz^{2+}$) for the $Ru(bpy)_2qpyMe_2^{4+}$ complex cannot be ruled out completely in light of the observed enantioselectivity. Two other binding modes will be compared and contrasted, and conclusions will be drawn based on the spectral evidence and on model building. Analogies to the $Ru(phen)_3^{2+}$, $Ru(DIP)_3^{2+}$, and $Ru(bpy)_2ppz^{2+}$ complexes will be drawn when necessary to characterize the different kinds of binding found for this series of complexes.

Results

Absorption Spectra

For the complex $Ru(bpy)_2qpy^{2+}$, the spectra shown in Figure VIII-1 indicate a larger decrease in intensity near the 475 nm MLCT band in the presence of DNA (hypochromic effect), with a somewhat smaller decrease near 430nm. For this complex, the qpy MLCT absorption band is not well resolved, yet resonance Raman spectra of the complex indicate that the red-shifted transition is due to the transitions to the qpy ligand.[231] For the complex $Ru(bpy)_2qpyMe^{3+}$, neither absorption band undergoes intensity changes and no wavelength shifts are evident in the presence of DNA (Figure VIII-1). The $Ru(bpy)_2qpyMe_2^{4+}$ complex is unique for the series of complexes, in that the MLCT band assigned to $qpyMe_2^{2+}$ shows a red-shifted absorption to 520 nm from 500nm,*and* a small **hyperchromic** effect (~5%) seen for both the bpy

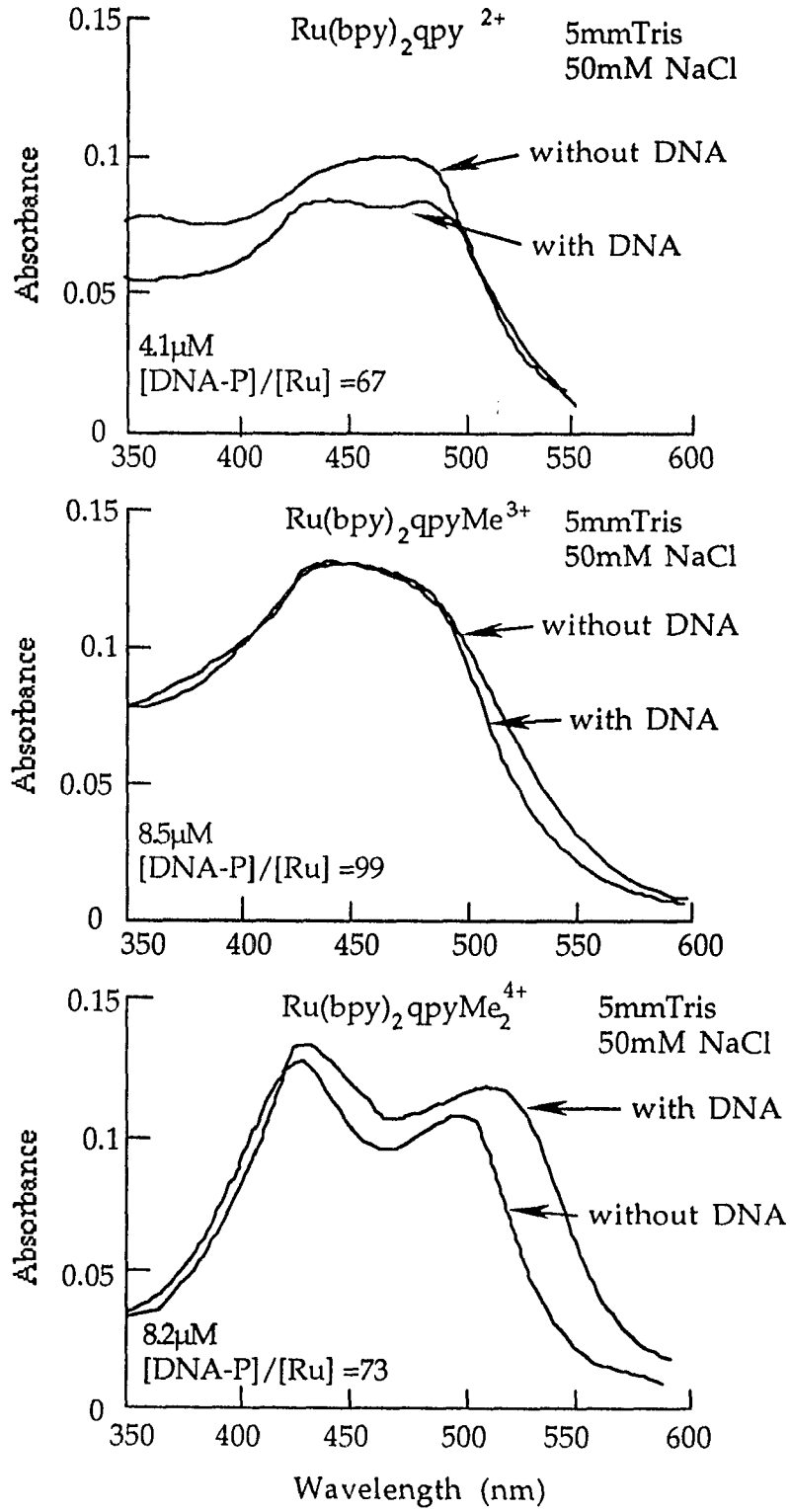

Figure VIII-1 Absorption Spectra for the qpy complexes with and without DNA.

and the $qpyMe_2^{2+}$ MLCT bands. For this series of complexes, changes are evident for both the $Ru(bpy)_2qpyMe_2^{4+}$ and $Ru(bpy)_2qpy^{2+}$ complexes, but not for the $Ru(bpy)_2qpyMe^{3+}$ complex. However, the effects are less pronounced for the bpy transitions.

Emission Enhancement (Increase in Quantum Efficiency)

Upon binding to DNA, no luminescence enhancement of the emission band occurring at 665nm is observed for the $Ru(bpy)_2qpy^{2+}$ or the $Ru(bpy)_2qpyMe^{3+}$ complex ion. Figure VIII-2 shows the emission enhancement for the $qpyMe_2^{2+}$ complex relative to its emission in free aqueous solution. The emission band observed is attributed to a transition from a π^* orbital on the qpy or methylated qpy ligand to the Ru(II) d orbital. $Ru(bpy)_2qpyMe_2^{4+}$ is unique for the series, where a small emission enhancement is evident and there is also a red-shift of ~25 nm. The quantum yield of emission of the $Ru(bpy)_2qpyMe_2^{4+}$ complex bound to DNA increases ~1.9-fold at large [DNA-P]/[Ru] ratios, while no changes are observed with the other complexes. Accompanying the emission enhancement for this complex is an increase in spectral bandwidth from a half-width (FWHM) of 2020 cm^{-1} in the free solution spectrum to 2223 cm^{-1} in the presence of DNA at a [DNA-P]/[Ru] ratio = 111.

Emission Lifetime

Changes in luminescence lifetime in the presence of DNA were only evident for the $Ru(bpy)_2qpyMe_2^{4+}$ complex, where the luminescence lifetime of the complex in buffer was found to be 64ns, and the lifetime of the bound complex decayed bi-exponentially with a short component of < 30ns and a long

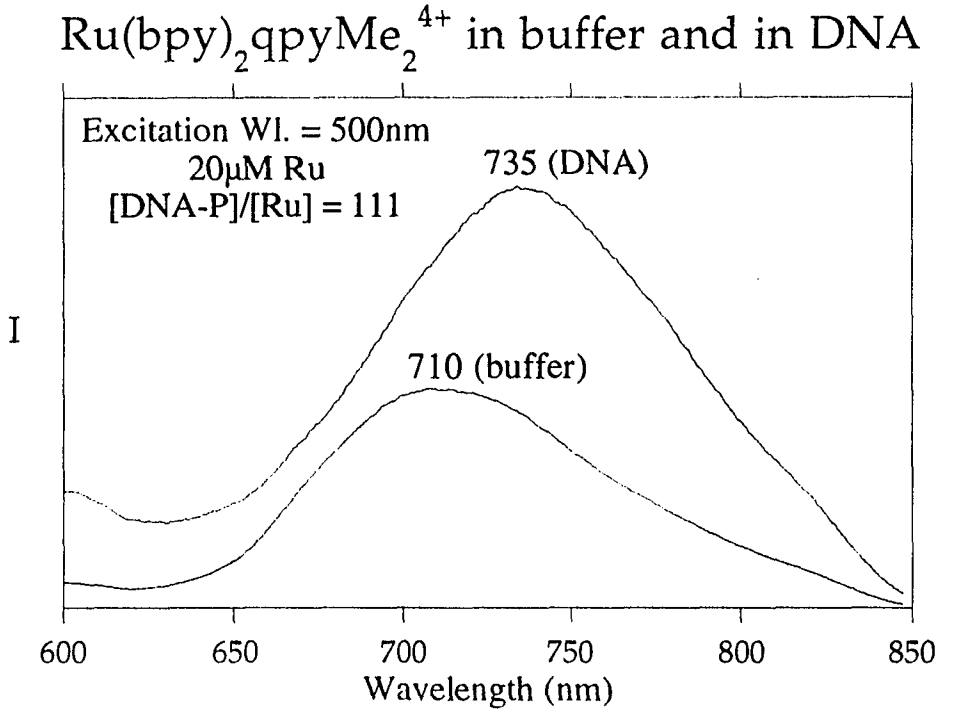

Figure VIII-2 Emission Spectra of $Ru(bpy)_2qpyMe_2^{4+}$ in the presence and absence of calf thymus DNA. All solutions in 5mM Tris, 50mM NaCl, pH 7.4.

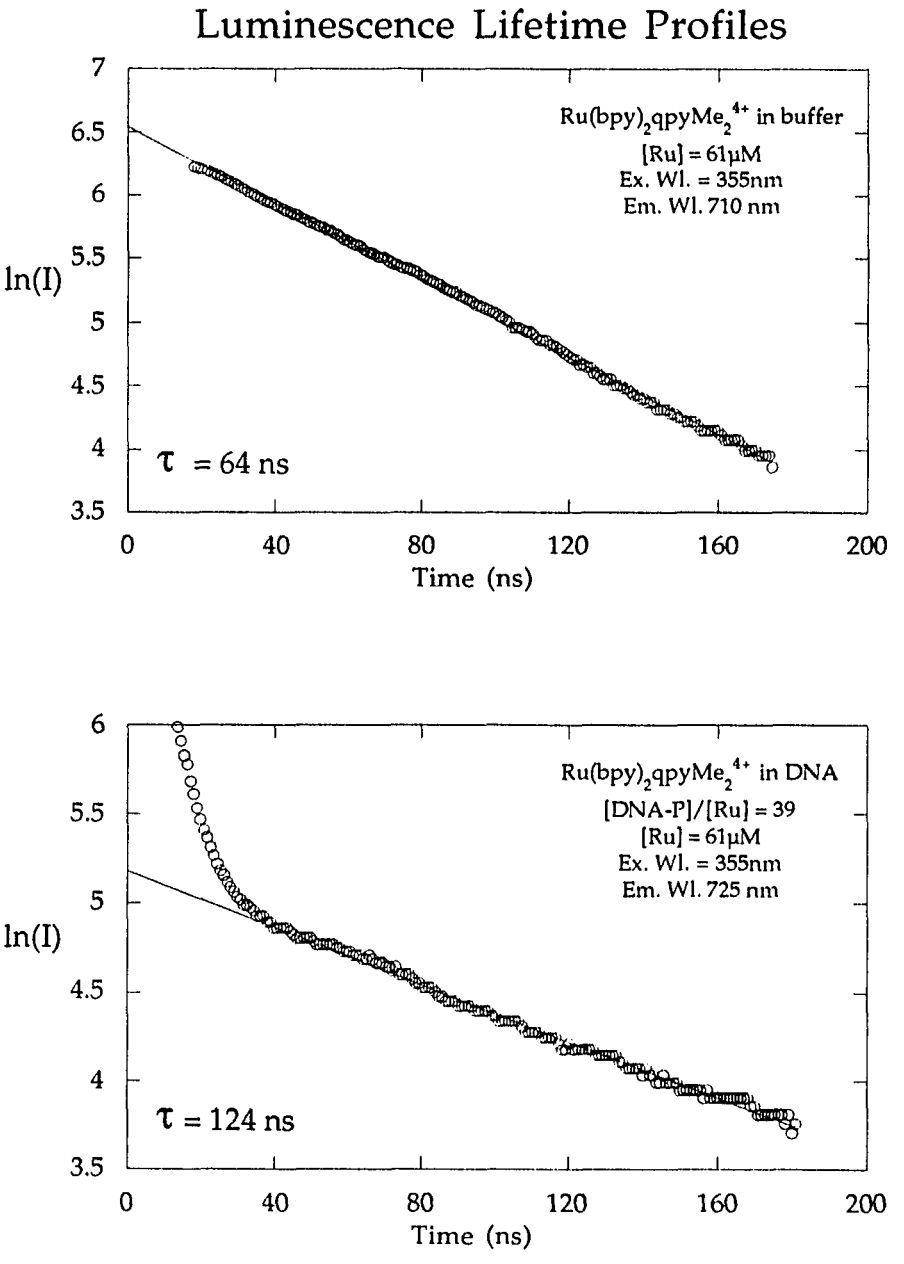

Figure VIII-3. Luminescence lifetime profiles of $qpyMe_2^{2+}$ with and without calf thymus DNA. Samples excited with the 355nm line of a Nd:YAG laser with a 7 ns pulse duration. Luminescence lifetimes (τ) as indicated. All samples in 5mM Tris, 50mM NaCl buffer, pH 7.4.

component of 124 ns (Figure VIII-3). The long component is attributed to the strongly bound mode, while the lifetime of the short component is somewhat shorter than the free solution value and requires further investigation. The different lifetimes may also be attributed to the two different enantiomers binding in different ways, (enantioselectively) and since the lifetime experiment was carried out for the racemic complex, both bound isomers would be seen in the lifetime profile. It is not possible to resolve this dilemma without looking at the lifetime profiles of the pure enantiomers.

The luminescence lifetime found for the $Ru(bpy)_2qpyMe^{3+}$ complex in free solution was bi-exponential, suggesting that the complex decomposed upon measuring the lifetime. Therefore, the reliability of this complex is questionable. The lifetime of the $Ru(bpy)_2qpy^{2+}$ complex does not change on binding to DNA, suggesting no intercalative interaction for this complex.

Emission Polarization

Steady state emission polarization measurements were performed only for the $Ru(bpy)_2qpyMe_2^{4+}$ complex, where a limiting polarization of ~0.07 was found. This seemingly large value of polarization is not surprising in light of the fact that the luminescence lifetime is so short (~120 ns) compared to, for example, the Δ $Ru(bpy)_2ppz^{2+}$ complex (~950 ns). In the timeframe of the luminescence of $Ru(bpy)_2qpyMe_2^{4+}$, less rotation of the bound chromophore occurs compared to the $Ru(bpy)_2ppz^{2+}$ complex (about 8 times less rotation), and hence a measurable polarization can arise from a rigidly held electrostatic or surface bound complex that doesn't have sufficient time to rotate during its

excited state. Measuring emission polarizations by steady state methods does not take into account the lifetime of the chromophore, and therefore lifetime data must be considered when comparing steady state polarizations.

It is important to compare the polarizations measured for the Δ and Λ isomers of $Ru(phen)_3^{2+}$, which showed small, measurable polarizations (~0.025 for Λ and ~0.036 for Δ),[6] yet have very long lifetimes in DNA (~2000 ns for the long component). Because the nature of the binding of the $Ru(phen)_3^{2+}$ complex is still a matter of controversy, it is possible to surmise that polarizations can be present for complexes in DNA even in the absence of intercalation.

Excitation polarization values for the $qpyMe_2^{2+}$ complex are given in Figure VIII-4. As in the case of the $Ru(bpy)_2ppz^{2+}$ complex, polarizations only arise from excitation of the $qpyMe_2^{2+}$ MLCT absorption bands.(480-530nm). The bpy bands do not give rise to polarization for this complex bound to DNA.

Emission Quenching

Emission intensity quenching was measured for the $Ru(bpy)_2qpyMe_2^{4+}$ complex, using $Fe(CN)_6^{4-}$ as the quencher. Free solution $Ru(bpy)_2qpyMe_2^{4+}$ was quenched very efficiently, (K_{sv} = 18000) while DNA bound $Ru(bpy)_2qpyMe_2^{4+}$ was quenched with more difficulty, yet this behavior was **not** similar to behavior found for the $Ru(bpy)_2ppz^{2+}$ complex. The increase in charge of the $Ru(bpy)_2qpyMe_2^{4+}$ complex compared to $Ru(bpy)_2ppz^{2+}$ in free solution can account for the increased quenching efficiency found for $Ru(bpy)_2qpyMe_2^{4+}$ in the absence of DNA. However, the quenching behavior of $Ru(bpy)_2qpyMe_2^{4+}$ in the presence of DNA (Ksv = 2980) is found to be similar to

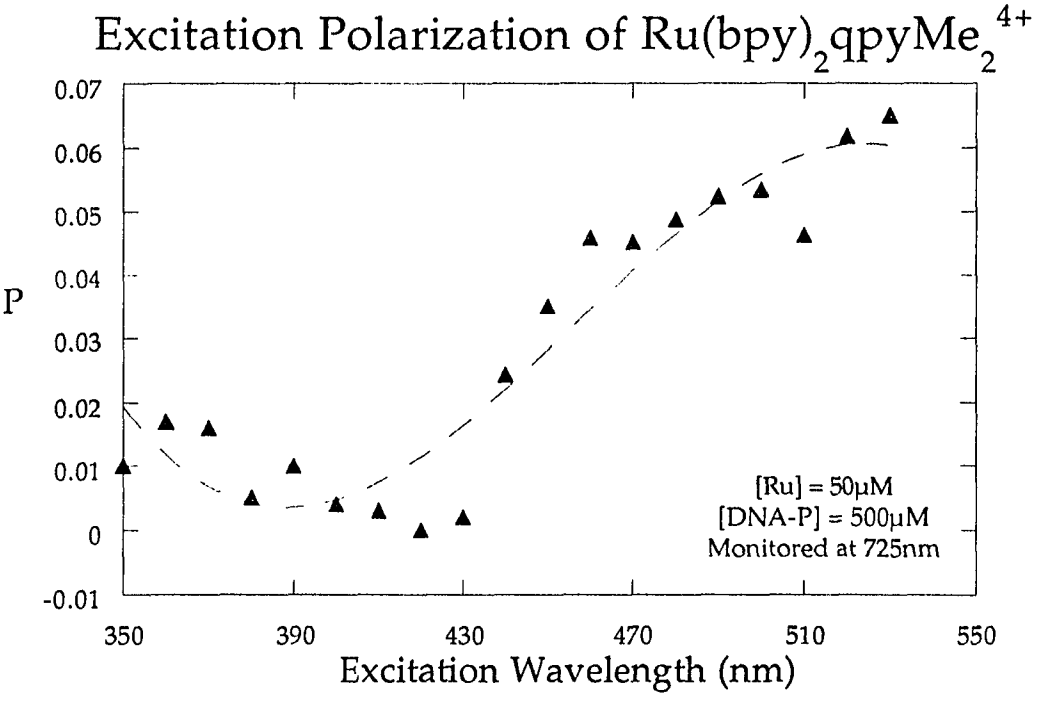

Figure VIII-4. Excitation polarization profile of $Ru(bpy)_2qpyMe_2^{4+}$ in the presence of DNA. Samples in 5mM Tris, 50mM NaCl, pH 7.4. Negligible polarization values were found for $Ru(bpy)_2qpyMe_2^{4+}$ in the absence of DNA.

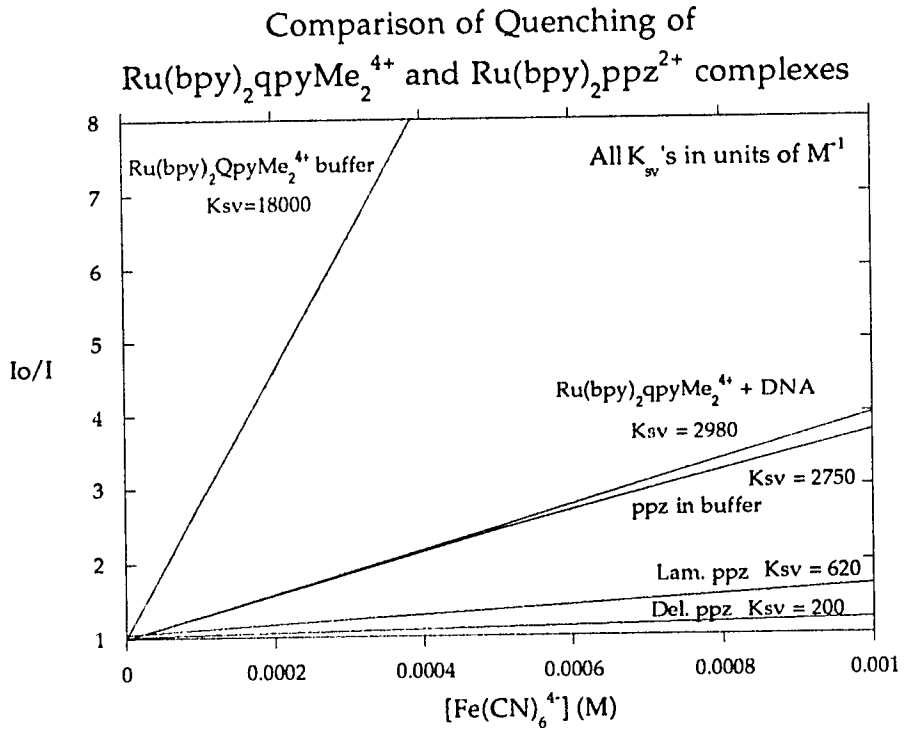

Figure VIII-5. Anionic quenching ($Fe(CN)_6^{4-}$) of $Ru(bpy)_2qpyMe_2^{4+}$ in the presence and absence of DNA. Concentrations used - [Ru] = 10μM, [DNA-phosphate] = 100μM. Quenching of $Ru(bpy)_2ppz^{2+}$ at the same [DNA-phosphate] ratio is included for comparison purposes. All solutions in 5mM Tris, 50mM NaCl, pH 7.4.

the quenching of $Ru(bpy)_2ppz^{2+}$ in free solution. (Ksv = 2750 for the $Ru(bpy)_2ppz^{2+}$ complex - See Figure VIII-5) These values of K_{sv} are indicative of diffusion limited bimolecular quenching. From the evidence presented here, we conclude that shielding from the solvent occurs to a certain extent with the $Ru(bpy)_2qpyMe_2^{4+}$ complex in the presence of DNA. However, the effect is less for this complex than the $Ru(bpy)_2ppz^{2+}$ complex, where quenching of this complex in the presence of DNA is **less** than diffusion limiting values. Downward curvature of the Stern-Volmer plots (found for the enantiomers of the $Ru(bpy)_2ppz^{2+}$ complex in the presence of DNA) were **not** found for the Stern-Volmer plot of the $Ru(bpy)_2qpyMe_2^{4+}$ complex in the presence of DNA, indicating a different type of interaction than that found for the $Ru(bpy)_2ppz^{2+}$ enantiomers. Dissimilar quenching behavior found for the $Ru(bpy)_2qpyMe_2^{4+}$ complex in the presence of DNA compared to the $Ru(bpy)_2ppz^{2+}$ complex in the presence of DNA leads to the description of the binding of the $Ru(bpy)_2qpyMe_2^{4+}$ complex to DNA as consisting of primarily electrostatic and/or surface binding, such that the chromophore is partially shielded from the bulk solvent, yet partially exposed to allow quenching to be diffusion limited.

Rate Constants

From the luminescence lifetime and emission quantum yield measurements, the parameters k_r, k_{nr}, and the radiative lifetime τ_r may be calculated. Assuming the strongly bound complex is associated with the long component of the emission lifetime in DNA found for the $Ru(bpy)_2qpyMe_2^{4+}$ complex, the increase in lifetime upon binding is ~1.9. The emission quantum

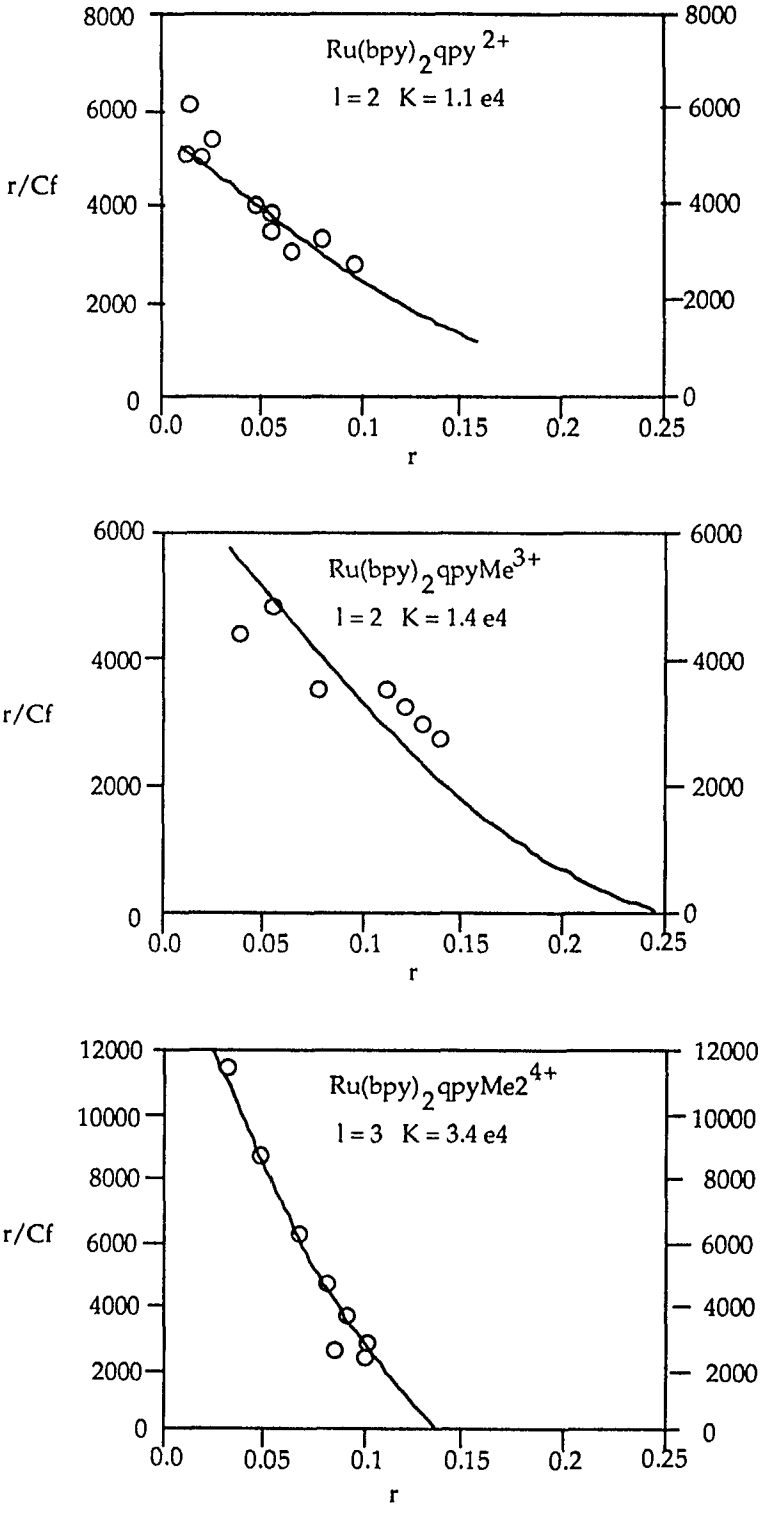

Figure VIII-6. Scatchard analysis of the series of complexes.

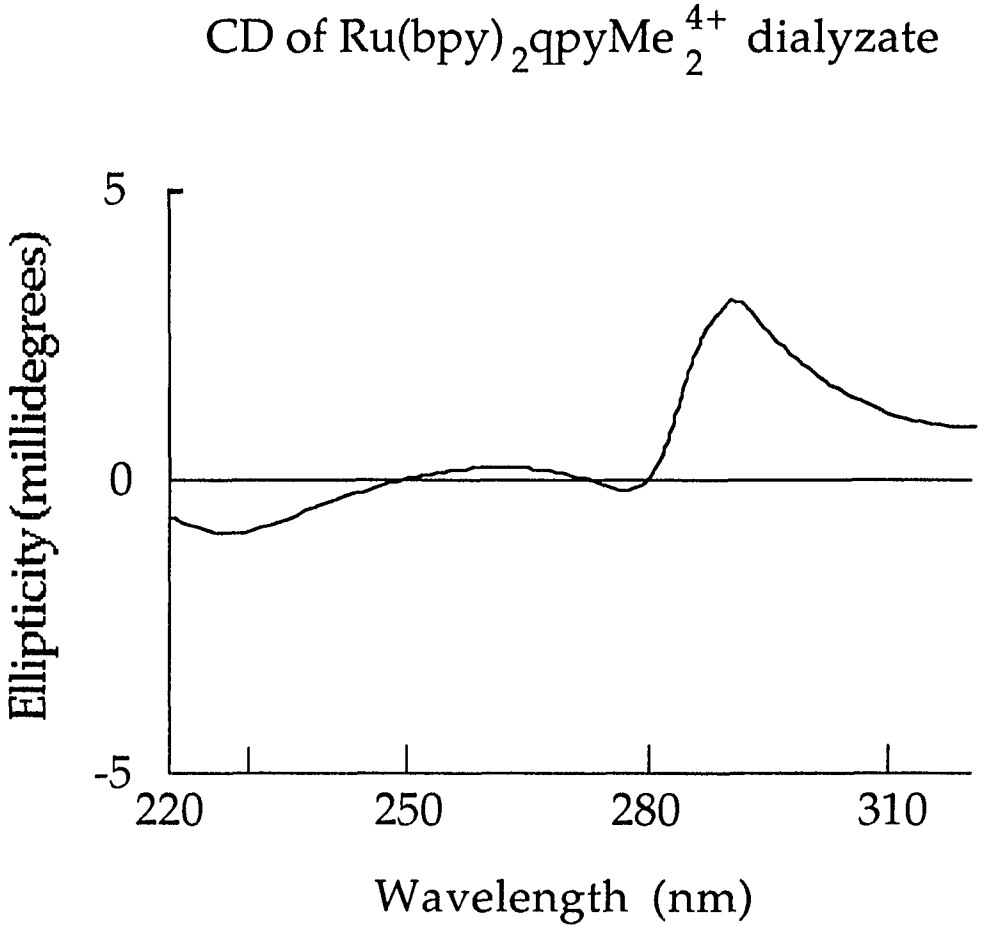

Figure VIII-7. CD spectrum (showing enantioselectivity) of 41hour dialyzate versus calf thymus DNA (1.6mM [DNA-phosphate]) Concentraion of [Ru] =13μM. Sample in 5mM Tris 50mM NaCl, pH 7.4.

yield increases by ~1.9 upon binding, and therefore does not alter significantly the radiative lifetime, τ_r. This is more characteristic of non-intercalative behavior, since the proposed intercalator Δ $Ru(bpy)_2ppz^{2+}$ has a radically altered τ_r value. The k_{nr} typically changes from one solvent system to another, and changes in k_{nr} are evident for the $Ru(bpy)_2qpyMe_2^{4+}$ complex in the absence and presence of DNA.

Equilibrium Dialysis

Equilibrium dialysis experiments for this series of complexes yield Scatchard plots[316] shown in Figure VIII-6. The binding constant (K_b) for the $Ru(bpy)_2qpyMe_2^{4+}$ complex was found to be larger than the other two complexes, perhaps reflecting its larger positive charge. The binding sites for these complexes were either 2 or 3.

Enantioselectivity

For the series of complexes, only the $Ru(bpy)_2qpyMe_2^{4+}$ complex was shown to bind enantioselectively. A measurable CD signal of the dialyzate indicated enrichment of the less favored isomer outside the bag (Figure VIII-7). The enantioselectivity is found to be smaller than for the $Ru(bpy)_2ppz^{2+}$ complex. This evidence **must** be taken into account to describe the binding behavior of the $Ru(bpy)_2qpyMe_2^{4+}$ complex.

Molecular modeling

Molecular modeling of the binding of $Ru(bpy)_2qpyMe_2^{4+}$ to B-DNA suggests that electrostatic binding can occur by bridging two of the phosphates on either the same or opposite strands of the DNA duplex. Peripheral charges

on the $qpyMe_2^{2+}$ ligand can effectively allow this type of binding, since the positive charges are delocalized onto the upper pyridyl rings of the $qpyMe_2^{2+}$ ligand. Enantioselectivity possibly arises from the way in which this bridging occurs. One can envision at least two binding modes, an electrostatic mode with the $qpyMe_2^{2+}$ ligand facing towards the helix with the bpy ligands exposed (Mode 1), and a combination of surface and electrostatic interactions, with the $qpyMe_2^{2+}$ ligand facing away from the helix, with the bpy ligands more deeply buried (Mode 2). From models, Mode 2 seems more plausible, based on consideration of the enantioselectivity. Mode 1 cannot to my satisfaction explain enantioselectivity. Mode 2 is a more probable explanation since the different orientations of the bpy ligands can interact differently within the DNA major groove can give rise to the enantioselectivity. While models suggest that the bpy ligands appear too large to allow the $Ru(bpy)_2qpyMe_2^{4+}$ complex to go into DNA with the bpy's pointing towards the helix, slight alteration of the DNA structure can allow the macromolecule to bend slightly, and cause a better interaction between the positive and negative charges on the $qpyMe_2^{2+}$ ligand and DNA respectively. Alteration of the DNA conformation can also make the major groove somewhat deeper, and more accommodating to the bpy ligands. Since the bpy ligands can be considered the more hydrophobic region of the complex, it seems only fitting that these ligands would go into a more hydrophobic region, with the hydrophilic(charged) portion of the complex aligned with the charges on the phosphate backbone. Stabilization of this binding via van der Waals interactions of the bpy ligands with atoms lining the

groove and electrostatic interactions of the charged quaternary nitrogens on the $qpyMe_2^{2+}$ ligand can account for the larger binding constant found for this complex. This mode of binding is consistent with the observed enantioselectivity.

Mode 1 can be envisioned as a binding mode possible for both enantiomers, but this mode does not explain the observed enantioselectivity, nor the increase in luminescence lifetime, decrease in quenching ability, or the observed absorption hyperchromism. With resolution of the enantiomers of this complex, which up to this point has not been achieved, the answers to these questions will be found.

Binding via an **intercalative** scheme is harder to imagine for the $Ru(bpy)_2qpyMe_2^{4+}$ complex, since a positive charge (hydrophilic region) on the end of the $qpyMe_2^{2+}$ ligand could prevent this portion of the molecule from entering the hydrophobic region (between the base pairs). The presence of positive charge in the middle of a chromophore is a more likely situation for intercalative binding, since most organic intercalators have positive charge located on the middle heterocyclic ring. Modeling also suggests that the distance from peripheral charges is too great to intercalate in a mode similar to the $Ru(bpy)_2ppz^{2+}$ complex. Modeling suggests that intercalation of one half of the $qpyMe_2^{2+}$ ligand could occur, but this mode is much harder to rationalize in light of the hyperchromism seen with this complex.

Resonance Raman Spectroscopy

Resonance enhanced Raman spectra of the $Ru(bpy)_2qpyMe_2^{4+}$ in the

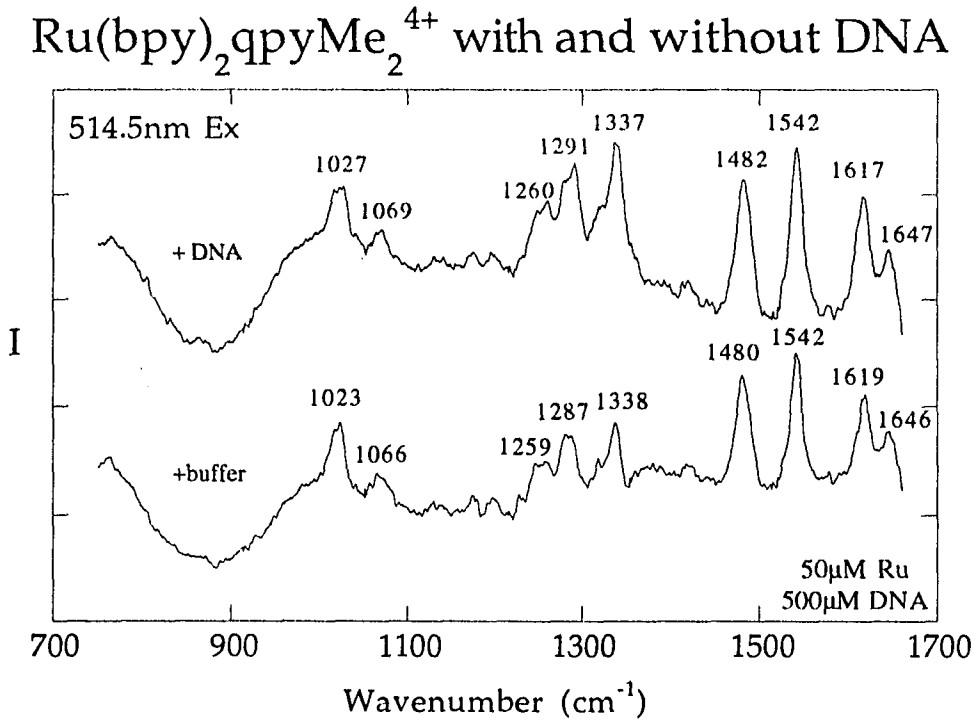

Figure VIII-8. Resonance Raman spectrum of $Ru(bpy)_2qpyme_2^{4+}$ with and without DNA using 514.5 Ar^+ excitation. Concentrations are as shown. All solutions in 5mM Tris, 50mM NaCl, pH 7.4.

presence and absence of DNA were obtained. This was the only complex analyzed in this series. The goal was to elucidate the possibility of enantioselective binding. (Figure VIII-8) Only very minor changes were evident in the comparison of the two spectra excited at 514.5nm, suggesting a much less intimate interaction with DNA than for the $Ru(bpy)_2ppz^{2+}$ complex, which showed noticeable changes for both enantiomers. This evidence is consistent with a non-intercalative binding mode, where the chromophore is only slightly perturbed upon binding, and not so greatly affected as in the case of intercalative binding. These spectra, however, cannot distinguish between Modes 1 and 2 discussed above.

Discussion

The evidence presented here is most consistent with the proposed model of electrostatic binding of the $Ru(bpy)_2qpyMe_2^{4+}$ to DNA via Mode 2, since all our evidence supports this mode, including emission enhancement, absorption hyperchromism, and small polarizations (taking into account the short lifetime of $Ru(bpy)_2qpyMe_2^{4+}$). Taking luminescence lifetime and emission quantum yield evidence together result in only a slight change in k_r, and therefore do not support an intercalative binding mode. Emission quenching data suggests some shielding from solvent, but not as much as is found with the $Ru(bpy)_2ppz^{2+}$ complex. Mode 1 binding is not well supported by the evidence for $Ru(bpy)_2qpyMe_2^{4+}$ because it cannot account for the enantioselective binding. For the other two complexes, only electrostatic binding is proposed based on the lack of emission enhancement and enantioselectivity, and a mode which

binds these complexes randomly to the negative backbone is the most likely type of binding.

Intercalative binding was proposed by Barton et. al.[3,345] for only the Δ isomer of $Ru(DIP)_3^{2+}$ which is structurally similar to complexes in this series, yet this mode of binding is not supported by molecular models. Due to the rotation of the upper phenyl rings (disfavoring planarity of the DIP ligand), and the way in which these rings point away from each other, the structure of $Ru(DIP)_3^{2+}$ does not appear suitable to induce intercalative binding via the major groove. Likewise, by analogy, our series of complexes should also not be able to bind in this way.

The binding constant increases as the series of complexes is further methylated, consistent with increasingly charged species being more attracted to a highly negative DNA molecule. Also, based on arguments by Barton, an anticipated decrease in hydrophobic-like binding as the qpy ligand is more highly methylated should be found. If this is true, then the non-methylated complex would be the most likely of the series to show intercalative interaction via the major groove. However, no emission enhancement is seen for the $Ru(bpy)_2qpy^{2+}$ or $Ru(bpy)_2qpyMe^{3+}$, which argues strongly against an intercalative mode of binding for these complexes to DNA.

It is proposed here that binding of these complexes to DNA is largely due to an electrostatic interaction which increases with increasing charge. The enantioselectivity found for the $Ru(bpy)_2qpyMe_2^{4+}$ complex reflects differential binding for the enantiomers, and the interaction of the ligands with the structure

of the DNA helix induces this effect. Resolution of this complex using a DNA-hydroxylapatite column will no doubt shed light on the binding characteristics of this complex. The complexes $Ru(bpy)_2qpy^{2+}$ and $Ru(bpy)_2qpyMe^{3+}$ show no enantioselectivity and therefore will not be resolvable using this separation technique. It can be inferred therefore that for these two complexes, the structure of the nucleic acid is less important in characterizing the binding of these two complexes to the DNA duplex. For the $Ru(bpy)_2qpyMe_2^{4+}$ complex, interaction of the complex with the right-handed screw sense of B-DNA **must** give rise to the enantioselectivity and account for the observed spectral perturbations.

Chapter IX. DNA binding of Ru(II) complexes which have interacting ligands of varying length.

Introduction

By comparing data gathered by Barton et. al.[4,5,6] for the $Ru(phen)_3^{2+}$ complex, and our data for the $Ru(bpy)_2ppz^{2+}$ complex, it is evident that variation in ligand length significantly alters the spectral properties of the Ru (II) polypyridyl probes when they interact with DNA. Previous studies with the complex $Ru(bpy)_2dppz^{2+}$, (dppz= dipyridophenazine, the "light-switch" complex) have shown strong emission enhancement in the presence of DNA.[27-30] This complex shows no emission in aqueous solution, but luminesces strongly in the presence of DNA, hence the name "light switch". The binding of this complex has been attributed to intercalation in the major groove, the same model proposed for the $Ru(phen)_3^{2+}$ complex bound to DNA.[27-30]

Two novel complexes were synthesized by our group which are structurally similar to $Ru(bpy)_2dppz^{2+}$. The $Ru(bpy)_2iso\text{-}ppz^{2+}$ complex (iso-ppz=a structural isomer of ppz) has one less fused benzene ring on the periphery of the dppz ligand, while the $Ru(bpy)_2nar^{2+}$ complex has an additional fused benzene ring on the periphery of the dppz ligand. (See Chapter II-page 41) Both complexes show enantioselective binding to DNA. However, binding of the $Ru(bpy)_2nar^{2+}$ complex appears to have significant non-intercalative contributions to the overall binding, while the $Ru(bpy)_2iso\text{-}ppz^{2+}$ complex displays mainly intercalative behavior. Both complexes luminesce in the presence and absence of DNA, in contrast to the $Ru(bpy)_2dppz^{2+}$ complex,

which shows negligible emission at room temperature in aqueous solution.[27] Both emissions are enhanced in the presence of DNA, but the $Ru(bpy)_2nar^{2+}$ complex shows an unusual emission enhancement phenomenon. Initially, upon adding DNA to an aqueous solution of $Ru(bpy)_2nar^{2+}$, the luminescence first decreases and then increases. This phenomenon is highly unusual, and may ultimately lead to a better understanding of the binding of this complex to DNA.

A study of complexes such as these can provide information regarding the extent to which ligand length plays a part in the way Ru(II) polypyridyl ligands penetrate the double helix via intercalation in the major groove. However, the interpretation of the spectral properties of this series is complicated because the $Ru(bpy)_2dppz^{2+}$ complex does not luminesce at all in aqueous solution.[27] This discontinuity complicates the analysis of the emission enhancement for this series of complexes because the enhancements and luminescence quantum yields are measured relative to aqueous solution values, and descriptions of the binding to DNA are based on these values.

Results and Discussion

Absorption Hypochromism

The absorption bands in this series of complexes are not resolved because all the π^* states of the ligands are similar in energy to bipyridine. The lack of red-shifted absorption for the "light-switch" complex has been discussed by Amouyal and coworkers, who concluded that the electronic structure of $Ru(bpy)_2dppz^{2+}$ is best described as a coupling of a $Ru(bpy)_3^{2+}$ chromophore

with a phenazine electron acceptor.[346] Hence, the MLCT transitions to the excited states of the ligands occur at overlapping energies, and the visible spectra for this series of complexes are broad and poorly resolved. The small hypochromic effects of the MLCT bands for all these complexes cannot be assigned unambiguously to transitions terminating on bpy or the modified ligand, because of the spectral overlap. (Figures IX-1,2,3). The bands at ~360-390 in the $Ru(bpy)_2dppz^{2+}$ spectrum show the largest hypochromism, followed by the 450nm MLCT band(s) in $Ru(bpy)_2iso\text{-}ppz^{2+}$. The 400-450 nm MLCT band(s) of $Ru(bpy)_2nar^{2+}$ show similar hypochromic effects as compared to $Ru(bpy)_2iso\text{-}ppz^{2+}$. Barton et. al. did not report on absorption hypochromism, nor aqueous free solution absorption spectra for the complex $Ru(bpy)_2dppz^{2+}$ and on the bis-phen derivatives $Ru(phen)_2dppz^{2+}$ and $Ru(phen)_2dppn^{2+}$.[27-30] (dppn = nar)

Emission Enhancement

Emission enhancement was found for all members of this series upon binding to DNA. The maximal effect was found for $Ru(bpy)_2dppz^{2+}$, while the minimal effect was observed with $Ru(bpy)_2nar^{2+}$. Normalized plots of emission enhancement vs. [DNA-P]/[Ru] ratio are given for both $Ru(bpy)_2nar^{2+}$ and $Ru(bpy)_2iso\text{-}ppz^{2+}$. An increase in emission quantum yield of 1.7 times was found for the $Ru(bpy)_2nar^{2+}$ complex, and 4.4 times for $Ru(bpy)_2iso\text{-}ppz^{2+}$ (Figures IX 4,5). Emission quantum yield increases for $Ru(bpy)_2dppz^{2+}$ in the presence of DNA of about 10^4 have been reported[27-30]. This number may be artificially high due to the total lack of luminescence of this complex in water.

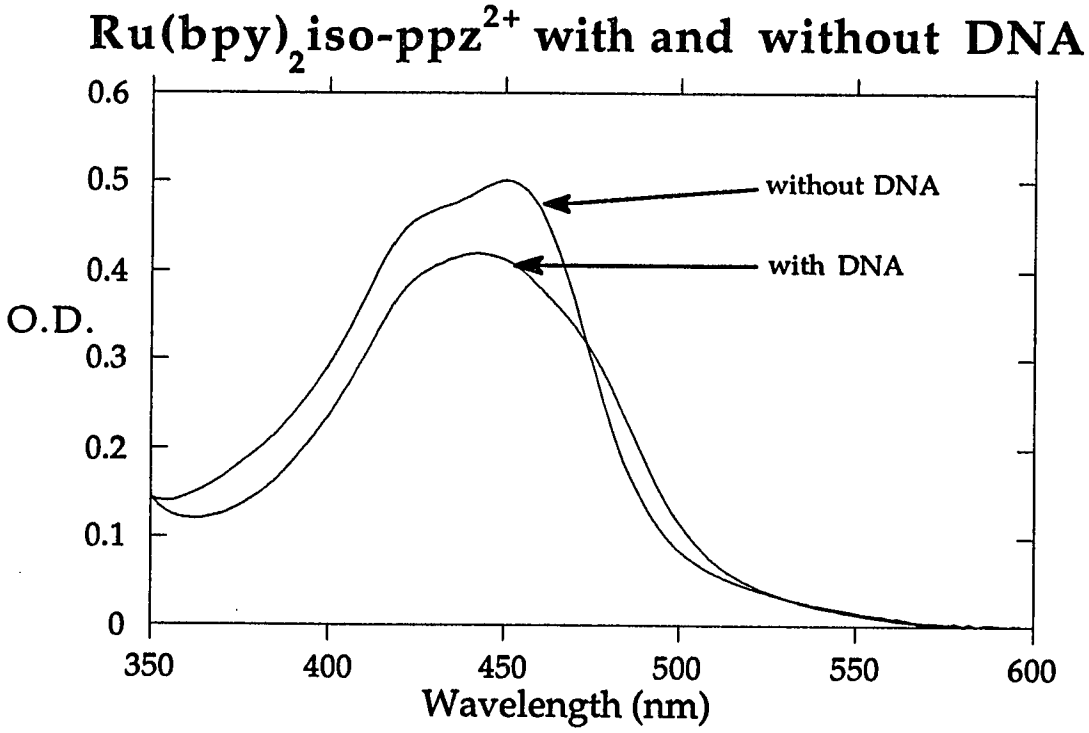

Figure IX-1. Visible absorption spectra of racemic $Ru(bpy)_2iso\text{-}ppz^{2+}$ (26μM) alone and in the presence of calf thymus DNA. [DNA-P]/[Ru] = 30. All solutions measured at 25°C in 5mM Tris, pH 7.4, 50mM NaCl.

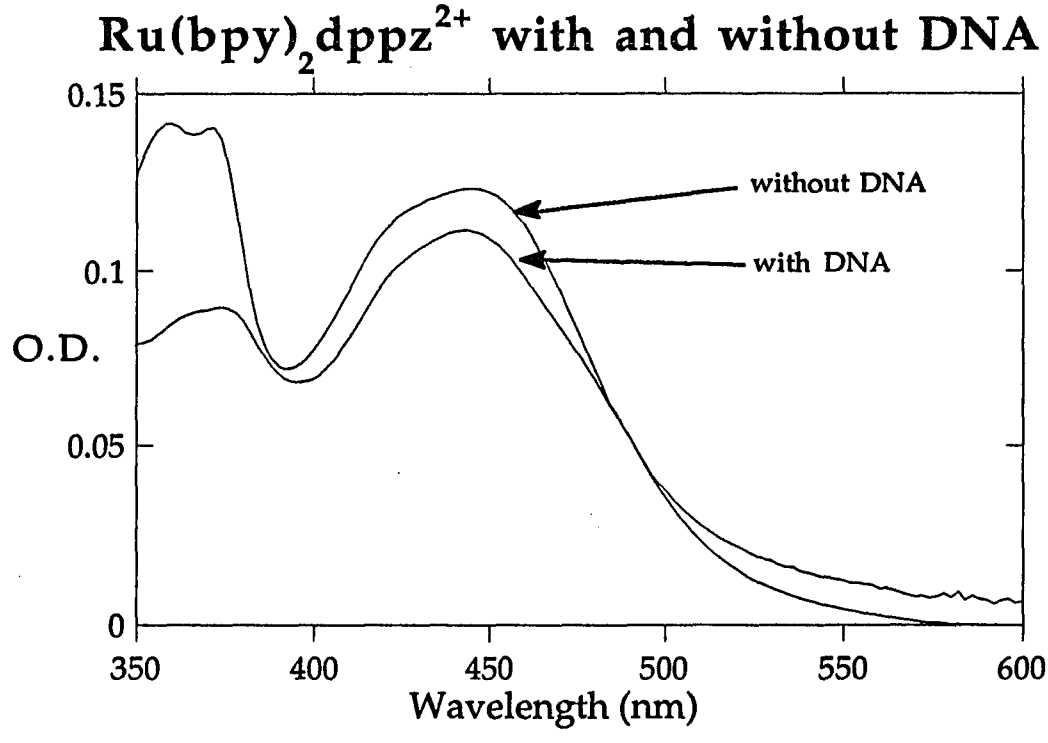

Figure IX-2. Visible absorption spectra of racemic $Ru(bpy)_2dppz^{2+}$ (5.4μM) alone and in the presence of calf thymus DNA. [DNA-P]/[Ru] = 146. All solutions measured at 25°C in 5mM Tris, pH 7.4, 50mM NaCl.

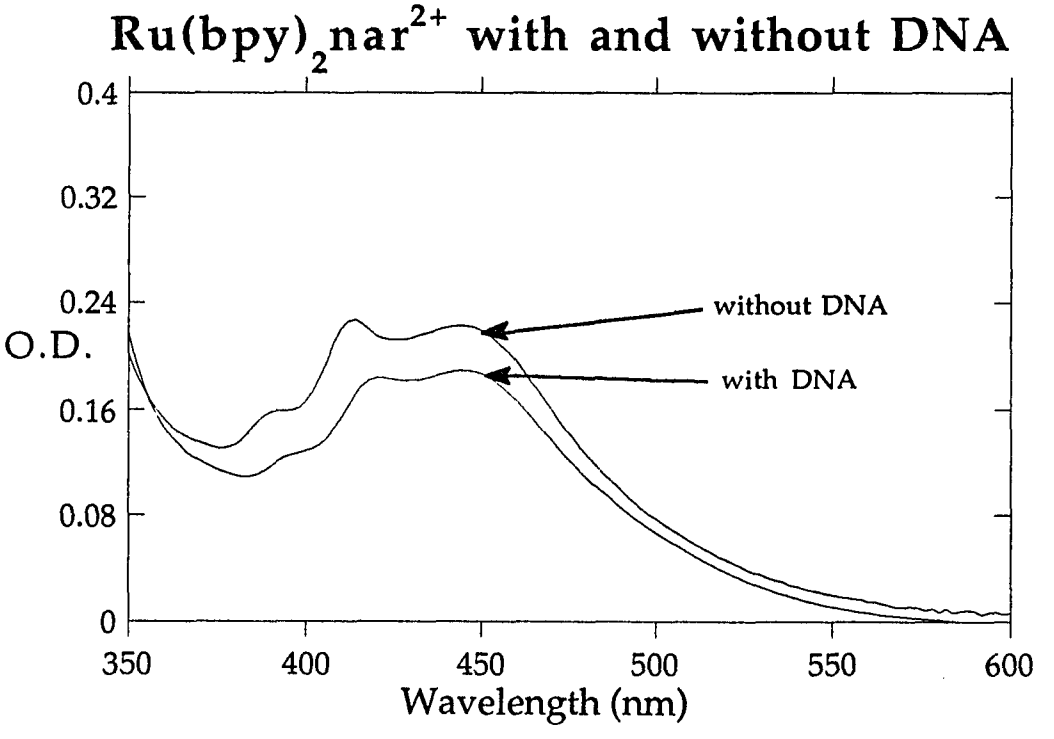

Figure IX-3. Visible absorption spectra of racemic $Ru(bpy)_2nar^{2+}$ (9.2μM) alone and in the presence of calf thymus DNA. [DNA-P]/[Ru] = 54. All solutions measured at 25°C in 5mM Tris, pH 7.4, 50mM NaCl.

The large emission enhancement found for $Ru(bpy)_2dppz^{2+}$ arises because the ligand is well shielded from water when bound, enhancing the luminescence tremendously by preventing water from deactivating the excited state non-radiatively. Barton and coworkers have carried out studies to observe the quenching effect of water with this complex, and they have come to the conclusion that protonation of a pyrazyl nitrogen leads to the quenching phenomenon in aqueous solution ("Light switch" effect)[30].

Interestingly, both $Ru(bpy)_2nar^{2+}$ and $Ru(bpy)_2iso\text{-}ppz^{2+}$ are luminescent at room temperature in fluid solution, with measured emission quantum yields in the **absence** of DNA of 0.011 and 0.019 respectively. Quantum yield of emission values at [DNA-P]/[Ru] ~200 are calculated to be 0.018 and 0.083, respectively, from the emission enhancement data. No values of emission quantum yields for $Ru(phen)_2nar^{2+}$, $Ru(bpy)_2dppz^{2+}$, or $Ru(phen)_2dppz^{2+}$ were reported for free aqueous solutions, however, emission enhancements relative to air-saturated $Ru(bpy)_3^{2+}$ were given for these complexes, and are listed in Table 1. Emission quantum yields were calculated from these values using 0.028 as the emission quantum yield of air-saturated $Ru(bpy)_3^{2+}$.[347] The emission quantum yield in the presence of DNA for $Ru(bpy)_2dppz^{2+}$ is approximately 0.0056, and 0.016 for $Ru(phen)_2nar^{2+}$. These values may be much smaller than maximal because the Barton group did not investigate [DNA-P]/[Ru] ratios higher than ~25,[30] while we investigated [DNA-P]/[Ru] ratios of ~200 to maximize the effect.

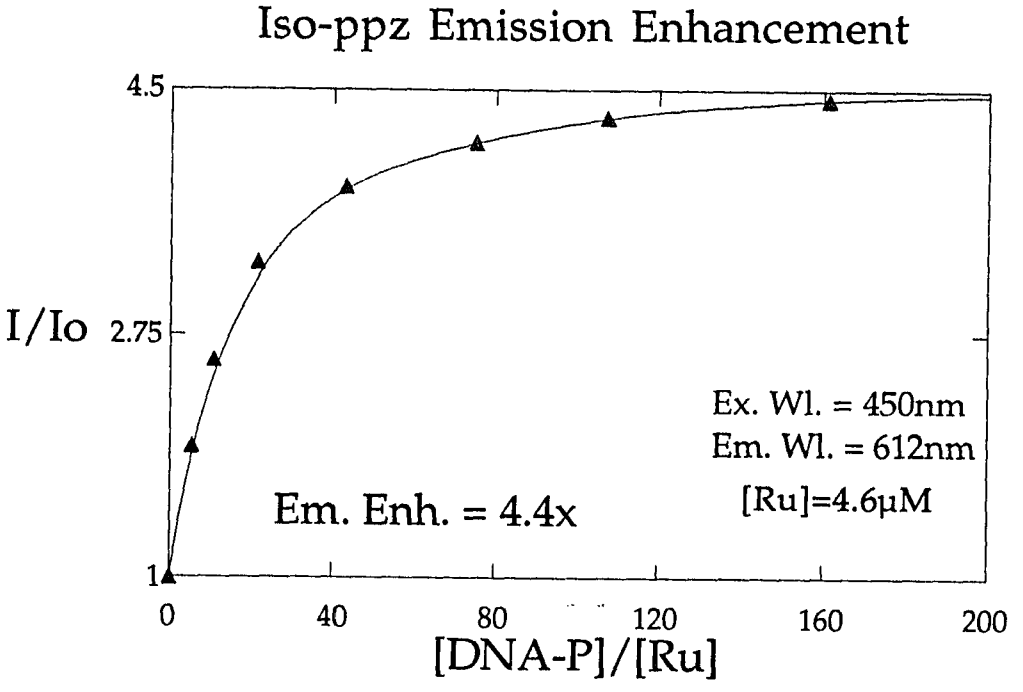

Figure IX-4. Emission enhancement vs. [DNA-phosphate] for $Ru(bpy)_2iso\text{-}ppz^{2+}$ (4.6μM) in the presence of calf thymus DNA. Samples in 5mM Tris, 50mM NaCl, pH 7.4.

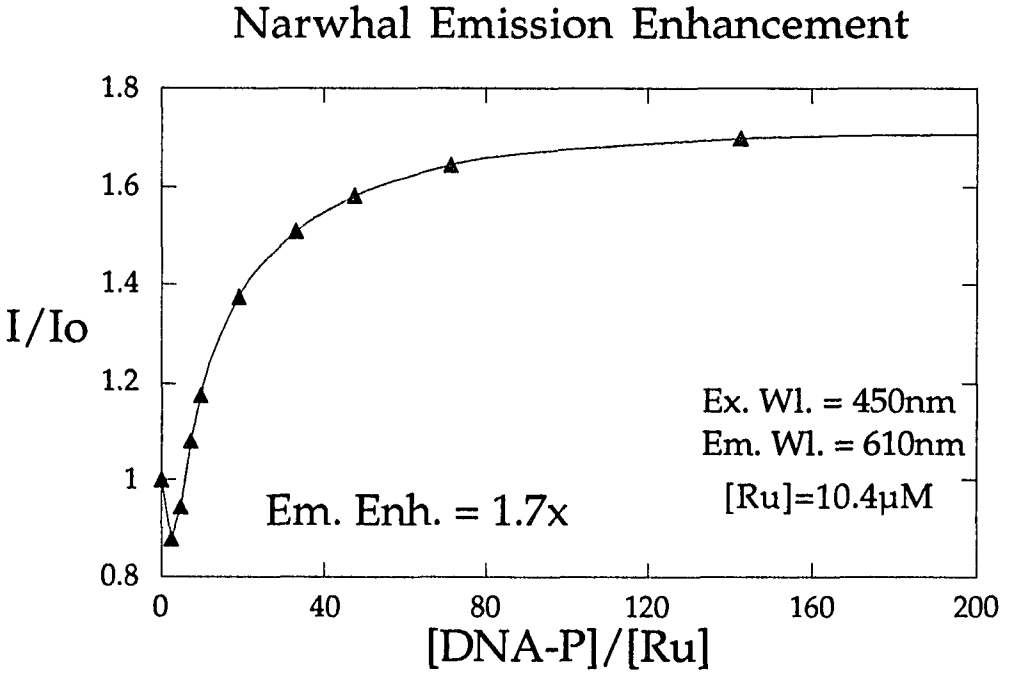

Figure IX-5. Emission enhancement vs. [DNA-phosphate] for $Ru(bpy)_2nar^{2+}$ (10.4μM) in the presence of calf thymus DNA. Samples in 5mM Tris, 50mM NaCl, pH 7.4.

Table 1

Emission Intensities relative to air-saturated $Ru(bpy)_3^{2+}$ at 298K.

Compound	Rel. Intensity (No DNA)	Rel. Intensity (With DNA)	λ_{max}	Enhancement at [DNA-P]/[Ru] =25
$Ru(phen)_2dppz^{2+}$ [a]	0	0.56	618	>100
$Ru(phen)_2nar^{2+}$ [a]	0.16	0.20	607	1.3
$Ru(bpy)_2dppz^{2+}$ [b]	0	0.16	621	>100
$Ru(bpy)_2iso\text{-}ppz^{2+}$	0.68	2.9	612	>4.4
$Ru(bpy)_2nar^{2+}$	0.39	0.68	610	>1.7

a-From reference 30. b-From reference 28. All other data collected at 298K in 5mM Tris, 50mM NaCl, pH 7.4 buffer.

From the emission quantum yield data, the $Ru(bpy)_2iso\text{-}ppz^{2+}$ complex shows the largest emission quantum yield in the presence of DNA (ϕ =0.083), which is even more emissive than N_2 purged $Ru(bpy)_3^{2+}$ in aqueous solution (ϕ =0.042). The $Ru(bpy)_2dppz^{2+}$ complex **with DNA** shows a value smaller than $Ru(bpy)_2iso\text{-}ppz^{2+}$ and $Ru(bpy)_2nar^{2+}$ in **free** aqueous solution.

Intercalative binding in the major groove of B-DNA, similar to the binding proposed for $Ru(phen)_3^{2+}$,[5] has been proposed for the complexes $Ru(bpy)_2dppz^{2+}$ and $Ru(phen)_2dppz^{2+}$[28,30] . For these complexes, changes in the emission properties are similar to those of $Ru(phen)_3^{2+}$ and $Ru(bpy)_2ppz^{2+}$.

For $Ru(bpy)_2iso\text{-}ppz^{2+}$, the enhancement is much less than

$Ru(bpy)_2dppz^{2+}$, perhaps due to the fact that this complex luminesces quite strongly in aqueous solution, and is apparently not quenched efficiently by interactions with aqueous solvent molecules as compared to the "light-switch" complexes. However, larger emission enhancement in the presence of DNA is found for the $Ru(bpy)_2iso\text{-}ppz^{2+}$ complex (4.4 times) compared to the $Ru(phen)_3^{2+}$ complex (1.9 times), and the emission quantum yield of $Ru(bpy)_2iso\text{-}ppz^{2+}$ upon binding to DNA is larger than $Ru(bpy)_3^{2+}$ in N_2 purged aqueous solution. Therefore, I propose that the $Ru(bpy)_2iso\text{-}ppz^{2+}$ complex binds intercalatively in the major groove, similar to $Ru(bpy)_2ppz^{2+}$.

For $Ru(bpy)_2nar^{2+}$, the enhancement is much less than for $Ru(bpy)_2iso\text{-}ppz^{2+}$, yet they both have somewhat similar free solution emission quantum yields. Also, the emission enhancement decreases initially and then increases to its limiting value of ~1.7 times. (Figure IX-5 at low [DNA-P]/[Ru] ratios) This decrease is highly uncharacteristic of intercalating complexes, and it may be inferred that the cause of this phenomenon is the size of the nar ligand, perhaps too large to intercalate in as many intercalation sites as, for example, $Ru(bpy)_2dppz^{2+}$. It therefore adopts a favorable electrostatic binding mode that quenches the excited state when all intercalating sites are occupied (i.e. lower [DNA-P]/[Ru] ratios), and then when more intercalating sites become available (i.e. higher [DNA-P]/[Ru] ratios), it finds these sites and intercalates there. Also, penetration of the large nar ligand may not occur to the same extent as it does in the dppz and iso-ppz complexes, and intercalative binding is partially inhibited. It can also be surmised that due to the flexibility of the DNA duplex,

some major groove intercalating sites are better suited for intercalation than others. Since the favorable intercalating sites may be somewhat more limited than the average intercalating sites, a much smaller number of $Ru(bpy)_2nar^{2+}$ ions become intercalated, and less emission enhancement is seen. This difference in intercalating sites may be more critical in determining the ability of the $Ru(bpy)_2nar^{2+}$ complex to bind intercalatively due to the increased length of the nar ligand compared to the other members of the series.

Emission Lifetime

Emission lifetimes for this series of complexes in the presence and absence of DNA were measured. Bi-exponential behavior is found for all complexes in this series in the presence of DNA.

For $Ru(bpy)_2iso\text{-}ppz^{2+}$, the free solution lifetime was measured to be 252ns. Upon binding to DNA, a short and a long component resulted, with lifetimes of 250ns and 1450ns respectively. Therefore, a 5.8x increase in luminescence lifetime (long component) accompanies a 4.4x increase in the emission quantum yield for this complex. These values indicate that the radiative rate constant of the chromophore is slightly decreased upon binding to DNA, and therefore the chromophore is perturbed slightly. The short component of the emission is similar to the free solution value, and can be assigned to the free and electrostatically bound modes.

For $Ru(bpy)_2nar^{2+}$, the free solution lifetime was measured to be 524ns. Upon binding to DNA, a bi-exponential decay resulted, with lifetimes of ~520ns and 908ns respectively. These were **not** well resolved however, due to the

large contribution of the short component even at [DNA-P]/[Ru] ratios of > 40. Here, a 1.7 fold increase in the emission lifetime is accompanied by a 1.7 fold increase in the emission quantum yield. These similar values indicate that the radiative rate constant of the chromophore is not altered significantly upon binding. Table 2 summarizes the data found for the $Ru(bpy)_2iso\text{-}ppz^{2+}$, $Ru(bpy)_2dppz^{2+}$, and $Ru(bpy)_2nar^{2+}$ complexes with and without DNA.

Table 2

Emission properties τ,ϕ in the presence and absence of DNA.

Compound	τ (No DNA)	ϕ (No DNA)	τ (ns)short and long (With DNA)	ϕ (With DNA)	τ_r (s) (No DNA)	τ_r (s) (With DNA)
$Ru(phen)_2dppz^{2+}$[a]	0	0	120,770	0.0045	Undefined	1.7×10^{-4}
$Ru(bpy)_2dppz^{2+}$	0	0	90,340	0.026	Undefined	1.3×10^{-5}
$Ru(bpy)_2iso\text{-}ppz^{2+}$	252	0.019	250,1450	0.083	1.3×10^{-5}	1.7×10^{-5}
$Ru(bpy)_2nar^{2+}$	524	0.011	524[b],908	0.019	4.7×10^{-5}	4.7×10^{-5}

a-From reference 28

b-not resolvable due to the large contribution of short component.

The luminescence lifetime of the $Ru(phen)_2dppz^{2+}$ complex is also bi-exponential in DNA, (τ = 120ns,770ns)[30] yet for this complex, the short component of the luminescence cannot be explained as it has for the other complexes. Due to its total lack of luminescence in aqueous solution, the short component cannot be assigned to the free or electrostatically bound complex,

since this species presumably would not luminesce either. Therefore, Barton put forth a model of two intercalative binding modes for this complex, one with the intercalating ligand going perpendicular to the long axis of the base pairs of DNA, and another side-on mode, where the ligand is partially exposed to solvent.[28] This model was used to explain the experimental data found for $Ru(bpy)_2dppz^{2+}$ complex, yet has not been characterized further.

Luminescence lifetimes are very sensitive probes of the local environment, and seem to indicate that intercalative binding interactions give rise to longer luminescence lifetimes and larger emission quantum yields than can be achieved by simply changing to a more hydrophobic solvent. A change in the **radiative** lifetime, or equivalently, a change in the intersystem crossing efficiency, is an important indicator of an **intercalative** interaction. **Differential changes in the luminescence lifetime and emission quantum yield are what give rise to changes in radiative lifetime (τ_r).** The alteration may either increase or decrease the τ_r, but if a change is seen, this appears to be a strong indicator of an intercalative interaction. For example, the radiative lifetime change found for Δ $Ru(bpy)_2ppz^{2+}$ when bound to DNA is an example of a complex which has a radically different τ_r value compared to its free solution value. Both enantiomers of $Ru(phen)_3^{2+}$ show change in their τ_r values, as does the $Ru(bpy)_2dppz^{2+}$ complex, where the change in τ_r is most dramatic. The lack of change in τ_r found for the $Ru(bpy)_2qpyMe_2^{4+}$ complex supports the conclusion that this complex only interacts electrostatically or via a surface bound mode. Since the radiative

lifetime is a property of the chromophore itself,[73] it becomes apparent that interactions which alter the chromophore significantly (e.g. intercalation) can change the radiative lifetime, and interactions that do not alter the chromophore (electrostatic and surface bound interactions) do not affect τ_r. It can also be stated that intercalation does not necessarily have to alter the τ_r, as is the case with the Λ isomer of $Ru(bpy)_2ppz^{2+}$, which has only a modest change in the τ_r. Some parallels can be drawn to the resonance Raman spectra for $Ru(bpy)_2ppz^{2+}$ and $Ru(bpy)_2qpyMe_2^{4+}$, where changes in intensities were evident for the $Ru(bpy)_2ppz^{2+}$ complex, and only small changes were found in the $Ru(bpy)_2qpyMe_2^{4+}$ spectrum with and without DNA. Changes in the rR spectrum upon binding to DNA are indicative of changes in going from the ground state to the singlet excited state, but may also indicate changes in the triplet (emissive) excited state as well, since both excited states are expected to be similar in structure on the timeframe of the absorption.

Based on the change in τ_r, it is proposed that for the $Ru(bpy)_2iso\text{-}ppz^{2+}$ complex, a change in radiative lifetime occurs, and therefore a substantial amount of this complex ion is bound in an intercalative fashion. Similar arguments can be made for $Ru(bpy)_2dppz^{2+}$, at least for the long component of the emission lifetime profile. For the $Ru(bpy)_2nar^{2+}$ complex, a lack of change in τ_r suggests that this complex has a ligand (nar) which due to its length cannot find as many suitable sites capable of allowing this complex to bind intercalatively, and therefore a larger contribution from electrostatic and/or surface bound modes to DNA is proposed, combined with smaller contributions

from intercalative binding modes relative to the other complexes in the series.

Emission Polarization

Limiting emission polarizations of ~0.06 for $Ru(bpy)_2iso\text{-}ppz^{2+}$ and ~0.05 for $Ru(bpy)_2nar^{2+}$ were found for these complexes in the presence of DNA ([DNA-P]/[Ru] >80). A reported value of 0.15 for the polarization of $Ru(bpy)_2dppz^{2+}$ was given at a [DNA-P]/[Ru] ratio = 100.[30] Since the long component lifetime of the $Ru(bpy)_2dppz^{2+}$ complex is shorter than the other two, and both luminescence lifetime and emission polarization must be taken into account to explain the measured static emission polarizations, the $Ru(bpy)_2dppz^{2+}$ complex can be assumed to be the most rigidly held of the series, followed by $Ru(bpy)_2iso\text{-}ppz^{2+}$ and $Ru(bpy)_2nar^{2+}$. These data are consistent with the proposed binding modes for each complex, with $Ru(bpy)_2dppz^{2+}$ being proposed as the best major groove intercalator for this series of complexes.

Emission Quenching

Quenching studies with the $Ru(bpy)_2iso\text{-}ppz^{2+}$ and $Ru(bpy)_2nar^{2+}$ complexes with ferrocyanide ion support the proposed binding of these complexes. Quenching for the $Ru(bpy)_2iso\text{-}ppz^{2+}$ is very similar to that of racemic $Ru(bpy)_2ppz^{2+}$, its structural isomer, in the presence and absence of DNA. The $Ru(bpy)_2nar^{2+}$ complex with ferrocyanide ion quenches somewhat more easily than the $Ru(bpy)_2iso\text{-}ppz^{2+}$ complex. (Figure IX-6) This may indicate that the $Ru(bpy)_2nar^{2+}$ complex has its nar ligand more exposed to solvent, where interactions with quencher lower the emission intensity faster

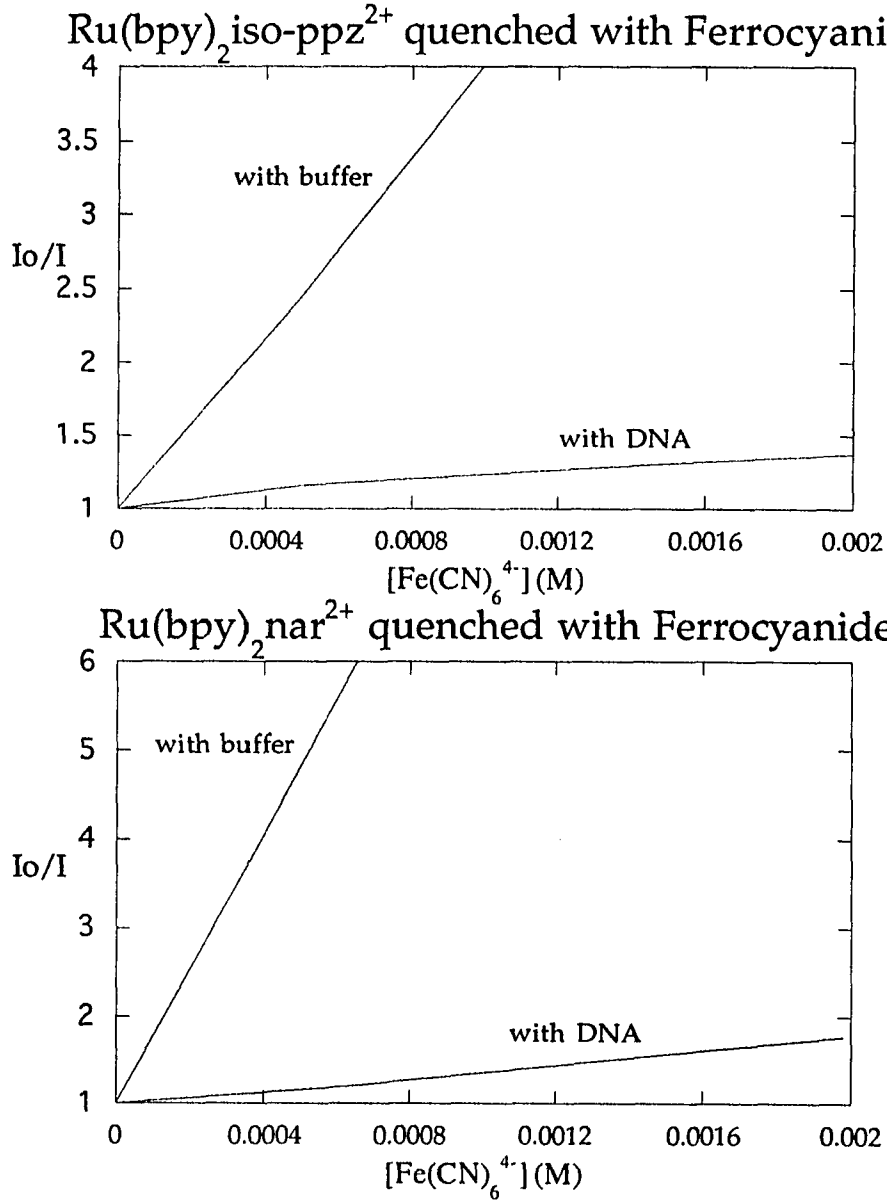

Figure IX-6. Quenching with $Fe(CN)_6^{4-}$ ion for $Ru(bpy)_2nar^{2+}$ and $Ru(bpy)_2iso\text{-}ppz^{2+}$ at [DNA-phosphate]/[Ru]=10. Quenching of each complex by $Fe(CN)_6^{4-}$ ion in the absence of DNA shown for comparison. All samples measured at 20°C in 5mM Tris, 50mM NaCl buffer, pH 7.4.

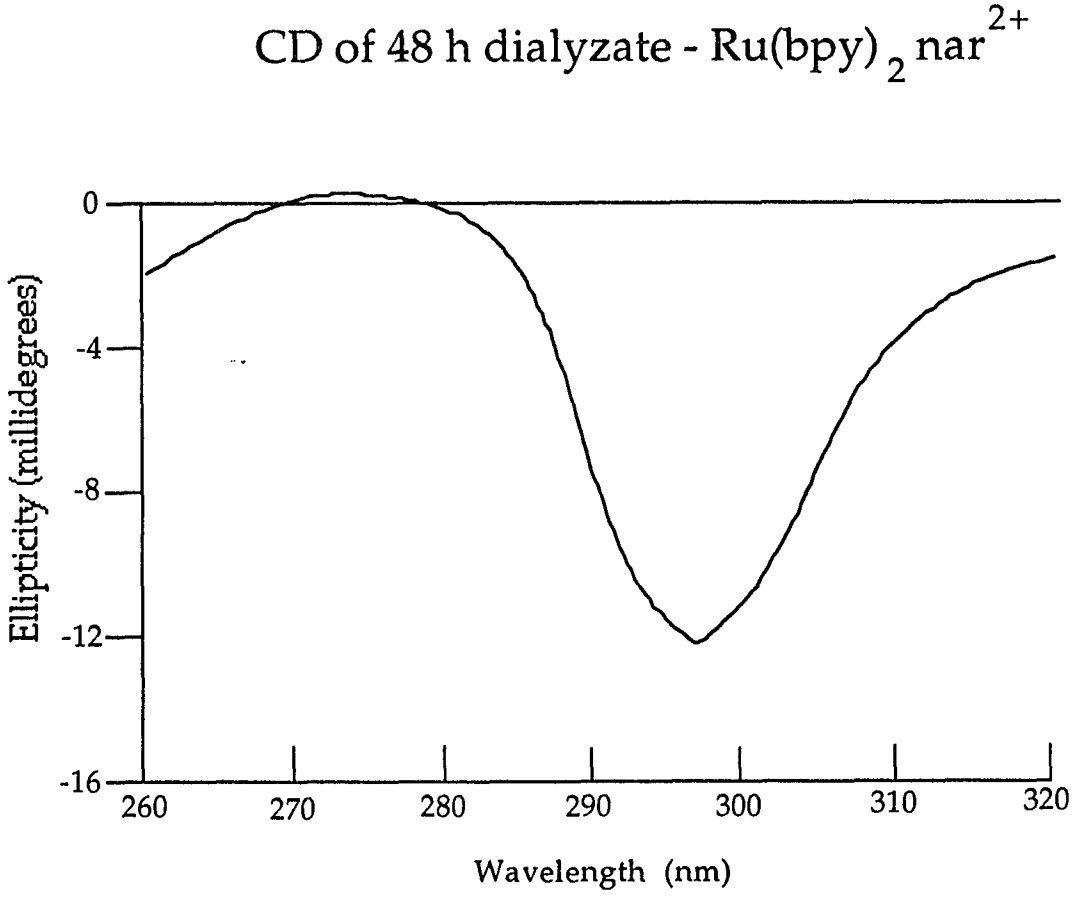

Figure IX-7. Circular dichroism spectra of 48hour dialyzate vs. calf thymus DNA ([DNA-P] = 1.6mM) for racemic $Ru(bpy)_2nar^{2+}$. Sample measured at 25°C in 5mM Tris, 50mM NaCl buffer, pH 7.4.

than if this complex were to adopt an intercalative interaction. (i.e. shielded from the quencher)

Enantioselectivity

The enantioselectivity found for both complexes must be taken into account to describe the binding mode. (Figure IX-7, only $Ru(bpy)_2nar^{2+}$ CD shown) Qualitatively, the $Ru(bpy)_2dppz^{2+}$ complex shows smaller enantioselectivity than $Ru(bpy)_2iso\text{-}ppz^{2+}$ or $Ru(bpy)_2nar^{2+}$, suggesting that both enantiomers may possess similar binding strengths with this complex, due to the increased length relative to $Ru(bpy)_2ppz^{2+}$ or $Ru(bpy)_2iso\text{-}ppz^{2+}$. This weak enantioselectivity may be the reason why reports on the resolved enantiomers of $Ru(bpy)_2dppz^{2+}$ have **not** appeared in the literature.

Enantioselectivity for $Ru(bpy)_2iso\text{-}ppz^{2+}$ can be understood from arguments made for $Ru(bpy)_2ppz^{2+}$ (Chapter VII). No conclusions regarding the origin of the enantioselectivity for the $Ru(bpy)_2nar^{2+}$ complex will be made in this dissertation.

Equilibrium Dialysis

Equilibrium dialysis studies performed on $Ru(bpy)_2iso\text{-}ppz^{2+}$ yield a binding constant of 9.0×10^4 for this complex, with a site size I = 2. This measured binding constant is somewhat higher yet still comparable to the $Ru(bpy)_2ppz^{2+}$ complex and the $Ru(bpy)_2qpyMe_2^{4+}$ complex, where binding constants on the order of 10^3 or 10^4 were found. Figure IX-8 is a Scatchard plot of the $Ru(bpy)_2iso\text{-}ppz^{2+}$ complex describing the binding to DNA.

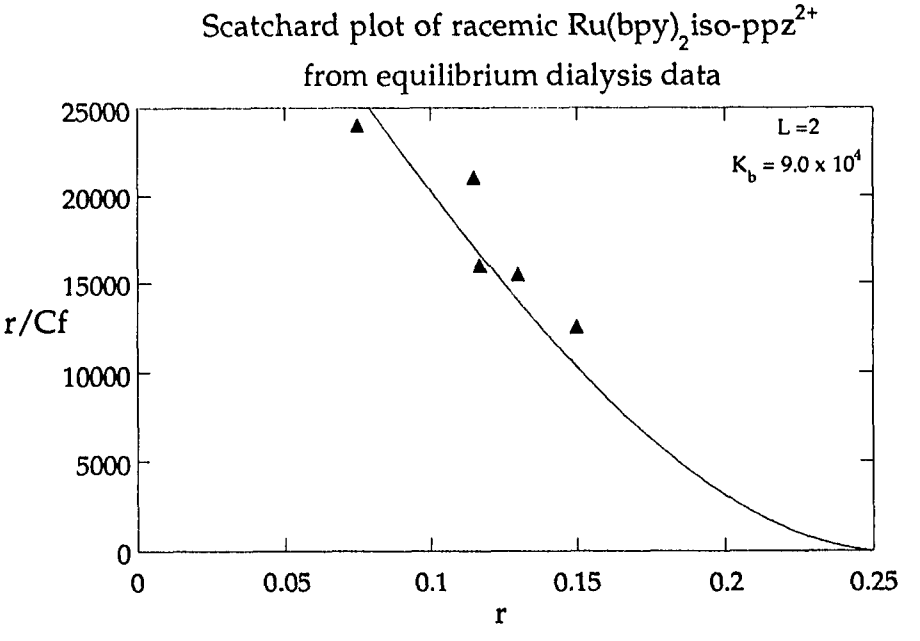

Figure IX-8. Scatchard analysis from equilibrium dialysis data for racemic $Ru(bpy)_2$iso-ppz^{2+}. (○) actual data, (——) best fit to the McGhee and von Hippel equation. Site sizes and binding constants are indicated in plot.

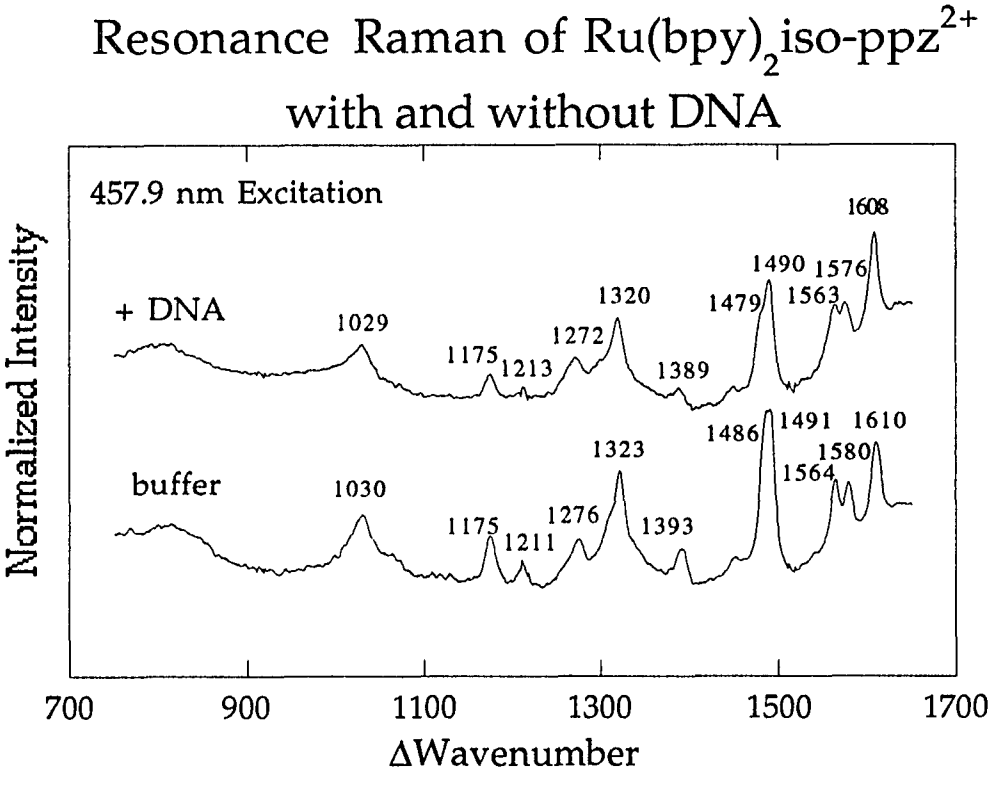

Figure IX-9. Resonance Raman spectrum of $Ru(bpy)_2$iso-ppz^{2+} without DNA and with [DNA-P]/[Ru] =36 using 457.9nm Ar^+ excitation and 4.0 cm^{-1} spectral bandwidth. [Ru] = 43μM for all spectra. All samples in 5mM Tris, 50mM NaCl, pH 7.4.

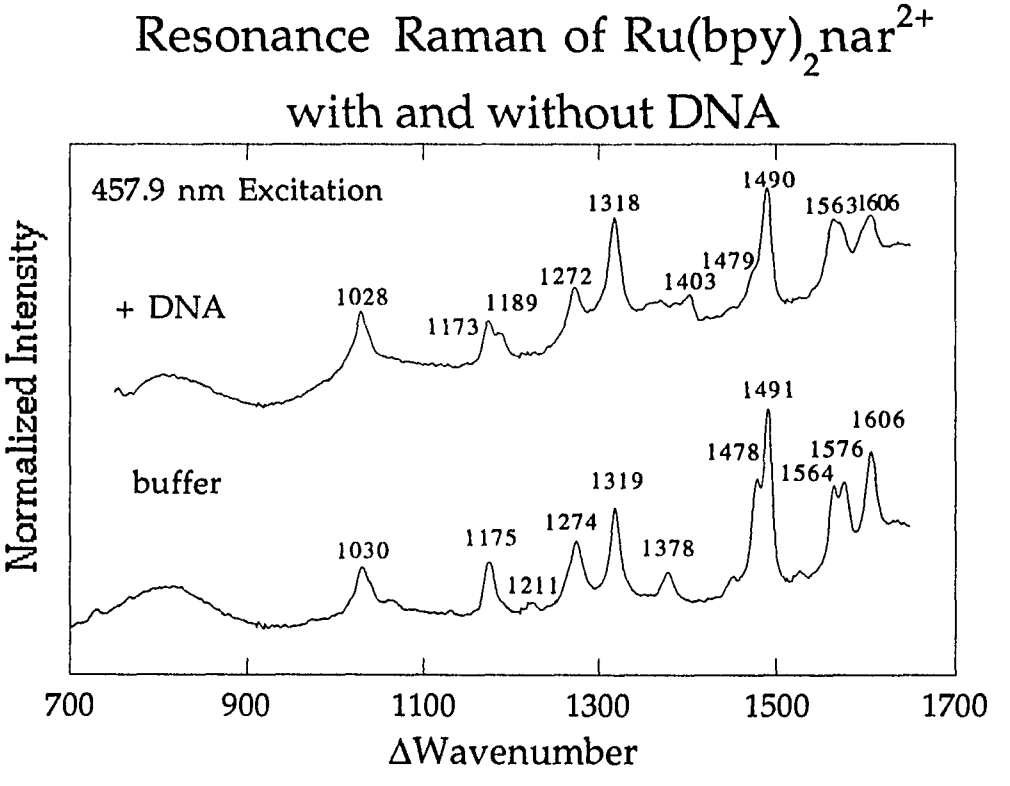

Figure IX-10. Resonance Raman spectrum of $Ru(bpy)_2nar^{2+}$ without DNA and with [DNA-P]/[Ru] =50 using 457.9nm Ar^+ excitation and 4.0 cm^{-1} spectral bandwidth. [Ru] = 47μM for all spectra. All samples in 5mM Tris, 50mM NaCl, pH 7.4.

Resonance Raman

The resonance enhanced Raman spectra for $Ru(bpy)_2iso\text{-}ppz^{2+}$ and $Ru(bpy)_2nar^{2+}$ in the presence and absence of DNA were measured using 457.9 nm excitation. Differences were found for both complexes , consistent with the proposed binding model for these complexes. Figures IX-9 and IX-10 portray the resonance Raman spectra of both complexes in the presence and absence of DNA. A [DNA-P]/[Ru] ratio of >30 was used for both complexes with DNA to observe the maximal effect. With these spectra, decreases in the intensities of bands not attributed to bpy are evident in the DNA spectra. For the $Ru(bpy)_2iso\text{-}ppz^{2+}$ complex in DNA, decreases in the bands at 1576,1479,1389, and 1213 cm^{-1} relative to the bpy band at ~1608 are similar to changes seen for the $Ru(bpy)_2ppz^{2+}$ complex. The bands at 1576,1479,1389, and 1213 cm^{-1} are not thought to be associated with bpy vibrations, since the bpy vibrational frequencies are well known. Rather, they can be attributed to modes associated with the iso-ppz ligand vibrations.

Similarly, changes upon DNA binding are evident in the resonance Raman spectrum of the $Ru(bpy)_2nar^{2+}$ complex. Here, a change in the intensity of the vibration at 1479 is evident upon binding to DNA. What is perhaps most noticeable in the spectra for this complex is that the relative intensities of the **bpy** bands change, by the comparison of the bands at 1274 and 1319, which are both attributed to vibrations of the bpy ligand. The intensity of the the 1274 vibrational band decreases in the DNA spectrum relative to the buffer spectrum. Several other more subtle changes in the bands associated with the transitions

to bpy can be seen in the spectra of $Ru(bpy)_2nar^{2+}$ with DNA.

Changes in intensities of both the bpy and nar vibrational bands are prevalent in the $Ru(bpy)_2nar^{2+}$ spectrum with DNA. However, in the $Ru(bpy)_2$iso-ppz^{2+} spectrum with DNA, the vibrational bands associated with the iso-ppz ligand show the most changes in intensity, with very small changes observed for the bpy vibrational intensities. In the nar spectrum, changes are observed for both bpy and nar vibrational intensities.

The rR evidence supports the proposed binding modes of these complexes, with both showing intercalative behavior. The changes in the intensities of the bpy ligand vibrations as well as the nar ligand vibrations for the $Ru(bpy)_2nar^{2+}$ complex when bound to DNA support the existence of a significant contribution to an electrostatic and/or surface bound interaction with DNA.

Summary

The spectroscopic and photophysical information presented here and evidence from the literature support strong intercalative interaction in the major groove for both $Ru(bpy)_2dppz^{2+}$ and $Ru(bpy)_2$iso-ppz^{2+} in the presence of calf thymus B-DNA, with the "light-switch" complex ($Ru(bpy)_2dppz^{2+}$) being proposed as the best intercalator of the series. Intercalation for $Ru(bpy)_2nar^{2+}$ is also proposed, however, a significant contribution to an electrostatic and/or surface bound mode competes appreciably with intercalation based on the spectroscopic evidence. Resolution of both of these complexes into their enantiomers and their subsequent study should shed new light on this subject,

and provide clearer evidence for the characterization of the binding behavior of these complexes to the DNA duplex.

Chapter X. Summary of the Spectroscopic and Photophysical Parameters measured for the complexes used in the DNA binding study.

All complexes listed contain two bpy ligands and one modified bpy ligand, except $Ru(phen)_3^{2+}$. They will be designated on the chart with just the name of the differentiating ligand. References cited for dppz and tris-phen data are from Barton et. al.[4,5,6,27-30] Some values were taken or derived from these references. All properties were measured with air-saturated solutions at room temperature in 5mM Tris, 50mM NaCl, pH 7.4 buffer.

Table 1. Absorption Properties

Property	Complex	Solution (Aqueous)
ε	tris-phen	1.9×10^4 @ 448nm
	bpy	1.4×10^4 @ 450nm
	dpp	1.2×10^4 @ 430nm
	ppz	1.1×10^4 @ 422nm
	qpy	2.3×10^4 @ 472nm
	$qpyMe^+$	1.3×10^4 @ 488nm
	$qpyMe_2^{2+}$	1.4×10^4 @ 492nm
	iso-ppz	1.5×10^4 @ 450nm
	nar	2.5×10^4 @ 444nm
	dppz	2.2×10^4 @ 440nm

	Complex	Solution (Aqueous)	With DNA
λ_{max}(vis)	tris-phen	448	452
	bpy	452	452
	dpp	430	430
	Δ ppz	422 (477) sh	422 (495) sh
	Λ ppz	422 (477) sh	422 (485) sh
	qpy	420, 473	420, 473
	$qpyMe^+$	425	425
	$qpyMe_2^{2+}$	426, 500	430, 518
	iso-ppz	429, 450	441
	nar	444	444
	dppz	446	445

Table 2. Emission Properties

Property	Complex	Solution (Aq.)	DNA Solution	λ Shift in DNA
λ_{max}	tris-phen	600	602	2
	bpy	610	610	0
	dpp	685	685	0
	ppz	690	668	-28
	Δ ppz	690	660	-30
	Λ ppz	690	670	-20
	qpy	665	665	0
	$qpyMe^{+}$	655	655	0
	$qpyMe_2^{2+}$	710	735	25
	iso-ppz	612	610	-2
	nar	610	612	2
	dppz	-----	618	----

Property	Complex	Solution (Aq.)	with DNA	Em. Enhance(max effect)
ϕ_{em}	tris-phen	0.032(Air Sat.)	0.061	1.9x
	bpy	0.028	0.028	1x
	dpp	0.0020	0.0020	1x
	ppz	0.0023	0.028	12x
	Δ ppz	0.0023	0.039	17x
	Λ ppz	0.0023	0.012	5.2x
	qpy	0.0056	0.0056	1x
	$qpyMe_2^{2+}$	0.00077	0.0015	1.9x
	iso-ppz	0.019	0.0836	4.4x
	nar	0.011	0.019	1.7x

Property	Complex	Aq. solution	short component	long component
τ_{em}(ns)				
	tris-phen	585	~500	~2000
	bpy	400	416	--
	dpp	125	125	--
	ppz	120-130	125	908
	Δ ppz	127	120	950
	Λ ppz	125	120	550
	qpy	440		
	$qpyMe^{+}$	Sample decomposes		
	$qpyMe_2^{2+}$	64	<30	124
	iso-ppz	250	250	1450
	nar	524	*	908
	dppz	--	120	750

* difficult to resolve from emission lifetime profile

Emission properties (continued)

Property	Complex	Solution (Aqueous)	With CT DNA(Max. Effect)
τ_r (μs)	tris-phen	18	32
	bpy	14	14
(Using	dpp	62	62
longest	Δ ppz	52	24
component	Λ ppz	52	47
of	$qpyMe_2^{2+}$	83	83
emission)	iso-ppz	13	17
	nar	47	48
k_r (s^{-1})	tris-phen	5.6×10^4	3.1×10^4
	bpy	7.1×10^4	7.1×10^4
(Using	dpp	1.6×10^4	1.6×10^4
longest	Δ ppz	1.9×10^4	4.1×10^4
component	Λ ppz	1.9×10^4	2.1×10^4
of	$qpyMe_2^{2+}$	1.2×10^4	1.2×10^4
emission)	iso-ppz	7.7×10^4	5.9×10^4
	nar	2.1×10^4	2.1×10^4
k_{nr} (s^{-1})	tris-phen	1.7×10^6	4.7×10^5
	bpy	1.7×10^6	1.7×10^6
(Using	dpp	2.4×10^6	2.4×10^6
longest	Δ ppz	8.2×10^6	1.0×10^6
component	Λ ppz	8.2×10^6	1.0×10^6
of	$qpyMe_2^{2+}$	1.6×10^7	8.1×10^6
emission)	iso-ppz	4.0×10^6	6.9×10^5
	nar	1.9×10^6	1.1×10^6

Emission properties (continued)

Property	Complex	Solution (Aqueous)	With CT DNA(Max. Effect)
P (static)	tris-phen	0.00±0.01	Δ 0.036 Λ 0.025
	bpy	0.00±0.01	0.00±0.01
	dpp	0.00±0.01	0.00±0.01
	ppz	0.00±0.01	0.09±0.01
	Δ ppz	0.00±0.01	0.085±0.01
	Λ ppz	0.00±0.01	0.10±0.01
	qpy	0.00±0.01	0.02±0.01
	$qpyMe^{+}$	0.00±0.01	0.02±0.01
	$qpyMe_2^{2+}$	0.00±0.01	0.07±0.01
	iso-ppz	0.00±0.01	0.06±0.01
	nar	0.00±0.01	0.05±0.01
	dppz	0.00±0.01	0.15

Table 3. Binding Constants (McGhee and von Hippel parameters)

Experiment	Complex	K_b	L = site size in base pairs
Equilibrium Dialysis	tris-phen	6.2×10^3	4
	bpy	$<10^3$	
	dpp	$<10^3$	
	ppz	6.0×10^3	3,4
	qpy	1.1×10^4	2
	$qpyMe^{+}$	1.4×10^4	2
	$qpyMe_2^{2+}$	3.4×10^4	3
	iso-ppz	9.0×10^4	2
Experiment	Complex	K_b	L = site size in base pairs
Emission Enhancement	Δ ppz	1.2×10^4	3
	Λ ppz	6.0×10^3	3,4

Table 4. Enantioselectivity

Complex	Evidence for Enantioselectivity
tris-phen	yes
bpy	no
dpp	no
ppz	yes
Δ ppz	----
Λ ppz	----
qpy	no
$qpyMe^{+}$	no
$qpyMe_2^{2+}$	yes
iso-ppz	yes
nar	yes
dppz	very small

Chapter XI. Experimental

Materials and Methods

Chemicals Used

$[Ru(bpy)_3]Cl_2$ and $[Ru(bpy)_2Cl_2]$ were either prepared by the procedure of Palmer and Piper,[37] or were purchased from Aldrich and recrystallized prior to use. HPLC grade solvents were used throughout. Calf Thymus DNA purchased from Sigma Chemical company was ethanol precipitated according to published procedures. $K_4Fe(CN)_6$ was used without further purification. Synthetic poly (dG•dC) • poly (dG•dC) and poly (dA•dT) • poly (dA•dT) was purchased and used as received. All solutions used for the DNA experiments used a "Tris" buffer (5mM tris acetate, 50mM NaCl, pH 7.4) unless otherwise specified.

The annelated bipyridine and terpyridine complexes were received as a gift from Dr. Randolph Thummel of the University of Houston. The other complexes used in this study were synthesized in our laboratories by refluxing $Ru(bpy)_2Cl_2$ with the appropriate ligand and purifying through successive recrystallizations. Preparations of the ligands were performed by published procedures,[80,220,231] were analyzed by NMR, and sent out for analysis to insure their purity.

Column Chromatography

Column chromatography was also employed to remove other impurities (e.g. dimer formation). A column of alumina (Neutral activity I) is poured from an acetone solution and allowed to settle. The column is packed by allowing

acetone to run through. The complex to be purified is then dissolved in acetonitrile or acetonitrile/methanol. Acetonitrile is often used as the eluent. If the bands didn't move fast enough then methanol is added until movement resumes. The column is cleaned after a run with methanol and may be used several times over.

Resolution of Enantiomers

Resolution of the enantiomeric pairs of $Ru(bpy)_2ppz^{2+}$ was achieved by use of a hydroxylapatite ($Ca_3(PO_4)_2$) column charged with calf thymus DNA.[33] The differential binding behavior of these two mirror image complexes to DNA is the basis for the separation. This technique, however, is not universal since some complexes show only minimal enantioselectivity with respect to calf thymus DNA.

Preparation and Measurements with Porous Vycor Glass (PVG)

Porous Vycor glass, code no. 7930, was received from Corning Glass Works. Samples of glass suitable for impregnation were refluxed in a Soxhlet extractor for 6 hours with water and then heated to 40°C under reduced pressure to remove bulk water. When the glass became transparent, it was placed in a muffle furnace and the temperature was raised from 25°C to 550°C at the rate of 100°C/hr. The glass was maintained at 550°C until impregnation began.

Impregnation onto Porous Vycor Glass (PVG) of compounds that are low vapor pressure solids was achieved by adsorption of a solution of known concentration. One clean PVG sample was weighed and mounted upright in an

Eastman Kodak Developing Jar containing ~50mL of 1 x 10^{-4} Ru complex in solution. The impregnating time was between 12 and 48 hours. The sample was removed and washed with solvent to prevent layering of the solution on the surface of the glass. The solvent was removed by placing the sample under high vacuum.

The adsorbate concentration was determined by measuring the absorbance of the MLCT band of the complex in solution before and after the glass was added to the developing jar. The number of adsorbed moles of compound, n_{ads}, is found by

$$n_{ads} = (A_i - A_f/A_i) \times n_i \qquad [1]$$

where A is the volume corrected optical density at the analyzing wavelength, n_i is the number of moles of adsorbate present in solution before impregnation, and the subscripts i and f indicate initial and final values. By taking the value of n_{ads} and dividing by the weight of the clean glass gives the number of adsorbed moles/gram of PVG. Typical samples of 10^{-4} to 10^{-8} moles/gram were prepared and used.

Equilibrium Dialysis

Equilibrium dialysis experiments to determine binding constants to DNA and enantioselectivity were performed by adding 1.0 ml of a ~1mg/ml DNA solution dissolved in buffer (5 mM Tris, 50mM NaCl, pH 7.4) to a dialysis bag of MWCO 8000-10000 and sealing it. Dialysis vs. 2.0mL of Ru(II) complex for 48 to 72 hours is carried out and analysis of the concentrations inside and outside of the bag are performed by using absorption spectroscopy or CD.[4]

Instrumentation and Physical Measurements

Electronic Absorption Spectra

Electronic Absorption Spectra were recorded either on an Aviv associates upgraded Cary 14 spectrophotometer interfaced to an AT&T model 6300 computer or a Hewlett-Packard model 8452 single beam diode array spectrophotometer interfaced to a 12MHz DTK 80286 PC clone through a GPIB interface. Either 1cm or 2mm cuvettes were used. Unless otherwise noted, all samples measured were air-saturated, unless N_2 purge was necessary for the experiment.

Spectra of PVG samples were obtained by placing the PVG sample within a rectangular cell in the sample beam and mounting a "blank" piece of PVG in the reference beam. A baseline was measured and subtracted to give the net optical density of the adsorbed complex.

Steady-State Emission Spectra

Room temperature emission spectra were recorded on either a Perkin-Elmer MPF-2A emission spectrometer or a P-E model MPF-66 interfaced to a model 7500 P-E professional computer. Both spectrometers were equipped with red-sensitive photomultiplier tubes, and both monitor the emission at 90° to the excitation beam. Suitable filters were used to avoid stray light effects. Samples were mounted in a thermostated cell holder and kept at a steady temperature for the duration of the experiment using a Haake Model FK-2 temperature control bath or similar water bath. When possible, corrected spectra are given. Quantum yields of luminescence were measured mainly on

the MPF-66 due to its higher reproducibility. Excitation spectra were also taken on the above mentioned equipment. All samples were measured with air-saturated solutions, unless otherwise noted.

Low-temperature (77K) emission spectra were measured using a specially constructed Dewar flask with a quartz window for measurement of samples. Samples were placed in capillaries with one closed end and slowly cooled to avoid cracking the tube. Samples were kept submerged for the duration of the experiment, and the quartz window was rinsed with EtOH when frosting occurred. Samples were often dissolved in CH_3CN to measure emission at 77K since the "glass" formed by CH_3CN is relatively transparent in the visible range.

Emission and Excitation Polarization Spectra

Polarized emission and excitation spectra were collected using a polarization accessory Model for the P-E Model MPF-66 emission spectrophotometer. Polarizing filters were rotated during the course of the experiment. Software written for the Model 7500 computer facilitated the measurement of polarization. Instrumental artifacts necessitated the calculation of a "G" factor to correct for grating biasing of light. Measurements were taken every 0.1 seconds for two minutes for each polarizer orientation and averaged. Reproduction of published results of emission polarization values gave confidence to the measurements taken. All polarization measurements were monitored very carefully for temperature fluctuation, which can seriously affect the values of P.

Time Resolved Emission Spectroscopy

A time-resolved emission lifetime and flash photolysis apparatus was built to measure emission intensities as a function of time in the nanosecond range. Using the 355nm line of a Quanta-Ray Model DCR-2A Nd:YAG laser as excitation (4ns pulses), emission light was monitored at 90° after passing through a Bausch and Lomb Model 33-86-76 grating monochromator set at the emission wavelength. An RCA C31034A photomultiplier, which was cooled with a Pacific Photometric Model 3470 AD/6 thermoelectrically cooled housing, was used as the principal detection system. Voltages between -1000 and -1800 V were supplied by a Tennelec Model TC941 negative high voltage power supply. The photomultiplier signal was sent to the 50Ω input of a Tektronix Model 7834 storage oscilloscope and recorded on Polaroid film. Triggering of the oscilloscope was accomplished by either internal triggering or external triggering with a TTL circuit designed and tested by Mr. Robert Bunch of the Queens College Physics Department. RG 58/AU 50Ω cables were used throughout the apparatus.

Once the photographs were taken subsequent workup of the data involved the digitization of the data for use in computer analysis. This was achieved by scanning the photograph with a Microtek Model 300Z Optical Scanner and importing the resultant graphic image into a computer program written for the Apple Macintosh computer by myself. The digitized data was further analyzed by the Simplex Method for fitting to an exponential equation, thus detecting the presence or absence of a multi-component decay.

Reported values of luminescence lifetime are defined as the time required for the initial emission intensity (t=0) to fall to a value of 1/e of the initial value. When multi-component decays are analyzed, each component is subjected to the method of component-stripping described by Demas,[348] and later fed into a simplex computer program to determine the lifetimes of each component.

Time Resolved Emission Studies of PVG Samples

Glass samples were mounted in evacuated cells and placed in a thermostated cell holder. Samples were monitored either through the edge of the glass or off the front surface and mounted at 80° to the excitation. The measured lifetimes were found to be orientation independent at all T. A fast temperature independent component of the emission (τ < 50 ns) was found to arise from the PVG itself, and therefore only the longer component was analyzed.

Resonance Raman Spectroscopy

Ground state resonance Raman spectra were recorded on a Raman spectrometer constructed by Dr. Thomas Strekas.[84] A Spectra-Physics Model 164-88 CW argon ion laser with lines at 457.9, 488, and 514.5nm was used for excitation. Samples were placed in capillaries and situated in the beam of the laser. Scattered light was collected at 90° to the excitation. Detection was achieved through a Spex 14018 monochromater dispersed onto a Princeton Instruments optical muti-channel analyzer (OSMA) equipped with an ST-100 detector controller and an IRY700G microchannel plate image intensified

photodiode array. The interface to a PC's Limited 80286 computer facilitated the collection and viewing of spectra. The spectra were calibrated using toluene as a standard. Scanning ranges were typically between 800 cm^{-1} and 1700 cm^{-1} with a bandwidth of ~2 cm^{-1} for each spectrum collected.

Circular Dichroism

Circular dichroism spectra were collected on a Jasco Model 500-C Spectropolarimeter. Samples were placed in 1 cm circular cuvettes designed for CD spectroscopy. Sensitivities were adjusted to give the smoothest spectra possible. Spectra were manually digitized for plotting purposes. CD was primarily used to determine the purities of enantiomers and detection of enantioselectivity in binding to DNA.

pH Measurements

pH measurements were made on a Corning Model 115 or Orion Research Model 601A pH meter. The machine was calibrated using a two-point calibration.

Photolysis Procedures

An evacuated cell containing an impregnated PVG sample was mounted in a cell holder thermostated with a Haake Model FK2 temperature bath. The sample was subsequently irradiated with 350nm light in a Rayonet Photochemical Reactor (Southern New England Ultraviolet). Excitation intensities were found using ferrioxalate actinometry, and the amount of adsorbed $Ru(bpy)_3^{2+}$ was calculated from the change in optical density at 452nm.

Emission Quantum Yield of $Ru(bpy)_3^{2+}$ and other Ru(II) complexes

Quantum yields of emission were determined using the equation[73]

$$\phi_x = \phi_r (Area_X/Area_R)(n_X^2/n_R^2) \quad [2]$$

where X and R refer to the sample and a reference. The reference was N_2 purged, and the concentrations were adjusted to give the same absorbance at the excitation wavelength. Concentrations were adjusted so as to achieve an "optically dilute" measurement as described by Demas and Crosby.[343] Areas under the emission band(s) were used and measured under equivalent conditions. The indices of refraction were assumed to be the same for each sample and therefore the ratio of the indices of refraction were assumed to be unity. The value of 0.042 for $Ru(bpy)_3^{2+}$ in aqueous N_2 purged solution was used as the standard for the quantum yield of luminescence of Ru(II) complexes at 298K.

Emission Quantum Yield of $Ru(bpy)_3^{2+}$ adsorbed onto PVG

Quantum yields of emission were determined using the equation[343]

$$\phi_x = \phi_r (I_X/I_R)(n_X^2/n_R^2) \quad [3]$$

where X and R refer to the sample and a reference. The reference was N_2 purged, and the concentrations were adjusted to give the same absorbance at the excitation wavelength. Emission intensities were used and measured under equivalent conditions except for variation in temperature. Once again, the value of 0.042 was used for the quantum yield of emission of $Ru(bpy)_3^{2+}$ at 298K. The indices of refraction, n_R and n_X were temperature independent in the range examined and were determined to be 1.33 for aqueous solutions and 1.51 for

PVG samples.

Photolysis of $Ru(bpy)_3^{2+}$ adsorbed onto PVG

Impregnated samples were mounted in rectangular cells, placed in a thermostated cell holder, and evacuated to a pressure of $\leq 10^{-4}$ Torr. $Ru(bpy)_3^{2+}$(ads) was irradiated with 457.9-nm light from a Spectra-Physics Model 164-08 Ar^+ laser. The excitation intensity incident on the cell, typically 6 x 10^{-7} einstein/(s cm^2), was measured with a Coherent Model 210 power meter, and that absorbed by $Ru(bpy)_3^{2+}$(ads) was calculated from an average of the initial and final absorbance of the complex at the excitation wavelength. Quantum yields were calculated from the initial rates of $[Ru(bpy)_2(bpy^-)]^+$(ads)[207] formation and the average absorbed intensity. Although the extent of reaction was limited to ≤20% in all experiments, there is a variation of ≤10% in quantum yield from sample to sample due to differences in light scattering and surface topology. To minimize this variation, quantum yields at different temperatures were determined for each of the individual samples.

The cell containing the impregnated sample was placed in a thermostated cell holder that defined four 6.5-mm-diameter regions near each corner of the PVG sample. With each sample, the initial measurement was at room temperature, 22±1 °C. The sample was then removed and placed in a constant-temperature bath at a higher temperature. After thermal equilibration, the cell holder was realigned to a second region with a bidirectional mount, the cell was inserted, and the quantum yield was measured at the new temperature.

Four independent measurements of quantum yield at different temperatures were made at the different locations on each sample.

References

1. Kalyanasundaram, K. *Coord. Chem. Rev.* **1982**, *46*, 159.

2. Juris, A.; Balzani, V.; Barigelletti, F.; Campagna, S.; Belser, P.; Von Zelewsky, A. *Coord. Chem. Rev.* **1988**, *84*, 279.

3. Barton, J. K.; Basile, L. A.; Danishefsky, A.; Alexandrescu, A. *Proc. Natl. Acad. Sci. USA* **1984**, *81*, 1961.

4. Barton, J. K.; Danishefsky, A; Goldberg, J. M. *J. Am. Chem. Soc.* **1984**, *106*, 2172.

5. Kumar, C.V.; Barton, J. K.; Turro, N. J. *J. Am. Chem. Soc.* **1985**, *107*, 5518.

6. Barton, J. K.; Goldberg, J. M.; Kumar, C.V.; Turro, N. J. *J. Am. Chem. Soc.* **1986**, *108*, 2081.

7. Kelly, J. M.; Tossi, A.B.; McConnell, D. J.; OhUigin, C. *Nuc. Acid. Res.* **1985**, *13*, 6017.

8. Barton, J. K. *Comm. Inorg. Chem.* **1985**, *3*, 321.

9. Pyle, A. M.; Barton, J. K. *Inorg. Chem.* **1987**, *26*, 3820.

10. Kelly, J. M.; McConnell, D. J.; OhUigin, C.; Tossi, A. B.; Kirsch-De Mesmaeker, A.; Masschelein, A.; Nasielski, J. *J. Chem. Soc., Chem. Commun.* **1987**, 1821.

11. Barton, J. K.; *C&EN News* **1988**, 30.

12. Kumar, C. V.; Barton, J. K.; Gould, I. R.; Turro, N. J.; Van Houten, J. *Inorg. Chem.* **1988**, *27*, 648.

13. Mei, H.; Barton, J. K. *Proc, Natl. Acad. Sci. USA* **1988**, *85*, 1339.

14. Tossi, A.B.; Kelly, J. M. *Photochem. and Photobiol.* **1989**, *49*, 545.

15. Pyle, A. M.; Rehmann, J. P.; Meshoyrer, R.; Kumar, C. V.; Turro, N. J.; Barton, J. K. *J. Am. Chem. Soc.* **1989**, *111*, 3051.

16. Kirsch-De Mesmaeker, A.; Orellana, G.; Barton, J. K.; Turro, N. J. *Photochem. and Photobiol.* **1990**, *52*, 461.

17. Hiort, C.; Nordén, B.; Rodger, A. *J. Am. Chem. Soc.* **1990**, *112,* 1971.

18. Pyle, A. M.; Chiang, M. Y.; Barton, J. K. *Inorg. Chem.* **1990**, *29*, 4487.

19. Rehmann, J. P.; Barton, J. K. *Biochemistry* **1990**, *29*, 1701.

20. Rehmann, J. P.; Barton, J. K. *Biochemistry* **1990**, *29*, 1710.

21. Haworth, I. S.; Elcock, A. H.; Freeman, J.; Rodger, A.; Richards, W. G. *J. Biomol. Struct. Dyn.* **1991**, *9*, 23.

22. Orellana, G.; Kirsch-De Mesmaeker, A.; Barton, J. K.; Turro, N. J. *Photochem. and Photobiol.* **1991**, *54*, 499.

23. Morgan, R. J.; Chatterjee, S.; Baker, A. D.; Strekas, T. C. *Inorg. Chem.* **1991**, *30*, 2687.

24. Baker, A. D.; Morgan, R. J.; Strekas, T. C. *J. Chem. Soc., Chem Commun.* **1992**, 1099.

25. Eriksson, M.; Leijon, M.; Hiort, C.; Nordén, B.; Gräslund, A. *J. Am. Chem. Soc.* **1992**, *114,* 4933.

26. Pyle, A. M.; Barton, J. K. In *Progress in Inorganic Chemistry: Bioinorganic Chemistry*; Lippard, S. J.,Ed.; John Wiley & Sons: New York. **1990**, Vol. 38.

27. Friedman, A. E.; Chambron, J. Sauvage, J.; Turro, N. J.; Barton, J. K. *J. Am. Chem. Soc.* **1990**, *112,* 4960.

28. Jenkins, Y.; Friedman, A. E.; Turro, N. J.; Barton, J. K. *Biochemistry* **1992**, *31*, 10809.

29. Friedman, A. E.; Kumar, C. V.; Turro, N. J.; Barton, J. K. *Nuc. Acid. Res.* **1991**, *19*, 2595.

30. Hartshorn, R. M.; Barton, J. K. *J. Am. Chem. Soc.* **1992**, *114,* 5919.

31. Basile, L. A.; Barton, J. K. *J. Am. Chem. Soc.* **1987**, *109,* 7548.

32. Sitlani, A.; Long, E. C.; Pyle, A. M.; Barton, J. K. *J. Am. Chem. Soc.* **1992**, *114*, 2303.

33. Baker, A. D.; Morgan, R. J.; Strekas, T. C. *J. Am. Chem. Soc.* **1991**, *113*, 1411.

34. Paris, J. P.; Brandt, W. W. *J. Am. Chem. Soc.* **1959**, *81*, 5001.

35. Porter, G. B.; Schläfer, H. L. *Ber. Bunsenges Phys. Chem.* **1964**, *68*, 316.

36. Crosby, G. A.; Perkins, W. G.; Klassen, D. M. *J. Chem. Phys.* **1965**, *43*, 1498.

37. Palmer, R. A.; Piper, T. S. *Inorg. Chem.* **1966**, *5*, 864.

38. Day, P.; Sanders, N. *J. Chem. Soc. A.* **1967**, 1536.

39. Klassen, D. M.; Crosby, G. A.; *Chem. Phys. Lett.* **1967**, *1*, 127.

40. Klassen, D. M.; Crosby, G. A.; *J. Chem. Phys.* **1968**, *48*, 1853.

41. Demas, J. N.; Crosby, G. A.; *J. Mol. Spectros.* **1968**, *26*, 72.

42. Zuloaga, F.; Kasha, M. *Photochem. and Photobiol.* **1968**, *7*, 549.

43. Hanazaki, I; Nagakura, S. *Inorg. Chem.* **1968**, *8*, 648.

44. Lytle, F. E.; Hercules, D. M. *J. Am. Chem. Soc.* **1969**, *91*, 253.

45. Demas, J. N.; Crosby, G. A.; *J. Am. Chem. Soc.* **1970**, *92*, 7262.

46. Demas, J. N.; Crosby, G. A.; *J. Am. Chem. Soc.* **1971**, *93*, 2841.

47. Fujita, I.; Kobayashi, H. *Inorg. Chem.* **1973**, *12*, 2758.

48. Harrigan, R. W.; Crosby, G. A.; *J. Chem. Phys.* **1973**, *59*, 3468.

49. Harrigan, R. W.; Hager, G. D.; Crosby, G. A.; *Chem. Phys. Lett.* **1973**, *21*, 487.

50. Crosby, G. A.; Hipps, K. W.; Elfring, W. H. *J. Am. Chem. Soc.* **1974**, *96*, 629.

51. Baker, D. C.; Crosby, G. A.; *Chem. Phys.* **1974**, *4*, 428.

52. Hager, G. D.; Crosby, G. A.; *J. Am. Chem. Soc.* **1975**, *97*, 7031.

53. Hager, G. D.; Watts, R. J.; Crosby, G. A.; *J. Am. Chem. Soc.* **1975**, *97*, 7037.

54. Hipps, K. W.; Crosby, G. A. *J. Am. Chem. Soc.* **1975**, *97*, 7042.

55. Van Houten, J.; Watts, R. J. *J. Am. Chem. Soc.* **1975**, *97*, 3843.

56. Van Houten, J.; Watts, R. J. *J. Am. Chem. Soc.* **1976**, *98*, 4853.

57. Bensasson, R. V.; Salet, C.; Balzani, V. *J. Am. Chem. Soc.* **1976**, *98*, 3722.

58. Allsopp, S. R.; Cox, A.; Jenkins, S. A.; Kemp, T. J.; Tunstall, S. M. *Chem. Phys. Lett.* **1976**, *43*, 135.

59. Allsopp, S. R.; Cox, A.; Kemp, T. J.; Reed, W. J. *J.Chem. Soc. Farad. Trans. 1* **1978**, *74*, 1275.

60. Lachish, U.; Infelta, P. P.; Grätzel, M.*Chem. Phys. Lett.* **1979**, *62*, 317.

61. Creutz, C.; Chou, M.; Netzel, T. L.; Okumura, M.; Sutin, N. *J. Am. Chem. Soc.* **1980**, *102*, 1309.

62. Bensasson, R. V.; Salet, C.; Balzani, V. *C. R. Acad. Sci. Ser. B* **1979**, *289*, 41.

63. Dallinger, R. F.; Woodruff, W. H. *J. Am. Chem.Soc.* **1979**, *101*, 4391.

64. Felix, F.; Ferguson, J.; Güdel, H. U.; Ludi, A.*Chem. Phys. Lett.* **1979**, *62*, 153.

65. Felix, F.; Ferguson, J.; Güdel, H. U.; Ludi, A.*J. Am. Chem.Soc.* **1980**, *102*, 4096.

66. DeArmond, M. K.; Carlin, C. M.; Huang, W. L. *Inorg. Chem.* **1980**, *19*, 62.

67. Hipps, K. W. *Inorg. Chem.* **1980**, *19*, 1390.

68. Elfring, W. H.; Crosby, G. A. *J. Am. Chem.Soc.* **1981**, *103*, 2863.

69. Belser, P. D.; Daul, C.; Von Zelewsky, A.*Chem. Phys. Lett.* **1981**, *79*, 596.

70. Motten, A. G.; Hanck, K.; DeArmond, M. K.*Chem. Phys. Lett.* **1981**, *79*, 541.

71. Ceulemans, A.; Van Quickenborne, L. G. *J. Am. Chem.Soc.* **1981**, *103*, 2238.

72. Forster, M.; Hester, R. E. *Chem. Phys. Lett.* **1981**, *81*, 42.

73. Parker, C. A. *Photoluminescence of Solutions* Elsevier: New York **1968.**

74. Crosby, G. A. *Acc. Chem. Res.* **1975**, *8*, 231.

75. Stone, M. L.; Crosby, G. A.*Chem. Phys. Lett.* **1981**, *79*, 169.

76. Crosby, G. A.; Elfring, W. H. *J. Phys. Chem.* **1976**, *80*, 2206.

77. Balzani, V.; Carassiti, V. *Photochemistry of Coordination Compounds* Academic Press: London **1970.**

78. Ohsawa, Y.; DeArmond, M. K.; Hanck, K. W.; Moreland, C. G. *J. Am. Chem. Soc.* **1985**, *107*, 5383.

79. Yersin, H.; Gallhuber, E.; Vogler, A.; Kunkely, H. *J. Am. Chem.Soc.* **1983**, *105*, 4155.

80. Braunstein, C. H.; Baker, A. D.; Strekas, T. C.; Gafney, H. D. *Inorg. Chem.* **1984**, *23*, 857.

81. DeArmond, M. K.; Carlin, C. M. *Abstr. IUPAC Conf. Photochem., Seerfield, Austria* **1980**, 146.

82. Caspar, J. V.; Westmoreland, T. D.; Allen, G. H.; Bradley, P. G.; Meyer, T. J.; Woodruff, W. H. *J. Am. Chem.Soc.* **1984**, *106*, 3492.

83. Mabrouk, P. A.; Wrighton, M. S. *Inorg. Chem.* **1986**, *25*, 526.

84. Strekas, T. C.; Gafney, H. D.; Tysoe, S. A.; Thummel, R. P; Lefoulon, F. *Inorg. Chem.* **1989**, *28*, 2964.

85. Shi. W. Ph. D. Thesis, City University of New York, **1986.**

86. Hercules, D. M.; Lytle, F. E. *J. Am. Chem.Soc.* **1966**, *88*, 4795.

87. Wallace, W.; Bard, A. J. *J. Phys. Chem.* **1979**, *83*, 1350.

88. Luttmer, J. R.; Bard, A. J. *J. Phys. Chem.* **1981**, *85*, 1155.

89. Itoh, K.; Honda, K. *Chem. Lett.* **1979**, 99.

90. Glass, R. S.; Faulkner, L. R. *J. Phys. Chem.* **1981**, *85*, 1160.

91. Lin, C. T.; Sutin, N. *J. Am. Chem.Soc.* **1975**, *97*, 3543.

92. Young, R. C.; Keene, F. R.; Meyer, T. J. *J. Am. Chem.Soc.* **1977**, *99*, 2468.

93. Laurence, G. S.; Balzani, V. *Inorg. Chem.* **1974**, *13*, 2976.

94. Bock, C. R.; Meyer, T. J.; Whitten, D. G. *J. Am. Chem.Soc.* **1974**, *96*, 4710.

95. Creutz, C.; Sutin, N. *Inorg. Chem.* **1976**, *15*, 496.

96. Ferreira, M. I. C.; Harriman, A. *J. Chem. Soc. Farad. Trans. 2* **1979**, *75*, 874.

97. Taylor, D. G.; Demas, J. N. *J. Phys. Chem.* **1979**, *71*, 1032.

98. Hazelton, M. A.; Lin, C. T.; Schwarz, H. A.; Sutin, N. *J. Am. Chem.Soc.* **1978**, *100*, 2383.

99. Baggott, J. E.; Pilling, M. J. *J. Phys. Chem.* **1980**, *84*, 3012.

100. Demas, J. N.; Addington, J. W. *J. Am. Chem.Soc.* **1976**, *98*, 5800.

101. Creutz, C.; Sutin, N. *J. Am. Chem.Soc.* **1976**, *98*, 6384.

102. Creutz, C. *Inorg. Chem.* **1979**, *17*, 1046.

103. DeLaguardia, R. A.; Thomas, J. K. *J. Phys. Chem.* **1983**, *87*, 3550.

104. Creutz, C.; Sutin, N.; Brunschwig, B. S. *J. Am. Chem.Soc.* **1979**, *101*, 1297.

105. Pelizzetti, E.; Mentasti, E.; Pramauro, E. *Inorg. Chem.* **1976**, *15*, 2898.

106. Lin, C. T.; Böttcher, W.; Chou, M.; Creutz, C.; Sutin, N. *J. Am. Chem.Soc.* **1976**, *98*, 6536.

107. Brunschwig, B. S.; Sutin, N. *Inorg. Chem.* **1979**, *18*, 1731.

108. Giro, G.; Casalbore, G.; Di Marco, P. G.*Chem. Phys. Lett.* **1981**, *71*, 476.

109. Brunschwig, B. S.; Sutin, N.*Chem. Phys. Lett.* **1981**, *77*, 63.

110. Gafney, H. D.; Adamson, A. W. *J. Am. Chem.Soc.* **1972**, *94*, 8238.

111. Fujita, I.; Kobayashi, H. *J. Chem. Phys.* **1970**, *52*, 4904.

112. Fujita, I.; Kobayashi, H. *J. Chem. Phys.* **1972**, *59*, 2902.

113. Fujita, I.; Kobayashi, H. *Ber. Bunsenges. Phys. Chem.* **1972**, *76*, 115.

114. Bock, C. R.; Conner, J. A.; Gutierrez, A. R.; Meyer, T. J.; Whitten, D. G.; Sullivan, B. P.; Nagle, J. K. *J. Am. Chem.Soc.* **1979**, *101*, 4815.

115. Bock, C. R.; Meyer, T. J.; Whitten, D. G. *J. Am. Chem.Soc.* **1975**, *97*, 2909.

116. Kalyanasundaram, K.; Kiwi, J.; Grätzel, M. *Helv. Chim. Acta.* **1978**, *61*, 2720.

117. Gaines, G. L. *J. Phys. Chem.* **1983**, *79*, 3088.

118. Takuma, K.; Kajiwara, M.; Matsuo, T. *Chem. Lett.* **1977**, 1199.

119. Amouyal, E.; Zidler, B.; Keller, P.; Moradpour, A.*Chem. Phys. Lett.* **1980**, *74*, 314.

120. Nagle, J. K.; Bernstein, J. S.; Young, R. C.; Meyer, T. J. *Inorg. Chem.* **1981**, *20*, 1760.

121. Nagle, J. K.; Young, R. C.; Meyer, T. J. *Inorg. Chem.* **1977**, *16*, 3366.

122. Balzani, V.; Bolletta, F.; Ciano, M.; Maestri, M. *J. Chem. Educ.* **1983**, *60*, 447.

123. Balzani, V.; Bolletta, F.; Gandolfi, M. T.; Maestri, M. *Top. Curr. Chem.* **1978**, *75*, 1.

124. Sutin, N.; Creutz, C. *Pure Appl. Chem.* **1980**, *52*, 2717.

125. Barigelletti, F.; Juris, A.; Balzani, V.; Belser, P.; Von Zelewsky, A. *Inorg. Chem.* **1988**, *22*, 3335.

126. Meyer, T. J. *Prog. Inorg. Chem.* **1983**, *30*, 389.

127. Balzani, V.; Juris, A.; Scandola, F.; Pelizzetti, E.; Serpone, N. *Homogeneous and Heterogeneous Photocatalysis* Reidel: Dordrecht **1986.**

128. Watts, R. J. *J. Chem. Ed.* **1983**, *60*, 834.

129. Whitten, D. G. *Acc. Chem. Res.* **1980**, *13*, 83.

130. Young, R. C.; Meyer, T. J.; Whitten, D. G. *J. Am. Chem.Soc.* **1973**, *97*, 4781.

131. Wacholtz, W. F.; Auerbach, R. A.; Schmehl, R. H. *Inorg. Chem.* **1986**, *25*, 227.

132. Lumpkin, R. S.; Kober, E. M.; Worl, L. A.; Murtaza, Z.; Meyer, T. J. *J. Phys. Chem.* **1990**, *94*, 239.

133. Seddon, E. A.; Seddon; K. R. *The Chemistry of Ruthenium* Elsevier: Amsterdam, **1984.**

134. Connolly, J. S. *Photochemical Conversion and Storage of Solar Energy* Academic Press: New York, **1981.**

135. Porter, G. in Coyle, J. D.; Hill, R. R.; Roberts, D. R. (Eds) *Light, Chemical Change and Life* Open University Press: Walton Hall, Milton Keynes, **1982.**

136. Harriman, A.; West, M. A. *Photogeneration of Hydrogen* Academic Press: New York, **1982.**

137. Grätzel, M. (Ed.) *Energy Resources through Photochemistry and Catalysis* Academic Press: New York, **1983.**

138. Grätzel, M. in Connolly, J. S. (Ed.) *Photochemical Conversion and Storage of Solar Energy* Academic Press: New York, **1981.**

139. Lehn, J. M. in Connolly, J. S. (Ed.) *Photochemical Conversion and Storage of Solar Energy* Academic Press: New York, **1981.**

140. Zamaraev, K. I.; Parmon, V. N. in Grätzel, M. (Ed.) *Energy Resources through Photochemistry and Catalysis* Academic Press: New York, **1983.**

141. Kiwi, J. in Grätzel, M. (Ed.) *Energy Resources through Photochemistry and Catalysis* Academic Press: New York, **1983.**

142. Watanabe, T.; Fujishima, A.; Honda, K. in Grätzel, M. (Ed.) *Energy Resources through Photochemistry and Catalysis* Academic Press: New York, **1983.**

143. Kalyanasundaram, K.; Kiwi, J.; Grätzel, M. *Helv. Chim. Acta.*, **1978**, *61*, 2720.

144. Yersin, H.; Gallhuber, E. *J. Am. Chem. Soc.* **1984**, *106*, 6582.

145. Moradpour, A.; Amouyal, E.; Keller, P.; Kagan, H. *Nouv. J. Chim.*, **1978**, *2*, 547.

146. Allsopp, S. R.; Cox, A.; Kemp, T. J.; Reed, W. J. *J. Chem. Soc. Farad. Trans. 1* **1979**, *75*, 353.

147. Kiwi, J.; Grätzel, M. *Angew. Chem. Int. Ed. Engl.* **1979**, *18*, 624.

148. Takuma, K.; Shuto, Y.; Matsuo, T. *Chem. Lett.* **1978**, 983.

149. Kiwi, J.; Grätzel, M. *Nature (London)* **1979**, *281*, 657.

150. Kiwi, J.; Grätzel, M. *J. Am. Chem. Soc.* **1979**, *101*, 7214.

151. Gohn, M.; Getoff, N. *Z. Naturforsch. Teif A* **1979**, *34*, 1135.

152. Okura, I.; Kim-Thuan, N. *J. Mol. Catal.* **1979**, *5*, 311.

153. Okura, I.; Nakamura, S.; Kim-Thuan, N.; Nakamura, K.I. *J. Mol. Catal.* **1979**, *5*, 311.

154. Keller, P.; Moradpour, A.; Amouyal, E.; Kagan, H. B. *Nouv. J. Chim.* **1980**, *4*, 377.

155. Keller, P.; Moradpour, A.; Amouyal, E.; Kagan, H. B. *J. Mol. Catal.* **1980**, *7*, 539.

156. Krasna, A. I. *Photochem. Photobiol.* **1980**, *31*, 75.

157. Amouyal, E.; Keller, P.; Moradpour, A. *J. Chem. Soc. Chem. Commun.* **1980**, 1019.

158. Keller, P.; Moradpour, A. *J. Am. Chem. Soc.* **1980**, *102*, 7193.

159. Okuno, Y.; Yonemitsu, O. *Chem. Lett.* **1980** 959.

160. Crutchley, R. J.; Lever, A. B. P. *J. Am. Chem. Soc.* **1980**, *102*, 7128.

161. Johansen, O.; Launikonis, A.; Mau, A. W. H.; Sasse, W. H. F. *Aust. J. Chem.* **1980**, *33*, 1643.

162. Borgarello, E.; Kiwi, J.; Pelizzetti, E.; Visca, M.; Grätzel, M. *J. Am. Chem. Soc.* **1981**, *103*, 6324.

163. Duonghong, D.; Borgarello, E.; Grätzel, M. *J. Am. Chem. Soc.* **1981**, *103*, 4685.

164. Miller, D.; McLendon, G. *Inorg. Chem.* **1981**, *20*, 950.

165. Okura, I.; Kim-Thuan, N. *J. Chem. Soc. Farad. Trans. 1* **1981**, *77*, 1411.

166. Okura, I.; Kim-Thuan, N.; Takeuchi, M. *Inorg. Chim. Acta* **1981**, *53*, L149.

167. Nishijima, T.; Nagamura, T.; Matsuo, T. *J. Polym. Sci. Polym. Lett.* **1981**, *19*, 65.

168. Ageishi, K.; Endo, T.; Okawara, M. *J. Polym. Sci. Polym. Chem.* **1981**, *19*, 1085.

169. Kiwi, J.; Borgarello, E.; Pelizzetti, E.; Visca, M.; Grätzel, M. *Angew. Chem. Int. Ed. Engl.* **1980**, *19*, 646.

170. Borgarello, E.; Kiwi, J.; Pelizzetti, E.; Visca, M.; Grätzel, M. *Nature (London)* **1981**, *289*, 158.

171. Rubenstein, I; Bard, A. J. *J. Am. Chem. Soc.* **1981**, *103*, 512.

172. Rillema, D. P.; Dressick, W. J.; Meyer, T. J. *J. Chem. Soc., Chem. Commun.* **1980**, 274.

173. Bolletta, F.; Balzani, V. *J. Am. Chem. Soc.* **1982**, *104*, 4250.

174. Bolletta, F.; Mulazzani, Q. G.; Venturi, M.; Serpone, N.; Balzani, V. *Gazz. Chim. Ital.* **1985**, *115*, 137.

175. Wheeler, J.; Thomas, J. K. *J. Phys. Chem.* **1982**, *86*, 4540.

176. Furlong, N. D.; Tricot, Y. M.; Swift, J. D.; Sasse, W. *Aust. J. Chem.* **1984**, *37*, 703.

177. DeLaguardia, R. A.; Thomas, J. K. *J. Phys. Chem.* **1983**, *87*, 990.

178. Krenske, D.; Abdo, S.; Van Damme, H.; Cruz, M.; Friapat, J. J.*J. Phys. Chem.* **1980**, *84*, 2447.

179. Ghosh, P. K.; Bard, A. J.*J. Phys. Chem.* **1984**, *88*, 5519.

180. Gaudiello, J. G.; Ghosh, P. K.; Bard, A. J. *J. Am. Chem. Soc.* **1985**, *107*, 3027.

181. Schoonheydt, R. A.; DePauw, P.; Vliers, D.; DeSchrijver, F. C. *J. Phys. Chem.* **1984**, *88*, 5113.

182. Nakamura, T.; Thomas, J. K. *Langmuir*, **1985**, *1*, 568.

183. Milosavijevic, B. H.; Thomas, J. K. *J. Phys. Chem.* **1983**, *87*, 616.

184. Milosavijevic, B. H.; Thomas, J. K. *Macromolecules* **1984**, *17*, 2244.

185. Milosavijevic, B. H.; Thomas, J. K. *J. Chem. Soc. Farad, Trans. 1* **1985**, *81*, 735.

186. Milosavijevic, B. H.; Thomas, J. K. *J. Phys. Chem.* **1985**, *89*, 1830.

187. Kaneto, M.; Motoyoshi, J.; Yamada, A. *Nature (London)* **1980**, *285*, 468.

188. Thornton, A. T.; Laurence, G. S. *J. Chem. Soc., Chem. Commun.* **1978**, 408.

189. Kurimura, Y.; Katzumata, K. *Bull. Chem. Soc. Jpn.* **1982**, *55*, 2560.

190. Quayle, W. H.; Lunsford, J. K. *Inorg. Chem.* **1981**, *20*, 97.

191. Alkaitis, S. A.; Beck, G.; Grätzel, M. *J. Am. Chem. Soc.* **1975**, *97*, 5723.

192. Szentirmay, M. N.; Prieto, N. E.; Martin, C. R. *J. Phys. Chem.* **1985**, *89*, 3017.

193. Turro, N. J.; Barton, J. K.; Tomalia, D. A. *Acc. Chem. Res.* **1991**, *24*, 332.

194. Kajiwara, T.; Hashimoto, K.; Kawai, T.; Sakata, T. *J. Phys. Chem.* **1982**, *86*, 4518.

195. Shi, W.; Wolfgang, S.; Strekas, T. C.; Gafney, H. D. *J. Phys. Chem.* **1985**, *89*, 974.

196. Fan, J.; Shi, W.; Tysoe, S. A.; Strekas, T. C.; Gafney, H. D. *J. Phys. Chem.* **1989**, *93*, 373.

197. Borgarello, E.; Kiwi, J.; Grätzel, M.; Pelizzetti, E.; Visca *J. Am. Chem. Soc.* **1982**, *104*, 2996.

198. Houlding, V. H.; Grätzel, M. *J. Am. Chem. Soc.* **1983**, *105*, 5695.

199. Furlong, D. N.; Wells, D.; Sasse, W. H. F. *J. Phys. Chem.* **1986**, *90*, 1107.

200. Clark, W. D. K.; Sutin, N. *J. Am. Chem. Soc.* **1977**, *99*, 4676.

201. Whitten, D. G.; Russell, J. C.; Scmel, R. H. *Tetrahedron*, **1982**, *38*, 2455.

202. Lee, L. Y.; Hurst, J. K.; Politi, M.; Kurihara, K.; Fendler, J. H. *J. Am. Chem. Soc.* **1983**, *105*, 370.

203. Tunneli, M. S.; Fendler, J. H. *J. Am. Chem. Soc.* **1981**, *103*, 2507.

204. Watts, R. J.; Crosby, G. A. *J. Am. Chem. Soc.* **1972**, *94*, 2606.

205. Thummel, R. P.; Jahng, Y. *Inorg. Chem.* **1986**, *25*, 2527.

206. Thummel, R. P.; Lefoulon, F.; Korp, J. D. *Inorg. Chem.* **1987**, *26*, 2370.

207. Kennelly, T.; Gafney, H. D.; Braun, M. *J. Am. Chem. Soc.* **1985**, *107*, 4431.

208. Washel, A. *Annu. Rev. Biophys. Bioeng.* **1977**, *6*, 273.

209. Peterson, S. H.; Demas, J. N. *J. Am. Chem. Soc.* **1976**, *98*, 7880.

210. Crutchley, R. J.; Kress, N.; Lever, A. B. P. *J. Am. Chem. Soc.* **1983**, *105*, 1170.

211. Giordano, P. J.; Bock, C. R.; Wrighton, M .S.; Interrante, L. V.; Williams, R. F. X. *J. Am. Chem. Soc.* **1977**, *99*, 3187.

212. Giordano, P. J.; Bock, C. R.; Wrighton, M .S. *J. Am. Chem. Soc.* **1978**, *100*, 6960.

213. Ferguson, J.; Sasse, W. H. F. *Chem. Phys. Lett.* **1979**, *68*, 21.

214. Lay, P. A.; Sasse, W. H. F. *Inorg. Chem.* **1984**, *23*, 4123.

215. Shimidzu, T.; Iyoda, T.; Izaki, K. *J. Phys. Chem.* **1985**, *89*, 642.

216. Hunziker, M.; Ludi, A. *J. Am. Chem. Soc.* **1977**, *99*, 7370.

217. Rillema, D. P.; Allen, G.; Meyer, T. J.; Conrad, D. *Inorg. Chem.* **1983**, *22*, 1617.

218. Caswell, D. S.; Spiro, T. G.*Inorg. Chem.* **1987**, *26*, 18.

219. Ford, P.; De Rudd, F. P.; Gaunder, R.; Taube, H. *J. Am. Chem. Soc.* **1968**, *90*, 1187.

220. Fuchs, Y.; Lofters, S.; Dieter, T.; Shi, W.; Morgan, R.; Strekas, T. C.; Gafney, H. D.; Baker, A. D. *J. Am. Chem. Soc.* **1987**, *109*, 2691.

221. Bodner, G. M. *J. Chem. Educ.* **1986**, *63*, 246.

222. Lasser, N.; Feitelson, J. *J. Phys. Chem.* **1973**, *77*, 1011.

223. Eigen, M.; Kruse, W.; Maass, G.; De Mayer, L. *Prog. React. Kinet.* **1964**, *2*, 285.

224. Vander Donckt, E. *Prog. React. Kinet.* **1966**, *5*, 273.

225. Brignell, P. J.; Johnson, C. D.; Katritzky, A. R.; Shakir, N.; Tarhan, H. O.; Walker, G. *J. Chem. Soc. B* **1967**, 1233.

226. Nakamoto, K. *J. Phys. Chem.* **1960**, *64*, 1420.

227. Krishnan, C. V.; Creutz, C.; Schwartz, H. A.; Sutin, N. *J. Am. Chem. Soc.* **1983**, *105*, 5617.

228. Hosek, W.; Tysoe, S. A.; Gafney, H. D.; Baker, A. D.; Strekas, T. C. *Inorg. Chem.* **1989**, *28*, 1228.

229. Calvert, J. G.; Pitts, J. N. *Photochemistry* John Wiley and Sons:New York, **1966.**

230. Turro, J. N. *Modern Molecular Photochemistry* Benjamin Cummings: California, **1978.**

231. Bierig, K.; Morgan, R. J.; Tysoe, S.; Gafney, H. D.; Strekas, T. C.; Baker, A. D. *Inorg. Chem.* **1991**, *30*, 4898.

232. Thummmel, R. P.; Lefoulon, F. *Inorg. Chem.* **1987**, *26*, 675.

233. Thummel, R. P.; Decloitre, Y.; Lefoulon, F. *Inorg. Chim. Acta* **1987**, *128*, 245.

234. Binamira-Soriga, E.; Sprouse, S. D.; Watts, R. J.; Kaska, W. C. *Inorg. Chim. Acta* **1984**, *84*, 135.

235. Klassen, D. M. *Inorg. Chem.* **1976**, *15*, 3166.

236. Anderson, S.; Seddon, S.; Wright, R. D. *Chem. Phys. Lett.* **1980**, *71*, 220.

237. Allen, G. H.; White, R. P.; Rillema, D. P.; Meyer, T. J. *J. Am. Chem. Soc.* **1984**, *106*, 2613.

238. Balzani, V.; Juris, A.; Barigelletti, F.; Belser, P.; Von Zelewsky, A. *Sci. Pap. Inst. Phys. Chem. Res. (Jpn.)* **1984**, *78*, 78.

239. Belser, P.; Von Zelewsky, A.; *Helv. Chim. Acta* **1980**, *63*, 1675.

240. Belser, P.; Von Zelewsky, A.; *Chem. Phys. Lett.* **1982**, *89*, 101.

241. Thummel, R. P.; Lefoulon, F.; Korp, J. D. *Inorg. Chem.* **1987**, *26*, 2370.

242. Thummel, R. P.; Lefoulon, F.; Mahadevan, R. *J. Org. Chem.* **1985**, *50*, 3824.

243. Henderson, L. J.; Fronczek, F. R.; Cherry, W. R. *J. Am. Chem. Soc.* **1984**, *106*, 5876.

244. Wolfgang, S.; Strekas, T. C.; Gafney, H. D.; Krause, R.; Krause, K. *Inorg. Chem.* **1984**, *23*, 2650.

245. Knorrs, C.; Gafney, H. D.; Baker, A. D.; Braunstein, C. H.; Strekas, T. C. *J. Raman Spectrosc.* **1983**, *14*, 32.

246. Chung, Y. C.; Leventis, N.; Wagner, P. J.; Leroi, G. E. *J. Am. Chem. Soc.* **1985**, *107*, 1414.

247. Smothers, W. K.; Wrighton, M. S. *J. Am. Chem. Soc.* **1983**, *105*, 1067.

248. Bradley, P. G.; Kress, N.; Hornberger, B. A.; Dallinger, R. F.; Woodruff, W. H. *J. Am. Chem. Soc.* **1979**, *101*, 4391.

249. Caswell, D. S.; Spiro, T. G. *Inorg. Chem.* **1987**, *26*, 18.

250. McClanahan, S.; Kincaid, J. *J. Raman Spectrosc.* **1984**, *15*, 173.

251. Tait, C. D.; MacQueen, D. B.; Donohoe, R. J.; DeArmond, M. K.; Hanck, K. W.; Wertz, D. W. *J. Phys. Chem.* **1986**, *90*, 1766.

252. Kober, E. M.; Meyer, T. J. *Inorg. Chem.* **1985**, *24*, 106.

253. Shi, W.; Gafney, H. D. *J. Phys. Chem.* **1988**, *92*, 2329.

254. Zerbi, G.; Sandroni, S. *Spectrochim. Acta, Part A* **1968**, *24A*, 511.

255. Kirchoff, J. R.; McMillin, D. R.; Marnot, P. A.; Sauvage, J. P. *J. Am. Chem. Soc.* **1985**, *107*, 1138.

256. Fan, J. W. Ph. D. Thesis, City University of New York, **1992.**

257. Agnew, S. F.; Stone, M. L.; Crosby, G. A. *Chem. Phys. Lett.* **1982**, *85*, 57.

258. Thomas, J. K. *Chem. Rev.* **1980**, *80*, 283.

259. Klassen, D. M.; Hudson, C. W.; Shaddix, E. L. *Inorg. Chem.* **1975**, *14*, 2733.

260. Young, R. C.; Nagle, J. K.; Meyer, T. J.; Whitten, D. G. *J. Am. Chem. Soc.* **1978**, *100*, 4773.

261. Downard, A. J.; Honey, G. E.; Steel, P. J. *Inorg.Chem.* **1991**, *30*, 3733.

262. Lytle, F. E.; Petrosky, L. M.; Carlson, L. R. *Anal. Chim. Acta* **1971**, *57*, 239.

263. Calvert, J. M.; Caspar, J. V.; Binstead, R. A.; Westmoreland, T. D.; Meyer, T. J. *J. Am. Chem.Soc.* **1982**, *104*, 6620.

264. Lumpkin, R. S.; Meyer, T. J. *J. Phys. Chem.* **1986**, *90*, 5307.

265. Danielson, E.; Lumpkin, R. S.; Meyer, T. J. *J. Phys. Chem.* **1987**, *91*, 1305.

266. Ferguson, J.; Krausz, E. F.; Maeder, M. *J. Phys. Chem.* **1985**, *89*, 1852.

267. Ferguson, J.; Krausz, E. F. *Chem. Phys. Lett.* **1986**, *127*, 551.

268. Kitamura, N.; Kim, H.; Kawanishi, Y.; Obata, R.; Tazuke, S. *J. Phys. Chem.* **1986**, *90*, 1488.

269. Kim, H.; Kitamura, N.; Tazuke, S. *Chem. Phys. Lett.* **1988**, *143*, 77.

270. Matsuo, T.; Takuma, K.; Nishizima, T.; Tsutsui, Y. *J. Coord. Chem.* **1980**, *10*, 195.

271. Rodgers, M. A. J.; Becker, J. C. *J. Phys. Chem.* **1980**, *84*, 2762.

272. Atik, S. S.; Thomas, J. K. *J. Am. Chem. Soc.* **1981**, *103*, 7403, 4367.

273. Willner, I.; Otvos, J. W.; Calvin, M. *J. Am. Chem. Soc.* **1981**, *103*, 3203.

274. Willner, I.; Yang, J. M.; Laane, C.; Otvos, J. W.; Calvin, M. *J. Phys. Chem.* **1981**, *85*, 3277.

275. Willner, I.; Degani, Y. *J. Am. Chem. Soc.* **1983**, *105*, 6228.

276. Shi, W.; Gafney, H. D. *J. Am. Chem. Soc.* **1987**, *109*, 1582.

277. Cant, N. W.; Little, L. H. *Can. J. Chem.* **1964**, *42*, 802.

278. Elmer, T. H.; Chapman, I. D.; Nordberg, M. E. *J. Phys. Chem.* **1962**, *66*, 1517.

279. Darsillo, M. S.; Gafney, H. D.; Paquette, M. S. *J. Am. Chem. Soc.* **1987**,*109*, 3275.

280. Martin, J. E.; Hart, E. J.; Adamson, A. W.; Gafney, H. D.; Halpern, J. *J. Am. Chem. Soc.* **1972**, *94*, 9238.

281. Krenske, D.; Abdo, S.; Van Damme, H.; Cruz, M.; Friapat, J. J. *J. Phys. Chem.* **1981**, *85*, 797.

282. Meisel, D.; Matheson, M. S.; Rabani, J. *J. Am. Chem. Soc.* **1978**, *100*, 117.

283. Baxendale, J. H.; Fiti, M. *J. Chem. Soc., Dalton Trans.* **1972**, 1995.

284. Baxendale, J. H. *Radiat. Res. Suppl.* **1964**, *4*, 139.

285. Hart, E. J.; Gordon, S.; Fielden, E. M. *J. Phys. Chem.* **1966**, *70*, 150.

286. Matheson, M. S.; *Adv. Chem. Ser.* **1965**, *No. 50*, 45.

287. Gale, E. F.; Cundliffe, F.; Reynolds, P. E.; Richmond, M. H.; Waring, M. J. *The Molecular Basis of Antibiotic Action*, Wiley: London **1972.**

288. Corcoran, J. W.; Hahn, F. E. (Eds.) *Antibiotics, III, Mechanism of Action of Antimicrobial and Antitumor Agents* Springer-Verlag: Berlin **1974.**

289. Hartmann, G.; Behr, W.; Beissner, K. A.; Honikel, K.; Sippel, A. *Angew. Chem. Int. Ed. Engl.* **1968**, *7*, 693.

290. Waring, M. J. *Annu. Rev. Biochem.* **1981**, *50*, 159.

291. Heidelberger, C. *Annu. Rev. Biochem.* **1975**, *44*, 78.

292. Marzilli, L. G. *Prog. Inorg. Chem.* **1977**, *23*, 255.

293. Lippard, S. J. *Accts. Chem. Res.* **1978**, *11*, 211.

294. Barton, J. K.; Lippard, S. J. *Metal Ions in Biology* **1980**, *1*, 31.

295. Lerman, L. S. *J. Mol. Biol.* **1961**, *3*, 18.

296. Watson, J. D.; Crick, F. H. C. *Nature* **1953**, *171*, 737.

297. Crick, F. H. C.; Watson, J. D. *Proc. Roy. Soc. (London) Ser. A.* **1954**, *223*, 80.

298. Wang, A. H.-J.; Quigley, G. J.; Kolpak, F. J.; Crawford, J. L.; Van Boom, J. H.; Van Der Marel, G.; Rich, A. *Nature (London)* **1979**, *282*, 680.

299. Moser, H. E.; Dervan, P. B. *Science* **1987**, *238*, 645.

300. Gellert, M.; Mizuuchi, M.; O'Dea, M. H.; Ohmori, H.; Tomizawa, J. *Cold Spring Harbor Symp. Quant. Biol.* **1979**, *43*, 35.

301. Lilley, D. M. J. *Proc. Nat. Acad. Sci. USA* **1980**, *77*, 6468.

302. Trifonov, E. N.; Sussman, J. L. *Proc. Nat. Acad. Sci. USA* **1980**, *77*, 3816.

303. Marini, J. C.; Levene, S. D.; Crothers, D. M.; Englund, P. T. *Proc. Nat. Acad. Sci. USA* **1982**, *79*, 7664.

304. Koo, H.-S.; Wu, H.-M.; Crothers, D. M. *Nature (London)* **1986**, *320*, 501.

305. Mokul'skii, M. A.; Kaiptarova, K. A.; Mokul'skaya, T. D. *Mol. Biol. (Moscow)* **1972**, *6*, 714.

306. Barton, J. K. *Science* **1986**, *233*, 727.

307. Peacocke, A. R.; Skerrett, J. N. H. *J. Chem. Soc., Farad. Trans.* **1956**, *52*, 261.

308. Neville, D. M.; Davis, D. R. *J. Mol. Biol.* **1966**, *17*, 57.

309. Isenberg, I.; Baird, S. L.; Bersohn, R. *Biopolymers* **1967**, *5*, 477.

310. Müller, W.; Crothers, D. M. *J. Mol. Biol.* **1968**, *35*, 251.

311. Fuller, W.; Waring, M. *Ber. Bunsenges. Phys. Chem.* **1964**, *68*, 805.

312. Weill, G.; Calvin, M. *Biopolymers* **1963**, *1*, 401.

313. Lerman, L. S. *Proc. Nat. Acad. Sci., Washington* **1963**, *49*, 94.

314. Blears, D. J.; Danyluk, S. S. *Biopolymers* **1967**, *5*, 535.

315. Gardner, B. J.; Mason, S. F. *Biopolymers* **1967**, *5*, 79.

316. Scatchard, G.; *Ann. N. Y. Acad. Sci.* **1949**, *51*, 660.

317. Crothers, D. *Biopolymers*, **1968**, *6*, 575.

318. Stone, A. L.; Bradley, D. F. *J. Am. Chem. Soc.* **1961**, *83*, 3627.

319. Marky, L. A.; Blumenfield, S.; Breslauer, K. J. *Nucl. Acid. Res.* **1983**, *11*, 2857.

320. Barton, J. K.; Dannenberg, J. J.; Raphael, A. L. *J. Am. Chem. Soc.* **1982**, *104*, 4967.

321. Gessner, R. V.; Quigley, G. J.; Wang, A. H.-J.; Van Der Marel, G. A.; Van Boom, J. H.; Rich, A. *Biochemistry*, **1985**, *24*, 237.

322. Wong, Y.-S.; Lippard, S. J.; *J. Chem. Soc., Chem. Commun.* **1977**, 824.

323. Jennette, K. W.; Lippard, S. J.; Vassiliades, G. A.; Bauer, W. R. *Proc. Nat. Acad. Sci. USA* **1974**, *71*, 3839.

324. Barton, J. K.; Raphael, A. L. *J. Am. Chem. Soc.* **1984**,*106*, 2466.

325. Lippard, S. J.; Bond, P. J.; Wu, K. C.; Bauer, W. R. *Science* **1976**, *194*, 726.

326. Wang, A. H.-J.; Nathans, J.; Van Der Marel, G.; Van Boom, J. H.; Rich, A. *Nature (London)* **1978**, *276*, 471.

327. Barton, J. K.; Raphael, A. L. *Proc, Natl. Acad. Sci. USA* **1985**, *82*, 6460.

328. Fleisher, M. B.; Waterman, K. C.; Turro, N. J.; Barton, J. K. *Inorg. Chem.* **1986**, *25*, 3549.

329. Kirshenbaum, M. R.; Tribolet, R.; Barton, J. K. *Nuc. Acid. Res.* **1988**, *16*, 7943.

330. Purugganan, M. D.; Kumar, C. V.; Turro, N. J.; Barton, J. K. *Science*, **1988**, *241*, 1645.

331. Chow, C. S.; Barton, J. K. *Biochemistry* **1992**, *31*, 5423.

332. Satyanaranya, S.; Dabrowiak, J. C.; Chaires, J. B. *Biochemistry* **1992**, *31*, 9320.

333. Cantor, C. R.; Schimmel, P. R. *Biophysical Chemistry* W. H. Freeman and Company: San Francisco, **1980.**

334. Waring, M. J. *J. Mol. Biol.* **1965**, *13*, 269.

335. Tinoco, I. in Weisbluth, M. (Ed.) *Molecular Biophysics* Academic Press: New York, **1965.**

336. Tysoe, S. A.; Morgan, R. A.; Baker, A. D.; Strekas, T. C. *J. Phys. Chem.* **1993**, *96*, in press.

337. Bittman, R. *J. Mol. Biol.* **1969**, *46*, 251.

338. McGhee, J. D.; Von Hippel, P. H. *J. Mol. Biol.* **1974**, *86*, 469.

339. Waring, M. J. *J. Mol. Biol.* **1970**, *54*, 247.

340. Dougherty, G.; Pilbrow, J. R. *Int. J. Biochem.* **1984**, *16*, 1179.

341. Bard, A. J.; Carter, M. T. *Bioconjugate Chem.* **1990**, *1*, 257.

342. Pyle, A. M; Morii, T.; Barton, J. K. *J. Am. Chem. Soc,* **1990**, *112*, 9432.

343. Demas, J. N.; Crosby, G. A. *J. Phys. Chem.* **1971**, *75*, 991.

344. Nakamaru, K.; *Bull. Chem. Soc. Jpn.* **1982**, *55*, 1639.

345. Goldstein, B. M.; Barton, J. K.; Berman, H. M. *Inorg. Chem.* **1986**, *25*, 842.

346. Chambron, J.-C.; Sauvage, J.-P.; Amouyal, E.; Koffi, P. *Nouv. J. Chim.* **1985**, *9*, 527.

347. Nakamaru, K.; *Bull. Chem. Soc. Jpn.* **1982**, *55*, 2697.

348. Demas, J. N. *Excited-State Lifetime Measurements* Academic Press: New York, **1983.**